First-Passage-Time Problems
in Time-Aware Networks

by

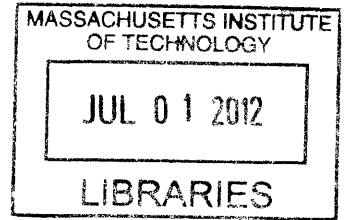## Watcharapan Suwansantisuk

Submitted to the Department of Electrical Engineering
and Computer Science
in partial fulfillment of the requirements for the degree of

Doctor of Philosophy

at the
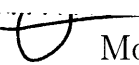
MASSACHUSETTS INSTITUTE OF TECHNOLOGY

June 2012

© Massachusetts Institute of Technology 2012. All rights reserved.

Author . . . .
Department of Electrical Engineering
and Computer Science
May 23, 2012

Certified by . . . .
Moe Z. Win
Associate Professor
Thesis Supervisor

Accepted by . . . .
Professor Leslie A. Kolodziejski
Chairman, Department Committee on Graduate Theses

First-Passage-Time Problems

in Time-Aware Networks

by

Watcharapan Suwansantisuk

Submitted to the Department of Electrical Engineering
and Computer Science
on May 23, 2012, in partial fulfillment of the
requirements for the degree of
Doctor of Philosophy

Abstract

First passage time or the first time that a stochastic process crosses a boundary is a random variable whose probability distribution is sought in engineering, statistics, finance, and other disciplines. The probability distribution of the first passage time has practical utility but is difficult to obtain because the values of the stochastic process at different times often constitute dependent random variables. As a result, most first-passage-time problems are still open and few of them are explicitly solved. In this thesis, we solve a large class of first-passage-time problems and demonstrate the applications of our solutions to networks that need to maintain common-time references.

Motivated by rich applications of first passage time, we solve first-passage-time problems, which are divided into four categories according to the form of stochastic processes and the type of the boundaries. The four categories cover Brownian motion with quadratic drift and the boundary that consists of two constants; Brownian motion with polynomial drift of an arbitrary degree and the boundary that consists of two constants; multi-dimensional Brownian motion with polynomial drift and a class of boundaries that are characterized by open sets in the Euclidean space; and a discrete-time process with a class of correlations and the boundary that consists of one constant. These first-passage-time problems are challenging yet important for practical utility.

The solutions to these first-passage-time problems range from an explicit expression to a bound of the first-passage-time distribution, reflecting the inherent difficulty in these first-passage-time problems. For Brownian motion with quadratic drift, the solution is explicit, consisting of elementary functions and functions that are characterized by Laplace transforms. For Brownian motion with polynomial drift of an arbitrary order, the solution involves analytical and numerical methods. For multi-dimensional Brownian motion, the solution is explicit for a certain shape of the boundary and is given by an upper bound and a lower bound for the other shapes. For the discrete-time process, the solution is explicit. The strength of our solutions

is that they cover a large class of first-passage-time problems and are easy to use.

The primary approach that allows us to solve these first-passage-time problems is transformation methodology. We apply various types of transformations, including transformation of probability measure, transformation of time, and integral transformation. Although these transformations are known, the combination of them in an appropriate order enables the solutions to previously-unsolved first-passage-time problems. We also discuss other problems that can be solved as consequences of the transformation methodology, including first-passage-time problems that involve a one-sided constant boundary, a moving boundary, and drifts such as logarithmic, exponential, sinusoidal, and square-root functions. A large class of first-passage-time problems confirms the utility of the transformation methodology.

We demonstrate an application of the first-passage-time problems in the context of network synchronization. In the first setting that we consider, the first passage time is the first time that a network loses synchronization with a reference clock. At the first passage time, clocks in the network need to be calibrated. In the second setting, the first passage time represents the first time that a node achieves a correct synchronization of frames or packets. At the first passage time, a node in the network is able to process the packets that are transmitted as parts of the calibration. In both settings, we consider two performance metrics—the average and the outage—which succinctly summarize the first passage time. These metrics give insight, for example, into the amount of time for networks to lose synchronization as a function of key parameters such as noise in the clocks and the number of nodes in the network. Given the large class of first-passage-time problems being solved, we expect the thesis results to be useful in many disciplines where first-passage-time problems appear.

Thesis Supervisor: Moe Z. Win
Title: Associate Professor

Acknowledgments

Contents

List of Figures

11

13

List of Tables

Chapter 1

Introduction

The first passage time, or the first time that a random process crosses a boundary, is of importance in many fields. The first passage time is a random variable that appears, for example, in biology, statistics, physics, finance, and engineering. In general, first-passage-time problems aim to determine the probability distributions or the equivalent characterizations.

First-Passage-Time problems are difficult to solve. The difficulty in first-passage-time problems is mainly due to the dependency across times of random processes. To solve the first-passage-time problem, we need to know the trajectory of the random process, a requirement for the joint probability of values of the random process at all times. Every unsolved first passage problem involves an infinite set of dependent random variables, a source of difficulty. Given this difficulty, most first-passage-time problems are open and few of them are solved explicitly.

Motivated by the rich applications of first-passage-time problems, we solve a large class of first-passage-time problems in this thesis. Then, we demonstrate the applications of our first-passage-time solutions to network synchronization. Solutions to these first-passage-time problems and their applications constitute the main research results in this thesis.

The class of problems that we aim to solve are divided into four categories, according to the form of the random processes and the boundaries. These four categories are as follows:

Brownian motion with quadratic drift: This first-passage-time problem involves Brownian motion with quadratic drift and a boundary that consists of two constants. Our solution to this first-passage-time problem is an explicit expression of the probability density function (PDF) for the first passage time. The solution has applications to clock synchronization.

Brownian motion with polynomial drift: This first-passage-time problem involves Brownian motion with polynomial drift and a boundary that consists of two constants. The polynomial may have an arbitrary degree although the case of polynomials with degree two is more suitable to be solved using the method for Brownian motion with quadratic drift (the first problem that we study). A class of polynomials is a dense subset of the class of continuous functions, making the class of polynomials an important class of drifts to study. Our solution to this first-passage-time problem is an expression of the PDF for the first passage time. The solution has applications to clock synchronization.

Multi-dimensional Brownian motion: This first-passage-time problem involves multi-dimensional Brownian motion with polynomial drift and a boundary that belongs to a family of open sets in the Euclidean space. Our solution to this first-passage-time problem is an expression of the cumulative density function (CDF) for certain open sets and the bounds of the CDF for other open sets. The solution has applications to network synchronization.

Discrete-Time process: This first-passage-time problem involves a discrete time process and a boundary consisting of a constant. The random process has a certain correlation across time. Our solution to this this first-passage-time problem is the expressions of the CDF and the expectation for the first passage time. The solution has applications to frame synchronization.

The most important mathematical technique that enables us to solve the first-passage-time problem is transformation methodology. To solve the first-passage-time problems that involve Brownian motion with quadratic drift and polynomial drift, we transform Brownian motion with drift into Brownian motion without drift, large time into small time, a stochastic integration into a Riemann integration with a

random integrand, a conditional expectation into an expectation, and an expectation into a solution to a differential equation. To solve the first-passage-time problems that involve multi-dimensional Brownian motion and discrete-time process, we apply rules in measure theory, probability theory, ordered statistics, and renewal theory. The combination of these approaches provides the solutions to the first-passage-time distributions.

To demonstrate rich applications of our solutions, we consider three important aspects of time-aware networks from a standpoint of synchronization. In the first setting, we aim to understand the amount of time until two clocks need to be calibrated. In the second setting, we aim to understand the amount of time until a network of clocks needs to be calibrated. In the third setting, we aim to understand the amount of time until frame synchronization is completed. The amount of time that appears in these settings are first passage times, whose probability distributions are immediate consequences of this research. We will characterize the first passage times in these settings by two performance metrics: the average and the outage. These performance metrics give insight into the amount of time to calibration and the amount of time time to successfully acquiring the frames or packets during the synchronization phase.

In summary, we study a large class of first-passage-time problems, motivated by their rich applications. First-passage-time problems are difficult to solve in general. But we are able to obtain the solutions by using transformation methodology and approaches from measure theory, probability theory, ordered statistics, and renewal theory. We demonstrate the applications of our first-passage-time distributions to network synchronization. We expect the contributions to have practical utility in many fields where first-passage-time problems appear.

The remaining part of this chapter is organized as follows. In Section 1.1, we state the objectives of this thesis. In Section 1.2, we describe the scope of the research. In Section 1.3, we provide lists of the acronyms, notations, and definitions that frequently appear in the thesis. In Section 1.4, we summarize the main contributions of this research. In the last paragraph of this chapter, we outline the organization of this thesis.

1.1 Objectives of this Research

The objectives of this research are the following:

1. To obtain the probability distribution of the first passage time of a Brownian motion with quadratic drift, to exit from a boundary consisting of two constants;

2. To obtain the probability distribution of the first passage time of a Brownian motion with polynomial drift, to exit from a boundary consisting of two constants;

3. To obtain and bound the probability distribution of the first passage time of a multi-dimensional Brownian motion with polynomial drift, to exit from a class of boundaries that are given by open sets in the Euclidean space;

4. To obtain the probability distribution of the amount of time to correctly acquire a packet;

5. To apply the results on first-passage-time distributions to time-aware networks.

We will discuss the research methodology that helps us achieve these objectives in Chap. 3. Then, we will provide the research results that address these objectives in Chap. 4.

1.2 Scope of this Research

This research focuses on certain types of clocks and a certain aspect of network synchronization. The scope of this research is as follows.

- Time process at a clock takes the form of Brownian motion with quadratic drift. This model is reasonable when the white frequency modulation noise is the dominant type of clock noises.

- Clocks in the network are to be synchronized with a reference clock. This model is suitable when the network needs to maintain the absolute time as opposed to the relative time.

The above scope allows this research to balance between applications and tractability.

1.3   Acronyms, Notations, and Definitions

Below is a summary of acronyms, notations, and definitions that frequently appear in the thesis.

Acronyms

a.e.	almost everywhere
a.s.	almost surely
ATM	asynchronous transfer mode
AWGN	additive white Gaussian noise
CDF	cumulative density function
CSS	conventional serial search
CMF	cumulative mass function
FSS-N_J	fixed-step serial search with a step size N_J
IBVP	initial-boundary value problem
IID	independent and identically distributed
MAT	mean acquisition time
MGF	moment generating function
MSS	marker spacing span
PDE	partial differential equation
PDF	probability density function
PMF	probability mass function
SNR	signal to noise ratio

Notations

The serif font indicates random variables and random processes, except for the Greek letter τ, which denotes a random time and does not have a serif font.

Here are the frequently-used symbols:

a	a real number, representing a barrier
b	a real number, representing a barrier, $a < b$
$\emptyset$	the empty set
$\mathbb{R}$	the set of real numbers
$\mathcal{A} \subset \mathcal{B}$	set $\mathcal{A}$ is a subset of set $\mathcal{B}$, i.e., every element of $\mathcal{A}$ is an element of $\mathcal{B}$. Note that $\mathcal{A} \subset \mathcal{A}$ for every set $\mathcal{A}$
$\lvert \mathcal{A} \rvert$	the number of elements in a finite set $\mathcal{A}$
(p, q)	a set of real numbers x's such that $p < x < q$
$\lim_{x \searrow x_0} f(x)$	the limit of function f as x approaches x_0 from the right, i.e., a number q such that $f(t_n) \to q$ as $n \to \infty$ for all sequences $\{t_n\}$ in (x_0, ∞) such that $t_n \to x_0$
f'	The derivative of function f
$\inf \mathcal{A}$	the greatest lower bound, or the infimum, of a set $\mathcal{A} \subset \mathbb{R}$. If $\mathcal{A}$ is an empty set, we define $\inf \mathcal{A} = \infty$. If $\mathcal{A}$ is not bounded from below (this case does not occur in this research), we define $\inf \mathcal{A} = -\infty$
$\mathcal{N}(\mu, \sigma^2)$	normal distribution with mean μ and variance σ^2
$\varphi(\cdot)$	the PDF of the standard normal, $\mathcal{N}(0, 1)$, random variable: $\varphi(x) = \frac{1}{\sqrt{2\pi}} e^{-x^2/2}$, for $x \in \mathbb{R}$
$\Phi(\cdot)$	the CDF of the standard normal, $\mathcal{N}(0, 1)$, random variable: $\Phi(x) = \int_{-\infty}^{x} \varphi(y) dy$
$Q(\cdot)$	the Gaussian Q-function: $Q(x) = 1 - \Phi(x)$
$1_{\mathcal{A}}(\cdot)$	the indicator function of set $\mathcal{A}$, i.e., $1_{\mathcal{A}}(x) = 1$ if $x \in \mathcal{A}$; and $1_{\mathcal{A}}(x) = 0$ if $x \notin \mathcal{A}$
$\Gamma(\cdot)$	the gamma function: $\Gamma(z) = \int_0^{\infty} t^{z-1} e^{-z} dt$ for any complex number z whose real part is positive
$\text{Ai}(\cdot), \text{Bi}(\cdot)$	Airy functions: $\text{Ai}(z) = c_1 f(z) - c_2 g(z)$ and $\text{Bi}(z) = \sqrt{3}[c_1 f(z) + c_2 g(z)]$ for any complex number z, where $f(z) = \sum_{k=0}^{\infty} 3^k \left(\frac{1}{3}\right)_k \frac{z^{3k}}{(3k)!}$, $g(z) = \sum_{k=0}^{\infty} 3^k \left(\frac{2}{3}\right)_k \frac{z^{3k+1}}{(3k+1)!}$, $c_1 = 3^{-2/3}\Gamma(2/3)$, $c_2 = 3^{-1/3}\Gamma(2/3)$, and $(z)_n = \Gamma(z+n)/\Gamma(z)$ (Pochhammer's symbol)

$\lceil x \rceil$	the smallest integer m such that $x \leq m$
$x \wedge y$	the minimum between x and y
X_t	a random process, for $t \geq 0$
$\mathbb{P}$	Probability measure corresponding to standard Brownian motion
$\mathbb{P}_x$	probability measure corresponding to Brownian motion with initial position $x \in \mathbb{R}$
$\boldsymbol{P}$	Probability measure corresponding to multi-dimensional Brownian motion with initial position at the origin
$\mathbb{E}$	Expectation with respect to probability measure $\mathbb{P}$
$\boldsymbol{E}$	Expectation with respect to probability measure $\boldsymbol{P}$
B_t	a standard Brownian motion with respect to the probability space $(\Omega, \mathcal{F}, \mathbb{P})$, for $t \geq 0$
$\sigma(\mathsf{X})$	the σ-algebra generated by random variable X
$\mathcal{F}_t$	the σ-algebra generated by $\{\mathsf{B}_s : 0 \leq s \leq t\}$
$\tau_{a,b}$	$\inf\{t \geq 0 : \mathsf{X}_t \notin (a,b)\}$, i.e., the first time that a random process X_t takes the value outside an open interval (a,b)
$\mathsf{T}_{a,b}$	$\inf\{t \geq 0 : \mathsf{B}_t \notin (a,b)\}$, i.e., the first time that a random process B_t takes the value outside an open interval (a,b)
$f_{\mathsf{X}}(\cdot)$	PDF of random variable X, i.e., if X is defined on the probability space $(\Omega, \mathcal{F}, P)$, then $P(dx) = f_{\mathsf{X}}(x)dx$

Definitions

First passage time (a random variable) is the first time that a random process takes the value outside an open set.

A time-aware network is a set of nodes (such as the transmitters, receivers, satellites, or other electronic devices) that need to maintain a common time reference.

1.4 Contributions of this Research

The main contributions of this research are as follows:

- A methodology involving transformation techniques to solve a large class of first-passage-time problems;

- A survey of mathematical models for the time process;

- A survey of methods to solve first-passage-time problems;

- Explicit expression for the probability distribution of the first time that Brownian motion with quadratic drift crosses a two-sided, constant boundary;

- Analytical expression for the probability distribution of the first time that Brownian motion with polynomial drift crosses a two-sided, constant boundary;

- Analytical expression and bounds for the probability distribution of the first time that a multi-dimensional Brownian motion exits a class of boundaries;

- Explicit expressions for probability distribution for the first time at which frame synchronization is correctly achieved;

- Proposal of two metrics (expectation and outage) that can be used to measure the calibration time in a network;

- Applications of first passage time to synchronization of a pair of clocks;

- Applications of first passage time to synchronization of a network; and

- Applications of first passage time to frame synchronization.

Given the rich applications of first-passage-time problems, we expect the contributions to be useful in many disciplines.

The remaining part of this thesis is organized as follows. In the next chapter (Chap. 2), we review existing work related to this research. In (Chap. 3), we outline the methodologies that help us achieve the objectives of this research. In Chap. 4, we present the research results, which address the above objectives. Finally, in Chap. 5, we conclude the thesis and summarize important findings.

Chapter 2

Literature Review

In this chapter, we survey existing work related to the thesis. In Section 2.1, we provide an overview on synchronization, which is a crucial task for transmitters and receivers employing digital transmissions. In Section 2.2, we discuss mathematical models for time processes of clocks. In Section 2.3, we provide an overview of first-passage-time problems. In Section 2.4, we survey known methods to solve first-passage-time problems. We now describe the existing work in detail.

2.1 Synchronization

Synchronization refers to the task of regulating the clocks among the transmitters and the receivers. Synchronization can be achieved at the frame level and at the waveform level, among many possibilities. At the frame level, the clocks are virtual clocks, which tick at the boundaries of the frames. The task of frame synchronization is achieved by the receivers, aiming to recover the boundaries of the frames. At the waveform level, the clocks are also virtual clocks, which tick at every symbol time. The task of waveform synchronization is also achieved by the receivers, aiming to obtain the time at which each symbol starts. In this section, we review existing work that is related to frame synchronization and waveform synchronization, which are fundamental types of synchronization for point-to-point transmission.[1]

---

[1]See [56,70,113,118,144–146] for other types of synchronization.
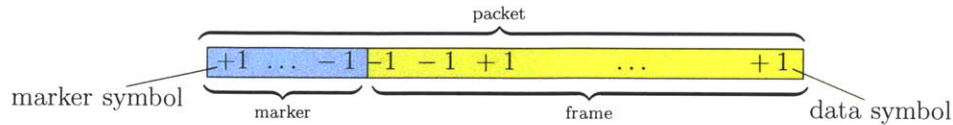
Figure 2-1: A packet consists of two parts: a marker and a frame. The marker indicates the start of a frame, while the frame contains transmitted messages and other relevant information, such as the frame lengths and the symbol pattern for channel estimation.

Frame Synchronization

Digital transmission requires a receiver to regulate its clock in synchronism with the transmitter clock. Clock synchronism is achieved at the waveform level (by an acquisition unit and a phase-locked loop), at the symbol level (by a bit synchronizer), and then at the frame level (by a frame synchronizer) [102] [118, pp. 7–8]. Here, we describe frame synchronization, which is a task of receivers aiming to recover the boundary of the frames given the sequence of the received symbols.

Frame synchronization involves the following steps. In the first step, the transmitter injects a fixed-length symbol pattern, called a marker, into the beginning of each frame[2] to form a marker and frame pair, which is known as a packet (Fig. 2-1).[3] Packets are then converted from symbols into a waveform and transmitted through the channel. The receiver detects the arrival of packets by searching for the marker, removes the markers from the data stream, and recovers the transmitted messages. Marker detection is the most important step for frame synchronization.

The division of symbols into frames may seem burdensome for the network, but it serves many purposes. Framing ensures that individual frames can be transmitted independently without requiring scheduling overhead. The ability to transmit individual frames independently implies that the frequency spectrum can be utilized intermittently according to its availability, resulting in efficient spectrum utilization. In the streaming of multimedia data (such as MPEG-4 video [135]), framing ensures that errors within one frame do not propagate to adjacent frames [98, 128]. In a

---

[2]Before injecting markers, the transmitter modifies the sequence of data symbols, if necessary, to ensure that the data symbols differ from the marker symbols.

[3]The marker is also known at the receiver.

(a) fixed-length frames

(b) variable-length frames
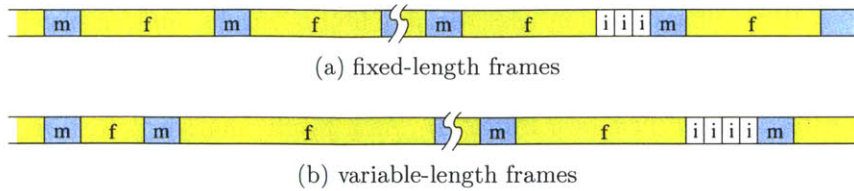
Figure 2-2: Idle fill characters keep the transmitter and receiver synchronized for continuous transmission. Here, region "m" indicates a marker, "f" indicates a frame, and "i" indicates an idle fill character.

Figure 2-3: The use of idle fill characters is not allowed in bursty transmission. Hence, the time between two packets is silent.

network that employs legacy transmission systems, such as asynchronous transfer mode (ATM) technology [44], framing ensures that frames have a length that can be handled by the underlying network infrastructure. These examples show that frame synchronization is important for various applications.

Several approaches can be employed to achieve frame synchronization. One approach, referred to as a continuous transmission of packets, is to reserve the communication link between the transmitter and receiver over the entire time of communication. Frames for continuous transmission may have a fixed length [9, 61, 76, 97] (such as those in ATM networks) or variable lengths [23–25] (such as those in MPEG-4 video streaming). In both cases, the transmitter sends a special character, known as an idle fill character, when it has no immediate packet to transmit (Fig. 2-2). The idle fill characters serve the purpose of keeping the transmitter and receiver synchronized. The use of idle fill characters is possible since the entire link is allocated to the transmitter and receiver during continuous transmission.

On the other hand, the link may not be allocated to the transmitter and receiver during the communications. This approach, referred to as bursty packet transmission, arises in practice, for example, in an 802.11 network and in the Internet. Bursty transmission provides benefits that include a low transmission overhead and efficient spectrum utilization. The drawback of bursty transmission is that transmission delay is difficult to control, which could be problematic for transmission of time-critical

27

information. Bursty transmission uses variable frame-lengths, and, unlike continuous transmission, idle fill characters cannot be used to maintain synchronization between the transmitter and receiver (see Fig. 2-3). As a result, marker detection strategies for continuous and bursty transmission are different.

Performance of frame synchronization has been improved through two broad design approaches. The first approach improves the performance through the design of a marker with good synchronization properties [4,34,52,53,117]. The second approach improves the performance through the design of optimal or near-optimal marker-detection strategies [23–25,76,97,148]. The problem of marker design, valid for both continuous and bursty transmission schemes, has been explored [4, 34, 52, 53, 117]. Performance of frame synchronization is usually obtained via Monte Carlo simulation [60, 62, 147].

Waveform Synchronization

Waveform synchronization is a task of digital receivers, aiming to obtain the time at which each symbol starts, based on the observed, received waveform. Waveform synchronization is a rich subject [48–50,68,79,87,94,121–124,126,127,132,150]. Here, we will focus on signal acquisition, which is an initial part of waveform synchronization.

Waveform synchronization is an important task for a digital receivers employing spread-spectrum techniques. Before communication commences, the receiver must search for a location of sequence phase within a required accuracy. The synchronization process occurs in two stages: the acquisition stage and the tracking stage [58, 82, 83, 114]. During the acquisition stage, the receiver coarsely aligns the sequence of the locally generated reference (LGR) with that of the received signal. The receiver then enters the tracking stage to finely align the two sequences and maintain the synchronization throughout the communication. It has been shown that an acquisition problem is a hypothesis testing problem [133].

The total number N_{unc} of phases or cells that the receiver needs to test depends on the temporal uncertainty range $[T_{begin}, T_{end})$ of a phase delay and the resolution

T_{res} to resolve the phase delay.[4] The expression for N_{unc} is given by

$$N_{\text{unc}} = \frac{T_{\text{end}} - T_{\text{begin}}}{T_{\text{res}}},\qquad(2.1)$$

which can range from a few cells to several thousand cells, depending on the application [85]. Without loss of generality, we index the cells from 1 to N_{unc}. Cell i, $1 \leq i \leq N_{\text{unc}}$, corresponds to a hypothesized phase delay in the range $[T_{\text{begin}} + (i - 1)T_{\text{res}}, T_{\text{begin}} + iT_{\text{res}})$. An uncertainty index set

$$\mathcal{U} = \{1, 2, 3, \ldots, N_{\text{unc}}\}\qquad(2.2)$$

denotes a collection of cells to test. Because the ratio $1/T_{\text{res}}$ is proportional to the transmission bandwidth, N_{unc} can be very large, especially, for a wide bandwidth transmission system [50]. In that scenario, acquisition of a received signal in a reasonable amount of time is a challenging task.

In a hash environment, such as dense urban or indoor environments, the received signal often consists of multiple propagation paths, which can be resolved via the use of wide bandwidth signals [138, 139]. The number of correct phases or in-phase cells, denoted by N_{hit}, in a dense multipath channel is proportional to the number of resolvable paths. Multiple resolvable paths tend to arrive in a cluster in dense multipath channels [20, 26, 27, 140–142], giving rise to consecutive in-phase cells, modulo-N_{unc}, in the uncertainty index set. The availability of consecutive in-phase cells can be utilized to aid the design of an acquisition system.

Designing an acquisition system involves two broad design aspects. One deals with how the decision is made at the detection layer. Examples of the relevant issues at this layer include combining methods for decision variables, the number of stages in a multi-dwell detector, a design choice for decision thresholds, and the evaluation of the detection and false-alarm probabilities. The other aspect deals with the procedure for finding a correct cell at the search layer. Examples of the relevant issues include the choice of search strategy (e.g., serial search [85], fully parallel search [94], or hybrid

---

[4]Subscript "unc" stands for uncertainty.

search [116]); and the selection of efficient search order (the sequence in which cells are tested). In general, the goal of the acquisition receiver is to find a correct sequence phase as fast as possible.

The performance of the acquisition system is measured typically by the mean acquisition time (MAT), the average duration required for the receiver to achieve acquisition. A common method for finding the MAT is to use a flow diagram. A flow diagram that describes the acquisition procedure in additive white Gaussian noise (AWGN) channels [86–88] or in frequency non-selective fading channels [51,64, 65, 68, 103, 106, 107] simply has one in-phase cell. On the other hand, in multipath fading channels, the flow diagram has multiple in-phase cells corresponding to the multiple resolvable paths [59, 66, 67, 111, 131, 149, 150, 152].

There are two major approaches to improve the MAT. The first approach improves the MAT at the detection layer. For example, a receiver may dedicate more resources, such as correlators, to form a decision variable [95, 104, 105, 111, 149, 150], use passive correlators to increase a decision rate [88], use an appropriate decision rule [18,19], or employ sequential techniques [6, 36, 37, 129, 134]. The second approach improves the MAT at the search layer. For example, a receiver may perform a hybrid search by using multiple correlators [29–32] or use a special search pattern such as an expanding zigzag window [15, 58, 86, 136] or a non-consecutive [59, 66, 67, 111, 131] serial search.

In a few special cases, the MAT of the conventional serial search (CSS)[5] is shown to be longer than that of a non-consecutive serial search (see also [59,66,67,111,131]). To gain some insight into this behavior, let us consider an idealized scenario in the absence of fading and noise. In this hypothetical scenario (see Fig. 2-4a), a receiver that skips some cells after each test will reach and find an in-phase cell faster than does the receiver that uses the CSS. This example indicates that multipath helps the signal acquisition, and indeed can be generalized to the case in the presence of fading and noise (see Fig. 2-4b).

Among different serial search techniques, a promising approach to improve the MAT is to examine signal phases (or cells) according to a specific order, a technique

---

[5]The CSS is a search order that tests consecutive cells serially.

30
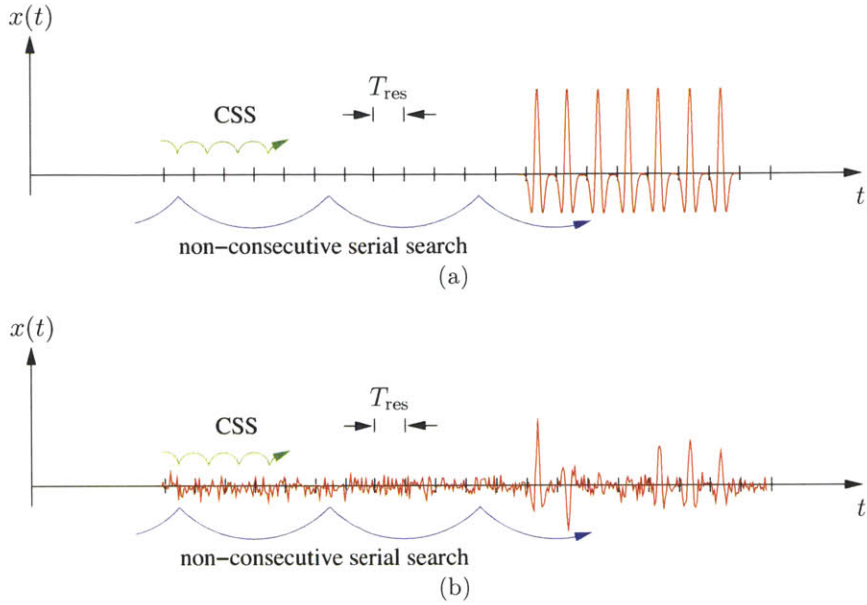
Figure 2-4: A correlator output $x(t)$ contains several resolvable peaks. In an idealized scenario (a), the output is free from fading and noise. In a realistic scenario (b), the output is corrupted by fading and noise.

known as a search strategy [121]. Examples of search strategies include the CSS [59, 124], the fixed-step serial search with a step size N_J (FSS-N_J) [124], the bit-reversal search [59], and the uniform randomized search [92, 123]. The CSS is the most commonly-used search strategy, giving the most natural order $\{1, 2, 3, \dots\}$ of cells to be examined. The FSS-N_J allows a jump size of N_J cells after an examination of each cell. The bit reversal search examines the cells in the order that approximately mimics the binary search in computer science. The uniform randomized search examines a cell randomly so that every cell is equally likely to be examined [92, 123]. A search strategy that yields small MAT is more attractive for the receiver design than a search strategy that yields large MAT. In general, we want to design the acquisition receiver using the search strategy that yields the minimum MAT.

The fixed-step serial search and the uniform randomized search are known to produce the MATs that are close to the optimal MAT, i.e., the minimum MAT among all possible search strategies. Under a wide range of operating environments, the fixed-step serial search with the step size N_{hit} is η-optimal (see [121, 124, 126]

31

for a precise mathematical statement). Similarly, under a wide range of operating environments, the uniform randomized search yields the MAT that is at most twice the MAT of the optimal search strategy [123, 125]. These properties make the fixed-step serial search and the uniform randomized search attractive for the design of acquisition receivers.

2.2   Existing Models for Time Processes of Clocks

In this section, we review existing models of clocks. First, we give a mathematical model for oscillators whose output generates a clock signal. Second, we review a fractional Brownian motion, which has been employed to model noises that exhibit a memory effect commonly found in clocks. Third, we outline a mathematical model based on stochastic differential equations for a clock signal.

2.2.1   Clock Modeling

Timing signal of a clock is obtained from the output, $\mathsf{S}(t)$, of a pseudo-periodic oscillator [70]

$$\mathsf{S}(t) = \Big(A + \epsilon(t)\Big) \sin \Phi(t),$$

where t is the time of a reference clock, A is the nominal amplitude (a constant), $\epsilon(t)$ is the derivation from the nominal amplitude, and $\Phi(t)$ is the phase of the oscillator (a random process). The deviation $\epsilon(t)$ is small relative to A and can be ignored in most timing applications [70] [16, Sec. 5.2]. The phase $\Phi(t)$ can be extracted from $\mathsf{S}(t)$ by using a phase-locked loop [71] or a tracking loop [72, Chap. 11]. The phase of the oscillator is a major source of timing error.

The phase $\Phi(t)$ of a non-ideal oscillator can be written as [46, 70] [16, Sec. 5.2]

$$\Phi(t) = 2\pi v_0 \left(\mathsf{q}_0 + t + \sum_{k=1}^{M} \frac{\mathsf{q}_k}{k!} t^k + \Psi(t) \right), \tag{2.3}$$

32

where v_0 is the nominal frequency (a constant); $\Psi(t)$ is a non-stationary noise with $\Psi(0) = 0$; M is a constant representing the highest order of clock drifts; and q_0, q_1, $\ldots$, q_M are random variables representing the magnitudes of the phase offset and clock drifts. The phase for an ideal oscillator is given by $\Phi_{\mathrm{id}}(t) = 2\pi v_0 t$.

The phase $\Phi(t)$ are related to the time process and the time deviation.[6] The time process and the time deviation are given by

$$\mathsf{T}(t) = q_0 + t + \sum_{k=1}^{M} \frac{q_k}{k!} t^k + \Psi(t) = \frac{1}{2\pi v_0} \Phi(t) \tag{2.4}$$

$$\mathsf{X}(t) = q_0 + \sum_{k=1}^{M} \frac{q_k}{k!} t^k + \Psi(t) = \mathsf{T}(t) - t, \tag{2.5}$$

respectively. The time deviation contains random quantities in $\Phi(t)$ and can be modeled by a stochastic integral [46, 153]. Through their relationships, $\Phi(t)$, $\mathsf{T}(t)$, and $\mathsf{X}(t)$ are equivalent characterizations of the oscillator's phase.

In the expressions for $\Phi(t)$, $\mathsf{T}(t)$, and $\mathsf{X}(t)$, the parameter M is usually taken to be $M = 2$ for simplicity and for practical purposes [16, Sec. 5.2], giving us $\{q_0, q_1, \ldots, q_M\} = \{q_0, q_1, q_2\}$. Random variable q_0 accounts for the phase error that arises from an imperfect calibration of the clock at time $t = 0$. Random variable q_1 accounts for the frequency error of the clock. Random variable q_2 accounts for the aging effect on clocks, the fact that clocks tend to run faster over time. Typical values of q_2 are reported in Table 2.1.

Noise $\Psi(t)$ in the oscillator's phase is usually characterized through a measurement of its derivative, $\Upsilon(t) \triangleq \frac{d\Psi(t)}{dt}$. The derivative $\Upsilon(t)$ can be measured either in the time domain or in the frequency domain. A time-domain measurement provides the variance, Allan variance [3], and modified Allan variance of Υ, among other metrics. A frequency-domain measurement provides the power-spectral density of $\Upsilon(t)$. Here, we focus on a frequency-domain approach, which is more relevant to this thesis.

The power spectral density of $\Upsilon(t)$ is denoted by S_Υ and has been observed to

---

[6]The time process is called "time function" in [16]. The time deviation is called "normalized phase deviation" in [46] and "phase deviation" in [153].

Table 2.1: The coefficient for the quadratic term depends on the type of clocks.

Clock	q_2 (per year)
Quartz oscillator	
Crystal Oscillator (XO)	$> 1 \times 10^{-6}$
Temperature-Compensated Crystal Oscillator (TCXO)	5×10^{-7}
Miniature single oven Oven-Controlled Crystal Oscillator (OCXO)	$2 \times 10^{-8} - 1 \times 10^{-7}$
Double oven OCXO	$1 \times 10^{-8} - 1 \times 10^{-7}$
Double oven Boîtier à Vieillissement Amélioré (BVA)† OCXO	$1 \times 10^{-9} - 4 \times 10^{-9}$
Atomic frequency standard	
Rubidium	$5 \times 10^{-11} - 5 \times 10^{-10}$
Caesium-beam	0
Hydrogen Microwave Amplification by Stimulated Emission of Radiation (MASER)	$< 10^{-13} - 5 \times 10^{-12}$

The table is adapted from [16, Tables. 6.1–6.3].
† The words mean "packaging for improved aging performance" in French [16, p. 285].

follow the power law

$$S_{\Upsilon}(f) = \sum_{k=-2}^{2} h_k |f|^k, \qquad \text{for } -f_{\mathrm{h}} \leq f \leq f_{\mathrm{h}}, \qquad (2.6)$$

and $S_{\Upsilon}(f) = 0$ otherwise. Frequency f_{h} is in the range 10–100 kHz for high-quality clocks (cited from [16, p. 248]). Parameters h_k's are constants representing noise intensities. The powers $k = -2, -1, 0, 1, 2$ are chosen empirically by curve fittings [22, 137] or to agree with a common noise construction, such as a random walk or a central limit theory [101, p. S307]. Not all types of power-law noise appear in every clock.

The power-law noises arise from various physical causes, which are documented in [16, p. 250]:

- f^{-2}-noise (random walk frequency modulation): This noise mainly arises from environmental effects and perturbation to frequency, such as mechanical shocks

34

or temperature variations. This noise could be difficult to measure due to a close proximity to the ideal timing signal.

- f^{-1}-noise (flicker frequency modulation): The origin of this noise in not well understood, but it may arise from the physical resonance mechanism of an active oscillator or from random phenomena that affect the control electronic devices. This noise is common in high-quality clocks, but it may be hidden by the f^0-noise and f-noise.

- f^0-noise (white frequency modulation noise): This noise mainly arises from a slave oscillator that locks into a resonance of another device. This noise is common in passive-resonator frequency standard, such as caesium-beam and rubidium clocks.

- f-noise (flicker phase modulation noise): This noise mainly arises from imperfect electronics, especially in the amplification output and frequency multipliers.

- f^2-noise (white phase modulation noise): This noise mainly arises from imperfect electronics and quantization error in the phase-locked loop. This noise is common in clocks that use digital control electronics and is often negligible in high-quality clocks.

Examples of the sample paths for power-law noise appear in Fig. 2-5 (see [16, p. 249] for the sample path of f^2-noise). The power-law noise accounts for important type of noise in clocks.

In addition to power-law noise, another type of noise, called the periodic noise, may arise in the measurements. The periodic noise is characterized by spikes at discrete frequencies in S_Υ. The periodic noise is caused by phenomena including interference from 50/60 Hz alternate current (AC) power line, seasonable variation of temperature, and sensitivity of clocks to acoustic or mechanical vibrations [16, Sec. 5.9.2]. The

35

(a) f-noise

(b) f^0-noise

(c) f^{-1}-noise

(d) f^{-2}-noise
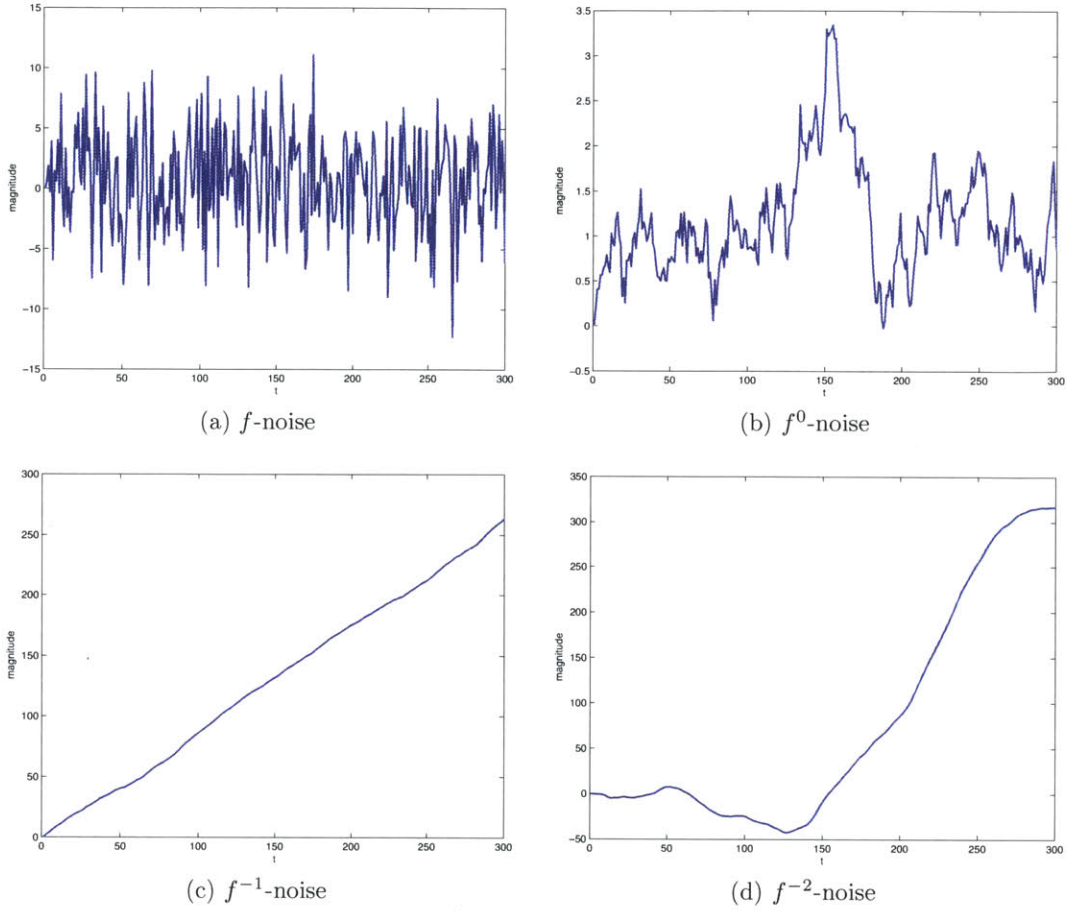
Figure 2-5: Sample paths of power-law noise exhibit memory.

periodic noise can be modeled by adding the term below to (2.6):[7]

$$S_{\Upsilon,\mathrm{pr}}(f) = \sum_{i=1}^{N_{\mathrm{sk}}} \beta_i \cdot \left[\delta_{\mathrm{sk}}(f + f_i) + \delta_{\mathrm{sk}}(f - f_i) \right], \qquad \text{for } -\infty < f < \infty,$$

where $\delta_{\mathrm{sk}}(\cdot)$ is a function representing a spike,[8] N_{sk} denotes the number of spikes, β_i's are intensities of spikes, and $\pm f_i$'s are frequencies at which the spikes occur. Next, we discuss a fractional Brownian motion, whose derivative can be used to model some of the power-law noise.

---

[7]For illustration purposes, [16, eq. 5.134] takes $N_{\mathrm{sk}} = 1$, although the number of spikes is usually larger than 1 in the measurements [16, Figs. 5.32, 5.35] [137, Fig. 3].

[8]Conceptually, δ_{sk} can be taken to equal the Dirac delta function. In the analysis, δ_{sk} can be taken to be a bounded, positive, even function with a narrow support and an area underneath of 1.

2.2.2 Fractional Brownian Motion

Fractional Brownian motion is a stochastic process that exhibits a power-law spectral density. Fractional Brownian motion can be continuous in time [5,45,73] or discrete in time [80,101]. Here, we focus on continuous-time fractional Brownian motion, which is more related to this thesis.

Continuous-time fractional Brownian motion is given by

$$
\mathsf{B}_H(t) = \frac{1}{\Gamma(H+1/2)} \left[\int_{-\infty}^{0} \left(|t-s|^{H-1/2} - |s|^{H-1/2} \right) d\mathsf{B}_s \right.
$$
$$
\left. + \int_{0}^{t} |t-s|^{H-1/2} d\mathsf{B}_s \right],
$$

where $0 < H < 1$, B_s is Brownian motion, and Γ is the gamma function. Fractional Brownian motion is a generalization of Brownian motion, which can be obtained by setting $H = 1/2$. Fractional Brownian motion is a zero-mean Gaussian process, with the covariance function

$$
R_{\mathsf{B}_H}(t,s) = \mathbb{E}\left\{ \mathsf{B}_H(t)\mathsf{B}_H(s) \right\} = \frac{V_H}{2} \left(|t|^{2H} + |s|^{2H} - |t-s|^{2H} \right), \qquad (2.7)
$$

where $V_H = \Gamma(1 - 2H)\frac{\cos \pi H}{\pi H}$. The autocorrelation function depends on both s and t, implying that B_H is not wide-sense stationary.

The derivative of B_H gives rise to the notion of the fractional Gaussian noise, a generalization of the additive white Gaussian noise. The fractional Gaussian noise is defined to be[9] [45, eq. (14)]

$$
\mathsf{B}'_H(t) \triangleq \lim_{\delta \to 0} \frac{\mathsf{B}_H(t+\delta) - \mathsf{B}_H(t)}{\delta}.
$$

Spectra of B_H and B'_H can be obtained through the concept of the Wigner-Ville spectrum.

---

[9]The notion of derivative can be made precise by distribution theory.

The Wigner-Ville spectrum for a process Z is given by

$$W_{\mathsf{Z}}(t, \omega_{\mathrm{a}}) \triangleq \int_{-\infty}^{\infty} R_{\mathsf{Z}}\left(t + \frac{s}{2}, t - \frac{s}{2}\right) e^{-\jmath\omega_{\mathrm{a}}s} ds, \qquad (2.8)$$

where $\omega_{\mathrm{a}} = 2\pi f$ is an angular frequency, $R_{\mathsf{Z}}(\cdot, \cdot)$ is the covariance function of Z, and $\jmath$ is the imaginary unit, i.e., $\jmath = \sqrt{-1}$. If Z is a stationary process, $W_{\mathsf{Z}}(t, \omega_{\mathrm{a}})$ is identical to the power spectral density of Z. The Wigner-Ville spectrum for the derivative Z' can be obtained by the expression [45, eq. (10)]

$$W_{\mathsf{Z}'}(t, \omega_{\mathrm{a}}) = \omega_{\mathrm{a}}^2 W_{\mathsf{Z}}(t, \omega_{\mathrm{a}}) + \frac{1}{4}\frac{\partial^2}{\partial t^2} W_{\mathsf{Z}}(t, \omega_{\mathrm{a}}). \qquad (2.9)$$

The Wigner-Ville spectra of fractional Brownian motion and fraction Gaussian noise are given by

$$W_{\mathsf{B}_H}(t, \omega_{\mathrm{a}}) = \left(1 - 2^{1-2H}\cos 2\omega_{\mathrm{a}}t\right)\frac{1}{|\omega_{\mathrm{a}}|^{2H+1}} \qquad (2.10)$$

$$W_{\mathsf{B}'_H}(t, \omega_{\mathrm{a}}) = \frac{1}{|\omega_{\mathrm{a}}|^{2H-1}}. \qquad (2.11)$$

Notice that the second equality does not depend on t.

The Wigner-Ville spectrum is related to measurement outputs from spectral analyzers. The measurement outputs can be viewed as the average Wigner-Ville spectrum over a measurement duration T [45, p. 198]:

$$S_{\mathsf{X}}(\omega_{\mathrm{a}}, T) = \frac{1}{T}\int_0^T W_{\mathsf{X}}(t, \omega_{\mathrm{a}}) dt.$$

The average spectrum for fractional Brownian motion is given by

$$S_{\mathsf{B}_H}(\omega_{\mathrm{a}}, T) = \left(1 - 2^{1-2H}\frac{\sin 2\omega_{\mathrm{a}}T}{2\omega_{\mathrm{a}}T}\right)\frac{1}{|\omega_{\mathrm{a}}|^{2H+1}},$$

which has the limit of

$$\lim_{T\to\infty} S_{\mathsf{B}_H}(\omega_{\mathrm{a}}, T) = \frac{1}{|\omega_{\mathrm{a}}|^{2H+1}}.$$

38

The average spectrum for the fractional Gaussian noise is given by

$$S_{\mathsf{B}'_H}(\omega_{\mathrm{a}}, T) = \frac{1}{|\omega_{\mathrm{a}}|^{2H-1}}.$$

Fractional Brownian motion and fraction Gaussian noise exhibit power-law spectrum, as obtained from the spectral analyzers' outputs. Recall that $0 < H < 1$, and hence $\mathsf{B}'_H(t)$ can be used to model the f^α power-law noise for $-1 < \alpha < 1$ by setting $H = (1 - \alpha)/2$.

2.2.3   Stochastic Model for Time Deviation

The time deviation X (c.f.(2.5)) can be modeled as a solution to a stochastic differential equation [46, 153]. As it will become apparent shortly, the stochastic differential equation can account for the maximum drift order of $M = 3$, two types of power-law noise (f^0 and f^{-2}), and a type of noise called random walk on frequency drift.

The stochastic differential equations are given by [153, eq. (1)]

$$d\mathsf{X}_t^{(1)} = \left(\mathsf{X}_t^{(2)} + \mu_1\right) dt + \sigma_1 d\mathsf{B}_t^{(1)}$$
$$d\mathsf{X}_t^{(2)} = \left(\mathsf{X}_t^{(3)} + \mu_2\right) dt + \sigma_2 d\mathsf{B}_t^{(2)}$$
$$d\mathsf{X}_t^{(3)} = \mu_3 dt + \sigma_3 d\mathsf{B}_t^{(3)},$$

with the initial condition $\mathsf{B}_0^{(i)} = c_i$; and $\mathsf{X}^{(1)} = \mathsf{X}$, the time deviation. Here, $\mathsf{B}^{(i)}$'s are independent Brownian motions, σ_i's are noise intensities, and μ_i's are drift terms.

Random processes $\mathsf{B}^{(i)}$'s produce three types of clock noise for time deviation $\mathsf{X}^{(1)}$. The process $\mathsf{B}_t^{(1)}$ produces noise on the phase and yields the f^0 power-law noise (white frequency modulation noise). Process $\mathsf{B}_t^{(2)}$ produces noise on the frequency and yields the f^{-2} power-law noise (the random walk on a frequency modulation noise). Process $\mathsf{B}_t^{(3)}$ produces a type of noise known as a random walk on a frequency drift. The stochastic equations satisfy the Lipschitz and linear-growth conditions [74, Thm. 3.1] and hence have a unique solution.

39

The solution for $\mathsf{X}(t) = \mathsf{X}_1(t)$ is given by [153, eq. 13]:

$$\mathsf{X}(t) = x(0) + y(0)t + \frac{\tilde{\mu}}{2}t^2 + \frac{\mu_3}{6}t^3$$
$$+ \sigma_1 \mathsf{B}_t^{(1)} + \sigma_2 \int_0^t (t-s)d\mathsf{B}_s^{(2)} + \sigma_3 \int_0^t \frac{1}{2}(t-s)^2 d\mathsf{B}_s^{(3)}, \quad (2.12)$$

where $x(0) = c_1$ is the initial phase, $y(0) = \mu_1 + c_2$ is the initial frequency, and $\tilde{\mu} = \mu_2 + c_3$ is the frequency drift. The random processes $\mathsf{B}_t^{(1)}$, $\int_0^t (t-s)d\mathsf{B}_s^{(2)}$, and $\int_0^t \frac{1}{2}(t-s)^2 d\mathsf{B}_s^{(3)}$ represent f^0-noise, f^{-2}-noise, and noise on the frequency drift, respectively. The model can be extended to incorporate the power-law noise, for example by adding the f-noise and f^{-1}-noise, which are modeled by fractional Brownian motion, to the right side of (2.12).

2.3   First-Passage-Time Problems

A first passage time, or the first time that a random process crosses a boundary, is of importance in many fields. First passage times are random variables that appear in biology [17, 41] statistics [39, 151] physics [21, 112], finance [11, 40], engineering [12, 89], and other fields. We consider two examples to illustrate the diversity and the applications of the first passage time problems.

Imagine that an investor buys a stock for \$1 and plan to sell it for profit as soon as the stock's price reaches \$2. The amount of time until the stock reaches the desired price is a random variable, depending on the trajectory of the stock's price (see Fig. 2-6). This amount of time affects the wealth and constitutes a quantity that the investor wants to understand.

Consider another example, which involves an oscillator and a digital clock. The oscillator generates a sinusoidal waveform that serves to drive a digital clock: when the waveform reaches +1 or −1, the digital clock advances a tick. The non-ideal oscillator generates a noisy, pseudo-sinusoidal waveform, reaching +1 or −1 at random times (see Fig. 2-7). The amount of time until the waveform reaches +1 or −1 affects the accuracy of the digital clock and constitutes a quantity that engineers want to
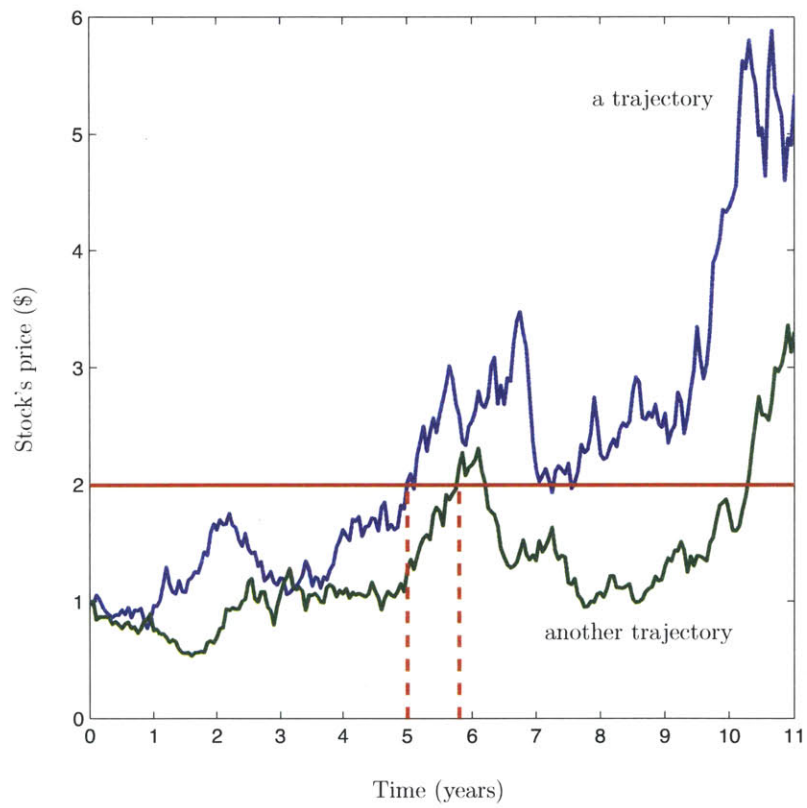
Figure 2-6: The first time that a stock's price doubles is a random variable.
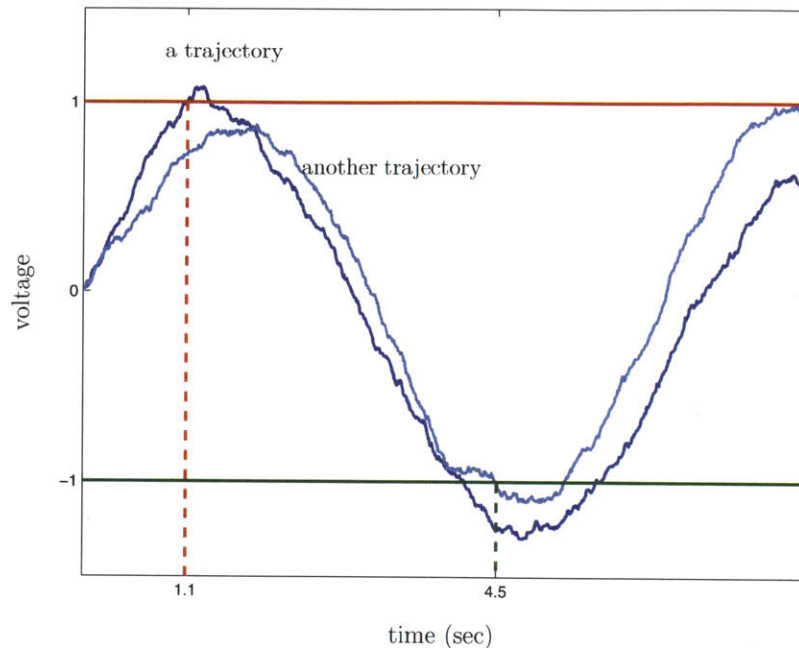
Figure 2-7: Noise corrupts an output of an oscillator, making the output reach a boundary at random time.

understand.

The above two examples are applications of first-passage-time problems to finance and engineering. A first-passage-time problem refers to a problem of obtaining a probabilistic characterization of a random variable called the first passage time. The probabilistic characterization includes the PDF, the CDF, the moment generating function (MGF), and the characteristic function. The first passage time is the time at which a random process first crosses a boundary for the first time. In the stock example, the first passage time is the time at which the stock's price first reaches $2. In the oscillator example, the first passage time is the time at which a noisy waveform first reaches $+1$ or -1. First passage time problems appear in other disciplines besides finance and engineering, making them important in application.

First passage time problems occur in many forms depending on the choice of random processes and boundaries. While we do not attempt to survey the literature, we give examples of random processes and boundaries that appear in first passage time problems. The random process might be discrete in time (e.g., [120, p. 3]),

42

continuous in time (e.g., [130, p. 60]), one-dimensional (e.g., [96]), multi-dimensional (e.g., [119, p. 516]), a Brownian motion (e.g., [63, p. 79]), a Brownian motion with linear drift (e.g., [63, p. 196]), a Brownian motion with quadratic drift (e.g., [55]), or a general process (e.g., [115]). For a one-dimensional process, the boundary might consist of one constant barrier (e.g., [38, p. 459]), two constant barriers (e.g., [33]), one moving barrier (e.g., [77]), or two moving barriers (e.g., [109]). For a multi-dimensional process, the boundary might be a set in the Euclidean space (e.g., [74, p. 11]). In the stock example, the random process takes non-negative values; the boundary is a constant barrier at \$2. In the oscillator example, the random process takes any real value; the boundary consists of two constant barriers at $+1$ and -1. The choice of a random process and a boundary is usually motivated by applications and tractability.

Most first-passage-time problems are difficult to solve. The main difficulty originates from the dependency across times of random processes. View a random process as an uncountably infinite set of random variables indexed by time. These random variables are dependent, often because of the physical constraints on the random process. In the stock example, the stock's price is influenced by economic outlook, interest rates, or other factors that linger, making the stock's prices at different times dependent. In the oscillator example, the waveform rises and falls at certain rates, making values of the waveform at different times dependent. To solve the first-passage-time problem, we need to know the trajectory of the random process, a requirement for the joint probability of values of the random process at all times. Every unsolved first passage problem involves an infinite set of dependent random variables, a source of difficulty. With the difficulty, few first-passage-time problems are solved for explicit solutions.

We survey the problems that have been solved and are similar to the problems in this thesis. The solutions exist for a Brownian motion and one constant barrier [12, eqs. (3.2)–(3.3)], [63, p. 88, Thm. 6.19; p. 96, Sec. 8.4], [38, Thm. 12.3.1], [33], [93, eqs. (7.7)–(7.10)]; a Brownian motion and two constant barriers [33]; a Brownian motion with linear drift and one constant barrier [63, p. 196, Sec. C], [33], [93, eqs. (7.16)–

43

(7.22)], [110]; a Brownian motion with linear drift and two constant barriers [33, 84]; and a Brownian motion with quadratic drift and one constant barrier [55, 100]. In the remaining part of this section, we summarize the solutions to these problems and the approaches to solve them.

2.3.1   Brownian motion and one-sided boundary

Let $\tau = \inf \{t \geq 0 : \mathsf{B}_t + x = \eta\}$, where x and η are constants. The probability distributions of τ are given by

$$\text{PDF}: \qquad f(t) = \frac{|\eta - x|}{\sqrt{2\pi t^3}} e^{-\frac{1}{2t}(\eta - x)^2}$$

$$\text{CDF}: \qquad F(t) = 2Q\left(\frac{|\eta - x|}{\sqrt{t}}\right)$$

$$\text{MGF}: \quad \mathbb{E}\left\{e^{-s\tau}\right\} = e^{-|\eta - x|\sqrt{2s}},$$

where $t > 0$ and $s > 0$. Approaches to obtain the above probability distributions include the reflection principle [38, Thm. 12.3.1] [63, p. 88, Thm. 6.19], a combination of Laplace transform and differential equation [33], the integral equation [12, eqs. (3.2)–(3.3)] [93, eqs. (7.7)–(7.10)], random walk [71, Sec. 7-4], and the exponential martingale [63, p. 96, Sec. 8.4].

2.3.2   Brownian motion with linear drift and one-sided boundary

Let $\tau = \inf \{t \geq 0 : \mathsf{B}_t + x + qt = \eta\}$, where x, q, and η are constants. The probability distributions of τ are given by

$$\text{PDF}: \qquad f(t) = \frac{|\eta - x|}{\sqrt{2\pi t^3}} e^{-\frac{1}{2t}(\eta - x - qt)^2}$$

$$\text{MGF}: \quad \mathbb{E}\left\{e^{-s\tau}\right\} = e^{q(\eta - x) - |\eta - x|\sqrt{q^2 + 2s}},$$

where $t > 0$ and $s > 0$. Approaches to obtain the above probability distributions include the method of image [93, eqs. (7.16)–(7.22)], a combination of Laplace transform and differential equation [33], the Cameron-Martin-Girsanov theorem [63, p. 196, Sec. C], and the Radon-Nikodym derivative [108, (17.1)] [110].

2.3.3 Brownian motion with quadratic drift and one-sided boundary

Let $\tau = \inf \left\{ t \geq 0 : \mathsf{B}_t + x + qt + \mu t^2 = \eta \right\}$ where x, q, μ and η are constants. Without loss of generality, we will consider $\mu > 0$.[10] If $x - \eta > 0$ and $q = 0$, the probability distribution of τ is given by

$$\text{PDF}: \quad f(t) = 2^{1/3} \mu^{2/3} \sum_{k=0}^{\infty} \frac{\mathrm{Ai}\left(\lambda_k + (2\mu)^{2/3}(x - \eta)\right)}{\mathrm{Ai}'(\lambda_k)} \exp\left(\lambda_k 2^{1/3} \mu^{2/3} t - \frac{2}{3} \mu^2 t^3\right),$$

for $t > 0$, where Ai is the Airy function and λ_k's are zeros of Ai on the negative real-line: $0 > \lambda_0 > \lambda_1 > \lambda_2 > \dots$. If $x - \eta < 0$, the probability distribution of τ is given by

$$\text{PDF}: \quad f(t) = \exp\left\{ -\frac{(t + 2q\mu)^3 - 8q^3\mu^3}{24\mu^2} - q\mu(\eta - x) \right\}$$
$$\int_{-\infty}^{\infty} e^{tu} \frac{B(u)A(u - x) - A(u)B(u - x)}{\pi[A^2(u) + B^2(u)]} du,$$

where $A(u) = \mathrm{Ai}\left(2\mu^{2/3}u\right)$ and $B(u) = \mathrm{Bi}\left(2\mu^{2/3}u\right)$. Approaches to obtain the above probability distributions include the Cameron-Martin-Girsanov theorem and a connection to a Bessel process (among other key steps) [55, Sec. 2]; a combination of Radon-Nikodym derivative and Feynman-Kac formula (among other key steps) [100, Sec. 3.2]; and the Cameron-Martin-Girsanov theorem and differential equations [75, p. 682].

---

[10]The case of $\mu < 0$ can be obtained as an immediate consequence, using the fact that Brownian motion is symmetric (see Section 2.4.1 for an example). The case of $\mu = 0$ appears in Section 2.3.2.

2.3.4 Brownian motion and two-sided boundary

Let $\tau = \inf \{t \geq 0 : \mathsf{B}_t + x \notin (a,b)\}$, where x, a, and b are constants such that $a < x < b$. The probability distributions of τ are given by

PDF :
$$f(t) = \frac{4\pi}{(b-a)^2} \sum_{k=0}^{\infty} \left\{ (-1)^k \left(k + \frac{1}{2}\right) \cos \left[\left(k + \frac{1}{2}\right) \frac{\pi(2x - b - a)}{b - a}\right] \right.$$
$$\left. \exp \left[-\frac{2\left(k + \frac{1}{2}\right)^2 \pi^2 t}{(b-a)^2}\right] \right\}$$

CDF :
$$F(t) = 1 - \frac{2}{\pi} \sum_{k=0}^{\infty} \left\{ \frac{(-1)^k}{k + \frac{1}{2}} \cos \left[\left(k + \frac{1}{2}\right) \frac{\pi(2x - b - a)}{b - a}\right] \right.$$
$$\left. \exp \left[-\frac{2\left(k + \frac{1}{2}\right)^2 \pi^2 t}{(b-a)^2}\right] \right\}$$

MGF :
$$\mathbb{E} \left\{e^{-s\tau}\right\} = \frac{\cosh[(b + a - 2x)\sqrt{s/2}]}{\cosh[(b-a)\sqrt{s/2}]},$$

where $t > 0$ and $s > 0$. Approaches to obtain the above probability distributions include a combination of Laplace transform and differential equation [33].

2.3.5 Brownian motion with linear drift and two-sided boundary

Let $\tau = \inf \{t \geq 0 : \mathsf{B}_t + x + qt \notin (a,b)\}$, where x, q, a, and b are constants such that $a < x < b$. The probability distribution of τ is given by

PDF :
$$f(t) = e^{-q^2 t/2} \left[e^{q(a-x)} ss_{b-x,b-a}(t) + e^{q(b-x)} ss_{x-a,b-a}(t)\right]$$

MGF :
$$\mathbb{E} \left\{e^{-s\tau}\right\} = \frac{e^{q(a-x)} \sinh \left[(b - x)\sqrt{2s + q^2}\right] + e^{q(b-x)} \sinh \left[(x - a)\sqrt{2s + q^2}\right]}{\sinh \left[(b - a)\sqrt{2s + q^2}\right]},$$

for $t > 0$ and $s > 0$, where

$$ss_{u,v}(t) = \sum_{k=-\infty}^{\infty} \frac{v - u + 2kv}{\sqrt{2\pi t^3}} e^{-\frac{1}{2t}(v-u+2kv)^2}.$$

Approaches to obtain the above probability distributions include random walk [84], a combination of Laplace transform and differential equation [33], and the Cameron-Martin-Girsanov theorem [13, p. 233].

2.4 Known Methods for Solving First-Passage-Time Problems

In this section, we survey known methods for solving first-passage-time problems and provide elementary examples, illustrating applications of these methods. The methods that we describe here are for continuous-time processes, Markov processes, and Brownian motion, which are the main random processes in this thesis. We do not attempt to survey the literature and the list of methods is not exhaustive.

In this section, B_t denotes a standard Brownian motion with respect to a probability space $(\Omega, \mathcal{F}, \mathbb{P})$ and $\mathcal{F}_t$ denotes the σ-algebra generated by $\{\mathsf{B}_s : 0 \leq s \leq t\}$.

2.4.1 Reflection Principle

Let $\mathbb{P}_x$ denote a probability measure of Brownian motion with the initial position at $x \in \mathbb{R}$. Brownian motion is a time-homogenous strong Markov process [74, Thm. 9.5, p. 90]. Hence, for any Borel set $\mathcal{A} \in \mathbb{R}$, we have

$$\mathbb{P}\left\{\mathsf{B}_{\tau+s} \in \mathcal{A} \mid \mathcal{F}_\tau\right\} = \mathbb{P}_{\mathsf{B}_\tau}\left\{\mathsf{B}_s \in \mathcal{A}\right\}, \qquad s > 0. \qquad (2.13)$$

Equation (2.13) can be used to derive the PDF of the first passage time for Brownian motion and one-sided, constant boundary.

For illustration, we will use the reflection principle to show that the PDF of

$$\mathsf{T}_\eta = \inf\left\{t \geq 0 : \mathsf{B}(t) = \eta\right\}$$

47

for $\eta \neq 0$ is given by

$$f_{T_\eta}(t) = \frac{|\eta|}{\sqrt{2\pi t^3}} e^{-\frac{1}{2t}\eta^2}, \qquad\qquad t > 0. \qquad (2.14)$$

The proof of the PDF is an adaptation of [38, Thm. 12.3.1] [63, Sec. 2.6.A, Thm. 6.19] and proceeds as follows.

By symmetry of Brownian motion (i.e., $-B_t$ is Brownian motion with respect to the probability space $(\Omega, \mathcal{F}, \mathbb{P})$), random variable T_η has the same distribution as random variable $T_{-\eta}$. Hence, we have for any $t > 0$,

$$\mathbb{P}\left\{T_\eta \leq t\right\} = \mathbb{P}\left\{T_{|\eta|} \leq t\right\}.$$

We write

$$\begin{aligned}
\mathbb{P}\left\{T_\eta \leq t\right\} &= \mathbb{P}\left\{T_{|\eta|} \leq t \text{ and } B_t > |\eta|\right\} + \mathbb{P}\left\{T_{|\eta|} \leq t \text{ and } B_t \leq |\eta|\right\} \\
&= \mathbb{P}\left\{B_t > |\eta|\right\} + \mathbb{P}\left\{B_t - |\eta| \leq 0 \,\middle|\, T_{|\eta|} \leq t\right\} \mathbb{P}\left\{T_{|\eta|} \leq t\right\} \\
&= \mathbb{P}\left\{B_t > |\eta|\right\} + \mathbb{P}\left\{B_t - B_{T_{|\eta|}} \leq 0 \,\middle|\, T_{|\eta|} \leq t\right\} \mathbb{P}\left\{T_{|\eta|} \leq t\right\} \\
&= \mathbb{P}\left\{B_t > |\eta|\right\} + \mathbb{P}\left\{B_t - B_{T_{|\eta|}} > 0 \,\middle|\, T_{|\eta|} \leq t\right\} \mathbb{P}\left\{T_{|\eta|} \leq t\right\} \\
&\qquad \text{(Reflection principle and symmetry of Brownian motion)} \\
&= \mathbb{P}\left\{B_t > |\eta|\right\} + \mathbb{P}\left\{T_{|\eta|} \leq t \text{ and } B_t > |\eta|\right\} \\
&= 2\mathbb{P}\left\{B_t > |\eta|\right\}.
\end{aligned}$$

For a fixed $t > 0$, random variable B_t has a normal $\mathcal{N}(0, t)$ distribution, giving us the CDF

$$\mathbb{P}\left\{T_\eta \leq t\right\} = 2\left[1 - \Phi\left(\frac{|\eta|}{\sqrt{t}}\right)\right],$$

where Φ is the CDF of normal $\mathcal{N}(0,1)$ random variable. Differentiation of the CDF

yields the PDF

$$f_{\mathsf{T}_\eta}(t) = \frac{|\eta|}{t^{3/2}} \cdot \varphi\left(\frac{\eta}{\sqrt{t}}\right),$$

where φ is the PDF of normal $\mathcal{N}(0,1)$ random variable. Substituting the expression for φ, we have (2.14).

2.4.2 Exponential Martingale

This method relies on the fact that random process

$$\mathsf{Z}(t) = \exp\left(\alpha\mathsf{B}_t - \frac{\alpha^2}{2}t\right),$$

is a martingale with respect to $\{\mathcal{F}_t\}$, for a fixed and given constant $\alpha \in \mathbb{R}$.[11] An application of the martingale stopping theory [74, Thm. 3.3, p. 11] can provide the MGF of the first passage time of Brownian motion and one-sided, constant boundary.

To demonstrate an application of the exponential martingale, we will show that

$$\mathbb{E}\left\{e^{-s\mathsf{T}_\eta}\right\} = e^{-|\eta|\sqrt{2s}}, \tag{2.15}$$

for $s \geq 0$ and $\eta \in \mathbb{R}$. The proof proceeds as follows.

Fix $\alpha \geq 0$ in the expression of Z_t, and suppose that $\eta \geq 0$. The case that $\eta < 0$ will be discussed separately. The random variable T_η is an $\{\mathcal{F}_t\}$-stopping time [74, Thm. 3.2, p. 11], and hence the martingale stopping theory [74, Thm. 3.3, p. 11] gives us

$$\mathbb{E}\left\{\mathsf{Z}(\mathsf{T}_\eta \wedge t) \mid \mathcal{F}_u\right\} = \mathsf{Z}(\mathsf{T}_\eta \wedge u),$$

for any $0 \leq u < t < \infty$, where $x \wedge y$ denotes the minimum between x and y. Setting $u = 0$, taking the expectation on both sides of the above equality, and evaluating

---

[11]The proof is simple, by verifying the definition of martingale: $\mathbb{E}\left\{\mathsf{Z}_t \mid \mathcal{F}_u\right\} = \mathsf{Z}_u$, for any $0 \leq u \leq t$.

$Z(T_\eta \wedge u) = Z_0 = 1$, we have

$$\mathbb{E}\left\{Z(T_\eta \wedge t)\right\} = 1.$$

Taking the limit as $t \to \infty$ gives us

$$\mathbb{E}\left\{\lim_{t\to\infty} \exp\left(\alpha B_{(T_\eta \wedge t)} - \frac{\alpha^2}{2}(T_\eta \wedge t)\right)\right\} = 1. \tag{2.16}$$

On the left side, we have interchanged the expectation and the limit. The interchange is justified by the dominated convergence theorem, where the dominating term is[12]

$$Z(T_\eta \wedge t) \le e^{\alpha B_{(T_\eta \wedge t)}} \le e^{\alpha \eta}.$$

Now, we evaluate the limit on the left side of (2.16) and have

$$\mathbb{E}\left\{\exp\left(\alpha\eta - \frac{\alpha^2}{2}T_\eta\right)\right\} = 1,$$

where we have utilized continuity of the exponential function, continuity of the sample paths of Brownian motion, and the fact that $B_{T_\eta} = \eta$. Setting $\alpha = \sqrt{2s}$ and arranging the term give us the expression

$$\mathbb{E}\left\{e^{-sT_\eta}\right\} = e^{-\eta\sqrt{2s}}, \qquad \text{for } \eta \ge 0 \text{ and } s \ge 0. \tag{2.17}$$

Now consider the case that $\eta < 0$. For any constant r, the probability distribution of T_r equals the probability distribution of T_{-r} because Brownian motion is symmetric at 0, i.e., $-B_t$ is Brownian motion with respect to the probability space $(\Omega, \mathcal{F}, \mathbb{P})$. Hence, for $\eta < 0$ and $s \ge 0$, we have

$$\mathbb{E}\left\{e^{-sT_\eta}\right\} = \mathbb{E}\left\{e^{-sT_{-\eta}}\right\}.$$

---

[12]Here, we use the fact that $\alpha \ge 0$ and $\eta \ge 0$ to bound $\alpha B_{(T_\eta \wedge t)} \le \alpha\eta$.

The right side is given by an application of (2.17), yielding the expression

$$\mathbb{E}\left\{e^{-sT_\eta}\right\} = e^{\eta\sqrt{2s}}, \qquad\qquad \text{for } \eta < 0 \text{ and } s \geq 0. \qquad (2.18)$$

Equations (2.17) and (2.18) imply the expression for the MGF in (2.15).

2.4.3   Integral Equation

An integral equation is based on the following theorem [81, Thm. 14.3, Thm. 14.4]. Let $g\colon (0,\infty) \to \mathbb{R}$ be a continuous function such that $\lim_{t\searrow 0} g(t) \geq 0$, and let

$$\tau = \inf\left\{t \geq 0 : \mathsf{B}_t \geq g(t)\right\}$$

be the first passage time of Brownian motion over g. Let F denote the CDF of τ, i.e., $F(t) = \mathbb{P}\left\{\tau \leq t\right\}$. Then, the following integral equation (called the Master Equation) holds:

$$Q\left(\frac{z}{\sqrt{t}}\right) = \int_0^t Q\left(\frac{z - g(s)}{t - s}\right) F(ds), \qquad (2.19)$$

for all $z \geq g(t)$ where $t > 0$. Here, $Q\left(\cdot\right)$ is the Gaussian Q-function: $Q\left(x\right) = 1 - \Phi(x)$. Furthermore, if g is continuously differentiable on $(0,\infty)$, then τ has a continuous PDF f, which satisfies

$$\frac{\partial}{\partial t}Q\left(\frac{g(t)}{\sqrt{t}}\right) = \frac{1}{2}f(t) + \int_0^t \frac{\partial}{\partial t}Q\left(\frac{g(t) - g(s)}{\sqrt{t - s}}\right) f(s)ds, \qquad (2.20)$$

for all $t > 0$. The proofs of (2.19) and (2.20) appear in [81, pp. 228–229, pp. 231–233]. See [81, Thm. 14.2] for a more general theorem for a strong Markov process.

We illustrate an application of the approach based on the integral equation. In particular, we will show that the CDF of T_η is given by

$$\mathbb{P}\left\{T_\eta \leq t\right\} = 2Q\left(\frac{|\eta|}{\sqrt{t}}\right), \qquad (2.21)$$

for $t > 0$ and $\eta \in \mathbb{R}$.

To obtain the distribution of T_η, we set $g(t) = |\eta|$. Note that $\lim_{t \searrow 0} g(t) = |\eta| \geq 0$ as required. For $z = g(t) = |\eta|$, equation (2.19) reads

$$Q\left(\frac{|\eta|}{\sqrt{t}}\right) = \int_0^t Q(0) \, f_{\mathsf{T}_{|\eta|}}(s) ds$$

for $t > 0$. Note that $Q(0) = \frac{1}{2}$, giving us an identity

$$Q\left(\frac{|\eta|}{\sqrt{t}}\right) = \frac{1}{2} \mathbb{P}\left\{\mathsf{T}_{|\eta|} \leq t\right\}.$$

Brownian motion is symmetric (i.e., $-\mathsf{B}_s$ is a Brownian motion with respect to $(\Omega, \mathcal{F}, \mathbb{P})$), implying that $\mathbb{P}\left\{\mathsf{T}_{|\eta|} \leq t\right\} = \mathbb{P}\left\{\mathsf{T}_\eta \leq t\right\}$. Hence, we have

$$Q\left(\frac{|\eta|}{\sqrt{t}}\right) = \frac{1}{2} \mathbb{P}\left\{\mathsf{T}_\eta \leq t\right\},$$

which simplifies to (2.21).

2.4.4   Method of Darling and Siegert

Method of Darling and Siegert [33] provides the first-passage-time distributions for time-homogenous Markov processes, such as Brownian motion and Brownian motion with linear drift. Here, we summarize a result that appears in [33].

Let X_t be a time-homogenous Markov process with continuous sample paths, for $t \geq 0$. Let $P(y|z,t)$ denote the transition probability, i.e.,[13]

$$P(y|z,t) = \mathbb{P}\left\{\mathsf{X}_{r+t} < z \mid \mathsf{X}_r = y\right\}, \qquad r > 0.$$

Suppose that P has a derivative,

$$p(y|z,t) = \frac{\partial}{\partial z} P(y|z,t),$$

---

[13]The right side does not depend on $r > 0$ because the process is time-homogenous.

that satisfies the diffusion equation:

$$\frac{\partial p}{\partial t} = A(y)\frac{\partial p}{\partial y} + \frac{1}{2}B^2(y)\frac{\partial^2 p}{\partial y^2},$$

with initial and boundary conditions $p(\infty|z,t) = p(-\infty|z,t) = 0$ and $p(y|z,0) = \delta(y - z)$ (the Dirac function). Note that $A(y)$ and $B(y)$ can be obtained from the stochastic differential equation for X_t [78, Thm. 7.3.3]. Let

$$\tau_{a,b} = \inf\{t \geq 0 : \mathsf{X}_t \notin (a,b)\}$$

for fixed constants a and b such that $a < \mathsf{X}_0 = x < b$. Then, the MGF of $\tau_{a,b}$ equals [33, Thm. 3.2 and Thm. 4.1]

$$\mathbb{E}\left\{e^{-s\tau_{a,b}}\right\} = \frac{v(x)[u(a) - u(b)] - u(x)[v(a) - v(b)]}{u(a)v(b) - u(b)v(a)}, \qquad (2.22)$$

where u and v are any two linearly independent solutions of the differential equation

$$\frac{1}{2}B^2(y)\frac{d^2w}{dy^2} + A(y)\frac{dw}{dy} - sw = 0.$$

We now illustrate an application of the method of Darling and Siegert to Brownian motion with two-sided constant boundary.

Consider $\mathsf{X}_t = x + \mathsf{B}_t$, Brownian motion starting from x. Let

$$\tau_{a,b} = \inf\{t \geq 0 : x + \mathsf{B}_t \notin (a,b)\},$$

where $a < x < b$. We will show that the MGF of $\tau_{a,b}$ is given by

$$\mathbb{E}\left\{e^{-s\tau_{a,b}}\right\} = \frac{\cosh[(b + a - 2x)\sqrt{s/2}]}{\cosh[(b - a)\sqrt{s/2}]}, \qquad s > 0. \qquad (2.23)$$

The solution proceeds as follows. For the process $\mathsf{X}_t = x + \mathsf{B}_t$, we have $A(y) = 0$ and $B(y) = 1$ [33, Sec. 5a] [93, (5.1)] [78, Ex. 7.3.4]. Hence, the corresponding

53

differential equation is

$$\frac{1}{2}w'' - sw = 0.$$

The differential equation has linearly independent solutions $u(y) = e^{-\sqrt{2s}y}$ and $v(y) = e^{\sqrt{2\lambda}y}$ for $s > 0$. Hence, (2.22) gives us the MGF in (2.23) after some algebra.

2.4.5   Change of Probability Measure

Let X_t denote a random process with respect to a probability space $(\Omega, \mathcal{F}, \mathbb{P})$. In the change of probability measure, the initial probability measure $\mathbb{P}$ is transformed into another probability measure $\tilde{\mathbb{P}}$ such that the probability distribution of X_t under a new measure $\tilde{\mathbb{P}}$ equals the probability distribution of $\tilde{X}_t$ under the initial measure $\mathbb{P}$. Here, $\tilde{X}_t$ is a random process that is simple to analyze under the measure $\mathbb{P}$. A change in probability measure is often achieved by the Radon-Nikodym derivative [108] or Cameron-Martin-Girsanov theorem [63, Sec. 3.5].

Here we describe the method based on the Cameron-Martin-Girsanov theorem [63, Thm 5.1]. Let $\mathbf{B}_t = \left(B_t^{(1)}, B_t^{(2)}, \ldots, B_t^{(n)}\right)$ denote an n-dimensional Brownian motion defined on a probability space $(\boldsymbol{\Omega}, \boldsymbol{\mathcal{F}}, \boldsymbol{P})$, with an initial position at the origin, i.e., $\boldsymbol{P}\{\mathbf{B}_0 = \mathbf{0}\} = 1$ where $\mathbf{0}$ is an n-dimensional vector of all components equal to zero. Let $\mathsf{H}_t = \left(H_t^{(1)}, H_t^{(2)}, \ldots, H_t^{(n)}\right)$ be a vector of measurable, adaptive process where each component satisfies

$$\mathbb{P}\left\{\int_0^T \left(H_t^{(i)}\right)^2 dt < \infty\right\} = 1,$$

for every $0 \leq T < \infty$ and $i = 1, 2, \ldots, n$. Let

$$Z_t = \exp\left(\sum_{i=1}^n \int_0^t H_s^{(i)} \, dB_s^{(i)} - \frac{1}{2}\sum_{i=1}^n \int_0^t \left(H_s^{(i)}\right)^2 ds\right),$$

and let $\tilde{\mathbf{B}}_t = (\tilde{\mathsf{B}}_1, \tilde{\mathsf{B}}_2, \ldots, \tilde{\mathsf{B}}_n)$ denote a random process defined by

$$\tilde{\mathsf{B}}_i = \mathsf{B}_i^{(i)} - \int_0^t \mathsf{H}_t^{(i)} ds,$$

for $0 \leq t < \infty$. If Z_t is a martingale, then for each fixed $T \in [0, \infty)$, the process $\tilde{\mathbf{B}}_t$ is an n-dimensional Brownian motion on $(\Omega, \mathcal{F}_T, \tilde{\boldsymbol{P}}_T)$, where $\mathcal{F}_T$ is the σ-algebra generated by $\{0 \leq t \leq T : \mathbf{B}_t\}$ and $\tilde{\boldsymbol{P}}_T$ is a probability measure defined on $\mathcal{F}_T$:

$$\tilde{\boldsymbol{P}}_T(\mathcal{A}) = \boldsymbol{E}\left\{1_\mathcal{A} \mathsf{Z}_T\right\}, \qquad\qquad \mathcal{A} \in \mathcal{F}_T.$$

From intuition, the Cameron-Martin-Girsanov theorem serves to remove the drift from the random process. For illustration, we will consider the first-passage-time problem that involves Brownian motion with linear drift.

Let $\mathsf{X}_t = qt + \mathsf{B}_t$ denote Brownian motion with linear drift, where $q \neq 0$ is a constant. Let

$$\tau_\eta = \inf\left\{t \geq 0 : \mathsf{X}_t = \eta\right\}$$

for $\eta \neq 0$. We want to show that the PDF of τ_η is

$$f_{\tau_\eta}(t) = \frac{|\eta|}{\sqrt{2\pi t^3}} \exp\left(-\frac{(\eta - qt)^2}{2t}\right), \qquad (2.24)$$

for $t > 0$.

The solution based on the Cameron-Martin-Girsanov theorem proceeds as follows. The random process $\tilde{\mathsf{B}}_t = \mathsf{B}_t - qt$ is a Brownian motion under the probability measure $\tilde{\mathbb{P}}$, which satisfies

$$\tilde{\mathbb{P}}(\mathcal{A}) = \mathbb{E}\left\{1_\mathcal{A} \mathsf{Z}_t\right\}, \qquad\qquad \mathcal{A} \in \mathcal{F}_t,$$

where $\mathsf{Z}_t = \exp\left(q\mathsf{B}_t - \frac{1}{2}q^2 t\right)$. Let $\mathsf{T}_\eta = \inf\left\{t \geq 0 : \mathsf{B}_t = \eta\right\}$ and take $\mathcal{A} = \{\mathsf{T}_\eta \leq t\}$. After an application of the martingale stopping theorem and some simplification

(see [63, p. 196]), we have

$$\tilde{\mathbb{P}}\left\{\mathsf{T}_\eta \leq t\right\} = \int_0^t \exp\left(q\eta - \frac{1}{2}q^2 s\right) \mathbb{P}\left\{\mathsf{T}_\eta \in ds\right\}.$$

The left side equals $\mathbb{P}\left\{\tau_\eta \leq t\right\}$ by the Cameron-Martin-Girsanov theorem. The right side can be simplified using the first-passage-time distribution for Brownian motion and one-sided boundary: $\mathbb{P}\left\{\mathsf{T}_\eta \in ds\right\} = \frac{|\eta|}{\sqrt{2\pi s^3}}\exp\left(-\frac{\eta^2}{2s}\right)ds$. Hence, we have the probability distribution

$$\mathbb{P}\left\{\tau_\eta \in dt\right\} = \frac{|\eta|}{\sqrt{2\pi t^3}}\exp\left(-\frac{(\eta - qt)^2}{2t}\right)dt,$$

$t > 0$. That is, the PDF of τ_η is given by (2.24).

Chapter 3

Research Methodology

In this chapter, we describe the research methodology that enables us to solve the first-passage-time problems and achieve the objectives of this thesis (see Section 1.1 for the list). We organize this chapter according to the research objectives: one section for each research objective. In Section 3.1, we describe the methodology for solving the first-passage-time problems that involve Brownian motion with quadratic drift and a two-sided, constant boundary. In Section 3.2, we describe the methodology for solving the first-passage-time problems that involve Brownian motion with polynomial drift and a two-sided, constant boundary. In Section 3.3, we describe the methodology for solving the first-passage-time problems that involve multi-dimensional Brownian motion with polynomial drift and a class of boundaries given by open sets in the Euclidean space. In Section 3.4, we describe the methodology for solving the first-passage-time problems that involve discrete-time process with certain correlation and a one-side, constant boundary. In Section 3.5, we describe the methodology for applying these first-passage-time solutions to time-aware networks.

3.1 For Brownian Motion with Quadratic Drift

The most important mathematical technique that enables us to solve the problem of Brownian motion with quadratic drift is transformation methodology. Transformation relates the original problem to an equivalent one that is easier to solve [69]. A

transformation methodology has been used to solve difficult problems [124, 143] and is appropriate for our first-passage-time problem.

Here is how we use transformation methodology. To derive the first-passage-time distribution, we apply five different types of transformations: transformations of the probability measure, the time, the stochastic integral, the conditional expectation, and the unconditional expectation. In the order that these transformations appear in the derivation, first, we transform Brownian motion with quadratic drift into Brownian motion without drift, using the Cameron-Martin-Girsanov theorem. Second, we transform large time into small time, using the martingale stopping theorem. Third, we transform the stochastic integration into a Riemann integration with a random integrand, using the Itô formula. Fourth, we transform the conditional expectation into the unconditional expectation, using the Laplace transform. Fifth, we transform the unconditional expectation into a solution of an ordinary differential equation, using the Feynman-Kac formula. The combination of these transformations yields the solution of the first-passage-time distribution.

3.2   For Brownian Motion with Polynomial Drift

The methodology for Brownian motion with polynomial drift is similar to the methodology for Brownian motion with quadratic drift. Namely, we also use transformation methodology. Like the case of quadratic drift (Section 3.1), the case of polynomial drift also involves five types of transformations. The distinction between the cases occurs at the last two transformations, where we now use another type of integral transform (instead of the Laplace transform) and need to solve a partial differential equation (PDE) (instead of an ordinary differential equation). The similarity between the methods for the quadric drift and polynomial drift is natural, reflecting the fact that a quadratic function is a special type of a polynomial.

For completeness, we describe the five types of transformation for Brownian motion with polynomial drift. They are transformations of the probability measure, the time, the stochastic integral, the conditional expectation, and the unconditional ex-

pectation. In particular, first, we transform Brownian motion with polynomial drift into Brownian motion without drift, using the Cameron-Martin-Girsanov theorem. Second, we transform large time into small time, using the martingale stopping theorem. Third, we transform the stochastic integration into a Riemann integration with a random integrand, using the Itô formula. Fourth, we transform the conditional expectation into the unconditional expectation, using the integration, which is invertible. Fifth, we transform the unconditional expectation into a solution of a PDE, using the Feynman-Kac formula. The combination of these five transformations yields the solution of the first-passage-time distribution.

3.3 For Multi-Dimensional Brownian Motion with Polynomial Drift

The methodology for multi-dimensional Brownian motion with polynomial drift is reduction and ordered statistics. In particular, we reduce the problem in multiple dimensions into several problems in one dimension and then apply rules of probability usually found in ordered statistics. The reduction simplifies the analysis and enables us to solve the original problem that consists of hundreds of dimensions.

Here is how we use the reduction and ordered statistics. We treat the n-dimensional process as n one-dimensional processes, exploiting independence among the random components of the n-dimensional process. Then, we obtain an upper bound and a lower bound for the CDF of the first passage time for the n-dimensional process using these approaches. For the lower bound, we relate the first passage time of the multi-dimensional process to an ordered statistic. The ordered statistics are the first passage times, placed in an increasing order, of the n one-dimensional random processes. We derive the probability distributions of the ordered statistics and obtain the lower bound. For the upper bound, we relate the first passage time of the multi-dimensional process to an appropriate event. Then, we evaluate the probability of this event and obtain the upper bound. The strength of our methodology is that

the upper bound and the lower bound are easy to obtain and valid for a large class of boundaries. For certain boundaries, we verify using rules of probability that the lower bound equal the exact probability distribution of the first-passage-time time. The combination of a reduction and ordered statistics give us a first-passage-time distribution.

3.4   For a Discrete-Time Process With Certain Correlations

The first-passage-time problem for a discrete-time process with certain corrections is motivated by frame synchronization. In particular, we want to characterize the duration to achieve frame synchronization using the framework of first passage time. The methodology for characterizing the duration to achieve frame synchronization is to decompose this duration into a random sum. Then we apply rules of probability and renewal theory to obtain the probability distribution of the random sum. Our method yields the expected time and the CDF of duration to achieve frame synchronization.

Here is how we use decomposition. We write the expected time and the CDF of duration to achieve frame synchronization as functions of a few basic terms. These basic terms are probabilities and conditional probabilities of certain first passage times for discrete-time processes and a one-sided, constant boundary. We derive explicit expressions for the probabilities and conditional probabilities using rules of probability (such as Bayes' theorem, the law of total probability, the law of large number), stopping time, and renewal theory. The expressions for the basic terms give us the expressions for the expected value and the CDF of time to correct frame synchronization.

3.5   For Applications to Time-Aware Networks

The methodology is to express key performance metrics in time-aware networks as first passage times. In particular, we consider three aspects of synchronization in time-

aware network: synchronization of two clocks, synchronization of a network of clocks, and synchronization of frames. The methodology for each aspect of synchronization is as follows.

For the synchronization of two clocks, we apply the frameworks for Brownian motion with quadratic drift and Brownian motion with polynomial drift. Brownian motion with drift represents the time error between the two clocks. The first time that Brownian motion with drift exits the boundary is the time that the two clocks need to be calibrated. We propose two performance measures for the calibration time: the average and the outage. We obtain the average and the outage of the calibration time using the first-passage-time distributions derived for Brownian motion with quadratic and polynomial drifts. Then, we plot the average and the outage as a function of key parameters such as severity of clock noise and the maximum allowable time error. The plots give insight into how often clocks need to be calibrated.

For synchronization of a network of clocks, we apply the framework for multi-dimensional Brownian motion with polynomial drift. The number of clocks equals the number of components of the multi-dimensional process. Each component of the multi-dimensional process represents the time error between each clock and a reference clock. The first time that multi-dimensional Brownian motion with polynomial drift exits a boundary is the time that a given number of clocks are simultaneously out of sync. At the first passage time, the network needs to be calibrated. We propose two performance measures for the network calibration time: the average and the outage. We obtain the exact expression (when available), the lower bound, and an upper bound for the average and the outage of the calibration time, using the first-passage-time distributions derived for multi-dimensional Brownian motion with quadratic and polynomial drifts. Then we plot the exact expression, the lower bound, and the upper bound as a function of key parameters such as severity of clock noise and the number of clocks in the network. The plots give insight into how often the network needs to be calibrated.

In the third setting, we apply the framework for discrete-time process to frame synchronization. The random process represents the decision variable at each discrete

61

time. The first passage time represents the time at which a receiver correctly acquires a frame (or a packet). We propose two performance measures to characterize time to correct frame synchronization: the average and the probability of correct acquisition within a given duration. Then we plot the two metrics as functions of key parameters such as the signal to noise ratio (SNR). These plots give insight into the duration until a node correctly acquires a packet.

Chapter 4

Research Results

In this chapter, we describe the research results that address the objectives of this thesis (see Section 1.1 for the list). We organize this chapter according to the research objectives: one section for each research objective. In Section 4.1, we solve first-passage-time problems that involve Brownian motion with quadratic drift and a two-sided, constant boundary. In Section 4.2, we solve first-passage-time problems that involve Brownian motion with polynomial drift and a two-sided, constant boundary. In Section 4.3, we solve first-passage-time problems that involve multi-dimensional Brownian motion with polynomial drift and a class of boundaries given by open sets in the Euclidean space. In Section 4.4, we solve first-passage-time problems that involve discrete-time process with certain correlation and a one-sided, constant boundary. In Section 3.5, we apply these first-passage-time solutions to time-aware networks.

4.1   Brownian Motion with Quadratic Drift

In this section, we solve first-passage-time problems involving Brownian motion with quadratic drift. The goal is to obtain the probability distribution of the first time that Brownian motion with quadratic drift crosses a two-sided boundary. Our main contributions from this section are

- a methodology involving transformation techniques to solve first-passage-time problems;

63
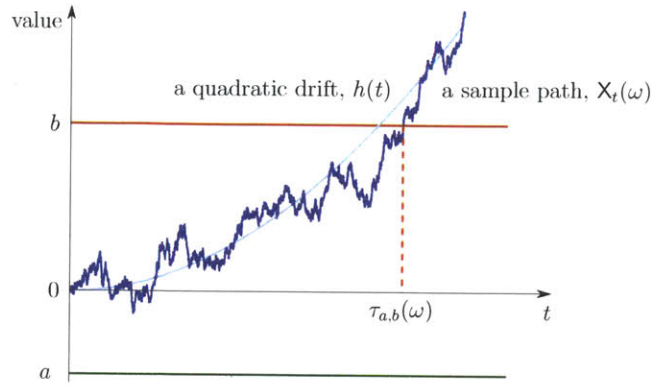
Figure 4-1: A sample path of Brownian motion with quadratic drift takes a value outside an open set (a, b) for the first time at time $\tau_{a,b}(\omega)$.

- an explicit expression of the PDF of the first time that Brownian motion with quadratic drift crosses a boundary consisting of two constants; and

- a PDF of a first passage time for scaled Brownian motion starting from an arbitrary position.

The solution to first-passage-time distribution has applications to clock synchronization.

This section is organized as follows. In Section 4.1.1, we state the first-passage-time problem that we aim to solve. In Section 4.1.2, we provide the solution to the first-passage-time distribution. In Section 4.1.3, we discuss important aspects and the consequences of our solution. In Section 4.1.4, we provide elementary examples demonstrating applications of our solution. In Section 4.1.5, we prove the main theorems that lead to the solution of the first-passage-time distribution.

4.1.1 Problem Statement

Let B_t denote a standard Brownian motion defined on a probability space $(\Omega, \mathcal{F}, \mathbb{P})$. Let X_t denote a random process

$$\mathsf{X}_t = \mathsf{B}_t + h(t), \qquad\qquad t \geq 0,$$

where $h(t) = qt + \mu t^2$ for constant $\mu \geq 0$ (without loss of generality) and constant $q \in \mathbb{R}$. Let $\tau_{a,b}$ denote the first time that X_t crosses a boundary consisting of two constants at a and b:

$$\tau_{a,b} = \inf\Big\{t \geq 0 : \mathsf{X}_t \notin (a,b)\Big\},$$

for finite numbers $a < 0 < b$. See Fig. 4-1 for an illustration. We want to obtain the probability distribution of $\tau_{a,b}$.

4.1.2   Solution to the First-Passage-Time Distribution

The PDF of $\tau_{a,b}$ is a sum of two terms:

$$f_{\tau_{a,b}}(t) = f_{\tau_{a,b}, \mathsf{X}_{\tau_{a,b}}}(t,a) + f_{\tau_{a,b}, \mathsf{X}_{\tau_{a,b}}}(t,b), \tag{4.1}$$

where

$$f_{\tau_{a,b}, \mathsf{X}_{\tau_{a,b}}}(t,a) = e^{aq - \frac{q^2}{2}t - \mu q t^2 - \frac{2}{3}\mu^2 t^3} f_{\mathrm{a}}(t), \tag{4.2}$$

$$f_{\tau_{a,b}, \mathsf{X}_{\tau_{a,b}}}(t,b) = e^{bq + [2\mu(b-a) - \frac{q^2}{2}]t - \mu q t^2 - \frac{2}{3}\mu^2 t^3} f_{\mathrm{b}}(t), \tag{4.3}$$

for almost every $t \geq 0$ (with respect to the Lebesgue measure). On the left side, $f_{\tau_{a,b}, \mathsf{X}_{\tau_{a,b}}}$ denotes a joint PDF of two random variables: the first passage time $\tau_{a,b}$ and the barrier $\mathsf{X}_{\tau_{a,b}}$ at which the random process first crosses at time $\tau_{a,b}$. On the right
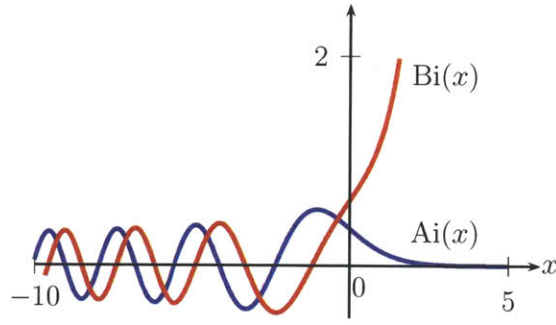
Figure 4-2: Airy functions $\mathrm{Ai}(x)$ and $\mathrm{Bi}(x)$ are linearly independent solutions of a differential equation $w''(x) - xw(x) = 0$.

side, f_a and f_b are given in terms of Laplace transforms:

$$\int_0^\infty e^{-st} f_a(t)dt = \begin{cases} \dfrac{b}{b-a}, & \mu = 0, s = 0, \\[3mm] \dfrac{\sinh[b\sqrt{2s}]}{\sinh[(b-a)\sqrt{2s}]}, & \mu = 0, s > 0, \\[3mm] \dfrac{\mathrm{Ai}(\gamma)\mathrm{Bi}(\beta b+\gamma)-\mathrm{Ai}(\beta b+\gamma)\mathrm{Bi}(\gamma)}{\mathrm{Ai}(\beta a+\gamma)\mathrm{Bi}(\beta b+\gamma)-\mathrm{Ai}(\beta b+\gamma)\mathrm{Bi}(\beta a+\gamma)}, & \mu > 0, s \geq 0, \end{cases} \qquad (4.4)$$

$$\int_0^\infty e^{-st} f_b(t)dt = \begin{cases} \dfrac{-a}{b-a}, & \mu = 0, s = 0, \\[3mm] \dfrac{\sinh[-a\sqrt{2s}]}{\sinh[(b-a)\sqrt{2s}]}, & \mu = 0, s > 0, \\[3mm] \dfrac{\mathrm{Ai}(\beta a+\gamma)\mathrm{Bi}(\gamma)-\mathrm{Ai}(\gamma)\mathrm{Bi}(\beta a+\gamma)}{\mathrm{Ai}(\beta a+\gamma)\mathrm{Bi}(\beta b+\gamma)-\mathrm{Ai}(\beta b+\gamma)\mathrm{Bi}(\beta a+\gamma)}, & \mu > 0, s \geq 0, \end{cases} \qquad (4.5)$$

and Ai and Bi are Airy functions (see Fig. 4-2) [2, Sec. 10.4.1, p. 446], $\beta = (4\mu)^{1/3}$, and $\gamma(s) = \dfrac{2(s-2\mu a)}{(4\mu)^{2/3}}$.

4.1.3 Important Aspects of the Solution and the Consequences

We discuss the important aspects of the solution and consider the other problems that can be solved as a consequence of our work.

Important Aspects of the Solution

We make the following remarks about the solution. First, for $\mu = 0$, the PDF in (4.1) reduces to a known result [14, p. 309, 3.0.1] for Brownian motion with linear drift. Second, f_a and f_b can be determined by numerically inverting the Laplace transforms (for example, see [1, Sec. 2]). Third, as it will be apparently shortly, to derive the first-passage-time distribution, we will evaluate a conditional expectation

$$\mathbb{E}\left\{ 1_{\left\{ \mathsf{B}_{\mathsf{T}_{a,b}} = \chi \right\}} e^{-\int_0^{\mathsf{T}_{a,b}} \mathsf{B}_u h''(u) du} \; \middle| \; \mathsf{T}_{a,b} = t \right\} \tag{4.6}$$

for each $t > 0$ and each $\chi \in \{a, b\}$. In the conditioning, $\mathsf{T}_{a,b}$ is the first time that a standard Brownian motion exits from an interval (a, b):

$$\mathsf{T}_{a,b} = \inf \left\{ t \geq 0 : \mathsf{B}_t \notin (a, b) \right\}. \tag{4.7}$$

The conditional expectation is difficult to evaluate directly, since conditioning on $\{\mathsf{T}_{a,b} = t\}$ alters the measure of process B_u. This difficulty is alleviated in our solution by finding the Laplace transform of

$$\mathbb{E}\left\{ 1_{\left\{ \mathsf{B}_{\mathsf{T}_{a,b}} = \chi \right\}} e^{-\int_0^{\mathsf{T}_{a,b}} \mathsf{B}_u h''(u) du} \; \middle| \; \mathsf{T}_{a,b} = t \right\} f_{\mathsf{T}_{a,b}}(t),$$

where $f_{\mathsf{T}_{a,b}}$ is the PDF of $\mathsf{T}_{a,b}$, i.e., $f_{\mathsf{T}_{a,b}}(t) dt = \mathbb{P}\left\{ \mathsf{T}_{a,b} \in dt \right\}$. See Step 4 of the proof in Section 4.1.5.

A Process not Starting from Zero with a Scaled Variance

The problem statement in Section 4.1.1 restricts X_t to start from zero, μ to be positive, and the variance of X_t to be that of the Brownian motion. In this section, we allow the random process to start from an arbitrary position, the value of μ to be negative, and the coefficient of B_t to be any value. This variation to the first-passage-time problem can be reduced to our original problem using the method described here.

The problem statement that we now want to solve is as follows. Let Y_t denote a

random process

$$\mathsf{Y}_t = \sigma \mathsf{B}_t + g(t), \qquad\qquad t \geq 0,$$

where σ is a non-zero constant and $g(t) = \breve{c} + \breve{q}t + \breve{\mu}t^2$ for constants $\breve{\mu}$, $\breve{c}$, and $\breve{q}$, where $\breve{\mu} \neq 0$. The case of $\breve{\mu} = 0$ is well-known and needs no consideration (see literature review, Section 2.3.5). Let $\breve{\tau}_{a_\mathsf{Y},b_\mathsf{Y}}$ denote the first time that Y_t crosses a boundary consisting of two constants at a_Y and b_Y:

$$\breve{\tau}_{a_\mathsf{Y},b_\mathsf{Y}} \triangleq \inf\Big\{ t \geq 0 : \mathsf{Y}_t \notin (a_\mathsf{Y}, b_\mathsf{Y}) \Big\},$$

for finite numbers $a_\mathsf{Y} < g(0) < b_\mathsf{Y}$. We want to obtain the probability distribution of $\breve{\tau}_{a_\mathsf{Y},b_\mathsf{Y}}$.

This first passage time problem can be reduced to the problem in the previous section by using the following observations. First, $-\mathsf{B}_t$ is a standard Brownian motion with respect to the probability space $(\Omega, \mathcal{F}, \mathbb{P})$. Hence the sign of σ does not affect the distribution of $\breve{\tau}_{a_\mathsf{Y},b_\mathsf{Y}}$. Second, the value of $\breve{\tau}_{a_\mathsf{Y},b_\mathsf{Y}}$ is not affected by scaling or shifting of a random process and the barriers along the y-axis. Hence we can scale and shift the random process and the barriers together to produce a Brownian motion with quadratic drift that begins at 0. These two observations provide a geometric interpretation of our solution.

A solution to the first passage time problem is as follows. The PDF of $\breve{\tau}_{a_\mathsf{Y},b_\mathsf{Y}}$ equals

$$f_{\breve{\tau}_{a_\mathsf{Y},b_\mathsf{Y}}}(t) = f_{\breve{\tau}_{a_\mathsf{Y},b_\mathsf{Y}}, \mathsf{Y}_{\breve{\tau}_{a_\mathsf{Y},b_\mathsf{Y}}}}(t, a_\mathsf{Y}) + f_{\breve{\tau}_{a_\mathsf{Y},b_\mathsf{Y}}, \mathsf{Y}_{\breve{\tau}_{a_\mathsf{Y},b_\mathsf{Y}}}}(t, b_\mathsf{Y}),$$

where, for almost $t \geq 0$ (with respect to the Lebesgue measure), the joint PDF

$f_{\check{\tau}_{a_Y,b_Y},Y_{\check{\tau}_{a_Y,b_Y}}}$ equals

$$f_{\check{\tau}_{a_Y,b_Y},Y_{\check{\tau}_{a_Y,b_Y}}}(t,a_Y)$$

$$= \begin{cases} A\left(\frac{\check{a}-\check{c}}{|\sigma|}, \frac{\check{b}-\check{c}}{|\sigma|}, \frac{\check{q}}{|\sigma|}, \frac{\check{\mu}}{|\sigma|}, t\right), & \check{\mu} > 0 \\ B\left(\frac{-\check{b}+\check{c}}{|\sigma|}, \frac{-\check{a}+\check{c}}{|\sigma|}, \frac{-\check{q}}{|\sigma|}, \frac{-\check{\mu}}{|\sigma|}, t\right), & \check{\mu} < 0 \end{cases}$$

$$f_{\check{\tau}_{a_Y,b_Y},Y_{\check{\tau}_{a_Y,b_Y}}}(t,b_Y)$$

$$= \begin{cases} B\left(\frac{\check{a}-\check{c}}{|\sigma|}, \frac{\check{b}-\check{c}}{|\sigma|}, \frac{\check{q}}{|\sigma|}, \frac{\check{\mu}}{|\sigma|}, t\right), & \check{\mu} > 0 \\ A\left(\frac{-\check{b}+\check{c}}{|\sigma|}, \frac{-\check{a}+\check{c}}{|\sigma|}, \frac{-\check{q}}{|\sigma|}, \frac{-\check{\mu}}{|\sigma|}, t\right), & \check{\mu} < 0. \end{cases}$$

Here, A and B are the right side of (4.2) and (4.3), respectively, viewing as functions of (a, b, q, μ, t). The proof is based on a scale and a shift of the random process and a symmetry in Brownian motion. The proof is omitted for brevity.

4.1.4 Elementary Examples

As an example, we consider a random process X_t with quadratic drift $h(t) = qt + \mu t^2$ where $q = 1$ and $\mu = \frac{1}{10}$ and consider the boundary at $a = -1$ and $b = 2$. We obtain the PDF of the first passage time using the method described in Section 4.1.2. The PDF is shown in Fig. 4-3 along with the joint PDF.

From the figure, the joint PDF, $f_{\tau_{a,b},X_{\tau_{a,b}}}$, matches intuition. For each $t > 0$ and $\chi \in \{a, b\}$, recall that $f_{\tau_{a,b},X_{\tau_{a,b}}}(t, \chi)$ is the probability density that the random process exits the boundary for the first time at time t and the exiting boundary is χ. When t is near zero, $f_{\tau_{a,b},X_{\tau_{a,b}}}(t, a)$ is larger than $f_{\tau_{a,b},X_{\tau_{a,b}}}(t, b)$. This trend arises because the barrier at $a = -1$ is closer to zero than the barrier at $b = 2$. As a consequence, the random process is more likely to exit from a than from b at small t when the drift approximates zero. From the figure when t is large, $f_{\tau_{a,b},X_{\tau_{a,b}}}(t, b)$ is greater than $f_{\tau_{a,b},X_{\tau_{a,b}}}(t, a)$. This trend arises because the drift moves the random process away from barrier a. As a consequence, the random process is more likely to exit from b than from a at large t. Adding the joint PDFs together gives us the PDF, which numerically integrates to one as we expect.
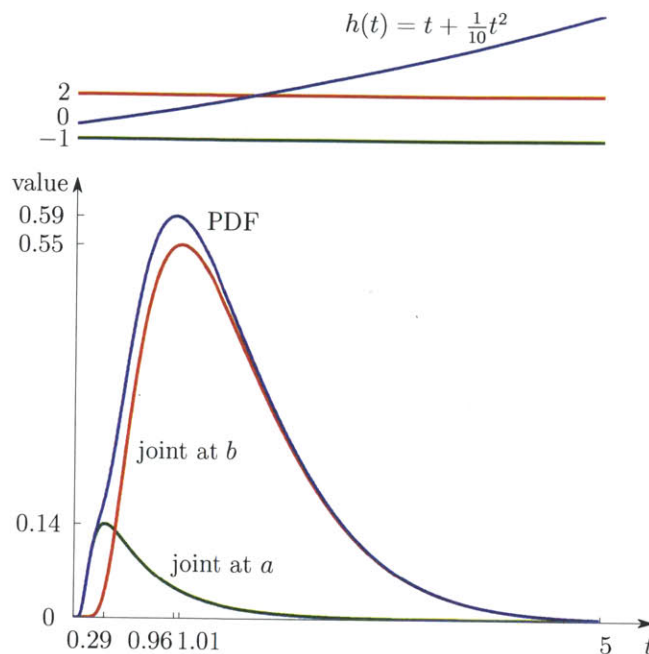
Figure 4-3: The PDF, the joint PDF evaluated at $a = -1$, and the joint PDF evaluated at $b = 2$ match intuition.

4.1.5   Proofs of the Key Theorems

Process X_t is continuous and hence exits the interval (a, b) *either* from a or from b, giving the equality in (4.1). It remains to derive (4.2) and (4.3).

The derivation of (4.2) and (4.3) employs the following ideas. First, we transform the process X_t into a standard Brownian motion using the Cameron-Martin-Girsanov theorem. Next, we replace a stochastic integration with a Riemann integration using Itô's formula or the stochastic integration-by-part formula. We then apply the martingale stopping theorem. Finally, we relate the conditional expectation in (4.6) to a differential equation using a Laplace transform and Feynman-Kac formula. The derivation is divided into several steps below.

Step 1: Transformation of measure

Let $\mathcal{F}_t$ denote the σ-algebra generated by $\{B_u : 0 \leq u \leq t\}$, and $\mathcal{F}_\infty$ denote the σ-algebra generated by $\{B_u : 0 \leq u\}$. The Cameron-Martin-Girsanov theorem [63,

Thm. 5.1, p. 191] implies that the process $\widetilde{\mathsf{B}}_t$, for

$$\widetilde{\mathsf{B}}_t = \mathsf{B}_t - \int_0^t h'(u)du = \mathsf{B}_t - h(t), \tag{4.8}$$

is a standard Brownian motion on $(\Omega, \mathcal{F}_\infty, \widetilde{\mathbb{P}})$, where $\widetilde{\mathbb{P}}$ is a unique probability measure satisfying [63, Cor. 5.2, p. 192]

$$\widetilde{\mathbb{P}}(\mathcal{E}) = \mathbb{E}\left\{1_{\mathcal{E}} \mathsf{Z}_t\right\}, \qquad \text{for every } t \geq 0 \text{ and every } \mathcal{E} \in \mathcal{F}_t. \tag{4.9}$$

On the right side, $\mathbb{E}\left\{\cdot\right\}$ is the expectation with respect to $\mathbb{P}$, and Z_t equals

$$\mathsf{Z}_t = e^{\int_0^t h'(u)d\mathsf{B}_u - \frac{1}{2}\int_0^t |h'(u)|^2 du} \tag{4.10}$$

$$= e^{h'(t)\mathsf{B}_t - \int_0^t \mathsf{B}_u h''(u)du - \frac{1}{2}\int_0^t |h'(u)|^2 du}. \tag{4.11}$$

The second equality for Z_t follows from Itô's formula or the stochastic integration-by-part formula [78, Thm. 4.1.5, p. 46]. Note from (4.10) that Z_t is an martingale (with respect to $\{\mathcal{F}_t\}$) by a straightforward verification of the martingale definition.

Under measure $\mathbb{P}$, process X_t is, by definition, a standard Brownian motion plus drift $h(t)$. Under measure $\widetilde{\mathbb{P}}$, process $\widetilde{\mathsf{B}}_t + h(t)$, or equivalently B_t (see (4.8)), is a standard Brownian motion plus drift $h(t)$. This parallelism between X_t and B_t implies the following:

$$\mathbb{P}\left\{\tau_{a,b} \leq t \text{ and } \mathsf{X}_{\tau_{a,b}} = a\right\} = \widetilde{\mathbb{P}}\{\mathsf{T}_{a,b} \leq t \text{ and } \mathsf{B}_{\mathsf{T}_{a,b}} = a\} \text{ and} \tag{4.12}$$

$$\mathbb{P}\left\{\tau_{a,b} \leq t \text{ and } \mathsf{X}_{\tau_{a,b}} = b\right\} = \widetilde{\mathbb{P}}\{\mathsf{T}_{a,b} \leq t \text{ and } \mathsf{B}_{\mathsf{T}_{a,b}} = b\}. \tag{4.13}$$

The right side can be written in terms of the expectations with respect to $\mathbb{P}$, using relationship (4.9) provided by the Cameron-Martin-Girsanov theorem.

Step 2: Derivation of $\mathbb{P}\left\{\tau_{a,b} \in dt \text{ and } \mathsf{X}_{\tau_{a,b}} = a\right\}$

71

Equation (4.12), together with (4.9) for $\mathcal{E} = \{\mathsf{T}_{a,b} \leq t \text{ and } \mathsf{B}_{\mathsf{T}_{a,b}} = a\}$, becomes

$$\mathbb{P}\left\{\tau_{a,b} \leq t \text{ and } \mathsf{X}_{\tau_{a,b}} = a\right\} = \mathbb{E}\left\{1_{\left\{\mathsf{T}_{a,b} \leq t \text{ and } \mathsf{B}_{\mathsf{T}_{a,b}} = a\right\}} Z_t\right\}.$$

Let $x \wedge y$ denote the minimum between x and y. The right side simplifies to

$$\mathbb{P}\left\{\tau_{a,b} \leq t \text{ and } \mathsf{X}_{\tau_{a,b}} = a\right\} \overset{(a)}{=} \mathbb{E}\left\{1_{\left\{\mathsf{T}_{a,b} \leq t \text{ and } \mathsf{B}_{\mathsf{T}_{a,b}} = a\right\}} \mathbb{E}\left\{Z_t \mid \mathcal{F}_{t \wedge \mathsf{T}_{a,b}}\right\}\right\}$$

$$\overset{(b)}{=} \mathbb{E}\left\{1_{\left\{\mathsf{T}_{a,b} \leq t \text{ and } \mathsf{B}_{\mathsf{T}_{a,b}} = a\right\}} Z_{t \wedge \mathsf{T}_{a,b}}\right\}$$

$$\overset{(c)}{=} \mathbb{E}\left\{1_{\left\{\mathsf{T}_{a,b} \leq t \text{ and } \mathsf{B}_{\mathsf{T}_{a,b}} = a\right\}} Z_{\mathsf{T}_{a,b}}\right\},$$

where (a) follows from an iterated expectation and the indicator random variable being $\mathcal{F}_{t \wedge \mathsf{T}_{a,b}}$-measurable, (b) follows from martingale stopping theorem [74, Thm. 3.3, p. 11], applied to a finite stopping time $(t \wedge \mathsf{T}_{a,b}) \leq t < \infty$, and (c) follows from the equality $(t \wedge \mathsf{T}_{a,b}) = \mathsf{T}_{a,b}$ on the set $\{\mathsf{T}_{a,b} \leq t \text{ and } \mathsf{B}_{\mathsf{T}_{a,b}} = a\}$.

Substitution of $Z_{\mathsf{T}_{a,b}}$ in (4.11) into the expectation gives us

$$\mathbb{P}\left\{\tau_{a,b} \leq t \text{ and } \mathsf{X}_{\tau_{a,b}} = a\right\}$$

$$\overset{(a)}{=} \mathbb{E}\left\{\mathbb{E}\left\{1_{\left\{\mathsf{T}_{a,b} \leq t \text{ and } \mathsf{B}_{\mathsf{T}_{a,b}} = a\right\}} e^{h'(\mathsf{T}_{a,b})a - \int_0^{\mathsf{T}_{a,b}} \mathsf{B}_u h''(u) du - \frac{1}{2} \int_0^{\mathsf{T}_{a,b}} |h'(u)|^2 du} \mid \mathsf{T}_{a,b}\right\}\right\}$$

$$\overset{(b)}{=} \mathbb{E}\left\{1_{\left\{\mathsf{T}_{a,b} \leq t\right\}} e^{h'(\mathsf{T}_{a,b})a - \frac{1}{2} \int_0^{\mathsf{T}_{a,b}} |h'(u)|^2 du} \mathbb{E}\left\{1_{\left\{\mathsf{B}_{\mathsf{T}_{a,b}} = a\right\}} e^{-\int_0^{\mathsf{T}_{a,b}} \mathsf{B}_u h''(u) du} \mid \mathsf{T}_{a,b}\right\}\right\},$$

where the conditioning is under $\sigma(\mathsf{T}_{a,b})$, the σ-algebra generated by random variable $\mathsf{T}_{a,b}$. Equation (a) follows from an iterated expectation. Equation (b) follows from the random variables outside the conditional expectation being $\sigma(\mathsf{T}_{a,b})$-measurable.

Random variables inside the expectation are functions of $\mathsf{T}_{a,b}$ [35, p. 20] [38, p. 340]. Hence, the expectation can be written as an integration involving the PDF of $\mathsf{T}_{a,b}$:

$$\mathbb{P}\left\{\tau_{a,b} \leq t \text{ and } \mathsf{X}_{\tau_{a,b}} = a\right\} = \int_0^t e^{ah'(v) - \frac{1}{2} \int_0^v |h'(u)|^2 du + cv} f_a(v) dv,$$

where

$$f_{\mathrm{a}}(v) = \mathbb{E}\left\{1_{\left\{\mathsf{B}_{\mathsf{T}_{a,b}}=a\right\}} e^{-\int_0^{\mathsf{T}_{a,b}}(\mathsf{B}_u h''(u)+c)du} \,\bigg|\, \mathsf{T}_{a,b} = v\right\} f_{\mathsf{T}_{a,b}}(v)$$

and $c = 2\mu|a|$. Constant c guarantees that the integrand in the expression of f_{a} is non-negative:

$$\mathsf{B}_u h''(u) + c = 2\mu\mathsf{B}_u - 2\mu a \geq 0, \qquad \text{for every } 0 \leq u \leq \mathsf{T}_{a,b}.$$

Step 3: Derivation of $\mathbb{P}\left\{\tau_{a,b} \in dt \text{ and } \mathsf{X}_{\tau_{a,b}} = b\right\}$

Starting from (4.13), using the relationship (4.9) for $\mathcal{E} = \{\mathsf{T}_{a,b} \leq t \text{ and } \mathsf{B}_{\mathsf{T}_{a,b}} = b\}$, and repeating the approach in the previous step, we have (4.3):

$$\mathbb{P}\left\{\tau_{a,b} \leq t \text{ and } \mathsf{X}_{\tau_{a,b}} = b\right\} = \int_0^t e^{bh'(v)-\frac{1}{2}\int_0^v |h'(u)|^2 du + cv} f_{\mathrm{b}}(v)dv,$$

where

$$f_{\mathrm{b}}(v) = \mathbb{E}\left\{1_{\left\{\mathsf{B}_{\mathsf{T}_{a,b}}=b\right\}} e^{-\int_0^{\mathsf{T}_{a,b}}(\mathsf{B}_u h''(u)+c)du} \,\bigg|\, \mathsf{T}_{a,b} = v\right\} f_{\mathsf{T}_{a,b}}(v).$$

It remains to show that $f_{\mathrm{a}}(t)$ and $f_{\mathrm{b}}(t)$ satisfy (4.4) and (4.5).

Step 4: Laplace transforms of f_{a} and f_{b}

Taking the Laplace transforms of f_{a} and f_{b} gives us

$$\int_0^\infty e^{-st} f_{\mathrm{a}}(t)dt = \int_0^\infty \mathbb{E}\left\{1_{\left\{\mathsf{B}_{\mathsf{T}_{a,b}}=a\right\}} e^{-\int_0^{\mathsf{T}_{a,b}}(\mathsf{B}_u h''(u)+c+s)ds} \,\bigg|\, \mathsf{T}_{a,b} = t\right\} f_{\mathsf{T}_{a,b}}(t)dt$$

$$= \mathbb{E}\left\{1_{\left\{\mathsf{B}_{\mathsf{T}_{a,b}}=a\right\}} e^{-\int_0^{\mathsf{T}_{a,b}}(\mathsf{B}_u h''(u)+c+s)du}\right\}, \qquad\qquad (4.14)$$

and

$$\int_0^\infty e^{-st} f_{\mathrm{b}}(t)dt = \mathbb{E}\left\{1_{\left\{\mathsf{B}_{\mathsf{T}_{a,b}}=b\right\}} e^{-\int_0^{\mathsf{T}_{a,b}}(\mathsf{B}_u h''(u)+c+s)du}\right\}, \qquad\qquad (4.15)$$

where s denotes the variable for Laplace transforms. Next, we evaluate the right sides

73

of (4.14) and (4.15).

Step 5: Evaluation of the expectation in (4.14)

Fix $s \geq 0$. By the Feynman-Kac formula [74, Thm. 8.1, p. 79], the expectation in (4.14) equals $y(0)$, where y is a unique solution for the ordinary differential equation

$$\frac{1}{2}y''(x) - (2\mu x + c + s)y(x) = 0, \qquad \text{for } a < x < b,$$

with boundary conditions

$$y(a) = 1 \quad \text{and} \quad y(b) = 0.$$

The differential equation has a unique solution due to our choices of c and s that make the integrand, $\mathsf{B}_u h''(u) + c + s$, non-negative [74, pp. 78–79]. The differential equation can be solved using standard techniques [28, Thm. 1, p. 51; Sec. 7, p. 126] [2, Sec. 10.4.1] and yields the solution

$$y(x) = \begin{cases} \frac{b-x}{b-a}, & \mu = 0 \text{ and } s = 0, \\[2ex] \frac{\sinh[(b-x)\sqrt{2s}]}{\sinh[(b-a)\sqrt{2s}]}, & \mu = 0 \text{ and } s > 0, \\[2ex] \frac{\text{Ai}(\beta x+\gamma)\text{Bi}(\beta b+\gamma) - \text{Ai}(\beta b+\gamma)\text{Bi}(\beta x+\gamma)}{\text{Ai}(\beta a+\gamma)\text{Bi}(\beta b+\gamma) - \text{Ai}(\beta b+\gamma)\text{Bi}(\beta a+\gamma)}, & \mu > 0, \end{cases}$$

where γ and β are defined in Section 4.1.2. Evaluation of $y(0)$ gives (4.4).

Step 6: Evaluation of the expectation in (4.15)

Fix $s \geq 0$. The Feynman-Kac formula implies that the expectation in (4.15) equals $z(0)$, where z is a unique solution for the ordinary differential equation

$$\frac{1}{2}z''(x) - (2\mu x + c + s)z(x) = 0, \qquad \text{for } a < x < b,$$

with boundary conditions

$$z(a) = 0 \quad \text{and} \quad z(b) = 1.$$

The differential equation has the solution

$$z(x) = \begin{cases} \frac{x-a}{b-a}, & \mu = 0 \text{ and } s = 0, \\[2ex] \frac{\sinh[(x-a)\sqrt{2s}]}{\sinh[(b-a)\sqrt{2s}]}, & \mu = 0 \text{ and } s > 0, \\[2ex] \frac{\text{Ai}(\beta a+\gamma)\text{Bi}(\beta x+\gamma)-\text{Ai}(\beta x+\gamma)\text{Bi}(\beta a+\gamma)}{\text{Ai}(\beta a+\gamma)\text{Bi}(\beta b+\gamma)-\text{Ai}(\beta b+\gamma)\text{Bi}(\beta a+\gamma)}, & \mu > 0. \end{cases}$$

Evaluation of $z(0)$ gives (4.5). The proof is complete.

4.2 Brownian Motion with Polynomial Drift of High Orders

In this section, we solve first-passage-time problems involving Brownian motion with polynomial drift. The goal is to obtain the probability distribution of the first time that Brownian motion with polynomial drift crosses a two-sided boundary. Our main contributions from this section are

- a methodology involving transformation techniques to solve first-passage-time problems;

- an expression of the PDF of the first time that Brownian motion with polynomial drift crosses a boundary consisting of two constants;

- an extension of the first-passage-time distribution to a large class of drifts that include functions with continuous third derivatives; and

- solution to the first-passage-time problems that involve one constant boundary and a moving boundary.

The solution to first-passage-time distribution has applications to clock synchronization.

This section is organized as follows. In Section 4.2.1, we state the first-passage-time problem that we aim to solve. In Section 4.2.2, we provide the solution to the

first-passage-time distribution. In Section 4.2.3, we discuss important aspects and the consequences of our solution. In Section 4.2.4, we provide elementary examples demonstrating applications of our solution. In Section 4.2.5, we prove the main theorems that lead to the solution of the first-passage-time distribution.

4.2.1 Problem Statement

Let B_t denote a standard Brownian motion defined on a probability space $(\Omega, \mathcal{F}, \mathbb{P})$. Let $\widetilde{\mathsf{X}}_t$ denote a Brownian motion with drift $\widetilde{h}(t)$:

$$\widetilde{\mathsf{X}}_t = \mathsf{B}_t + \widetilde{h}(t), \qquad\qquad t \geq 0,$$

where $\widetilde{h}$ is a polynomial with $\widetilde{h}(0) = 0$, i.e., $\widetilde{h}(t) = \sum_{i=1}^{m} c_i t^i$ for a finite $m \geq 1$ and constants $c_1, c_2, \ldots, c_m$.[1] We want to obtain the probability distribution of $\widetilde{\tau}_{a,b}$, where $\widetilde{\tau}_{a,b}$ is the first time that $\widetilde{\mathsf{X}}_t$ crosses a boundary consisting of two constants at a and b:

$$\widetilde{\tau}_{a,b} \triangleq \inf\left\{ t \geq 0 : \widetilde{\mathsf{X}}_t \notin (a, b) \right\},$$

for finite constants $a < \widetilde{h}(0) = 0 < b$.

4.2.2 Solution to the First-Passage-Time Distribution

In this section, we summarize our solution to the first-passage-time distribution. A proof for the solution is postponed until Section 4.2.5. A solution to drifts that are more general than polynomials will be discussed later (see "Solution to a class of accelerating drifts" on page 81).

The PDF of the first passage time $\widetilde{\tau}_{a,b}$ equals a sum of two terms:

$$f_{\widetilde{\tau}_{a,b}}(t) = f_{\widetilde{\tau}_{a,b}, \widetilde{\mathsf{X}}_{\widetilde{\tau}_{a,b}}}(t, a) + f_{\widetilde{\tau}_{a,b}, \widetilde{\mathsf{X}}_{\widetilde{\tau}_{a,b}}}(t, b), \tag{4.16}$$

---

[1]Later (see (4.29)), we will remove the condition $\widetilde{h}(0) = 0$ and allow the random process to start from an arbitrary position.

for almost every $t > 0$ with respect to the Lebesgue measure. The notation $f_{\widetilde{\tau}_{a,b}, \widetilde{X}_{\widetilde{\tau}_{a,b}}}$ denotes the joint PDF of two random variables: the first passage time $\widetilde{\tau}_{a,b}$, and the barrier $\widetilde{X}_{\widetilde{\tau}_{a,b}}$ at which the random process crosses at time $\widetilde{\tau}_{a,b}$. These terms equal

$$f_{\widetilde{\tau}_{a,b}, \widetilde{X}_{\widetilde{\tau}_{a,b}}}(t, a) = e^{a\widetilde{h}'(t) - \frac{1}{2}\int_0^t |\widetilde{h}'(u)|^2 du + \widetilde{c}t} \, g_{\mathrm{a}}'(t) \tag{4.17}$$

$$f_{\widetilde{\tau}_{a,b}, \widetilde{X}_{\widetilde{\tau}_{a,b}}}(t, b) = e^{b\widetilde{h}'(t) - \frac{1}{2}\int_0^t |\widetilde{h}'(u)|^2 du + \widetilde{c}t} \, g_{\mathrm{b}}'(t), \tag{4.18}$$

where $\widetilde{c}$ is a constant, g_{a} and g_{b} are functions relating to conditional expectations, and prime (') denotes the derivative. The constant $\widetilde{c}$ and the functions g_{a} and g_{b} are obtained as follows.

The constant $\widetilde{c}$ depends on the supremum norm $\sup_{s \geq 0} |\widetilde{h}''(s)|$. For a finite supremum norm, $\widetilde{c}$ is chosen to be any constant such that

$$\widetilde{c} \geq \max\left\{ -b \inf_{s \geq 0} \widetilde{h}''(s), -a \sup_{s \geq 0} \widetilde{h}''(s) \right\}, \qquad \text{(finite supremum norm).} \tag{4.19}$$

For an infinite supremum norm, $\widetilde{c}$ is chosen to be any constant such that

$$\widetilde{c} \geq \max\left\{ -b \inf_{0 \leq s \leq t_{\max}} \widetilde{h}''(s), -a \sup_{0 \leq s \leq t_{\max}} \widetilde{h}''(s) \right\}, \quad \text{(infinite supremum norm),} \tag{4.20}$$

where $t_{\max}$ is any positive number. For both cases of the supremum norm, $\widetilde{c}$ is finite and non-negative.

The functions $g_{\mathrm{a}}(t)$ and $g_{\mathrm{b}}(t)$ are obtained from PDEs and limit operations. Both functions depend on the supremum norm $\sup_{s \geq 0} |\widetilde{h}''(s)|$. For a finite supremum norm, g_{a} and g_{b} are defined to be functions on $t \in (0, \infty)$. For an infinite supremum norm, g_{a} and g_{b} are defined to be functions on $t \in (0, t_{\max}]$.

Function g_{a} is obtained as follows. Fix $t \in (0, \infty)$ or $t \in (0, t_{\max}]$, depending on the domain of g_{a}. The value of $g_{\mathrm{a}}(t)$ equals

$$g_{\mathrm{a}}(t) = \lim_{\varepsilon \searrow 0} y(0, 0, t, \varepsilon), \tag{4.21}$$

where $y(x, s, t, \varepsilon)$, for $0 < \varepsilon < b - a$, satisfies the PDE

$$\frac{\partial}{\partial s} y(x, s) + \frac{1}{2} \frac{\partial^2}{\partial x^2} y(x, s) - (x\widetilde{h}''(t) + \widetilde{c})y(x, s) = 0, \quad a < x < b, \, 0 \le s < t, \quad (4.22)$$

and boundary conditions

$$y(a, s) = 1, \qquad\qquad\qquad\qquad 0 \le s \le t \qquad\qquad (4.23\text{a})$$

$$y(b, s) = 0, \qquad\qquad\qquad\qquad 0 \le s \le t \qquad\qquad (4.23\text{b})$$

$$y(x, t) = \phi(x) = \max\{1 - (x - a)/\varepsilon, 0\}, \qquad a \le x \le b. \qquad (4.23\text{c})$$

In the PDE and the boundary conditions, we suppress variables t and ε for notational simplicity.

Function g_b is obtained by a similar method. Fix t in the domain of g_b. The value of $g_\text{b}(t)$ equals

$$g_\text{b}(t) = \lim_{\varepsilon \searrow 0} z(0, 0, t, \varepsilon). \qquad\qquad\qquad (4.24)$$

Function $z(x, s, t, \varepsilon)$, for $0 < \varepsilon < b - a$, satisfies the same PDE in (4.22) where y's are replaced by z's but the boundary conditions now become

$$z(a, s) = 0, \qquad\qquad\qquad\qquad 0 \le s \le t \qquad\qquad (4.25\text{a})$$

$$z(b, s) = 1, \qquad\qquad\qquad\qquad 0 \le s \le t \qquad\qquad (4.25\text{b})$$

$$z(x, t) = \psi(x) = \max\{1 + (x - b)/\varepsilon, 0\}, \qquad a \le x \le b. \qquad (4.25\text{c})$$

The critical step on obtaining the first-passage-time distribution reduces to solving the initial-boundary value problems (IBVPs), i.e., PDEs with given boundary conditions. It turns out that the IBVPs that appear in (4.22), (4.23) and (4.25) have unique solutions y and z, involve parabolic PDEs, and can be solved numerically by a mathematical software package.

4.2.3 Important Aspects of the Solution and the Consequences

We discuss the IBVPs that appear in the previous section; the methods to select $\widetilde{c}$, $t_{\max}$, and ε; and the consequences of our solution described in Section 4.2.2.

Initial-boundary Value Problems

The IBVPs that appear in our solution are difficult to solve due to the boundary conditions. To illustrate the difficulty, we temporarily ignore the boundary conditions and consider the PDE in (4.22). This PDE is a Schrödinger equation and has a solution

$$w(x,s) = \frac{1}{\sqrt{2\pi s}} \exp \left\{ \frac{\left[x - \widetilde{h}(s) \right]^2}{2s} + x\widetilde{h}'(s) - \frac{1}{2} \int_0^s |\widetilde{h}'(u)|^2 du - \widetilde{c}s \right\}. \qquad (4.26)$$

The solution is again obtained from a transformation methodology: transform the PDE into a heat-conduction equation, following the method of [42] [57, p. 9]. Now, consider the PDE together with the boundary conditions. The method that yields the solution to (4.26) will not solve the IBVP. The transformation of the PDE also transforms the boundary conditions into complicated forms. Furthermore, the method described in [42] [57, p. 9] does not guarantee the most general form of solutions. In such cases, the IBVP can be solved numerically.

Values of $\widetilde{c}$, ε, g_{a}, and g_{b}

To obtain the first-passage-time distribution, we select $\widetilde{c}$ and ε and solve the PDEs numerically and obtain g_{a}, g_{b}, and their derivatives. We then use (4.16)–(4.18) to produce the PDF at a given time t. The PDF can be obtained for each $t \in (0, \infty)$ or $t \in (0, t_{\max}]$ depending on the domain of g_{a} and g_{b}.

The value of $t_{\max}$ is arbitrary. Note, however, that a large value of $t_{\max}$ produces a large value of $\widetilde{c}$ since the right side of (4.20) is an increasing function of $t_{\max}$. A large $\widetilde{c}$ results in a large exponential $e^{\widetilde{c}t}$ (see the expression of PDF in (4.17) and (4.18)), which requires significant precision in the evaluation of $g_{\mathrm{a}}'(t)$ and $g_{\mathrm{b}}'(t)$. To reduce

79

the need for numerical precision, we select the smallest possible $t_{\max}$, for example, one that just gives us $\mathbb{P}\left\{\widetilde{\tau}_{a,b} \leq t_{\max}\right\} \approx 1$.

We now turn our discussion to $\widetilde{c}$. It will turn out that parameter $\widetilde{c}$ serves to shift an exponent so that the expectations that appear later in the proof (Step 8 of Section 4.2.5) are bounded. Parameter $\widetilde{c}$ depends on the infimum and the supremum of $\widetilde{h}''$ (see (4.19) and (4.20)). If the infimum and supremum can be evaluated explicitly, we set $\widetilde{c}$ to equal the right side of (4.19) or (4.20). Otherwise, we bound the supremum from above and the infimum from below, and set $\widetilde{c}$ to a value that is greater than or equal to the right side of (4.19) or (4.20). Similar to $t_{\max}$, parameter $\widetilde{c}$ should be chosen to be as small as possible to reduce the need for numerical precision.

Another consideration in obtaining g_a and g_b is the evaluations of the limits in (4.21) and (4.24). To evaluate the limits, we will need to select the value of ε. Fix t in the domain of g_a and g_b. To evaluate $g_a(t)$, we set ε in (4.21) to equal a constant ε_a (to be determined shortly), solve the IBVP for y, and approximate $g_a(t)$ by $y(0, 0, t, \varepsilon_a)$. Similarly, to evaluate $g_b(t)$, we set ε in (4.21) to equal a constant ε_b (to be determined shortly), solve the IBVP for z, and approximate $g_b(t)$ by $z(0, 0, t, \varepsilon_b)$. The values of ε_a and ε_b that we should select depend on the amount of error that we can accept from approximating the limit by the numerical value. In particular, if

$$0 < \varepsilon_a < \min\left\{b - a, \frac{|a|d\sqrt{2\pi e}}{1 + d\sqrt{2\pi e}}\right\} \text{ and} \tag{4.27a}$$

$$0 < \varepsilon_b < \min\left\{b - a, \frac{bd\sqrt{2\pi e}}{1 + d\sqrt{2\pi e}}\right\}, \tag{4.27b}$$

then the approximation error is at most d:

$$|y(0, 0, t, \varepsilon_a) - g_a(t)| < d \text{ and} \tag{4.28a}$$

$$|y(0, 0, t, \varepsilon_b) - g_b(t)| < d. \tag{4.28b}$$

A proof that (4.27a) implies (4.28a) and that (4.27b) implies (4.28b) appears in Section 4.2.5. With a suitable choice for ε_a and ε_b, we can evaluate $g_a(t)$ and $g_b(t)$

at a desired level of accuracy.

Solution to a class of accelerating drifts

By inspecting the proof in Section 4.2.5, we see that the solution for the first-passage-time distribution given in Section 4.2.2 is valid for other drifts besides the polynomials. In this section, we will describe the class of drifts whose first-passage-time distributions are also given by Section 4.2.2.

This class of drifts will be referred to as the class of accelerating drifts, due to a requirement on the second derivatives. In particular, we define the class of accelerating drifts to be the set of functions, $\widetilde{h} \colon [0, \infty) \to \mathbb{R}$, with the following property: for each $T > 0$, there exist $M > 0$ and $\alpha > 0$ such that

$$\left| x \widetilde{h}''(s) - y \widetilde{h}''(t) \right| \leq M \Big(|x - y| + |s - t| \Big)^{\alpha},$$

for every $x, y \in [a, b]$ and every $s, t \in [0, T]$. In other words, the mapping $(x, t) \mapsto x \widetilde{h}''(t)$ satisfies the Hölder condition with order α, for $(x, t) \in [a, b] \times [0, T]$. The probability distribution of

$$\widetilde{\tau}_{a,b} \triangleq \inf \Big\{ t \geq 0 : \widetilde{\mathsf{X}}_t \notin (a, b) \Big\},$$

where $\widetilde{h}(0) = 0$ and $\widetilde{h}$ is an accelerating drift, is also given by Section 4.2.2.

The class of accelerating drifts is a large class of functions. Examples of the functions in this class include $\widetilde{h}(t) = 0$ (no drift); $\widetilde{h}(t) = \breve{q}t$ (linear drift); $\widetilde{h}(t) = \breve{q}t + \breve{\mu}t^2$ (quadratic drift); $\widetilde{h}(t) = t^3$ (cubic drift); $\widetilde{h}(t) = \sin(\omega t)$ (sinusoidal drift); $\widetilde{h}(t) = \ln(1+t)$ (logarithmic drift); $\widetilde{h}(t) = 1 - e^{-t}$ (exponentially decaying drift); $\widetilde{h}(t) = 1 - e^{-t^n}$ for $n = 1, 2, 3, \dots$ (super-exponentially decaying drift); $\widetilde{h}(t) = \sqrt{1+t} - 1$ (square root drift); $\widetilde{h}(t) = (1 + t)^{\nu} - 1$ for $-\infty < \nu \leq 2$ (sub-quadratic drift); $\widetilde{h}(t) = t^n e^{-t}$ for $n = 1, 2, 3, \dots$ (a product of polynomial and exponentially decaying drift); any $\widetilde{h}(t)$ that has a continuous third-derivative on $t \in [0, \infty)$; a scalar multiplication of any of these examples; and a linear combination of these examples. A solution

in Section 4.2.2 solves a large class of drifts and a large class of first-passage-time problems.

A Random Process not Starting from Zero with a Scaled Variance

The problem statement in Section 4.2.1 restricts $\widetilde{\mathsf{X}}_t$ to start from 0 and the coefficient of B_t to be 1. In this section, we allow the random process to start from an arbitrary position and the coefficient of B_t to be any value. This variation to the first-passage-time problem can be reduced to our original problem using the method described here.

The problem statement that we now want to solve is as follows. Let Y_t denote a random process

$$\mathsf{Y}_t = \sigma\mathsf{B}_t + g(t), \qquad\qquad t \geq 0,$$

where $\sigma \neq 0$ and g belongs to the class of accelerating drifts. Let $\check{\tau}_{a_\mathsf{Y}, b_\mathsf{Y}}$ denote the first time that Y_t crosses a boundary consisting of two finite constants at a_Y and b_Y:

$$\check{\tau}_{a_\mathsf{Y}, b_\mathsf{Y}} \triangleq \inf\left\{ t \geq 0 : \mathsf{Y}_t \notin (a_\mathsf{Y}, b_\mathsf{Y}) \right\},$$

for $a_\mathsf{Y} < g(0) < b_\mathsf{Y}$. The goal is to obtain the probability distribution of $\check{\tau}_{a_\mathsf{Y}, b_\mathsf{Y}}$.

This first-passage-time problem can be reduced to the problem of Brownian motion with drift by using the following ideas. First, by symmetry, $-\mathsf{B}_t$ is standard Brownian motion with respect to probability space $(\Omega, \mathcal{F}, \mathbb{P})$. Hence, the sign of σ does not affect the distribution of $\check{\tau}_{a_\mathsf{Y}, b_\mathsf{Y}}$. Second, the value of $\check{\tau}_{a_\mathsf{Y}, b_\mathsf{Y}}$ is invariant to a scaling or a shifting along the y-axis of the random process together with the boundary. Hence, we can scale and shift the random process and the boundary to produce Brownian motion with drift. These two ideas lead to a solution.

Our solution to the first-passage-time problem is as follows. The PDF of $\check{\tau}_{a_\mathsf{Y}, b_\mathsf{Y}}$

equals

$$f_{\breve{\tau}_{a_{\mathrm{Y}},b_{\mathrm{Y}}}}(t) = f_{\breve{\tau}_{a_{\mathrm{Y}},b_{\mathrm{Y}}},\mathsf{Y}_{\breve{\tau}_{a_{\mathrm{Y}},b_{\mathrm{Y}}}}}(t, a_{\mathrm{Y}}) + f_{\breve{\tau}_{a_{\mathrm{Y}},b_{\mathrm{Y}}},\mathsf{Y}_{\breve{\tau}_{a_{\mathrm{Y}},b_{\mathrm{Y}}}}}(t, b_{\mathrm{Y}}), \tag{4.29}$$

for almost $t \geq 0$ (with respect to the Lebesgue measure), where $f_{\breve{\tau}_{a_{\mathrm{Y}},b_{\mathrm{Y}}},\mathsf{Y}_{\breve{\tau}_{a_{\mathrm{Y}},b_{\mathrm{Y}}}}}$ is a joint PDF of two random variables: the exit time $\breve{\tau}_{a_{\mathrm{Y}},b_{\mathrm{Y}}}$ and the exit barrier $\mathsf{Y}_{\breve{\tau}_{a_{\mathrm{Y}},b_{\mathrm{Y}}}}$. The values of $f_{\breve{\tau}_{a_{\mathrm{Y}},b_{\mathrm{Y}}},\mathsf{Y}_{\breve{\tau}_{a_{\mathrm{Y}},b_{\mathrm{Y}}}}}(t, a_{\mathrm{Y}})$ and $f_{\breve{\tau}_{a_{\mathrm{Y}},b_{\mathrm{Y}}},\mathsf{Y}_{\breve{\tau}_{a_{\mathrm{Y}},b_{\mathrm{Y}}}}}(t, b_{\mathrm{Y}})$ equal the right side of (4.17) and (4.18), respectively, with the following substitutions:

$$a = \frac{a_{\mathrm{Y}} - g(0)}{|\sigma|} \tag{4.30}$$

$$b = \frac{b_{\mathrm{Y}} - g(0)}{|\sigma|} \tag{4.31}$$

$$\widetilde{h}(t) = \frac{g(t) - g(0)}{|\sigma|}. \tag{4.32}$$

This solution reduces the problem to the case that we have already solved, the case of Brownian motion with drift.

The proof of (4.29) proceeds as follows. We write $\breve{\tau}_{a_{\mathrm{Y}},b_{\mathrm{Y}}}$ as

$$\begin{aligned}
\breve{\tau}_{a_{\mathrm{Y}},b_{\mathrm{Y}}} &= \inf\left\{t \geq 0 : \sigma\mathsf{B}_t + g(t) \geq b_{\mathrm{Y}} \text{ or } \sigma\mathsf{B}_t + g(t) \leq a_{\mathrm{Y}}\right\} \\
&= \inf\left\{t \geq 0 : \frac{\sigma}{|\sigma|}\mathsf{B}_t + \widetilde{h}(t) \geq b \text{ or } \frac{\sigma}{|\sigma|}\mathsf{B}_t + \widetilde{h}(t) \leq a\right\}
\end{aligned}$$

(subtract by $g(0)$ and divide by $|\sigma|$),

where a, b, and $\widetilde{h}(t)$ are defined in (4.30)–(4.32). The value of $\frac{\sigma}{|\sigma|}$ is 1 or -1, implying that $\frac{\sigma}{|\sigma|}\mathsf{B}_t$ is a standard Brownian motion. Hence, $\breve{\tau}_{a_{\mathrm{Y}},b_{\mathrm{Y}}}$ has the same distribution as the distribution of the first passage time for the barriers and the drift that appear in (4.30)–(4.32).

A Constant Barrier

Consider the following first-passage-time problem. Let $\widetilde{\mathsf{X}}_t = \mathsf{B}_t + \widetilde{h}(t)$, where $\widetilde{h}$ is an accelerating drift and $\widetilde{h}(0) = 0$. Let $\widetilde{\tau}_\eta$ denote the first time that random process $\widetilde{\mathsf{X}}_t$

crosses a constant barrier at η:

$$\tilde{\tau}_\eta = \inf\left\{ t \geq 0 : \widetilde{\mathsf{X}}_t = \eta \right\},$$

where η is a non-zero constant.[2] The goal is to obtain the probability distribution of $\tilde{\tau}_\eta$.

Before we provide the solution and the proof for this first-passage-time problem, we discuss the key ideas in the proof. This problem can be reduced to the problem of two constant barriers by using the following observations. A constant barrier at η is equivalent to two constant barriers: one at η; and the other at $-\infty$ if $\eta > 0$ or at ∞ if $\eta < 0$. Since the barriers a and b in the formulation of our problem in Section 4.2.1 must be finite, we set a to be a large negative number for $\eta > 0$ or set b to be a large positive number for $\eta < 0$. This observation suggests that the first-passage-time distribution in Section 4.2.1 can be adapted with appropriate values of a and b for the one-constant-barrier problem. The essence of our solution is to quantify the magnitude of a and b that achieve the desired level of accuracy.

Our solution to the first-passage-time problem is as follows. Let $0 < \delta < 1$ and $T_{\max} > 0$ be given. If $\eta > 0$ and if

$$a \leq \inf_{0 \leq s \leq T_{\max}} \widetilde{h}(s) - \sqrt{2T_{\max} \ln \frac{1}{\delta}} \qquad (4.33a)$$

$$b = \eta, \qquad (4.33b)$$

then the CDF of $\widetilde{\tau}_{a,b}$ obtained from the solution in Section 4.2.2 satisfies

$$\left| \mathbb{P}\left\{ \widetilde{\tau}_{a,b} \leq t \right\} - \mathbb{P}\left\{ \tilde{\tau}_\eta \leq t \right\} \right| \leq \delta, \qquad (4.34)$$

---

[2]The case that $\eta = 0$ is trivial because $\tilde{\tau}_0$ is identically zero.

for every $0 < t \leq T_{\max}$. In another case of η, if $\eta < 0$ and if

$$a = \eta \tag{4.35a}$$

$$b \geq \sup_{0 \leq s \leq T_{\max}} \widetilde{h}(s) + \sqrt{2T_{\max} \ln \frac{1}{\delta}}, \tag{4.35b}$$

then the CDF of $\widetilde{\tau}_{a,b}$ obtained from the solution in Section 4.2.2 is close to the CDF of $\widetilde{\tau}_{\eta}$

$$|\mathbb{P}\left\{\widetilde{\tau}_{a,b} \leq t\right\} - \mathbb{P}\left\{\widetilde{\tau}_{\eta} \leq t\right\}| \leq \delta, \tag{4.36}$$

for every $0 < t \leq T_{\max}$. See Section 4.2.5 for a proof of the above statements. Hence, the CDF of $\widetilde{\tau}_{a,b}$ can be used to approximate the CDF of $\widetilde{\tau}_{\eta}$ at a desired level δ of accuracy.

A Moving Barrier

Consider the following first-passage-time problem. Let τ denote the first time that Brownian motion crosses a moving barrier:

$$\tau = \inf\left\{t \geq 0 : \mathsf{B}_t = p(t)\right\},$$

where $p(0) \neq 0$ and p is an accelerating drift. The goal is to obtain the probability distribution of τ.

A solution to this first-passage-time problem is to rewrite the expression of τ and reduce the problem to a case that we can solve, i.e.,

$$\tau = \inf\left\{t \geq 0 : \mathsf{B}_t + \widetilde{h}(t) = \eta\right\},$$

where $\widetilde{h}(t) = -p(t) + p(0)$ and $\eta = p(0)$. Thus, we effectively reduce the problem to the case of Brownian motion with drift and one constant barrier, the case that we just solved (see "A Constant Barrier" on page 83).

85

4.2.4 Elementary Examples

We consider two sets of examples. The first set covers Brownian motion with quadratic drift and two-sided boundary; and Brownian motion and a moving square-root barrier. For this set of examples, we obtain the PDFs using the methodology developed in Section 4.2.2 (see also "A Moving Barrier" on page 85). Then the solutions of these first-passage-time distributions are obtained using alternative methods in Section 4.1.2 and [77]. The results from Section 4.2.2 and the results from the alternative methods agree, thus verifying our approach.

The second set covers drifts that are not well-studied in literature but are important elementary functions. The second set of examples show that our method can solve first-passage-time problems that involve drifts such as polynomial, sinusoidal, logarithmic, and exponential functions. For this set of examples, the first-passage-time distributions have the shapes that match intuition and, as expected, integrate to one. The examples from the first and second sets are organized in subsections: one subsection for each example.

Quadratic Drift

Here, we obtain the PDFs of first passage time of Brownian motion with quadratic drift using our method in Section 4.2.2. For illustration, we consider $\widetilde{h}(t) = t + \frac{1}{10}t^2$ for the drift and $a = -1$ and $b = 2$ for the boundary (see Fig. 4-4a). Then, we verify that PDFs are consistent with the PDFs obtained by an alternative method described in Section 4.1.2.

To obtain the PDFs, we use the results in Section 4.2.2 and the methodology in Section 4.2.3 to select key parameters (see "Values of $\widetilde{c}$, ε, g_a, and g_b" on page 79). We set $\widetilde{c} = -2a\breve{\mu}$ to shift the exponent (see (4.19)) and set $d = 10^{-8}$ to control the numerical error (see (4.27a) and (4.27b)). We obtain the joint PDFs and sum them to form the marginal PDF in Fig. 4-4b.

We also superimpose the PDF of the first-passage-time using the alternative method of Section 4.1.2. The results that are obtained by the methods in Section 4.2.2

and Section 4.1.2 agree, as can be observed in Fig. 4-4b. This good agreement shows that the method in Section 4.2.2 is general and can be used to solve several first-passage-time problems.

Square-Root Barrier

Here, we obtain the PDFs of the first passage time of standard Brownian motion (without drift) and a moving boundary using our method described in "A Moving Barrier" (page 85). In particular, let τ denote the first time that standard Brownian motion (without drift) crosses a moving square-root barrier,

$$\tau = \inf \left\{ t \geq 0 : \mathsf{B}_t = \tilde{a} + \tilde{b}\sqrt{t + \tilde{c}} \right\},$$

for $\tilde{c} \geq 0$ and $\tilde{a} + \tilde{b}\sqrt{\tilde{c}} > 0$. For illustration, we consider $\tilde{a} = 0$, $\tilde{b} = 1$, and $\tilde{c} = 1$ (see Fig. 4-5a). Then, we verify that the PDF is consistent with the PDF obtained by an alternative method of [77].

To obtain the PDF, we follow the approach in "A Moving Barrier" (page 85). We rewrite the expression of τ, arriving at Brownian motion with drift and one constant barrier:

$$\tau = \inf \left\{ t \geq 0 : \mathsf{B}_t + \widetilde{h}(t) = b \right\},$$

where $\widetilde{h}(t) = \tilde{b}\sqrt{\tilde{c}} - \tilde{b}\sqrt{t + \tilde{c}}$ and $b = \tilde{a} + \tilde{b}\sqrt{\tilde{c}}$. The CDF of τ is given by the CDF of $\widetilde{\tau}_{a,b}$, where

$$\widetilde{\tau}_{a,b} = \inf \left\{ t \geq 0 : \mathsf{B}_t + \widetilde{h}(t) \notin (a, b) \right\}$$

and $a = -30$. Per a discussion in "A Constant Barrier" (page 83), this choice of a guarantees that the difference between these CDFs is smaller than 10^{-17} for $0 \leq t \leq T_{\max} = 5$ (see (4.34)). For consistency with other figures, we plot the PDF instead of the CDF. The PDF of $\widetilde{\tau}_{a,b}$ is shown in Fig. 4-5b.

To verify our results, we plot the probability distribution using the alternative
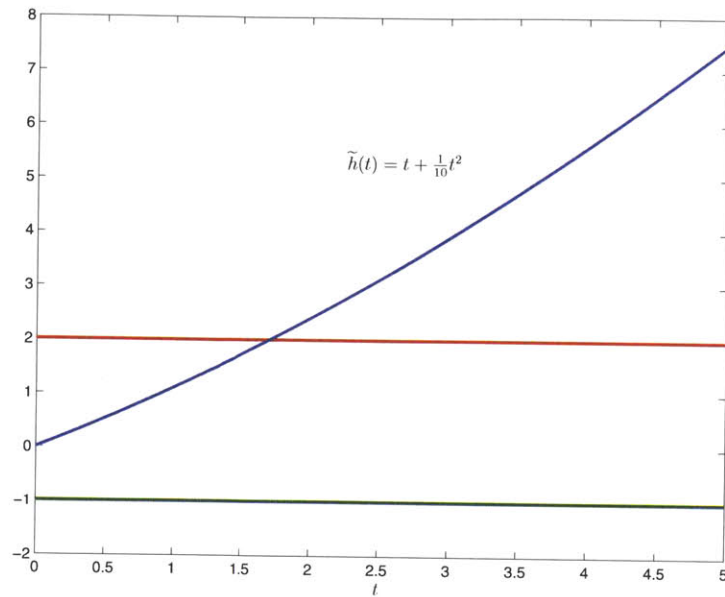
(a) boundaries at $a = -1$ and $b = 2$
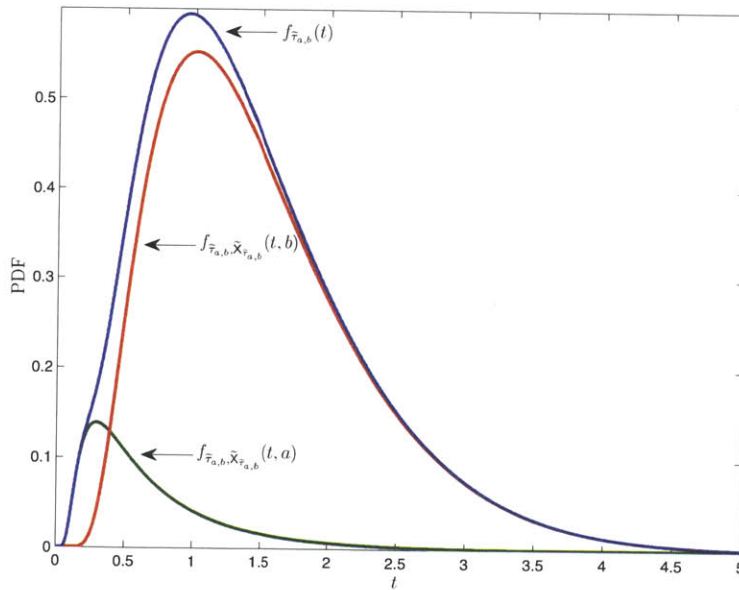
(b) PDFs

Figure 4-4: The PDFs for a quadratic drift from two of our methods (Section 4.1.2 and Section 4.2.2) are consistent with each other (drift $\widetilde{h}(t) = t + \frac{1}{10}t^2$ and the boundaries $a = -1$ and $b = 2$).

method of [77]. The probability distributions from our method and the alternative method appear in Fig. 4-5b. The probability distributions from these two methods agree.

Cubic Drift

Consider $\widetilde{h}(t) = t^3$ and the boundary at $a = -1$ and $b = 1$ (see Fig. 4-6a). For this drift, the supremum norm $\sup_{s \geq 0} |\widetilde{h}''(s)|$ is infinite, implying that we select a range $0 < t \leq t_{\max}$ to plot the first-passage-timedistribution. We set $t_{\max} = 1.65$, which is large enough so that the PDF approximately integrates to one for $0 < t < t_{\max}$.[3] We define $\widetilde{c}$ to equal the right side of (4.20): $\widetilde{c} = -6at_{\max}$. The joint and marginal PDFs are shown in Fig. 4-6b.

The probability distributions match our intuition (see Fig. 4-6b). When t is small, the joint PDFs $f_{\widetilde{\tau}_{a,b}, \mathsf{X}_{\widetilde{\tau}_{a,b}}}(t, a)$ and $f_{\widetilde{\tau}_{a,b}, \mathsf{X}_{\widetilde{\tau}_{a,b}}}(t, b)$ are approximately equal, meaning that the process is equally likely to cross barriers a and b at small t. This characteristic is intuitive and arises from symmetry of the barriers (i.e., $|a| = b$) and from the cubic drift, which equals approximately zero at small t. As t increases, the joint PDFs rise and decay, with the peak of $f_{\widetilde{\tau}_{a,b}, \mathsf{X}_{\widetilde{\tau}_{a,b}}}(\cdot, b)$ occurring at a later time than the peak of $f_{\widetilde{\tau}_{a,b}, \mathsf{X}_{\widetilde{\tau}_{a,b}}}(\cdot, a)$. The characteristic of the peaks is intuitive: as the drift moves away from barrier a, the process is less likely to cross barrier a at large t. The marginal PDF is obtained by summing the two joint PDFs.

Sinusoidal Drift

Consider $\widetilde{h}(t) = \sin t$ and the boundary at $a = -1$ and $b = \frac{3}{2}$ (see Fig. 4-7a). For this drift, the supremum norm $\sup_{s \geq 0} |\widetilde{h}''(s)|$ is finite so we let $\widetilde{c}$ equal the right side of (4.19): $\widetilde{c} = -a$. The joint and marginal PDFs are shown in Fig. 4-7b.

The probability distributions match our intuition (see Fig. 4-7b). When t is small, the joint PDF $f_{\widetilde{\tau}_{a,b}, \mathsf{X}_{\widetilde{\tau}_{a,b}}}(t, a)$ is larger than the joint PDF $f_{\widetilde{\tau}_{a,b}, \mathsf{X}_{\widetilde{\tau}_{a,b}}}(t, b)$, meaning that the process is more likely to cross barrier a than barrier b. This characteristic is

---

[3]That is, we select $t_{\max} = 1.65$, plot the PDF for $0 < t < t_{\max}$, and verify that an area under the PDF is approximately one.
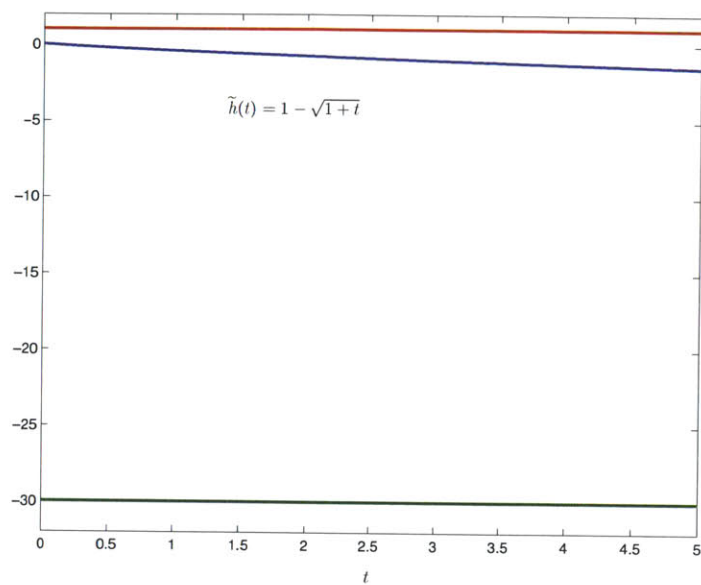
(a) boundaries at $a = -30$ and $b = 1$
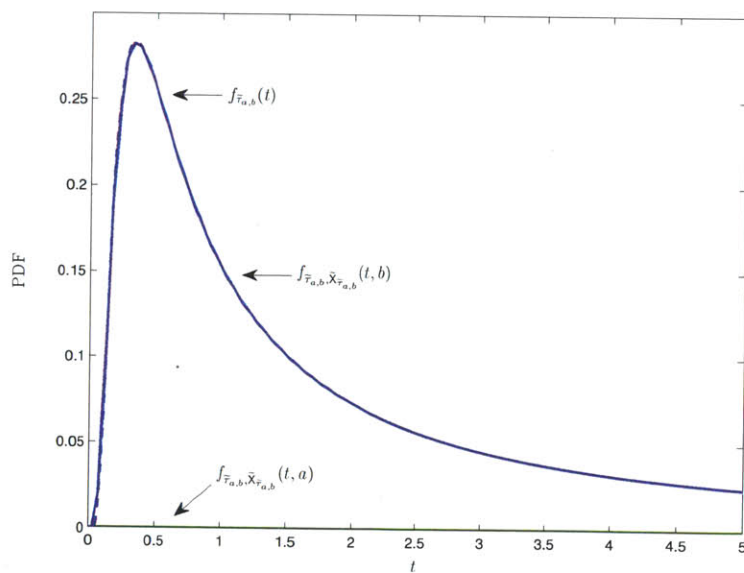
(b) PDFs

Figure 4-5: The PDF for a square-root drift matches the PDF obtained from existing work, which uses a different method (drift $\widetilde{h}(t) = 1 - \sqrt{1+t}$ and the boundaries $a = -30$ and $b = 1$).
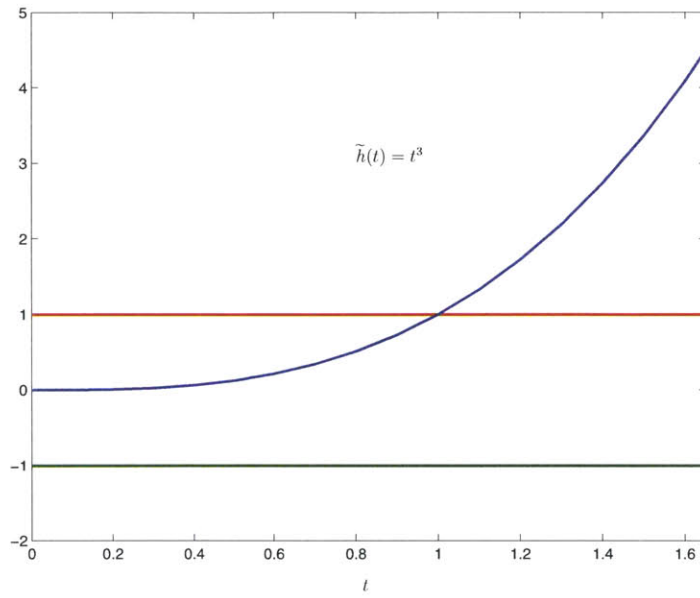
(a) boundaries at $a = -1$ and $b = 1$
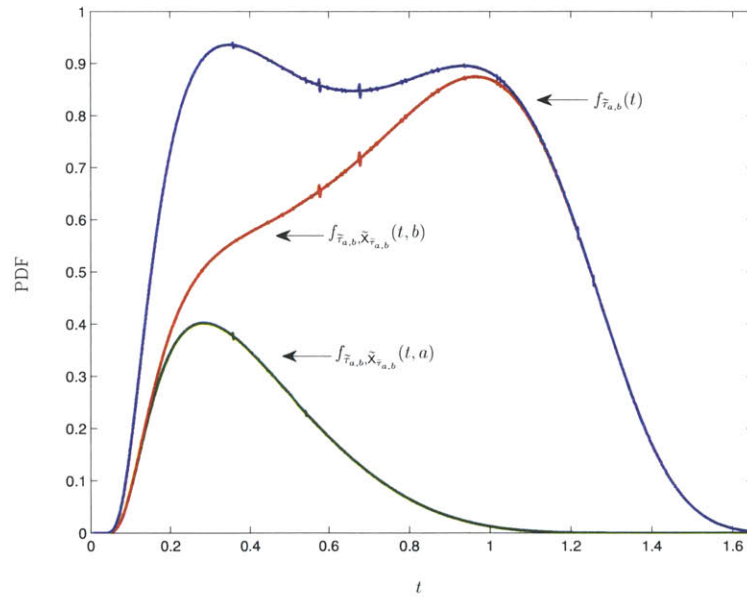
(b) PDFs

Figure 4-6: The PDF for a polynomial drift matches intuition (drift $\widetilde{h}(t) = t^3$ and the boundaries $a = -1$ and $b = 1$).

91
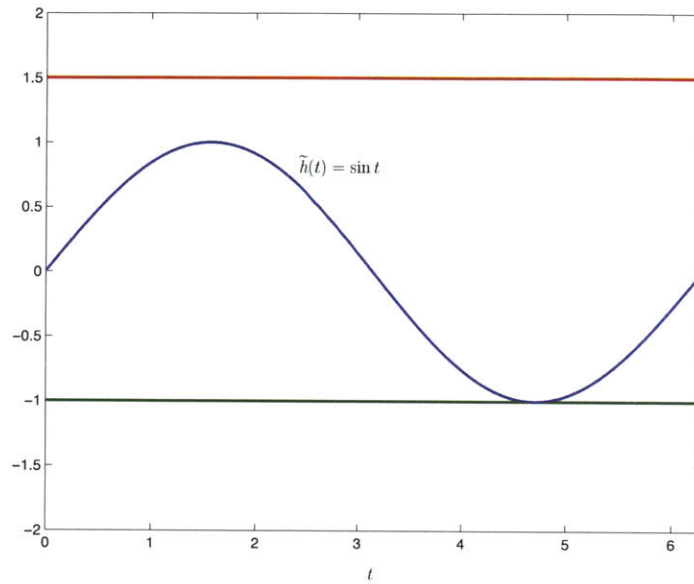
(a) boundaries at $a = -1$ and $b = \frac{3}{2}$
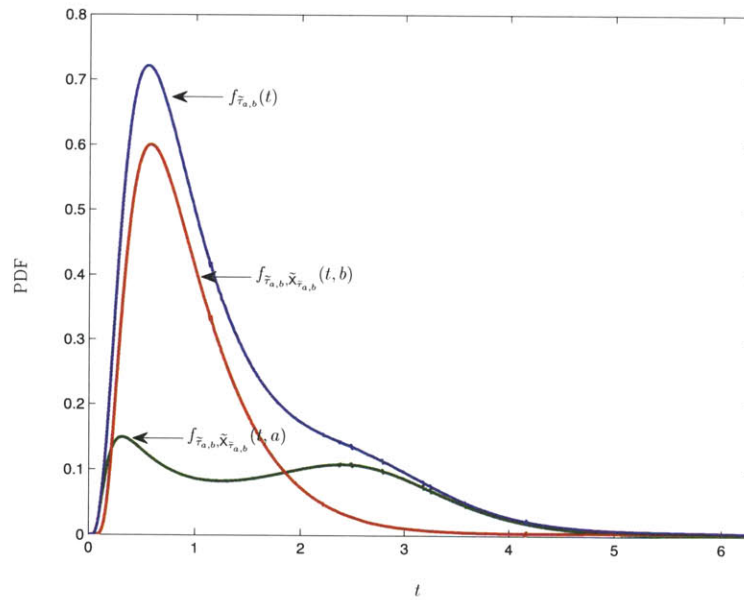
(b) PDFs

Figure 4-7: The PDF for a sinusoidal drift matches intuition (drift $\widetilde{h}(t) = \sin t$ and the boundaries $a = -1$ and $b = \frac{3}{2}$).

intuitive and arises from the fact that the initial location of the process (i.e., zero) is closer to barrier a than to barrier b. The joint PDF $f_{\widetilde{\tau}_{a,b}, \widetilde{X}_{\widetilde{\tau}_{a,b}}}(\cdot, a)$ consists of two visible peaks, while the joint PDF $f_{\widetilde{\tau}_{a,b}, \widetilde{X}_{\widetilde{\tau}_{a,b}}}(\cdot, b)$ consists of one. Appearances of these peaks are intuitive: two peaks because the drift approximates zero at small t and moves toward barrier a at a later time; one peak because the drift moves toward barrier b and by the time it moves toward and touches barrier a, the random process most likely exited the boundary, eliminating remaining peaks. The marginal PDF is obtained by summing the two joint PDFs.

Logarithmic Drift

Consider $\widetilde{h}(t) = \ln(t+1)$ and the boundary at $a = -2$ and $b = 1$ (see Fig. 4-8a). For this drift, the supremum norm $\sup_{s \geq 0} |\widetilde{h}''(s)|$ is finite, and we set $\widetilde{c}$ to equal the right side of (4.19): $\widetilde{c} = b$. The joint and marginal PDFs are shown in Fig. 4-8b.

The PDFs match our intuition. The joint PDF $f_{\widetilde{\tau}_{a,b}, \widetilde{X}_{\widetilde{\tau}_{a,b}}}(t, b)$ is larger than the joint PDF $f_{\widetilde{\tau}_{a,b}, \widetilde{X}_{\widetilde{\tau}_{a,b}}}(t, a)$, meaning that the process is more likely to cross barrier b than barrier a. This characteristic is intuitive and arises because the initial position of the process (i.e., zero) is closer to barrier b than to barrier a is and because the drift moves away from barrier a. The marginal PDF is obtained by summing the two joint PDFs.

Exponential Drift

Consider $\widetilde{h}(t) = 1 - e^t$ and the boundary at $a = -2$ and $b = 1/2$ (see Fig. 4-9a). For this drift, the supremum norm $\sup_{s \geq 0} |\widetilde{h}''(s)|$ is infinite, implying that we select a range $0 < t \leq t_{\max}$ to plot the probability distributions. For illustration, we select $t_{\max} = 2$. We define $\widetilde{c}$ to equal the right side of (4.20): $\widetilde{c} = be^{t_{\max}}$. The joint and marginal PDFs are shown in Fig. 4-9b.

The PDFs match our intuition. When t is small, the joint PDF $f_{\widetilde{\tau}_{a,b}, \widetilde{X}_{\widetilde{\tau}_{a,b}}}(t, b)$ is larger than the joint PDF $f_{\widetilde{\tau}_{a,b}, \widetilde{X}_{\widetilde{\tau}_{a,b}}}(t, a)$, meaning that the process is more likely to cross barrier b than barrier a. This characteristic is intuitive and arises because barrier b is closer to zero than barrier a is. The joint PDFs rise and decay, with the
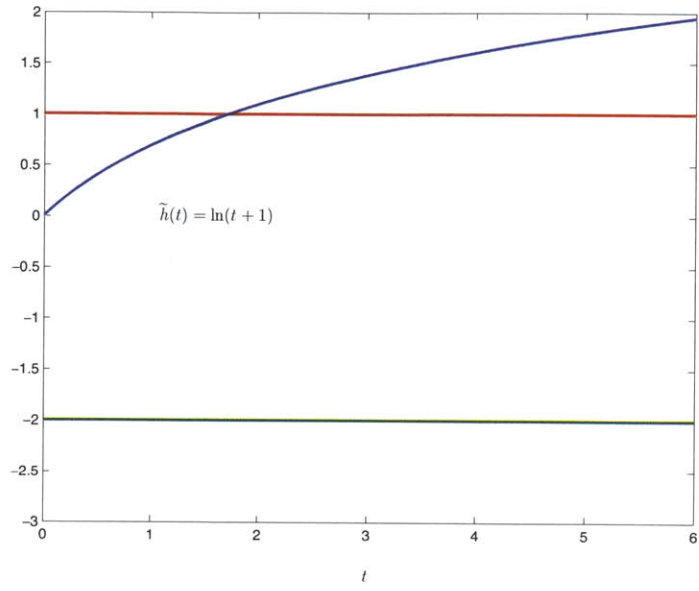
(a) boundaries at $a = -2$ and $b = 1$
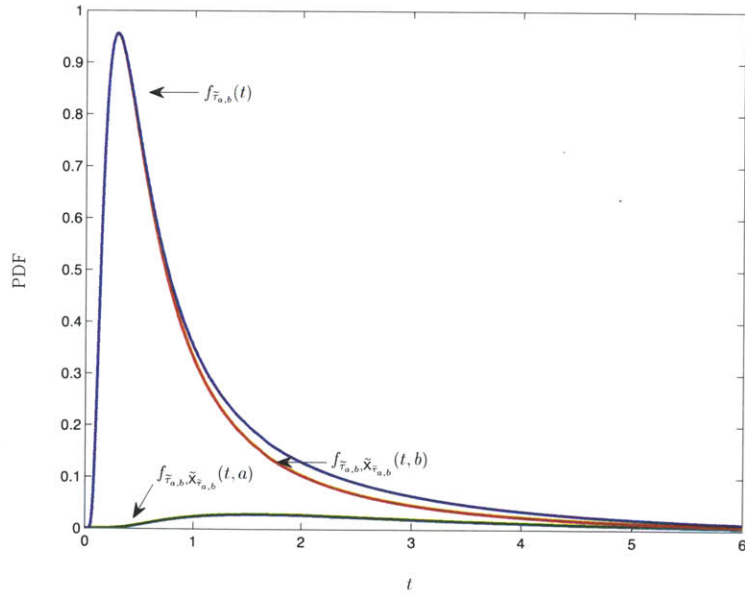
(b) PDFs

Figure 4-8: The PDF for a logarithmic drift matches intuition (drift $\widetilde{h}(t) = \ln(t+1)$ and the boundaries $a = -2$ and $b = 1$).

94
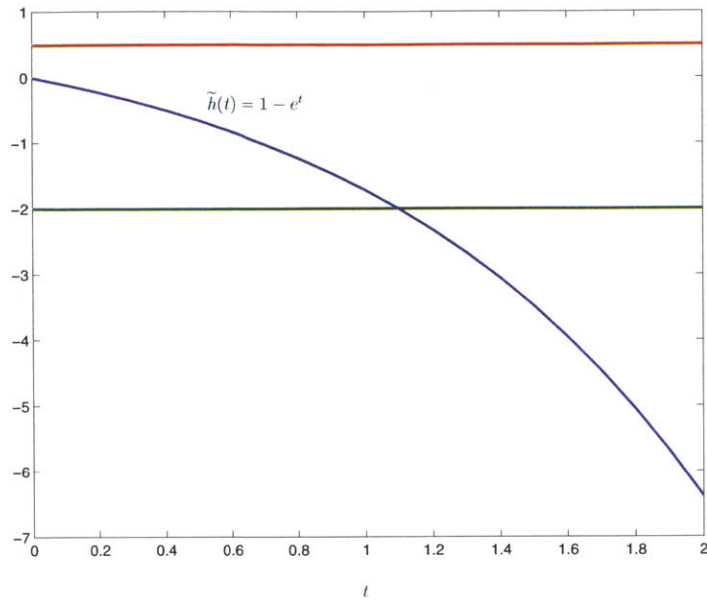
(a) boundaries at $a = -2$ and $b = 1/2$
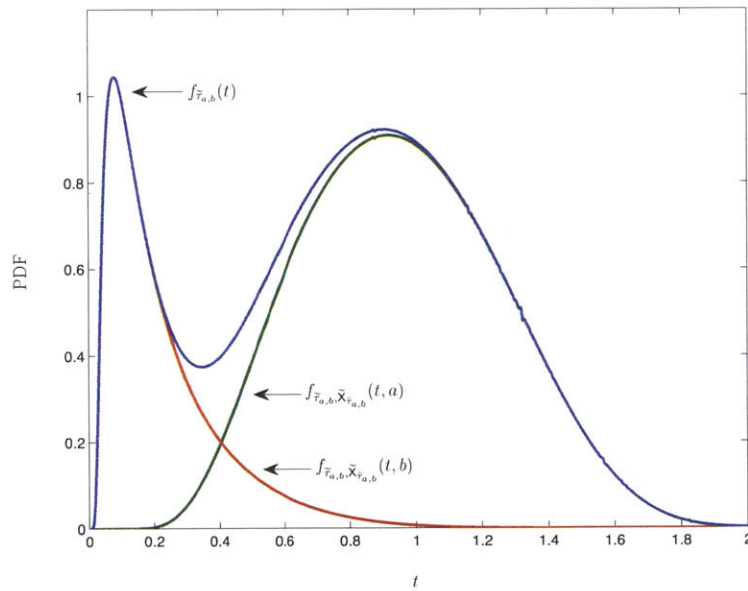
(b) PDFs

Figure 4-9: The PDF for an exponential drift matches intuition (drift $\widetilde{h}(t) = 1 - e^t$ and the boundaries $a = -2$ and $b = 1/2$).

Table 4.1: The proof of the main theorem consists of ten steps

Step	Name
1	Transformation of the probability measure
2	Martingale property
3	A consequence of the transformation
4	A simplification
5	A consequence of the martingale property
6	Substitution of $Z_{T_{a,b}}$
7	Integration forms and the derivatives
8	An adjustment to the exponent
9	Integration transform
10	Relating the expectations to the IBVPs

peak of $f_{\widetilde{\tau}_{a,b},\widetilde{X}_{\widetilde{\tau}_{a,b}}}(\cdot, b)$ occurs earlier than the peak of $f_{\widetilde{\tau}_{a,b},\widetilde{X}_{\widetilde{\tau}_{a,b}}}(\cdot, a)$. This characteristic of the peaks occurs because the drift moves away from barrier b. The marginal PDF is obtained by summing the two joint PDFs.

4.2.5 Proofs of the Key Theorems

Examples in the previous section show that the PDFs match known results, agree with intuition, and can be obtained using numerical and analytical methods. In this section, we prove that the expressions for the PDFs and the bounds in our numerical methods are correct. We begin with the most important proof for this section, the proof for the expressions of the PDFs.

Proof of the First-Passage-Time Distribution

The proof for the first-passage-time distribution, which appears in Section 4.2.2, is organized in ten steps as shown in Table 4.1. The key idea in the proof is to use various transformation techniques.

Step 1: Transformation of the probability measure

Let $\widetilde{B}_t = B_t - \widetilde{h}(t)$. By the Cameron-Martin-Girsanov Theorem [63, Thm. 5.1, p. 191], $\widetilde{B}_t$ is a standard Brownian motion with respect to the probability space

$(\Omega, \mathcal{F}_\infty, \widetilde{\mathbb{P}})$, where $\mathcal{F}_\infty$ is the σ-algebra generated by $\{\mathsf{B}_u : 0 \leq u\}$ and $\widetilde{\mathbb{P}}$ is the probability measure defined to be [63, Cor. 5.2, p. 192]

$$\widetilde{\mathbb{P}}(\mathcal{E}) = \mathbb{E}\left\{1_\mathcal{E} \mathsf{Z}_t\right\}, \qquad \text{for every } t \geq 0 \text{ and every } \mathcal{E} \in \mathcal{F}_t. \tag{4.37}$$

In (4.37), $\mathcal{F}_t$ is the σ-algebra generated by $\{\mathsf{B}_u : 0 \leq u \leq t\}$; $\mathbb{E}\{\cdot\}$ is the expectation with respect to $\mathbb{P}$; and

$$\mathsf{Z}_t = e^{\int_0^t \widetilde{h}'(u)d\mathsf{B}_u - \frac{1}{2}\int_0^t |\widetilde{h}'(u)|^2 du} \tag{4.38}$$

is an $\mathcal{F}_t$-martingale, which will be shown in the next step.

Step 2: Martingale property

Random process Z_t is an $\mathcal{F}_t$-martingale. This can be verified directly by using the definition of a martingale: for $0 \leq s \leq t$,

$$\begin{aligned}
\mathbb{E}\left\{\mathsf{Z}_t \mid \mathcal{F}_s\right\} &= e^{\int_0^s \widetilde{h}'(u)d\mathsf{B}_u - \frac{1}{2}\int_0^t |\widetilde{h}'(u)|^2 du} \mathbb{E}\left\{e^{\int_s^t \widetilde{h}'(u)d\mathsf{B}_u} \mid \mathcal{F}_s\right\} && \text{(measurability with respect to } \mathcal{F}_s) \\
&= e^{\int_0^s \widetilde{h}'(u)d\mathsf{B}_u - \frac{1}{2}\int_0^t |\widetilde{h}'(u)|^2 du} \mathbb{E}\left\{e^{\int_s^t \widetilde{h}'(u)d\mathsf{B}_u}\right\} && \text{(independence of } \mathcal{F}_s) \\
&= e^{\int_0^s \widetilde{h}'(u)d\mathsf{B}_u - \frac{1}{2}\int_0^t |\widetilde{h}'(u)|^2 du} e^{\frac{1}{2}\int_s^t |\widetilde{h}'(u)|^2 du}
\end{aligned}$$

$$\text{(a zero-mean normal random variable with variance } \frac{1}{2}\int_s^t |\widetilde{h}'(u)|^2 du)$$

$$= \mathsf{Z}_s.$$

Alternatively, we can verify the Novikov condition [63, p. 199, Cor. 5.13], which also shows that Z_t is a martingale.

Step 3: A consequence of the transformation

Recall that under measure $\widetilde{\mathbb{P}}$, process $\widetilde{\mathsf{B}}_t + \widetilde{h}(t) = \mathsf{B}_t$, is a Brownian motion with drift $\widetilde{h}(t)$. Thus, random processes $\widetilde{\mathsf{X}}_t$ under measure $\mathbb{P}$ plays a similar role to random process B_t under measure $\widetilde{\mathbb{P}}$. This similarity is a basis of the next portion of our proof.

The similarity between random processes $\widetilde{\mathsf{X}}_t$ and B_t has an implication for the

first passage times that they generate. Let

$$\mathsf{T}_{a,b} = \inf\left\{t \geq 0 : \mathsf{B}_t \notin (a,b)\right\}.$$

The similarity between $(\widetilde{\mathsf{X}}_t, \widetilde{\tau}_{a,b})$ under measure $\mathbb{P}$ and $(\mathsf{B}_t, \mathsf{T}_{a,b})$ under measure $\widetilde{\mathbb{P}}$ implies that

$$\mathbb{P}\left\{\widetilde{\tau}_{a,b} \leq t \text{ and } \widetilde{\mathsf{X}}_{\tau_{a,b}} = a\right\} = \widetilde{\mathbb{P}}\{\mathsf{T}_{a,b} \leq t \text{ and } \mathsf{B}_{\mathsf{T}_{a,b}} = a\} \text{ and} \qquad (4.39)$$

$$\mathbb{P}\left\{\widetilde{\tau}_{a,b} \leq t \text{ and } \widetilde{\mathsf{X}}_{\tau_{a,b}} = b\right\} = \widetilde{\mathbb{P}}\{\mathsf{T}_{a,b} \leq t \text{ and } \mathsf{B}_{\mathsf{T}_{a,b}} = b\}. \qquad (4.40)$$

The left side is the joint density that we wish to obtain.

Step 4: A simplification

Let $x \wedge y$ denote the minimum between x and y. Equation (4.39) simplifies to

$$\mathbb{P}\left\{\widetilde{\tau}_{a,b} \leq t \text{ and } \widetilde{\mathsf{X}}_{\tau_{a,b}} = a\right\}$$

$$= \mathbb{E}\left\{1_{\left\{\mathsf{T}_{a,b} \leq t \text{ and } \mathsf{B}_{\mathsf{T}_{a,b}} = a\right\}} \mathsf{Z}_t\right\}$$

$$\text{(use of (4.37) with } \mathcal{E} = \{\mathsf{T}_{a,b} \leq t \text{ and } \mathsf{B}_{\mathsf{T}_{a,b}} = a\}) \qquad (4.41)$$

$$= \mathbb{E}\left\{\mathbb{E}\left\{1_{\left\{\mathsf{T}_{a,b} \leq t \text{ and } \mathsf{B}_{\mathsf{T}_{a,b}} = a\right\}} \mathsf{Z}_t \,\Big|\, \mathcal{F}_{t \wedge \mathsf{T}_{a,b}}\right\}\right\}$$

$$\text{(Law of iterated expectation)}$$

$$= \mathbb{E}\left\{1_{\left\{\mathsf{T}_{a,b} \leq t \text{ and } \mathsf{B}_{\mathsf{T}_{a,b}} = a\right\}} \mathbb{E}\left\{\mathsf{Z}_t \,|\, \mathcal{F}_{t \wedge \mathsf{T}_{a,b}}\right\}\right\}$$

$$(\mathcal{F}_{t \wedge \mathsf{T}_{a,b}}\text{-measurable}). \qquad (4.42)$$

Similarly, (4.40) simplifies to

$$\mathbb{P}\left\{\widetilde{\tau}_{a,b} \leq t \text{ and } \widetilde{\mathsf{X}}_{\tau_{a,b}} = b\right\} = \mathbb{E}\left\{1_{\left\{\mathsf{T}_{a,b} \leq t \text{ and } \mathsf{B}_{\mathsf{T}_{a,b}} = b\right\}} \mathbb{E}\left\{\mathsf{Z}_t \,|\, \mathcal{F}_{t \wedge \mathsf{T}_{a,b}}\right\}\right\}. \qquad (4.43)$$

The conditional expectation $\mathbb{E}\left\{\mathsf{Z}_t \,|\, \mathcal{F}_{t \wedge \mathsf{T}_{a,b}}\right\}$ can be evaluated explicitly using a martingale property of Z_t.

A consequence of the martingale property is that

$$\mathbb{E}\left\{Z_t \mid \mathcal{F}_{t \wedge T_{a,b}}\right\} = Z_{t \wedge T_{a,b}},$$

by the martingale stopping theorem [74, Thm. 3.3, p. 11], applied to a finite stopping time, $(t \wedge T_{a,b}) \leq t < \infty$. With the martingale property, the right sides of (4.42) and (4.43) can be further simplified.

Step 5: A consequence of the martingale property

Equation (4.42) simplifies to

$$\mathbb{P}\left\{\widetilde{\tau}_{a,b} \leq t \text{ and } \widetilde{\mathsf{X}}_{\tau_{a,b}} = a\right\}$$

$$= \mathbb{E}\left\{1_{\left\{T_{a,b} \leq t \text{ and } B_{T_{a,b}} = a\right\}} Z_{t \wedge T_{a,b}}\right\} \quad \text{(martingale property)}$$

$$= \mathbb{E}\left\{1_{\left\{T_{a,b} \leq t \text{ and } B_{T_{a,b}} = a\right\}} Z_{T_{a,b}}\right\} \quad (t \wedge T_{a,b} = T_{a,b} \text{ on the set } \{T_{a,b} \leq t\}).$$

$$(4.44)$$

Similarly, (4.43) simplifies to

$$\mathbb{P}\left\{\widetilde{\tau}_{a,b} \leq t \text{ and } \widetilde{\mathsf{X}}_{\tau_{a,b}} = b\right\} = \mathbb{E}\left\{1_{\left\{T_{a,b} \leq t \text{ and } B_{T_{a,b}} = b\right\}} Z_{T_{a,b}}\right\}. \quad (4.45)$$

Note that the expression in (4.44) is similar to the expression in (4.41) except that Z_t is replaced by $Z_{T_{a,b}}$. The replacement of t by $T_{a,b}$ is a transformation of time and requires several steps including an application of the martingale theory. In the next step, we substitute the expression of $Z_{T_{a,b}}$.

Step 6: Substitution of $Z_{T_{a,b}}$

The expression of Z_t in (4.38) involves a stochastic integration and is difficult to manipulate. To alleviate this difficulty, we apply Itô's formula or the stochastic integration-by-part formula [78, Thm. 4.1.5, p. 46], and transform Z_t into the Riemann

integration

$$Z_t = e^{\tilde{h}'(t)\mathsf{B}_t - \int_0^t \mathsf{B}_u \tilde{h}''(u)du - \frac{1}{2}\int_0^t |\tilde{h}'(u)|^2 du}.$$

A continuation of (4.44) gives us

$$\mathbb{P}\left\{\tilde{\tau}_{a,b} \leq t \text{ and } \widetilde{\mathsf{X}}_{\tau_{a,b}} = a\right\}$$

$$= \mathbb{E}\left\{\mathbb{E}\left\{1_{\left\{\mathsf{T}_{a,b}\leq t \text{ and } \mathsf{B}_{\mathsf{T}_{a,b}}=a\right\}} Z_{\mathsf{T}_{a,b}} \,\middle|\, \mathsf{T}_{a,b}\right\}\right\}$$

(Conditioning on $\mathsf{T}_{a,b}$ or equivalently on the σ-algebra generated by $\mathsf{T}_{a,b}$)

$$= \mathbb{E}\left\{\mathbb{E}\left\{1_{\left\{\mathsf{T}_{a,b}\leq t \text{ and } \mathsf{B}_{\mathsf{T}_{a,b}}=a\right\}} e^{\tilde{h}'(\mathsf{T}_{a,b})\mathsf{B}_{\mathsf{T}_{a,b}} - \int_0^{\mathsf{T}_{a,b}} \mathsf{B}_u \tilde{h}''(u)du - \frac{1}{2}\int_0^{\mathsf{T}_{a,b}} |\tilde{h}'(u)|^2 du} \,\middle|\, \mathsf{T}_{a,b}\right\}\right\}$$

(substituting the expression of $Z_{\mathsf{T}_{a,b}}$).

We further simplify the expression using these steps. First, we factor $1_{\left\{\mathsf{T}_{a,b}\leq t \text{ and } \mathsf{B}_{\mathsf{T}_{a,b}}=a\right\}} = 1_{\left\{\mathsf{T}_{a,b}\leq t\right\}} 1_{\left\{\mathsf{B}_{\mathsf{T}_{a,b}}=a\right\}}$. Then, we set $e^{\tilde{h}'(\mathsf{T}_{a,b})\mathsf{B}_{\mathsf{T}_{a,b}}} = e^{\tilde{h}'(\mathsf{T}_{a,b})a}$ because the expectation applies to the set $\left\{\mathsf{B}_{\mathsf{T}_{a,b}} = a\right\}$. Finally, we move the random variables that are functions of only $\mathsf{T}_{a,b}$ out of the conditional expectation. These steps result in

$$\mathbb{P}\left\{\tilde{\tau}_{a,b} \leq t \text{ and } \widetilde{\mathsf{X}}_{\tau_{a,b}} = a\right\}$$
$$= \mathbb{E}\left\{1_{\left\{\mathsf{T}_{a,b}\leq t\right\}} e^{\tilde{h}'(\mathsf{T}_{a,b})a - \frac{1}{2}\int_0^{\mathsf{T}_{a,b}} |\tilde{h}'(u)|^2 du} \mathbb{E}\left\{1_{\left\{\mathsf{B}_{\mathsf{T}_{a,b}}=a\right\}} e^{-\int_0^{\mathsf{T}_{a,b}} \mathsf{B}_u \tilde{h}''(u)du} \,\middle|\, \mathsf{T}_{a,b}\right\}\right\}. \quad (4.46)$$

Similarly, a continuation of (4.45) gives us

$$\mathbb{P}\left\{\tilde{\tau}_{a,b} \leq t \text{ and } \widetilde{\mathsf{X}}_{\tau_{a,b}} = b\right\}$$
$$= \mathbb{E}\left\{1_{\left\{\mathsf{T}_{a,b}\leq t\right\}} e^{\tilde{h}'(\mathsf{T}_{a,b})b - \frac{1}{2}\int_0^{\mathsf{T}_{a,b}} |\tilde{h}'(u)|^2 du} \mathbb{E}\left\{1_{\left\{\mathsf{B}_{\mathsf{T}_{a,b}}=b\right\}} e^{-\int_0^{\mathsf{T}_{a,b}} \mathsf{B}_u \tilde{h}''(u)du} \,\middle|\, \mathsf{T}_{a,b}\right\}\right\}. \quad (4.47)$$

Step 7: Integration forms and the derivatives

The conditional expectations are functions of $\mathsf{T}_{a,b}$ [35, p. 20] [38, p. 340], and so are the random variables outside the conditional expectations. As a consequence, we

100

can write the expectations in terms of the integrations and the PDF of $\mathsf{T}_{a,b}$.

Let $f_{\mathsf{T}_{a,b}}$ denote the PDF of $\mathsf{T}_{a,b}$, i.e., $f_{\mathsf{T}_{a,b}}(v) = \frac{d}{dv}\mathbb{P}\left\{\mathsf{T}_{a,b} \leq v\right\}$. We write (4.46) as

$$\mathbb{P}\left\{\widetilde{\tau}_{a,b} \leq t \text{ and } \widetilde{\mathsf{X}}_{\tau_{a,b}} = a\right\}$$
$$= \int_0^t e^{\widetilde{h}'(v)a - \frac{1}{2}\int_0^v |\widetilde{h}'(u)|^2 du} \,\mathbb{E}\left\{1_{\left\{\mathsf{B}_{\mathsf{T}_{a,b}} = a\right\}} e^{-\int_0^{\mathsf{T}_{a,b}} \mathsf{B}_u \widetilde{h}''(u) du} \;\middle|\; \mathsf{T}_{a,b} = v\right\} f_{\mathsf{T}_{a,b}}(v) dv.$$

Taking the derivative with respect to t, we have the joint PDF

$$f_{\widetilde{\tau}_{a,b}, \widetilde{\mathsf{X}}_{\widetilde{\tau}_{a,b}}}(t, a) = e^{a\widetilde{h}'(t) - \frac{1}{2}\int_0^t |\widetilde{h}'(u)|^2 du}\,\mathbb{E}\left\{1_{\left\{\mathsf{B}_{\mathsf{T}_{a,b}} = a\right\}} e^{-\int_0^{\mathsf{T}_{a,b}} \mathsf{B}_u \widetilde{h}''(u) du} \;\middle|\; \mathsf{T}_{a,b} = t\right\} f_{\mathsf{T}_{a,b}}(t),$$

(4.48)

for almost everywhere (a.e.) for $t > 0$ by Lebesgue's differentiation theorem [38, Thm. 7.2.1, p. 228]. Similarly, a continuation of (4.47) gives us the joint PDF

$$f_{\widetilde{\tau}_{a,b}, \widetilde{\mathsf{X}}_{\widetilde{\tau}_{a,b}}}(t, b) = e^{b\widetilde{h}'(t) - \frac{1}{2}\int_0^t |\widetilde{h}'(u)|^2 du}\,\mathbb{E}\left\{1_{\left\{\mathsf{B}_{\mathsf{T}_{a,b}} = b\right\}} e^{-\int_0^{\mathsf{T}_{a,b}} \mathsf{B}_u \widetilde{h}''(u) du} \;\middle|\; \mathsf{T}_{a,b} = t\right\} f_{\mathsf{T}_{a,b}}(t),$$

(4.49)

a.e. for $t > 0$. It remains to characterize the conditional expectations.

Step 8: An adjustment to the exponent

To simply the proof, we make the exponent of e non-negative. In particular, we multiply the right side of (4.48) by $e^{\widetilde{c}t}e^{-\widetilde{c}t}$ and rearrange the expression, where $\widetilde{c}$ is defined as in Section 4.2.2. These steps give us

$$f_{\widetilde{\tau}_{a,b}, \widetilde{\mathsf{X}}_{\widetilde{\tau}_{a,b}}}(t, a) = e^{a\widetilde{h}'(t) - \frac{1}{2}\int_0^t |\widetilde{h}'(u)|^2 du + \widetilde{c}t}\,\mathbb{E}\left\{1_{\left\{\mathsf{B}_{\mathsf{T}_{a,b}} = a\right\}} e^{-\int_0^{\mathsf{T}_{a,b}} (\mathsf{B}_u \widetilde{h}''(u) + \widetilde{c}) du} \;\middle|\; \mathsf{T}_{a,b} = t\right\} f_{\mathsf{T}_{a,b}}(t).$$

(4.50)

By construction of $\widetilde{c}$, the exponent is now non-negative:

$$\mathsf{B}_u h''(u) + \widetilde{c} \geq 0, \qquad\qquad \text{for every } 0 \leq u \leq \mathsf{T}_{a,b}. \qquad (4.51)$$

101

To verify (4.51), we bound $a \leq \mathsf{B}_u \leq b$, apply an inequality $\mathsf{T}_{a,b} = t \leq t_{\max}$, bound $\inf_{0 \leq t \leq t_{\max}} \widetilde{h}''(t) \leq \widetilde{h}''(u) \leq \sup_{0 \leq t \leq t_{\max}} \widetilde{h}''(t)$, and substitute $\widetilde{c}$.

Similarly, we multiply (4.49) by $e^{\widetilde{c}t} e^{-\widetilde{c}t}$ and arrive at

$$f_{\widetilde{\tau}_{a,b}, \widetilde{\mathsf{X}}_{\widetilde{\tau}_{a,b}}}(t, b) = e^{b\widetilde{h}'(t) - \frac{1}{2} \int_0^t |\widetilde{h}'(u)|^2 du + \widetilde{c}t} \, \mathbb{E}\left\{ 1_{\left\{ \mathsf{B}_{\mathsf{T}_{a,b}} = b \right\}} e^{- \int_0^{\mathsf{T}_{a,b}} (\mathsf{B}_u \widetilde{h}''(u) + \widetilde{c}) du} \,\Bigg|\, \mathsf{T}_{a,b} = t \right\} f_{\mathsf{T}_{a,b}}(t).$$

$$(4.52)$$

The conditional expectations are difficult to evaluate with a direct method because the condition "$\mathsf{T}_{a,b} = t$" alters the measure of random process B_u. To alleviate this difficulty, we use a transformation.

Step 9: Integration transform

We write the joint probability density as a product of two terms: the term that is easy to evaluate and the term that is difficult:

$$f_{\widetilde{\tau}_{a,b}, \widetilde{\mathsf{X}}_{\widetilde{\tau}_{a,b}}}(t, a) = e^{a\widetilde{h}'(t) - \frac{1}{2} \int_0^t |\widetilde{h}'(u)|^2 du + \widetilde{c}t} \, \widetilde{f}_{\mathrm{a}}(t),$$

where

$$\widetilde{f}_{\mathrm{a}}(t) = \mathbb{E}\left\{ 1_{\left\{ \mathsf{B}_{\mathsf{T}_{a,b}} = a \right\}} e^{- \int_0^{\mathsf{T}_{a,b}} (\mathsf{B}_u \widetilde{h}''(u) + \widetilde{c}) du} \,\Bigg|\, \mathsf{T}_{a,b} = t \right\} f_{\mathsf{T}_{a,b}}(t). \qquad (4.53)$$

The term $\widetilde{f}_{\mathrm{a}}$ is difficult to evaluate due to the conditional expectation. To characterize $\widetilde{f}_{\mathrm{a}}$, we take an integral transform of $\widetilde{f}_{\mathrm{a}}$, resulting in a function g_{a}:

$$g_{\mathrm{a}}(t) = \int_0^t \widetilde{f}_{\mathrm{a}}(v) dv.$$

The transformation is invertible by taking the derivative of g_{a}. Substituting $\widetilde{f}_{\mathrm{a}}$, we have

$$g_{\mathrm{a}}(t) = \mathbb{E}\left\{ 1_{\left\{ \mathsf{B}_{\mathsf{T}_{a,b}} = a \right\}} 1_{\left\{ \mathsf{T}_{a,b} \leq t \right\}} e^{- \int_0^{\mathsf{T}_{a,b}} (\mathsf{B}_u \widetilde{h}''(u) + \widetilde{c}) du} \right\}, \qquad (4.54)$$

which no longer has the conditional expectation and is easier to obtain than $\widetilde{f}_{\mathrm{a}}$.

Similarly, we write

$$f_{\widetilde{T}_{a,b}, \widetilde{X}_{\widetilde{T}_{a,b}}}(t,b) = e^{b\widetilde{h}'(t) - \frac{1}{2}\int_0^t |\widetilde{h}'(u)|^2 du + \widetilde{c}t} \, \widetilde{f}_{\mathsf{b}}(t),$$

where

$$\widetilde{f}_{\mathsf{b}}(t) = \mathbb{E}\left\{ 1_{\left\{\mathsf{B}_{\mathsf{T}_{a,b}}=b\right\}} \, e^{-\int_0^{\mathsf{T}_{a,b}}(\mathsf{B}_u \widetilde{h}''(u)+\widetilde{c})du} \,\Big|\, \mathsf{T}_{a,b}=t \right\} f_{\mathsf{T}_{a,b}}(t). \qquad (4.55)$$

Taking an integral transform of $\widetilde{f}_{\mathsf{b}}$, we have

$$\begin{aligned}
g_{\mathsf{b}}(t) &= \int_0^t \widetilde{f}_{\mathsf{b}}(v)dv \\
&= \mathbb{E}\left\{ 1_{\left\{\mathsf{B}_{\mathsf{T}_{a,b}}=b\right\}} 1_{\left\{\mathsf{T}_{a,b}\leq t\right\}} \, e^{-\int_0^{\mathsf{T}_{a,b}}(\mathsf{B}_u \widetilde{h}''(u)+\widetilde{c})du} \right\}.
\end{aligned} \qquad (4.56)$$

The right sides of (4.54) and (4.56) can be obtained from using a limit operation and a connection to the PDE. It remains to verify that g_{a} and g_{b} satisfy (4.21) and (4.24).

Step 10: Relating the expectations to the IBVPs

The Feynman-Kac formula [74, Thm. 8.2, p. 81] implies that

$$\begin{aligned}
\mathbb{E}\left\{ 1_{\left\{\mathsf{T}_{a,b}\leq t\right\}} 1_{\left\{\mathsf{B}_{\mathsf{T}_{a,b}}=a\right\}} \, e^{-\int_0^{\mathsf{T}_{a,b}}(\mathsf{B}_u \widetilde{h}''(u)+\widetilde{c})du} \right\} & \\
+ \mathbb{E}\left\{ 1_{\left\{\mathsf{T}_{a,b}>t\right\}} \phi(\mathsf{B}_t) e^{-\int_0^t (\mathsf{B}_u \widetilde{h}''(u)+\widetilde{c})du} \right\} &= y(0,0,t,\varepsilon), \quad (4.57)
\end{aligned}$$

where y is a unique solution to the differential equation (4.22) with the boundary conditions in (4.23) and when $0 < \varepsilon < b-a$. If ε is too large, the boundary conditions (4.23b) and (4.23c) will be inconsistent at (a,t), implying that the IBVP has no solution, so ε needs to be small for (4.57) to hold. Uniqueness follows from certain properties [74, p. 81, eq. (8.17)] of the boundary conditions and Hölder continuity for $x\widetilde{h}''(t)$. Writing the first expectation as $g_{\mathsf{a}}(t)$, taking the limit of (4.57) as $\varepsilon \searrow 0$, and switching the limit and the expectation (by dominated convergence theorem [99,

103

Thm. 1.34]), we have

$$g_a(t) + \mathbb{E}\left\{1_{\{T_{a,b}>t\}}\left(\lim_{\varepsilon\searrow 0}\phi(\mathsf{B}_t)\right)e^{-\int_0^t(\mathsf{B}_u\tilde{h}''(u)+\tilde{c})du}\right\} = \lim_{\varepsilon\searrow 0}y(0,0,t,\varepsilon).$$

The limit inside the expectation is zero, giving us (4.21).

Similarly, for a fixed $r > 0$, a fixed $s \geq 0$, and any $0 < \varepsilon < b - a$ we have

$$\mathbb{E}\left\{1_{\{T_{a,b}\leq t\}}1_{\{\mathsf{B}_{T_{a,b}}=b\}}e^{-\int_0^{T_{a,b}}(\mathsf{B}_u\tilde{h}''(u)+\tilde{c})du}\right\}$$
$$+ \mathbb{E}\left\{1_{\{T_{a,b}>t\}}\psi(\mathsf{B}_t)e^{-\int_0^t(\mathsf{B}_u\tilde{h}''(u)+\tilde{c})du}\right\} = z(0,0,t,\varepsilon), \quad (4.58)$$

where z is a unique solution to a PDE and the boundary conditions in Section 4.2.2. Taking the limit of (4.58) as $\varepsilon \searrow 0$ gives us (4.24). The proof is complete.

Proof of the Inequalities (4.27a) and (4.27b)

We want to show that if ε_a and ε_b satisfy (4.27a) and (4.27b), then

$$0 \leq y(0,0,t,\varepsilon_a) - g_a(t) < d \text{ and}$$
$$0 \leq y(0,0,t,\varepsilon_b) - g_b(t) < d.$$

The proofs for ε_a and ε_b are similar. For brevity, we show the proof only for ε_a.

Fix t in the domain of g_a (either $t > 0$ or $t \in (0, t_{\max}]$). We start from (4.57), which is valid because $0 < \varepsilon_a < b - a$, and then replace the first expectation with g_a in (4.54), resulting in

$$y(0,0,t,\varepsilon_a) - g_a(t) = \mathbb{E}\left\{1_{\{T_{a,b}>t\}}\phi(\mathsf{B}_t,\varepsilon_a)e^{-\int_0^t(\mathsf{B}_u\tilde{h}''(u)+\tilde{c}+s)du}\right\}. \quad (4.59)$$

Here, we write $\phi(\cdot,\varepsilon_a)$ to emphasize the dependence of the right side on ε_a.

The argument of the expectation is non-negative, giving us the first inequality:

$$0 \leq y(0,0,t,\varepsilon_a) - g_a(t).$$

104

To show the other inequality, we bound

$$\mathbb{E}\left\{1_{\{\mathsf{T}_{a,b}>t\}}\phi(\mathsf{B}_t,\varepsilon_{\mathrm{a}})e^{-\int_0^t(\mathsf{B}_u\tilde{h}''(u)+\tilde{c}+s)du}\right\} \leq \mathbb{E}\left\{1\cdot 1_{\{a\leq \mathsf{B}_t\leq a+\varepsilon_{\mathrm{a}}\}}\cdot 1\right\}$$

$$= \mathbb{P}\left\{a\leq \mathsf{B}_t\leq a+\varepsilon_{\mathrm{a}}\right\}. \qquad (4.60)$$

Recall that B_t is a zero-mean normal random variable with variance t. Hence, we can write the right side in terms of the integration and bound it:

$$\begin{aligned}
\mathbb{P}\left\{a\leq \mathsf{B}_t\leq a+\varepsilon_{\mathrm{a}}\right\} &= \int_a^{a+\varepsilon_{\mathrm{a}}}\frac{1}{\sqrt{2\pi t}}e^{-\frac{1}{2t}x^2}dx \\
&\leq \frac{\varepsilon_{\mathrm{a}}}{\sqrt{2\pi t}}\max\left\{e^{-\frac{1}{2t}a^2},e^{-\frac{1}{2t}(a+\varepsilon_{\mathrm{a}})^2}\right\} \\
&= \frac{\varepsilon_{\mathrm{a}}}{\sqrt{2\pi t}}e^{-\frac{1}{2t}(a+\varepsilon_{\mathrm{a}})^2} \qquad\qquad \text{(because } \varepsilon_{\mathrm{a}}\leq 2|a|) \\
&\leq \frac{\varepsilon_{\mathrm{a}}}{\sqrt{2\pi e}|a+\varepsilon_{\mathrm{a}}|}. \qquad\qquad\qquad (4.61)
\end{aligned}$$

The last line is a maximization over $t>0$, by taking the first and second derivatives of the previous line. Equation (4.59), together with inequalities (4.60) and (4.61), gives us

$$y(0,0,t,\varepsilon_{\mathrm{a}}) - g_{\mathrm{a}}(t) \leq \frac{1}{\sqrt{2\pi e}}\frac{\varepsilon_{\mathrm{a}}}{|a+\varepsilon_{\mathrm{a}}|}.$$

Using the bound $0 < \varepsilon_{\mathrm{a}} < \frac{|a|d\sqrt{2\pi e}}{1+d\sqrt{2\pi e}}$, we can show that $a+\varepsilon_{\mathrm{a}}<0$, $|a+\varepsilon_{\mathrm{a}}| = -a-\varepsilon_{\mathrm{a}}$, and

$$\frac{1}{\sqrt{2\pi e}}\frac{\varepsilon_{\mathrm{a}}}{|a+\varepsilon_{\mathrm{a}}|} < d.$$

The proof is complete.

Proof that (4.33) implies (4.34) and that (4.35) implies (4.36)

Fix $0<\delta<1$ and $t\in(0,T_{\max}]$. We want to prove two statements. First, if $\eta>0$, if $b=\eta$, and if a satisfies (4.33a), then $0\leq \mathbb{P}\left\{\tilde{\tau}_{a,b}\leq t\right\} - \mathbb{P}\left\{\tilde{\tau}_\eta\leq t\right\}\leq \delta$. Second, if $\eta<0$, if $a=\eta$, and if b satisfies (4.35b), then $0\leq \mathbb{P}\left\{\tilde{\tau}_{a,b}\leq t\right\} - \mathbb{P}\left\{\tilde{\tau}_\eta\leq t\right\}\leq \delta$. The

proofs for the two statements are similar. For brevity, we only show the proof of the first statement.

Note that

$$\left\{ s \geq 0 : \widetilde{\mathsf{X}}_s \geq b \right\} \subseteq \left\{ s \geq 0 : \widetilde{\mathsf{X}}_s \leq a \text{ or } \widetilde{\mathsf{X}}_s \geq b \right\},$$

and, by taking the infimum of both sides, we have $\tilde{\tau}_b \geq \widetilde{\tau}_{a,b}$, which implies that

$$\{\widetilde{\tau}_{a,b} \leq t\} \supseteq \{\tilde{\tau}_b \leq t\}.$$

Taking the probability of both sides gives us the first inequality:

$$0 \leq \mathbb{P}\left\{\widetilde{\tau}_{a,b} \leq t\right\} - \mathbb{P}\left\{\tilde{\tau}_b \leq t\right\}.$$

To verify the other inequality, we start from the inclusion and write

$$\mathbb{P}\left\{\widetilde{\tau}_{a,b} \leq t\right\} - \mathbb{P}\left\{\tilde{\tau}_b \leq t\right\} = \mathbb{P}\left\{\{\widetilde{\tau}_{a,b} \leq t\} \setminus \{\tilde{\tau}_b \leq t\}\right\}, \qquad (4.62)$$

where "$\setminus$" denotes the set difference. The event on the right side satisfies a relationship

$$
\begin{aligned}
\{\widetilde{\tau}_{a,b} \leq t\} \setminus \{\tilde{\tau}_b \leq t\} &= \{\widetilde{\tau}_{a,b} \leq t \text{ and } \tilde{\tau}_b > t\} \\
&= \{\tilde{\tau}_a \leq t \text{ and } \tilde{\tau}_b > t\} \quad \text{(the random process exits from barrier } a \text{ at time } \widetilde{\tau}_{a,b}) \\
&\subseteq \{\tilde{\tau}_a \leq t\}.
\end{aligned}
$$

Hence,

$$\mathbb{P}\left\{\{\widetilde{\tau}_{a,b} \leq t\} \setminus \{\tilde{\tau}_b \leq t\}\right\} \leq \mathbb{P}\left\{\tilde{\tau}_a \leq t\right\}. \qquad (4.63)$$

Next, we show an inclusion

$$\{\tilde{\tau}_a \leq t\} \subseteq \{T_\alpha \leq t\},$$

where $\alpha = \sup_{0 \leq r \leq t}[a - \widetilde{h}(r)]$ and

$$T_\eta = \inf \left\{ s \geq 0 : \mathsf{B}_s = \alpha \right\},$$

the first time that a Brownian motion crosses a constant barrier at α. Take $\omega \in \Omega$ such that $\tilde{\tau}_a(\omega) \leq t$. Then,

$$\left\{ 0 \leq s \leq t : \mathsf{B}_s(\omega) \leq a - \widetilde{h}(s) \right\} \subseteq \left\{ 0 \leq s \leq t : \mathsf{B}_s(\omega) \leq \sup_{0 \leq r \leq t} [a - \widetilde{h}(r)] \right\}$$

$$\subseteq \left\{ 0 \leq s : \mathsf{B}_s(\omega) \leq \alpha \right\}.$$

Taking the infimum of the first and last sets and replacing $\widetilde{\mathsf{X}}_s(\omega) = \mathsf{B}_s(\omega) + \widetilde{h}(s)$, we have

$$\inf \left\{ 0 \leq s \leq t : \widetilde{\mathsf{X}}_s(\omega) \leq a \right\} \geq \inf \left\{ 0 \leq s : \mathsf{B}_s(\omega) \leq \alpha \right\}.$$

The left side equals $\tilde{\tau}_a(\omega)$ since $\tilde{\tau}_a(\omega) \leq t$. The right side equals $T_\alpha(\omega)$ since $\alpha < 0$ from the hypothesis that $\alpha = a - \inf_{0 \leq r \leq t} \widetilde{h}(r) \leq -\sqrt{2 T_{\max} \ln \frac{1}{\delta}} < 0$. Hence,

$$\tilde{\tau}_b(\omega) \geq T_\alpha(\omega),$$

which implies that $t \geq T_\alpha(\omega)$.

Taking the probability of the inclusion results in

$$\mathbb{P}\left\{ \tilde{\tau}_a \leq t \right\} \leq \mathbb{P}\left\{ T_\alpha \leq t \right\}. \tag{4.64}$$

The right side can be bounded:

$$\mathbb{P}\left\{ T_\alpha \leq t \right\} \leq \mathbb{P}\left\{ T_\alpha \leq T_{\max} \right\}$$

$$= 2Q\left(\frac{|\alpha|}{\sqrt{T_{\max}}} \right) \quad \text{(the reflection principle [63, p. 80, eq. (6.2)])}$$

$$\leq e^{-\frac{\alpha^2}{2 T_{\max}}}. \tag{4.65}$$

107

The last inequality is from $Q(x) \le \frac{1}{2}e^{-x^2/2}$ for $x \ge 0$. By the definitions of α and a, we have

$$\alpha \le -\sqrt{2T_{\max}\ln\frac{1}{\delta}} < 0,$$

which gives us

$$e^{-\frac{\alpha^2}{2T_{\max}}} \le \delta. \tag{4.66}$$

Combining (4.62)–(4.66), we have

$$\mathbb{P}\left\{\widetilde{\tau}_{a,b} \le t\right\} - \mathbb{P}\left\{\widetilde{\tau}_b \le t\right\} \le \delta.$$

4.3 Multi-Dimensional Brownian Motion with Polynomial Drift

In this section, we solve first-passage-time problems involving multi-dimensional Brownian motion with polynomial drift. The goal is to obtain the probability distribution of the first time that n-dimensional Brownian motion with polynomial drift crosses a boundary that is an open sets in the Euclidean space. The shape of the boundary depends on an index k, where $k = 1, 2, \ldots, n$. Our main contributions from this section are

- a methodology involving reduction and ordered statistics to solve first-passage-time problems;

- an expression of the CDF of the first time that multi-dimensional Brownian motion with polynomial drift crosses a boundary for the case that $k = 1$; and

- expressions for a lower bound and an upper bound for the CDF of the first time that multi-dimensional Brownian motion with polynomial drift crosses a boundary for the case that $k \ge 2$.

The solution to first-passage-time distribution has applications to network synchronization.

The remaining parts of this section are organized as follows. In Section 4.3.1, we state the first-passage-time problem that we aim to solve. In Section 4.3.2, we provide the solution to the first-passage-time distribution. In Section 4.3.3, we discuss important aspects and the consequences of our solution. In Section 4.3.4, we provide elementary examples demonstrating applications of our solution. In Section 4.3.5, we prove the main theorems that lead to the solution of the first-passage-time distribution.

4.3.1   Problem Statement

Let $\mathbf{B}_t = \left(\mathsf{B}_t^{(1)}, \mathsf{B}_t^{(2)}, \ldots, \mathsf{B}_t^{(n)} \right)$ denote an n-dimensional Brownian motion defined on a probability space $(\Omega, \mathcal{F}, \boldsymbol{P})$, with an initial position at the origin, i.e., $\boldsymbol{P}\{\mathbf{B}_0 = \mathbf{0}\} = 1$ where $\mathbf{0}$ is an n-dimensional vector of all components equal to zero. Let $\mathbf{X}_t = \left(\mathsf{X}_t^{(1)}, \mathsf{X}_t^{(2)}, \ldots, \mathsf{X}_t^{(n)} \right)$ denote an n-dimensional random process

$$\mathsf{X}_t^{(i)} = \mathsf{B}_t^{(i)} + h_i\left(t\right), \qquad\qquad t \geq 0 \text{ and } i = 1, 2, \ldots, n,$$

where $h_i\left(t\right)$ is a polynomial in t. For each $k = 1, 2, \ldots, n$, let $\tau_{\alpha,\beta}\left(k\right)$ denote the first time that k components out of n components of $\mathbf{X}_t$ cross a boundary consisting of two constants at α and β:

$$\tau_{\alpha,\beta}\left(k\right) = \inf\left\{ t \geq 0 : \exists\, \mathcal{J} \subset \{1, 2, \ldots, n\} \text{ such that } |\mathcal{J}| = k \text{ and } \forall j \in \mathcal{J}\ \mathsf{X}_t^{(j)} \notin (\alpha, \beta) \right\},$$

for finite numbers α and β such that $\alpha < h_i\left(0\right) < \beta$ for each $i = 1, 2, \ldots, n$. For each $k = 1, 2, \ldots, n$, we want to bound or, if possible, derive, the probability distribution of $\tau_{\alpha,\beta}\left(k\right)$.

4.3.2 Solution to the First-Passage-Time Distribution

We discuss two cases separately: $k = 1$ and $k \geq 2$. For the first case, we are able to obtain the expression of the CDF of $\tau_{\alpha,\beta}(k)$. For the second case, we provide a lower bound and an upper bound on the CDF.

Our solution for the case of $k = 1$ is as follows. For $t \geq 0$, the CDF of $\tau_{\alpha,\beta}(1)$ is given by

$$P\left\{\tau_{\alpha,\beta}(1) \leq t\right\} = 1 - \prod_{i=1}^{n}\left[1 - F_{\tau_{\alpha,\beta}^{(i)}}(t)\right], \tag{4.67}$$

where $F_{\tau_{\alpha,\beta}^{(i)}}(t)$ is the CDF of random variable $\tau_{\alpha,\beta}^{(i)}$, i.e., $F_{\tau_{\alpha,\beta}^{(i)}}(t) = P\left\{\tau_{\alpha,\beta}^{(i)} \leq t\right\}$, and $\tau_{\alpha,\beta}^{(i)}$ denote the first time that Brownian motion with polynomial drift crosses a boundary at (α, β):

$$\tau_{\alpha,\beta}^{(i)} = \inf\left\{t \geq 0 : \mathsf{X}_t^{(i)} \notin (\alpha, \beta)\right\}.$$

The CDF of $F_{\tau_{\alpha,\beta}^{(i)}}(t)$ is given by an integration of the PDF of $\tau_{\alpha,\beta}^{(i)}$. For a polynomial $h_i(t)$ of degree two or less, i.e., for $h_i(t) = c_{i,0} + c_{i,1}t + c_{i,2}t^2$, the PDF of $\tau_{\alpha,\beta}^{(i)}$ is given in Section 4.1.2 with these specific values of the barriers and the drift: if $c_{i,2} \geq 0$, we set

$$a = \alpha - c_{i,0}, \quad b = \beta - c_{i,0}, \quad h(t) = c_{i,1}t + c_{i,2}t^2,$$

and if $c_{i,2} < 0$, we set

$$a = c_{i,0} - \alpha, \quad b = c_{i,0} - \beta, \quad h(t) = -c_{i,1}t - c_{i,2}t^2.$$

For a polynomial of degree three or more, the PDF of $\tau_{\alpha,\beta}^{(i)}$ is given in Section 4.2.2 with these specific values of the barriers and the drift:

$$a = \alpha - h_i(0), \quad b = \beta - h_i(0), \quad \widetilde{h}(t) = h_i(t) - h_i(0).$$

This specification yields the PDF of the first passage time $\tau_{\alpha,\beta}(1)$.

For the case of $2 \leq k \leq n$ and for $t \geq 0$, the CDF of $\tau_{\alpha,\beta}(k)$ satisfies the lower bound and the upper bound

$$\sum_{i=k}^{n} \sum_{\substack{\mathcal{J} \subset \{1,2,\dots,n\} \\ |\mathcal{J}|=i}} \left(\prod_{j \in \mathcal{J}} p_j(t) \right) \prod_{\ell \in \{1,2,\dots,n\} \setminus \mathcal{J}} \left(1 - p_\ell(t) \right)$$

$$\leq P\{\tau_{\alpha,\beta}(k) \leq t\}$$

$$\leq \sum_{i=k}^{n} \sum_{\substack{\mathcal{J} \subset \{1,2,\dots,n\} \\ |\mathcal{J}|=i}} \left(\prod_{j \in \mathcal{J}} q_j(t) \right) \prod_{\ell \in \{1,2,\dots,n\} \setminus \mathcal{J}} \left(1 - q_\ell(t) \right), \quad (4.68)$$

where the product over an empty index, $\prod_{\ell \in \emptyset}(\cdot)$, is defined to be 1,

$$p_i(t) = \begin{cases} 0, & t = 0 \\ 1 - \Phi\left(\frac{\beta - h_i(t)}{\sqrt{t}}\right) + \Phi\left(\frac{\alpha - h_i(t)}{\sqrt{t}}\right), & t > 0, \end{cases}$$

$$q_i(t) = F_{\tau_{\alpha,\beta}^{(i)}}(t),$$

and $\Phi(\cdot)$ is the CDF of the standard normal random variable: $\Phi(z) = \int_{-\infty}^{z} \frac{1}{\sqrt{2\pi}} e^{-y^2/2} dy$.

4.3.3 Important Aspects of the Solution and the Consequences

For a special case when $h_1(t) = h_2(t) = \cdots = h_n(t)$ for all $t \geq 0$, the solution in Section 4.3.2 can be simplified. When the drifts are identical, each random process $X_t^{(i)}$ is Brownian motion with drift $h_1(t)$. Hence, the first passage times $\tau_{\alpha,\beta}^{(1)}, \tau_{\alpha,\beta}^{(2)}, \dots, \tau_{\alpha,\beta}^{(n)}$ are identically distributed. This observation gives us a simplification: when the drifts are equal, (4.67) becomes

$$P\{\tau_{\alpha,\beta}(1) \leq t\} = 1 - \left[1 - F_{\tau_{\alpha,\beta}^{(1)}}(t)\right]^n, \qquad (4.69)$$

111

and (4.68) becomes

$$\sum_{i=k}^{n} \binom{n}{i} \Big[p_1\left(t\right) \Big]^{i} \Big[1 - p_1\left(t\right) \Big]^{n-i}$$

$$\leq \boldsymbol{P}\left\{ \tau_{\alpha,\beta}\left(k\right) \leq t \right\}$$

$$\leq \sum_{i=k}^{n} \binom{n}{i} \Big[q_1\left(t\right) \Big]^{i} \Big[1 - q_1\left(t\right) \Big]^{n-i}. \quad (4.70)$$

The case of identical drifts has applications for synchronization to homogenous clocks (see Section 4.5.2).

4.3.4   Elementary Examples

As an example, we consider a random process $\mathbf{X}_t = \left(\mathsf{X}_t^{(1)}, \mathsf{X}_t^{(2)}, \ldots, \mathsf{X}_t^{(n)} \right)$ for

$$\mathsf{X}_t^{(i)} = \mathsf{B}_t^{(i)} + h_i\left(t\right), \qquad\qquad t \geq 0 \text{ and } i = 1, 2, \ldots, n,$$

where $n = 10$ and $h_i\left(t\right) = t + \frac{1}{10}t^2$. We set the boundary to $a = -1$ and $b = 2$. We consider various values of k, namely $k = 1, 2, 10$. For the case that $k = 1$, we obtain the CDF of the first passage time using the expression in (4.67). For other k's, we bound the CDF of the first passage time using the expressions in (4.68). The CDF and the bounds are shown in Fig. 4-10–Fig. 4-11 for different k's.

From the figures, the CDF for $k = 1$ and the bounds on the CDFs for $k = 2, 10$ take positive values on $x \geq 0$, increase with x, and reach the value of 1 as x approaches infinity. These behaviors are expected for the CDF ($k = 1$), and also expected for the lower bounds and the upper bounds because these bounds are valid CDFs. The strengths of these bounds are that they are easy to obtain even for large values of k and n. The CDF and the bounds on CDFs are useful in characterizing the time that a network lose synchronization (see Section 4.5.2).
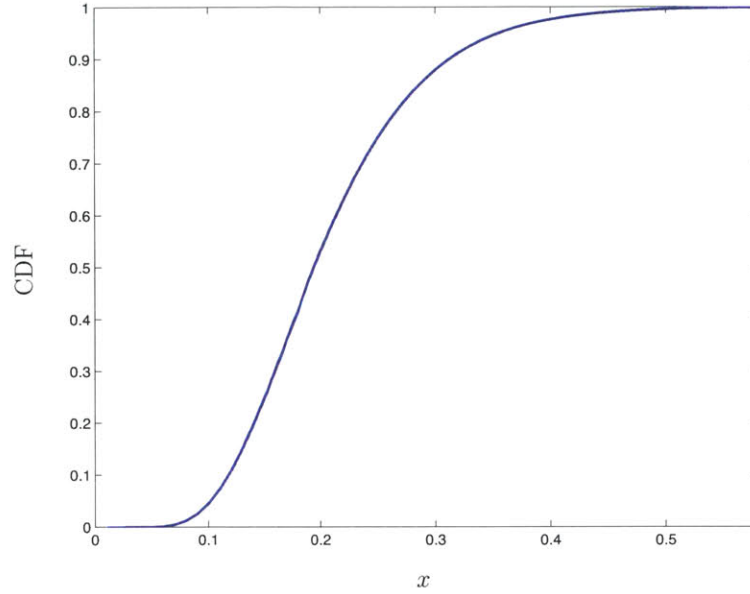
Figure 4-10: The CDF for $k = 1$ can be obtained easily using the expression in (4.67).

4.3.5 Proofs of the Key Theorems

This section contains the proofs of the equality in (4.67) and the bounds in (4.68). The proofs are simple and rely on the availability of the first-passage-time distributions for Brownian motion with polynomial drift that we derived in Section 4.1 and Section 4.2.

Proof of (4.67)

For $k = 1$, the idea for the proof is simple. The first passage time $\tau_{\alpha,\beta}(1)$ is the first time at which any of the random processes $\mathsf{X}_t^{(1)}, \mathsf{X}_t^{(2)}, \ldots, \mathsf{X}_t^{(i)}$ crosses a boundary. Thus, for $k = 1$, the first-passage-time problem, which involves the n-dimensional process, reduces to the first-passage-time problems, which involve several one-dimensional processes.

The proof is divided into two steps. First, we show that

$$\tau_{\alpha,\beta}(1) = \min\left\{\tau_{\alpha,\beta}^{(1)}, \tau_{\alpha,\beta}^{(2)}, \ldots, \tau_{\alpha,\beta}^{(n)}\right\} \tag{4.71}$$

almost surely (a.s.) on $\mathbf{\Omega}$. Then, we obtain the probability distribution of the mini-

113
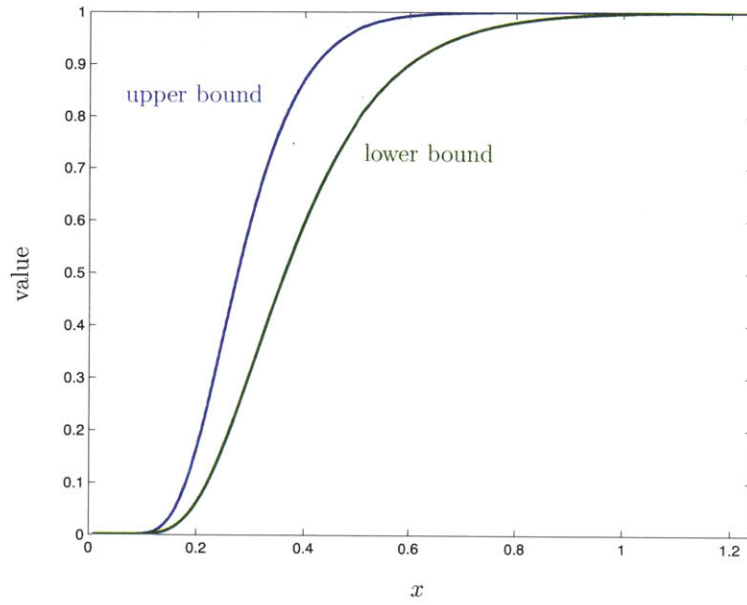
(a) $k = 2$
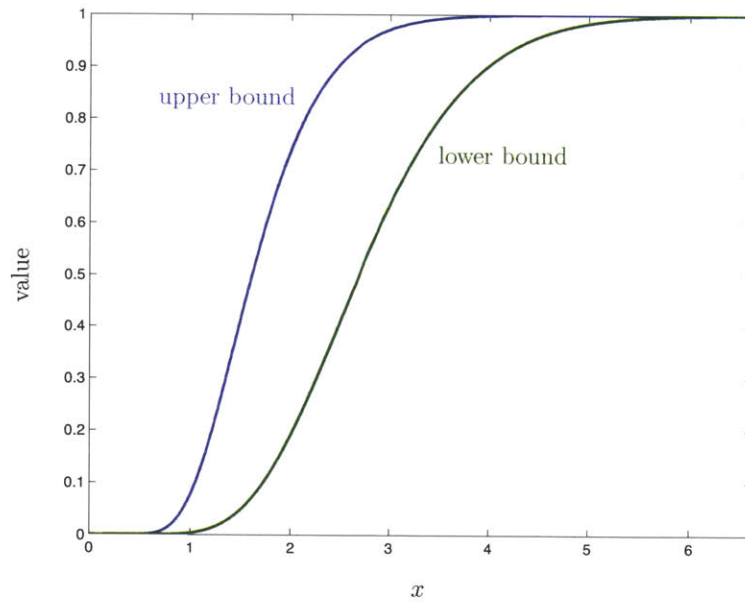
(b) $k = 10$

Figure 4-11: For $k \geq 2$, we provide the lower bound and the upper bound on the CDF. The bounds themselves are valid CDFs.

mum, the right side of (4.71). The proof proceeds as follows.

Step 1: Equality of two random variables

Let $\boldsymbol{\omega} \in \boldsymbol{\Omega}$. For each $i = 1, 2, \ldots, n$, we have

$$\left\{ t \geq 0 : \mathsf{X}_t^{(i)}(\boldsymbol{\omega}) \notin (\alpha, \beta) \right\} \subset \left\{ t \geq 0 : \exists \, 1 \leq j \leq n \, \mathsf{X}_t^{(j)} \notin (\alpha, \beta) \right\},$$

and by taking the infimum of these sets, we have $\tau_{\alpha,\beta}^{(i)}(\boldsymbol{\omega}) \geq \tau_{\alpha,\beta}(1, \boldsymbol{\omega})$. Hence,

$$\min \left\{ \tau_{\alpha,\beta}^{(1)}(\boldsymbol{\omega}), \tau_{\alpha,\beta}^{(2)}(\boldsymbol{\omega}), \ldots, \tau_{\alpha,\beta}^{(n)}(\boldsymbol{\omega}) \right\} \geq \tau_{\alpha,\beta}(1, \boldsymbol{\omega}). \tag{4.72}$$

Next, we want to verify the inequality

$$\min \left\{ \tau_{\alpha,\beta}^{(1)}(\boldsymbol{\omega}), \tau_{\alpha,\beta}^{(2)}(\boldsymbol{\omega}), \ldots, \tau_{\alpha,\beta}^{(n)}(\boldsymbol{\omega}) \right\} \leq \tau_{\alpha,\beta}(1, \boldsymbol{\omega}). \tag{4.73}$$

If $\tau_{\alpha,\beta}(1, \boldsymbol{\omega}) = \infty$, the inequality is trivial. If $\tau_{\alpha,\beta}(1, \boldsymbol{\omega}) < \infty$, then, by definition of $\tau_{\alpha,\beta}(1)$, we have $\mathsf{X}_s^{(j)}(\omega) \notin (\alpha, \beta)$ for some $1 \leq j \leq n$ and for $s = \tau_{\alpha,\beta}(1, \boldsymbol{\omega})$. Hence, $\tau_{\alpha,\beta}^{(j)}(\boldsymbol{\omega}) \leq s = \tau_{\alpha,\beta}(1, \boldsymbol{\omega})$, giving us (4.73). The inequalities (4.72) and (4.72) imply (4.71).

Step 2: Probability distribution of the minimum

For any t, we have

$$\begin{aligned} \boldsymbol{P} \left\{ \tau_{\alpha,\beta}(1) \leq t \right\} &= \boldsymbol{P} \left\{ \min \left\{ \tau_{\alpha,\beta}^{(1)}, \tau_{\alpha,\beta}^{(2)}, \ldots, \tau_{\alpha,\beta}^{(n)} \right\} \leq t \right\} \\ &= 1 - \boldsymbol{P} \left\{ \tau_{\alpha,\beta}^{(1)} > t, \ \tau_{\alpha,\beta}^{(2)} > t, \ \ldots, \ \text{and } \tau_{\alpha,\beta}^{(n)} > t \right\}. \end{aligned}$$

Random variables $\tau_{\alpha,\beta}^{(1)}, \tau_{\alpha,\beta}^{(2)}, \ldots, \tau_{\alpha,\beta}^{(n)}$ are independent, giving us the expression in (4.67).

115

Proof of the Lower Bound in (4.68)

To verify the left-most inequality in (4.68), we proceed as follows. First, we verify an inclusion

$$\left\{ \exists\, \mathcal{J} \subset \{1, 2, \ldots, n\} \text{ such that } |\mathcal{J}| = k \text{ and } \forall j \in \mathcal{J} \; \mathsf{X}_t^{(j)} \notin (\alpha, \beta) \right\}$$
$$\subset \left\{ \tau_{\alpha, \beta}(k) \leq t \right\}. \quad (4.74)$$

Then, we verify that the probability of the event on the left side of (4.74) is given by the right-most expression in (4.68). The proof of the upper bound in (4.68) is simple and appears in steps.

Step 1: An inclusion

Fix $k = 1, 2, \ldots, n$, fix $t \geq 0$, and take $\boldsymbol{\omega} \in \Omega$ that belongs to the event on the left side of (4.74). By an existence of index set $\mathcal{J}$, we have

$$t \in \left\{ s \geq 0 : \exists\, \mathcal{M} \subset \{1, 2, \ldots, n\} \text{ such that } |\mathcal{M}| = k \text{ and } \forall m \in \mathcal{M} \; \mathsf{X}_t^{(m)}(\boldsymbol{\omega}) \notin (\alpha, \beta) \right\}.$$
$$(4.75)$$

Hence, t is greater than or equal to the infimum of the set in (4.75), or equivalently, $t \geq \tau_{\alpha, \beta}(k, \boldsymbol{\omega})$.

Step 2: Probability of an event

We write the event on the left side of (4.74) as a union of disjoint events and have

$$\boldsymbol{P}\left\{ \exists\, \mathcal{J} \subset \{1, 2, \ldots, n\} \text{ such that } |\mathcal{J}| = k \text{ and } \forall j \in \mathcal{J} \; \mathsf{X}_t^{(j)} \notin (\alpha, \beta) \right\}$$
$$= \sum_{i=k}^{n} \sum_{\substack{\mathcal{J} \subset \{1, 2, \ldots, n\} \\ |\mathcal{J}| = i}} \left(\prod_{j \in \mathcal{J}} \boldsymbol{P}\left\{ \mathsf{X}_t^{(j)} \notin (\alpha, \beta) \right\} \right) \left(\prod_{\ell \in \{1, 2, \ldots, n\} \setminus \mathcal{J}} \boldsymbol{P}\left\{ \mathsf{X}_t^{(\ell)} \in (\alpha, \beta) \right\} \right). \quad (4.76)$$

Recall that $\mathsf{X}_0^{(i)} = h_i(0) \in (\alpha, \beta)$ by construction of α and β and recall that, for $s > 0$, $\mathsf{X}_s^{(i)}$ has a normal distribution with mean $h_i(s)$ and variance s. Hence, the right side of (4.76) evaluates to the left-most expression of (4.68).

116

Step 3: Lower bound for the CDFs of $\tau_{\alpha,\beta}(k)$

For given k and t, the inclusion in step one of the proof gives us

$$P\left\{\exists\, \mathcal{J} \subset \{1, 2, \ldots, n\} \text{ such that } |\mathcal{J}| = k \text{ and } \forall j \in \mathcal{J}\ \mathsf{X}_t^{(j)} \notin (\alpha, \beta)\right\}$$
$$\leq P\left\{\tau_{\alpha,\beta}(k) \leq t\right\}.$$

Step two of the proof gives us the expression of the probability on the left side. Combining step one and step two, we have the left-most inequality in (4.68). The proof is complete.

Proof of the Upper Bound in (4.68)

To verify the right-most inequality in (4.68), we proceed as follows. First, we show that the random variable $\tau_{\alpha,\beta}(k)$ is lower bounded by Y_k, where $\mathsf{Y}_1 \leq \mathsf{Y}_2 \leq \cdots \leq \mathsf{Y}_n$ are the values of $\tau_{\alpha,\beta}(1), \tau_{\alpha,\beta}(2), \ldots, \tau_{\alpha,\beta}(n)$ placed in the increasing order. Second, we derive the probability distribution of Y_k. The derivation is a simple generalization of the derivation that appears in ordered statistics. A difference between our derivation and the derivation in the ordered statistics is that for our case $\tau_{\alpha,\beta}(1), \tau_{\alpha,\beta}(2), \ldots, \tau_{\alpha,\beta}(n)$ may have different probability distributions. The proof of the upper bound in (4.68) is simple and appears in steps.

Step 1: Lower bound for $\tau_{\alpha,\beta}(k)$

For each $k = 1, 2, \ldots, n$, we will verify that

$$\mathsf{Y}_k \leq \tau_{\alpha,\beta}(k) \tag{4.77}$$

a.s. on Ω. Take $\omega \in \Omega$. If $\tau_{\alpha,\beta}(k, \omega) = \infty$, then (4.77) is trivial. If $\tau_{\alpha,\beta}(k, \omega) < \infty$, then take $\mathcal{J} \subset \{1, 2, \ldots, n\}$ such that $|\mathcal{J}| = k$ and

$$\mathsf{X}_s^{(j)} \notin (\alpha, \beta), \qquad\qquad \forall j \in \mathcal{J},$$

117

for $s = \tau_{\alpha,\beta}(k, \boldsymbol{\omega})$. By definition of $\tau_{\alpha,\beta}^{(1)}(\boldsymbol{\omega}), \tau_{\alpha,\beta}^{(2)}(\boldsymbol{\omega}), \ldots, \tau_{\alpha,\beta}^{(n)}(\boldsymbol{\omega})$, we have

$$\tau_{\alpha,\beta}^{(j)}(\boldsymbol{\omega}) \leq \tau_{\alpha,\beta}(k, \boldsymbol{\omega}), \qquad\qquad \forall j \in \mathcal{J}.$$

Taking the maximum of the right sides over $j \in \mathcal{J}$, we have

$$\max\left\{\tau_{\alpha,\beta}^{(j)}(\boldsymbol{\omega}) : j \in \mathcal{J}\right\} \leq \tau_{\alpha,\beta}(k, \boldsymbol{\omega}). \qquad (4.78)$$

By definition, $\mathsf{Y}_k(\boldsymbol{\omega})$ is the k-th smallest number among $\tau_{\alpha,\beta}^{(1)}(\boldsymbol{\omega}), \tau_{\alpha,\beta}^{(2)}(\boldsymbol{\omega}), \ldots, \tau_{\alpha,\beta}^{(n)}(\boldsymbol{\omega})$, so

$$\mathsf{Y}_k(\boldsymbol{\omega}) \leq \max\left\{\tau_{\alpha,\beta}^{(j)}(\boldsymbol{\omega}) : j \in \mathcal{J}\right\}. \qquad (4.79)$$

Combining (4.79) and (4.78), we have (4.77).

Step 2: CDF of Y_k

For each $k = 1, 2, \ldots, n$ and for each $t \in \mathbb{R}$, we will verify that $\boldsymbol{P}\{\mathsf{Y}_k \leq t\}$ equals the left-most expression of (4.68).

Let

$$\mathsf{C}_i = \begin{cases} 1, & \text{if } \tau_{\alpha,\beta}^{(i)} \leq t, \\ 0, & \text{otherwise,} \end{cases}$$

and let $\mathsf{C} = \mathsf{C}_1 + \mathsf{C}_2 + \cdots + \mathsf{C}_n$. Random variable C counts the number of values $\tau_{\alpha,\beta}^{(1)}, \tau_{\alpha,\beta}^{(2)}, \ldots, \tau_{\alpha,\beta}^{(n)}$ that are less than or equal to t. Since events $\{\mathsf{Y}_k \leq t\}$ and $\{\mathsf{C} \geq k\}$ mean k or more of $\tau_{\alpha,\beta}^{(i)}$'s are less than or equal to t, we have the equality

$$\boldsymbol{P}\{\mathsf{Y}_k \leq t\} = \boldsymbol{P}\{\mathsf{C} \geq k\}.$$

We write the event $\{C \geq k\}$ as a union of disjoint events, giving us

$$P\{C \geq k\} = \sum_{j=k}^{n} \sum_{\substack{\mathcal{J} \subset \{1,2,\ldots,n\} \\ |\mathcal{J}|=j}} P\Big\{ \forall j \in \mathcal{J},\ C_j = 1 \text{ and}$$

$$\forall \ell \in \{1, 2, \ldots, n\} \backslash \mathcal{J},\ C_\ell = 0 \Big\}.$$

The random variables C_i's are independent, giving us the CDF:

$$P\{Y_k \leq t\} = \sum_{i=k}^{n} \sum_{\substack{\mathcal{J} \subset \{1,2,\ldots,n\} \\ |\mathcal{J}|=i}} \left(\prod_{j \in \mathcal{J}} p_j(t) \right) \prod_{\ell \in \{1,2,\ldots,n\} \backslash \mathcal{J}} \Big(1 - p_\ell(t) \Big).$$

Step 3: Upper bound for the CDFs of $\tau_{\alpha,\beta}(k)$

For given k and t, step one of the proof gives us $P\{\tau_{\alpha,\beta}(k) \leq t\} \leq P\{Y_k \leq t\}$. Step two of the proof gives us the expression of $P\{Y_k \leq t\}$. Combining step one and step two, we have the right-most inequality in (4.68). The proof is complete.

4.4 A Discrete-Time Process With Certain Correlations

In this section, we consider a specific class of first-passage-time problems, where the random process is a discrete time process and the boundary is a constant. The motivation for this form of the random process and boundary comes from applications in frame synchronization. In particular, the time until a receiver correctly acquires a frame is a random variable, whose probability distribution can be obtained by solving first-passage-time problems. Here, we provide the probability distribution of time to complete frame synchronization.

In this section, we solve first passage time problems involving discrete-time process with certain correlation. Our main contributions this this section are

- a methodology involving Markov chain, stopping time, and renewal theory to solve first-passage-time problems;

119

- an expression of the expected time until a receiver correctly acquires a frame; and

- an expression of the probability mass function (PMF) of the during until a receiver correctly acquires a frame.

The solution to first-passage-time distribution gives insight into the amount of time required for frame synchronization.

This section is organized as follows. In Section 4.4.1, we state the first-passage-time problem that we aim to solve. In Section 4.4.2, we provide the solution to the first-passage-time distribution. In Section 4.4.3, we discuss important aspects and the consequences of our solution. In Section 4.4.4, we provide elementary examples demonstrating applications of our solution. In Section 4.4.5, we prove the main theorems that lead to the solution of the first-passage-time distribution.

4.4.1 Problem Statement

In this section we start by describing aspects of the transmitter and receiver which are relevant to the frame synchronization problem. We then present the marker acquisition procedure and introduce the concept of arrival process.

The transmitter delimits a long sequence of data to generate frames of variable lengths. Frame lengths or the number of data symbols per frame, $\{\mathsf{L}_i^{\mathrm{d}} : i \geq 1\}$, can be modeled as independent and identically distributed (IID) random variables. The transmitter injects a marker, $(c_1, c_2, \ldots, c_{\ell_{\max}^{\mathrm{m}}})$, of fixed length, $\ell_{\max}^{\mathrm{m}} \geq 2$ symbols, before each frame to form a packet. A modulator then generates a waveform from a sequence of data and marker symbols to be transmitted through the channel.

Adjacent packets are separated by an interval of length $\mathsf{L}_i^{\mathrm{s}}$, where $\{\mathsf{L}_i^{\mathrm{s}} : i \geq 1\}$ are IID and independent of $\mathsf{L}_i^{\mathrm{d}}$ (see Fig. 4-12). Each $\mathsf{L}_i^{\mathrm{s}}$ corresponds to the length of the idle fill characters in the case of continuous transmission or the length of silence in the case of bursty transmission. The waveform representing the packets and separation intervals is corrupted by noise and fading. The corrupted waveform becomes an input to the receiver.

120

(a) continuous transmission

(b) bursty transmission
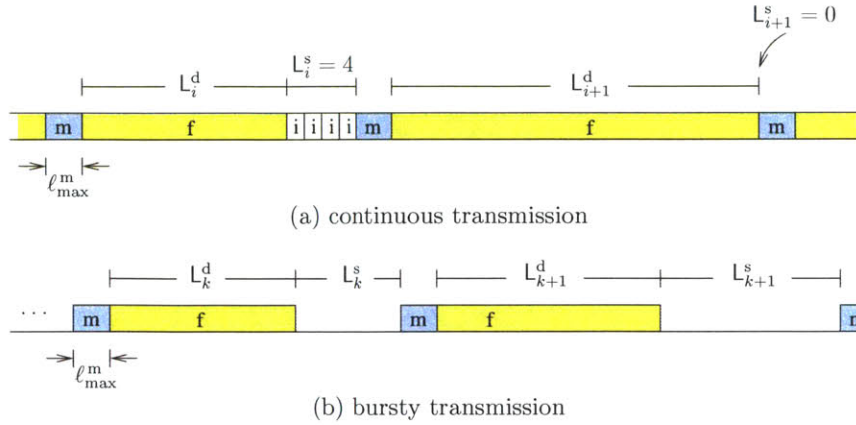
Figure 4-12: Two adjacent packets are separated by an interval, during which the transmitter has no data to send.

Upon receiving an input waveform, the receiver generates a sequence of soft decision variables, $\{X_j : j \geq 1\}$, which forms the input for the frame synchronizer. Variable X_j represents a corrupted marker symbol, a corrupted data symbol, or a corrupted symbol corresponding to the silent transmission. The frame synchronizer is said to acquire a marker at an index k if it decides, either correctly or incorrectly, that the soft-decision variable X_k corresponds to the first symbol of the marker.

To acquire a marker, the frame synchronizer forms a real-valued decision variable,[4]

$$V_j = g(X_{j:j+\ell_{\max}^m-1}),$$

for each symbol time, $j \geq 1$, where $x_{j:k}$ denotes a vector $[x_j\, x_{j+1}\, \ldots\, x_k]$ for $j \leq k$. If the decision variable V_j belongs to a predetermined set, $\mathcal{R}$, of real numbers, the frame synchronizer acquires a marker at index j.[5] Otherwise, the frame synchronizer

---

[4]Recall that the length of markers is $\ell_{\max}^m$. We consider the case, in which only $\ell_{\max}^m$ consecutive X_j's are required in forming the decision variable.

[5]For example, the set $\mathcal{R}$ can be $[\eta, \infty)$ for the case that $L_i^s = 0$ and for binary antipodal modulation, where η is known as a threshold.

tests the next decision variable, V_{j+1}. Examples of g are given by

$$g_1(X_{j:j+\ell_{\max}^m-1}) = \sum_{k=1}^{\ell_{\max}^m} c_k X_{j+k-1}, \tag{4.80}$$

$$g_2(X_{j:j+\ell_{\max}^m-1}) = \sum_{k=1}^{\ell_{\max}^m} \left[c_k X_{j+k-1} - |X_{j+k-1}| \right], \tag{4.81}$$

for antipodal marker symbols [24, 25]. Note that random variables $\{V_j\}$ are not mutually independent. In fact, this property makes the exact derivations of the performance metrics prohibitively difficult.

In this setting, the classical method [87] for analyzing the problem of synchronizing spread-spectrum waveforms does not apply since it assumes a constant frame length (which equals the spreading sequence period). In contrast, the spacing, $L_i^d + L_i^s + \ell_{\max}^m$, between the adjacent markers in frame synchronization varies from one packet to another. Here, we propose to analyze the frame synchronization problem by employing mathematical tools developed for studying the arrival processes.

A systematic approach to obtain performance metrics for frame synchronization involves the use of an arrival process, $\{J_i\}$, in which $1 \leq J_1 < J_2 < J_3 < \cdots$ denote arrival times of markers. An arrival is said to occur at time $j \in \mathbb{Z}_+$, if the first symbol of the marker begins at index j (and hence the decision variable V_j belongs to $\mathcal{R}$ under an ideal case).[6] We refer to a sequence of discrete time $\{j : J_i < j \leq J_{i+1}\}$ as a marker spacing span (MSS), with the convention that $J_0 < 1$. It will be apparent that the time until the first arrival, J_1, and interarrival times, $T_i \triangleq J_{i+1} - J_i = L_i^d + L_i^s + \ell_{\max}^m$, play an important role in the analysis.[7]

We consider a time invariance property for the decision variables. In particular, the probabilities

$$P \left\{ V_{J_i+1:J_{i+1}} \in \mathcal{R}^c \mid V_{J_i-\ell_{\max}^m+2:J_i} \in \mathcal{R}^c \right\}$$

---

[6]The symbol $\mathbb{Z}_+$ denotes the set of all positive integers.

[7]In general, the time until the first arrival J_1 and interarrival time T_i have different distributions.
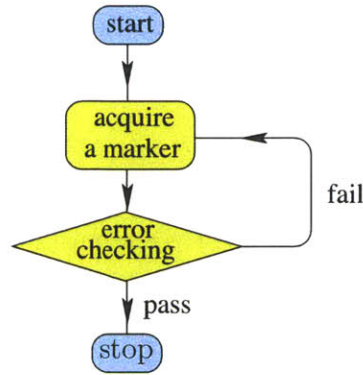
Figure 4-13: The diagram represents the frame synchronization process, which terminates after the correct acquisition of a marker.

are identical for any i, and so are

$$P\left\{\mathsf{V}_{\mathsf{J}_i+1:\mathsf{J}_{i+1}-1} \in \mathcal{R}^c, \mathsf{V}_{\mathsf{J}_{i+1}} \in \mathcal{R} \,\middle|\, \mathsf{V}_{\mathsf{J}_i-\ell_{\max}^{\mathrm{m}}+2:\mathsf{J}_i} \in \mathcal{R}^c\right\}.$$

Intuitively, the time invariance property states that statistical properties of the decision variables within an MSS do not depend on the choice of MSS. Time invariance property is valid when the probability of transmitting a given symbol, the channel statistics, and the decision rule do not change during frame synchronization.

4.4.2 Solution to the First-Passage-Time Distribution

This subsection contains two parts: the solution for the expected time until a correct frame acquisition; and the solution for the PMF of the time until a correct frame acquisition. Instead of seconds or other absolute time, we measure the amount of time in terms of the number of MSSs to provide fair comparisons of synchronization algorithms of short frames and long frames.

Expected Number of MSSs Required for a Correct Acquisition

The frame-synchronization process ends when the receiver acquires a correct marker. When an incorrect marker acquisition occurs, we assume that data symbols in the frame will be recognized as incorrect, for example by means of verifying the frame

123

structure or by means of cyclic redundancy check (CRC). After an incorrect acquisition is detected, the search for a marker starts all over again. These procedures are represented by the diagram in Fig. 4-13.

To measure the amount of time required to synchronize correctly, we count the number of MSSs that are needed for a correct acquisition. Such a number is denoted by a random sum, M, which is equal to

$$M = \sum_{i=1}^{K} M_i, \qquad (4.82)$$

where $K \geq 1$ is a random variable representing the number of attempts until frame synchronization ends and $M_i \geq 1$ are random variables representing the required number of MSSs for attempt i. The expected number of MSSs required for a correct acquisition, $E\{M\}$, is a suitable metric for frame synchronization.

We consider $\{M_i\}$ to be IID and K to have a geometric distribution with probability of success p_{cAcq}, where p_{cAcq} denotes the probability that a marker acquisition is correct. This can be justified as follows. Typically, an error-checking process lasts on the order of the frame length. Hence, different synchronization attempts examine different portions of the MSSs, implying that $\{M_i\}$ are independent. Furthermore, it is reasonable to model a time instant at which an incorrect acquisition occurs as a random variable. Therefore the arrival processes observed during different attempts are identically distributed, implying that $\{M_i\}$ are identically distributed. Therefore, $\{M_i\}$ are IID, and K has a geometric distribution with probability of success p_{cAcq}.

Using the above model, we show in Appendix A.1 that[8]

$$E\{M\} = E\{M_1\} E\{K\}. \qquad (4.83)$$

Substituting $E\{K\} = 1/p_{\text{cAcq}}$ gives

$$E\{M\} = E\{M_1\} / p_{\text{cAcq}}. \qquad (4.84)$$

---

[8]Note that the equation is not a direct application of the iterated law of expectation [8, p. 323] since we do not require K and M_1 to be independent.

Defining[9]

$$p_{\text{nal}} \triangleq P\left\{\mathsf{V}_{1:\mathsf{J}_1} \in \mathcal{R}^c\right\}, \tag{4.85a}$$

$$p_{\text{det}} \triangleq P\left\{\mathsf{V}_{1:\mathsf{J}_1-1} \in \mathcal{R}^c, \mathsf{V}_{\mathsf{J}_1} \in \mathcal{R}\right\}, \tag{4.85b}$$

$$p_{\text{nal-nal}} \triangleq P\left\{\mathsf{V}_{1:\mathsf{J}_2} \in \mathcal{R}^c\right\}, \tag{4.85c}$$

$$p_{\text{nal-det}} \triangleq P\left\{\mathsf{V}_{1:\mathsf{J}_2-1} \in \mathcal{R}^c, \mathsf{V}_{\mathsf{J}_2} \in \mathcal{R}\right\}, \tag{4.85d}$$

$$c_{\text{nal}} \triangleq P\left\{\mathsf{V}_{\mathsf{J}_2+1:\mathsf{J}_3} \in \mathcal{R}^c \mid \mathsf{V}_{\mathsf{J}_2-\ell_{\max}^{\mathrm{m}}+2:\mathsf{J}_2} \in \mathcal{R}^c\right\}, \tag{4.85e}$$

and

$$c_{\text{det}} \triangleq P\{\mathsf{V}_{\mathsf{J}_2+1:\mathsf{J}_3-1} \in \mathcal{R}^c, \mathsf{V}_{\mathsf{J}_3} \in \mathcal{R} \mid \mathsf{V}_{\mathsf{J}_2-\ell_{\max}^{\mathrm{m}}+2:\mathsf{J}_2} \in \mathcal{R}^c\}, \tag{4.85f}$$

we show in Appendix A.2 that

$$p_{\text{cAcq}} = \begin{cases} p_{\text{det}} + p_{\text{nal-det}}, & \text{if } c_{\text{nal}} = 1; \\[2mm] p_{\text{det}} + p_{\text{nal-det}} + \frac{p_{\text{nal-nal}} c_{\text{det}}}{1-c_{\text{nal}}}, & \text{if } 0 \le c_{\text{nal}} < 1, \end{cases} \tag{4.86}$$

and, in Appendix A.3 that

$$E\left\{\mathsf{M}_1\right\} = \begin{cases} 1 + p_{\text{nal}} + \frac{p_{\text{nal-nal}}}{1-c_{\text{nal}}}, & \text{if } 0 \le c_{\text{nal}} < 1; \\[2mm] 1 + p_{\text{nal}}, & \text{if } c_{\text{nal}} = 1 \text{ and } p_{\text{nal-nal}} = 0; \\[2mm] \infty, & \text{if } c_{\text{nal}} = 1 \text{ and } 0 < p_{\text{nal-nal}} \le 1. \end{cases} \tag{4.87}$$

For convenience, the probabilities in (4.85) will be referred to as the transition probabilities. In the next section, we will derive another performance metric, which is suitable for bursty transmission.

---

[9]When $\mathsf{J}_1 = 1$, we define $p_{\text{det}} \triangleq P\left\{\mathsf{V}_{\mathsf{J}_1} \in \mathcal{R}\right\}$. The subscript "det" stands for "detection," which refers to a detection of the marker. The subscript "nal" stands for "no alarm," which refers to the situation that decision variables under consideration belong to $\mathcal{R}^c$.

Probability of Correction Acquisition Within a Given Duration

The performance metric introduced in the previous section is suitable for transmission systems without delay constraints. For systems with delay constraints, e.g., bursty transmission systems, an appropriate performance metric is the probability of correct acquisition within a given duration.

The probability of correct acquisition within m MSSs is equal to $P\{\mathsf{M} \leq m\}$, where the random variable M is defined in Section 4.4.2. Then,

$$P\{\mathsf{M} \leq m\} = \sum_{k=1}^{\infty} P\{\mathsf{M}_1 + \mathsf{M}_2 + \cdots + \mathsf{M}_\mathsf{K} \leq m \mid \mathsf{K} = k\} P\{\mathsf{K} = k\}$$

$$= \sum_{k=1}^{m} \underbrace{P\{\mathsf{M}_1 + \mathsf{M}_2 + \cdots + \mathsf{M}_k \leq m\}}_{\triangleq \gamma(k,m)} (1 - p_{\mathrm{cAcq}})^{k-1} p_{\mathrm{cAcq}},$$

where $(1 - p_{\mathrm{cAcq}})^0 \triangleq 1$. The upper limit of the summation becomes finite since

$$P\{\mathsf{M}_1 + \mathsf{M}_2 + \cdots + \mathsf{M}_k \leq m\} = 0$$

for $m < k$, owing to the fact that $\mathsf{M}_i \geq 1$. The function $\gamma(k, m)$ for $1 \leq k \leq m$ is given by a recursive formula (see Appendix A.4)

$$\gamma(1, m) = 1 - P\{\mathsf{M}_1 \geq m + 1\}, \qquad \text{for } 1 \leq m \qquad (4.88\text{a})$$

$$\gamma(k + 1, m) = \sum_{n=1}^{m-k} \gamma(k, m - n) P\{\mathsf{M}_1 = n\}, \qquad \text{for } 0 < k < m, \qquad (4.88\text{b})$$

where

$$P\{\mathsf{M}_1 = n\} = P\{\mathsf{M}_1 \geq n\} - P\{\mathsf{M}_1 \geq n + 1\}, \qquad \text{for } n = 1, 2, 3, \ldots,$$

and according to Appendix A.3,

$$P\{\mathsf{M}_1 \geq n\} = \begin{cases} 1, & \text{for } n = 1; \\[2mm] p_{\text{nal}}, & \text{for } n = 2; \\[2mm] p_{\text{nal-nal}}, & \text{for } n = 3; \\[2mm] p_{\text{nal-nal}}(c_{\text{nal}})^{n-3}, & \text{for } n \geq 4. \end{cases}$$

This completes the derivation of the second performance metric.

4.4.3 Important Aspects of the Solution and the Consequences

This section assesses the computation time as a function of system parameters, $\ell_{\text{max}}^{\text{m}}$, $\ell_{\text{max}}^{\text{d}}$, and $\ell_{\text{max}}^{\text{s}}$.

Computation time T_{comp} required for evaluating the transition probabilities arises from two subtasks. The first subtask is to evaluate the joint probability terms that appear in the expressions for the transition probabilities. The second subtask is to multiply these joint probability terms and sum them during the evaluation of the transition probabilities. Total computation time equals computation time $T_{\text{comp}}^{(1)}$ for the first subtask plus the computation time $T_{\text{comp}}^{(2)}$ for the second subtask.

Computation time for the first subtask depends on the number of distinct joint probabilities and is given by

$$T_{\text{comp}}^{(1)} = \sum_{k=1}^{\ell_{\text{max}}^{\text{m}}} \tilde{N}(k)\, E(k), \tag{4.89}$$

where $E(k)$ denotes the computation time of a k-joint probability and $\tilde{N}(k)$ denotes the number of k-joint probabilities required to evaluate the transition probabilities. If the transition probabilities are derived according to the previous section, the value

of $\tilde{N}(k)$ satisfies (see Appendix A.6)

$$2 \le \tilde{N}(k) \le 2k + 1, \text{ for } 1 \le k \le \ell_{\max}^{m} - 2, \tag{4.90a}$$

$$3\ell_{\max}^{m} - 2 \le \tilde{N}(\ell_{\max}^{m} - 1) \le 5\ell_{\max}^{m} - 4, \tag{4.90b}$$

$$3\ell_{\max}^{m} - 1 \le \tilde{N}(\ell_{\max}^{m}) \le 5\ell_{\max}^{m} - 2. \tag{4.90c}$$

According to the appendix, the left inequalities are satisfied with equality if $\mathsf{L}_i^s = 0$, a typical case for continuous transmission without any idle fill character. The right inequalities are satisfied with equality if $\mathsf{L}_i^s \ge 2\ell_{\max}^{m} - 2$, a typical case for a transmission with large number of idle fill characters or a bursty transmission with long silent periods. The value of $E(k)$ depends on a specific application. For example, an exponential function, $E(k) = c^k$ for a constant $c > 1$, is a reasonable model for computation time of a k-nested integration using a conventional approach [90, p. 161]. In that case, $T_{\text{comp}}^{(1)}$ in (4.89) becomes [54, eq. 0.113]

$$T_{\text{comp}}^{(1)} = O\left(\ell_{\max}^{m} c^{\ell_{\max}^{m}}\right),$$

which gives a computation time for the first subtask.

Computation time for the second subtask is dominated by time required to evaluate $p_{\text{nal-nal}}$. Hence,

$$T_{\text{comp}}^{(2)} = \begin{cases} O\left((\ell_{\max}^{d})^2 (\ell_{\max}^{d} + \ell_{\max}^{m})^2\right), \\ \qquad\qquad\qquad \text{if } \ell_{\max}^{s} = 0; \\ O\left((\ell_{\max}^{d})^2 (\ell_{\max}^{s})^2 (\ell_{\max}^{d} + \ell_{\max}^{s} + \ell_{\max}^{m})^2\right), \\ \qquad\qquad\qquad \text{if } \ell_{\max}^{s} \ge \ell_{\max}^{m} - 1. \end{cases}$$

Therefore, total computation time is

$$
T_{\text{comp}} = \begin{cases} O\Big((\ell_{\max}^{\text{d}})^2(\ell_{\max}^{\text{d}} + \ell_{\max}^{\text{m}})^2 + \ell_{\max}^{\text{m}}c^{\ell_{\max}^{\text{m}}}\Big), \\[1em] \qquad\qquad\qquad\qquad \text{if } \ell_{\max}^{\text{s}} = 0; \\[1em] O\Big((\ell_{\max}^{\text{d}})^2(\ell_{\max}^{\text{s}})^2(\ell_{\max}^{\text{d}} + \ell_{\max}^{\text{s}} + \ell_{\max}^{\text{m}})^2 \\[0.5em] \qquad + \ell_{\max}^{\text{m}}c^{\ell_{\max}^{\text{m}}}\Big), \qquad \text{if } \ell_{\max}^{\text{s}} \geq \ell_{\max}^{\text{m}} - 1. \end{cases}
$$

4.4.4 Elementary Examples

To illustrate our framework, we consider a simple example. The example involves continuous transmission of binary symbols over the AWGN channel and the specific settings for frame synchronization. Next, we describe these settings.

The transmitted data symbols, $\{\mathsf{D}_j\}$, are IID binary-valued Bernoulli random variables, equally likely to be -1 and $+1$. The length of each frame is uniform over the set, $\{30, 31, \ldots, 40\}$. We consider a continuous transmission, so that the length of silence period is zero: $\mathsf{L}_i^{\text{s}} = 0$. The marker is given by $(c_1, \ldots, c_8) = (+1, -1, +1, +1, +1, -1, -1, -1)$, which has good correlation properties [102].

The frame synchronizer decides whether a marker begins at index j by considering two hypotheses: H_1 and H_0. Here, H_1 denote the hypothesis that a marker begins at index j, whereas H_0 denotes the hypothesis that a marker does not begin at index j:

$$
\mathsf{H}_1 : \mathsf{X}_i = c_{i-j+1} + \mathsf{N}_i, \qquad\qquad j \leq i \leq j + 7
$$

$$
\mathsf{H}_0 : \mathsf{X}_i = \mathsf{D}_i + \mathsf{N}_i, \qquad\qquad j \leq i \leq j + 7.
$$

We consider AWGN channel, where $\{\mathsf{N}_i\}$ are IID standard normal random variables (zero-mean and variance of one). The decision rule is to compare the correlation to a threshold:

$$
\mathsf{V}_j \triangleq \sum_{k=1}^{\ell_{\max}^{\text{m}}} c_k \mathsf{X}_{j+k-1} \underset{\mathsf{H}_0}{\overset{\mathsf{H}_1}{\gtrless}} \eta,
$$

where the threshold η is selected according to the Neyman-Pearson criteria to achieve

129
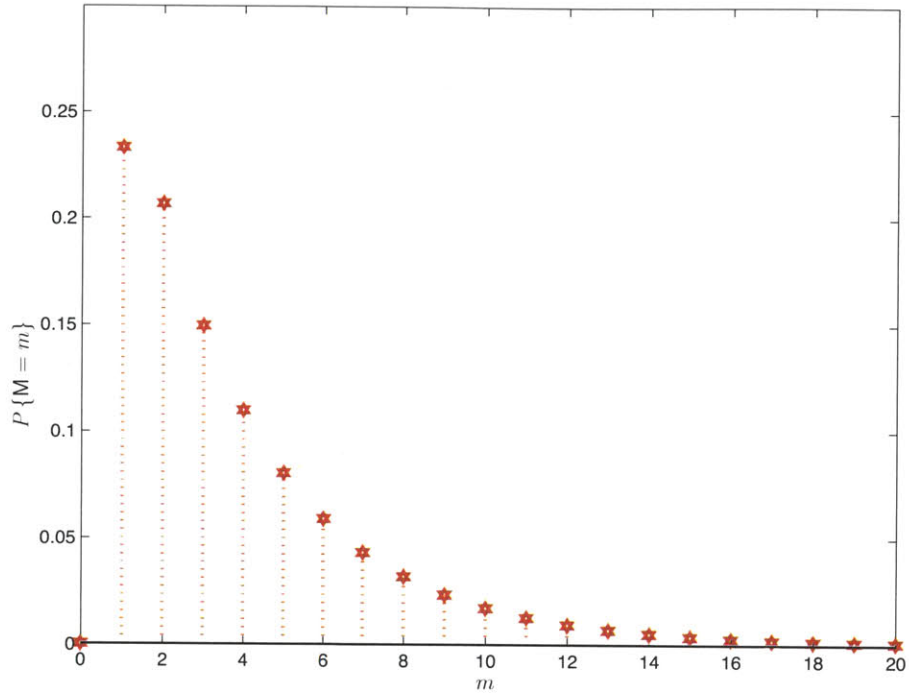
Figure 4-14: The PMF of M characterizes the amount of time to correct frame synchronization.

a target value, α, of probability of false alarm. For illustration, the target value is set to be $\alpha = 1\%$. Using this setting, we can obtain the probability distribution and the expected value of M, the duration (in terms of the number of MSS) to correct marker acquisition.

We plot the PMF of M in Fig. 4-14. The expected value $E\{M\}$ can be obtained from the PMF or, alternatively, from the expression in (4.87). The expectation turns out to be 3.87, meaning that on average the frame synchronizer passes by 3.87 markers before making a correct decision of frame acquisition. A more comprehensive example, which gives the performance as a function of the SNR, is given later in Section 4.5.3.

4.4.5 Proofs of the Key Theorems

To obtain the performance metrics derived in previous two sections, we need to evaluate the transition probabilities given in (4.85). This section outlines approaches to derive these transition probabilities.
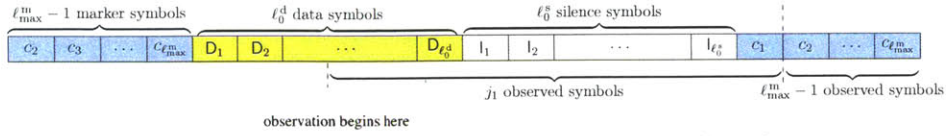
(a) Sequence of symbols satisfying the condition $\{J_1 = j_1, L_0^d = \ell_0^d, L_0^s = \ell_0^s\}$
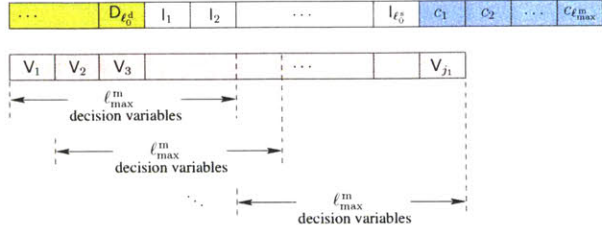
(b) Blocks of length ℓ_{max}^m, each of which corresponds to a different ℓ_{max}^m-joint probability term in the numerator
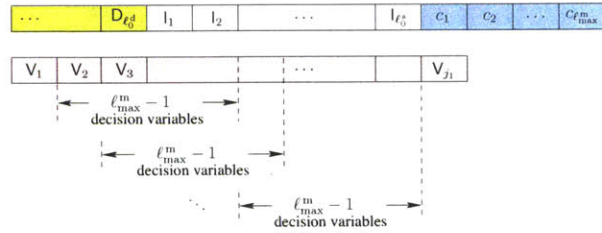
(c) Blocks of length $\ell_{max}^m - 1$, each of which corresponds to a different $(\ell_{max}^m - 1)$-joint probability term in the denominator

Figure 4-15: Pictorial representation of the MSSs helps to aid the interpretation of equation (4.92)

Derivation for p_{nal}

Let ℓ_{max}^d denote the maximum frame length and ℓ_{max}^s denote the maximum length of silent transmission: $L_1^d \leq \ell_{max}^d$ and $L_1^s \leq \ell_{max}^s$. Let L_0^d and L_0^s denote the length of the frame and the length of silent transmission, respectively, of the MSS that contains

131

the first observed symbol. We write

$$p_{\text{nal}} = P\left\{\mathsf{V}_{1:\mathsf{J}_1} \in \mathcal{R}^c\right\}$$

$$= \sum_{\ell_0^{\text{d}}=1}^{\ell_{\text{max}}^{\text{d}}} \sum_{\ell_0^{\text{s}}=0}^{\ell_{\text{max}}^{\text{s}}} \sum_{j_1=1}^{\ell_0^{\text{d}}+\ell_0^{\text{s}}+\ell_{\text{max}}^{\text{m}}} P\{\mathsf{V}_{1:\mathsf{J}_1} \in \mathcal{R}^c \mid \mathsf{J}_1 = j_1, \mathsf{L}_0^{\text{d}} = \ell_0^{\text{d}}, \mathsf{L}_0^{\text{s}} = \ell_0^{\text{s}}\}$$

$$\times P\left\{\mathsf{J}_1 = j_1 \mid \mathsf{L}_0^{\text{d}} = \ell_0^{\text{d}}, \mathsf{L}_0^{\text{s}} = \ell_0^{\text{s}}\right\} \times P\left\{\mathsf{L}_0^{\text{d}} = \ell_0^{\text{d}}\right\} P\left\{\mathsf{L}_0^{\text{s}} = \ell_0^{\text{s}}\right\},$$

where each probability term inside the summation can be obtained as follows.

The probabilities $P\left\{\mathsf{L}_0^{\text{d}} = \ell_0^{\text{d}}\right\}$ and $P\left\{\mathsf{L}_0^{\text{s}} = \ell_0^{\text{s}}\right\}$ are given by (see Appendix A.5)

$$P\left\{\mathsf{L}_0^{\text{d}} = \ell_0^{\text{d}}\right\} = \left(\frac{\ell_0^{\text{d}} + E\left\{\mathsf{L}_1^{\text{s}}\right\} + \ell_{\text{max}}^{\text{m}}}{E\left\{\mathsf{L}_1^{\text{d}}\right\} + E\left\{\mathsf{L}_1^{\text{s}}\right\} + \ell_{\text{max}}^{\text{m}}}\right) P\left\{\mathsf{L}_1^{\text{d}} = \ell_0^{\text{d}}\right\} \qquad (4.91\text{a})$$

$$P\left\{\mathsf{L}_0^{\text{s}} = \ell_0^{\text{s}}\right\} = \left(\frac{\ell_0^{\text{s}} + E\left\{\mathsf{L}_1^{\text{d}}\right\} + \ell_{\text{max}}^{\text{m}}}{E\left\{\mathsf{L}_1^{\text{d}}\right\} + E\left\{\mathsf{L}_1^{\text{s}}\right\} + \ell_{\text{max}}^{\text{m}}}\right) P\left\{\mathsf{L}_1^{\text{s}} = \ell_0^{\text{s}}\right\}. \qquad (4.91\text{b})$$

On the other hand, the conditional probability $P\left\{\mathsf{J}_1 = j_1 \mid \mathsf{L}_0^{\text{d}} = \ell_0^{\text{d}}, \mathsf{L}_0^{\text{s}} = \ell_0^{\text{s}}\right\}$ is uniform over the length of the MSS, since the first observed symbol can be anywhere in the MSS:

$$P\left\{\mathsf{J}_1 = j_1 \mid \mathsf{L}_0^{\text{d}} = \ell_0^{\text{d}}, \mathsf{L}_0^{\text{s}} = \ell_0^{\text{s}}\right\} = \begin{cases} \frac{1}{\ell_0^{\text{d}}+\ell_0^{\text{s}}+\ell_{\text{max}}^{\text{m}}}, & \text{for } 1 \leq j_1 \leq \ell_0^{\text{d}} + \ell_0^{\text{s}} + \ell_{\text{max}}^{\text{m}}; \\ 0, & \text{otherwise.} \end{cases}$$

The conditional probability

$$P\left\{\mathsf{V}_{1:\mathsf{J}_1} \in \mathcal{R}^c \mid \mathsf{J}_1 = j_1, \mathsf{L}_0^{\text{d}} = \ell_0^{\text{d}}, \mathsf{L}_0^{\text{s}} = \ell_0^{\text{s}}\right\}$$

for $1 \leq j_1 \leq \ell_{\text{max}}^{\text{m}}$ can be obtained by integrating the conditional joint probability density function (pdf) over the region $(\mathcal{R}^c)^{j_1}$.[10] For $j_1 \geq \ell_{\text{max}}^{\text{m}} + 1$, we obtain the

---

[10]The symbol $\mathcal{A}^{j_1}$ for a set $\mathcal{A}$ refers to the Cartesian product $\mathcal{A} \times \mathcal{A} \times \cdots \times \mathcal{A}$, where $\mathcal{A}$ appears j_1 times.

conditional probability through the expansion:

$$P\{V_{1:J_1} \in \mathcal{R}^c : J_1 = j_1, L_0^d = \ell_0^d, L_0^s = \ell_0^s\}$$

$$= P\left\{V_{1:\ell_{\max}^m} \in \mathcal{R}^c \mid J_1 = j_1, L_0^d = \ell_0^d, L_0^s = \ell_0^s\right\}$$

$$\times \prod_{k=\ell_{\max}^m+1}^{j_1} P\left\{V_k \in \mathcal{R}^c \mid V_{k-\ell_{\max}^m+1:k-1} \in \mathcal{R}^c, J_1 = j_1, L_0^d = \ell_0^d, L_0^s = \ell_0^s\right\}$$

$$= P\left\{V_{1:\ell_{\max}^m} \in \mathcal{R}^c \mid J_1 = j_1, L_0^d = \ell_0^d, L_0^s = \ell_0^s\right\}$$

$$\times \prod_{k=\ell_{\max}^m+1}^{j_1} \frac{P\left\{V_{k-\ell_{\max}^m+1:k} \in \mathcal{R}^c \mid J_1 = j_1, L_0^d = \ell_0^d, L_0^s = \ell_0^s\right\}}{P\left\{V_{k-\ell_{\max}^m+1:k-1} \in \mathcal{R}^c \mid J_1 = j_1, L_0^d = \ell_0^d, L_0^s = \ell_0^s\right\}}$$

$$= \underbrace{\left[\prod_{k=1}^{j_1-\ell_{\max}^m} \frac{P\left\{V_{k:k+\ell_{\max}^m-1} \in \mathcal{R}^c \mid J_1 = j_1, L_0^d = \ell_0^d, L_0^s = \ell_0^s\right\}}{P\left\{V_{k+1:k+\ell_{\max}^m-1} \in \mathcal{R}^c \mid J_1 = j_1, L_0^d = \ell_0^d, L_0^s = \ell_0^s\right\}}\right]}_{\triangleq \Lambda_{\text{pnal}}(j_1, \ell_0^d, \ell_0^s)}$$

$$\times P\left\{V_{J_1-\ell_{\max}^m+1:J_1} \in \mathcal{R}^c \mid J_1 = j_1, L_0^d = \ell_0^d, L_0^s = \ell_0^s\right\}. \tag{4.92}$$

Equation (4.92) can be interpreted with the help of Fig. 4-15 as follows. The condition $\{J_1 = j_1, L_0^d = \ell_0^d, L_0^s = \ell_0^s\}$ indicates that the observed symbols are the last j_1 symbols of an MSS with length $\ell_0^d + \ell_0^s + \ell_{\max}^m$, followed by $\ell_{\max}^m - 1$ marker symbols (see Fig. 4-15a). These observed symbols generate a total of j_1 decision variables. Each of the $j_1 - \ell_{\max}^m + 1$ terms in the numerator is a $\ell_{\max}^m$-joint probability, and each of the $j_1 - \ell_{\max}^m$ terms in the denominator is a $(\ell_{\max}^m - 1)$-joint probability.[11] Different terms in the numerator correspond to different segments of length $\ell_{\max}^m$, which are time-shifted versions of one another (see Fig. 4-15b). Similarly, different terms in the denominator correspond to different segments of length $\ell_{\max}^m - 1$, which are also time-shifted versions of one another (see Fig. 4-15c). In general, these joint-probability terms need to be obtained numerically.[12]

---

[11]We use the term *k-joint probability* to refer to a joint probability of k random variables.

[12]Each probability term in (4.92) can be obtained by integrating the conditional joint pdf of V_k's over the corresponding region.

Derivation for p_{det}

A similar approach to the previous section gives

$$p_{\text{det}} = P\left\{\mathsf{V}_{1\,:\,\mathsf{J}_1-1} \in \mathcal{R}^c, \mathsf{V}_{\mathsf{J}_1} \in \mathcal{R}\right\}$$

$$= \sum_{\ell_0^{\mathrm{d}}=1}^{\ell_{\max}^{\mathrm{d}}} \sum_{\ell_0^{\mathrm{s}}=0}^{\ell_{\max}^{\mathrm{s}}} \sum_{j_1=1}^{\ell_0^{\mathrm{d}}+\ell_0^{\mathrm{s}}+\ell_{\max}^{\mathrm{m}}} P\{\mathsf{V}_{1\,:\,\mathsf{J}_1-1} \in \mathcal{R}^c, \mathsf{V}_{\mathsf{J}_1} \in \mathcal{R} : \mathsf{J}_1 = j_1, \mathsf{L}_0^{\mathrm{d}} = \ell_0^{\mathrm{d}}, \mathsf{L}_0^{\mathrm{s}} = \ell_0^{\mathrm{s}}\}$$

$$\times \left(\frac{1}{\ell_0^{\mathrm{d}} + \ell_0^{\mathrm{s}} + \ell_{\max}^{\mathrm{m}}}\right) P\left\{\mathsf{L}_0^{\mathrm{d}} = \ell_0^{\mathrm{d}}\right\} P\left\{\mathsf{L}_0^{\mathrm{s}} = \ell_0^{\mathrm{s}}\right\}.$$

The conditional probability for $j_1 = 1$ is given by

$$P\{\mathsf{V}_{1\,:\,0} \in \mathcal{R}^c, \mathsf{V}_1 \in \mathcal{R} \,|\, \mathsf{J}_1 = 1, \mathsf{L}_0^{\mathrm{d}} = \ell_0^{\mathrm{d}}, \mathsf{L}_0^{\mathrm{s}} = \ell_0^{\mathrm{s}}\}$$

$$\triangleq P\left\{\mathsf{V}_1 \in \mathcal{R} \,|\, \mathsf{J}_1 = 1, \mathsf{L}_0^{\mathrm{d}} = \ell_0^{\mathrm{d}}, \mathsf{L}_0^{\mathrm{s}} = \ell_0^{\mathrm{s}}\right\}$$

$$= 1 - P\left\{\mathsf{V}_1 \in \mathcal{R}^c \,|\, \mathsf{J}_1 = 1, \mathsf{L}_0^{\mathrm{d}} = \ell_0^{\mathrm{d}}, \mathsf{L}_0^{\mathrm{s}} = \ell_0^{\mathrm{s}}\right\},$$

where the term on the right-hand side has already appeared during the evaluation of p_{nal}. The conditional probability for $2 \leq j_1 \leq \ell_{\max}^{\mathrm{m}}$ can be written as

$$P\left\{\mathsf{V}_{1\,:\,\mathsf{J}_1-1} \in \mathcal{R}^c, \mathsf{V}_{\mathsf{J}_1} \in \mathcal{R} \,|\, \mathsf{J}_1 = j_1, \mathsf{L}_0^{\mathrm{d}} = \ell_0^{\mathrm{d}}, \mathsf{L}_0^{\mathrm{s}} = \ell_0^{\mathrm{s}}\right\}$$

$$= P\left\{\mathsf{V}_{1\,:\,\mathsf{J}_1-1} \in \mathcal{R}^c \,|\, \mathsf{J}_1 = j_1, \mathsf{L}_0^{\mathrm{d}} = \ell_0^{\mathrm{d}}, \mathsf{L}_0^{\mathrm{s}} = \ell_0^{\mathrm{s}}\right\}$$

$$- P\left\{\mathsf{V}_{1\,:\,\mathsf{J}_1} \in \mathcal{R}^c \,|\, \mathsf{J}_1 = j_1, \mathsf{L}_0^{\mathrm{d}} = \ell_0^{\mathrm{d}}, \mathsf{L}_0^{\mathrm{s}} = \ell_0^{\mathrm{s}}\right\}. \quad (4.93)$$

The second probability term on the right-hand side has appeared during the evaluation of p_{nal}. The first probability has not appeared before and needs to be evaluated. The conditional probability for $j_1 \geq \ell_{\max}^{\mathrm{m}} + 1$ can be written as

$$P\left\{\mathsf{V}_{1:\mathsf{J}_1-1} \in \mathcal{R}^c, \mathsf{V}_{\mathsf{J}_1} \in \mathcal{R} \ : \ \mathsf{J}_1 = j_1, \mathsf{L}_0^{\mathrm{d}} = \ell_0^{\mathrm{d}}, \mathsf{L}_0^{\mathrm{s}} = \ell_0^{\mathrm{s}}\right\}$$

$$= \left[\prod_{k=1}^{j_1-1} \frac{P\left\{\mathsf{V}_{k:k+\ell_{\max}^{\mathrm{m}}-1} \in \mathcal{R}^c \ \middle| \ \mathsf{J}_1 = j_1, \mathsf{L}_0^{\mathrm{d}} = \ell_0^{\mathrm{d}}, \mathsf{L}_0^{\mathrm{s}} = \ell_0^{\mathrm{s}}\right\}}{P\left\{\mathsf{V}_{k+1:k+\ell_{\max}^{\mathrm{m}}-1} \in \mathcal{R}^c \ \middle| \ \mathsf{J}_1 = j_1, \mathsf{L}_0^{\mathrm{d}} = \ell_0^{\mathrm{d}}, \mathsf{L}_0^{\mathrm{s}} = \ell_0^{\mathrm{s}}\right\}}\right]$$

$$\times P\left\{\mathsf{V}_{\mathsf{J}_1-\ell_{\max}^{\mathrm{m}}+1:\mathsf{J}_1-1} \in \mathcal{R}^c, \mathsf{V}_{\mathsf{J}_1} \in \mathcal{R} \ \middle| \ \mathsf{J}_1 = j_1, \mathsf{L}_0^{\mathrm{d}} = \ell_0^{\mathrm{d}}, \mathsf{L}_0^{\mathrm{s}} = \ell_0^{\mathrm{s}}\right\}$$

$$= \Lambda_{\mathrm{pnal}}(j_1, \ell_0^{\mathrm{d}}, \ell_0^{\mathrm{s}}) \left[P\left\{\mathsf{V}_{\mathsf{J}_1-\ell_{\max}^{\mathrm{m}}+1:\mathsf{J}_1-1} \in \mathcal{R}^c \ \middle| \ \mathsf{J}_1 = j_1, \mathsf{L}_0^{\mathrm{d}} = \ell_0^{\mathrm{d}}, \mathsf{L}_0^{\mathrm{s}} = \ell_0^{\mathrm{s}}\right\} \right.$$

$$\left. - P\left\{\mathsf{V}_{\mathsf{J}_1-\ell_{\max}^{\mathrm{m}}+1:\mathsf{J}_1} \in \mathcal{R}^c \ \middle| \ \mathsf{J}_1 = j_1, \mathsf{L}_0^{\mathrm{d}} = \ell_0^{\mathrm{d}}, \mathsf{L}_0^{\mathrm{s}} = \ell_0^{\mathrm{s}}\right\} \right], \qquad (4.94)$$

where all terms have already appeared in (4.92) during the evaluation of p_{nal}.[13]

Derivation for $p_{\mathrm{nal\text{-}nal}}$

A similar approach to the previous section gives

$$p_{\mathrm{nal\text{-}nal}} = P\left\{\mathsf{V}_{1:\mathsf{J}_2} \in \mathcal{R}^c\right\}$$

$$= \sum_{\ell_0^{\mathrm{d}}=1}^{\ell_{\max}^{\mathrm{d}}} \sum_{\ell_0^{\mathrm{s}}=0}^{\ell_{\max}^{\mathrm{s}}} \sum_{j_1=1}^{\ell_0^{\mathrm{d}}+\ell_0^{\mathrm{s}}+\ell_{\max}^{\mathrm{m}}} \sum_{\ell_1^{\mathrm{d}}=1}^{\ell_{\max}^{\mathrm{d}}} \sum_{\ell_1^{\mathrm{s}}=0}^{\ell_{\max}^{\mathrm{s}}} P\{\mathsf{V}_{1:\mathsf{J}_2} \in \mathcal{R}^c \ : \ \mathsf{J}_1 = j_1, \mathsf{L}_0^{\mathrm{d}} = \ell_0^{\mathrm{d}}, \mathsf{L}_0^{\mathrm{s}} = \ell_0^{\mathrm{s}}, \mathsf{L}_1^{\mathrm{d}} = \ell_1^{\mathrm{d}}, \mathsf{L}_1^{\mathrm{s}} = \ell_1^{\mathrm{s}}\}$$

$$\times \left(\frac{1}{\ell_0^{\mathrm{d}} + \ell_0^{\mathrm{s}} + \ell_{\max}^{\mathrm{m}}}\right) P\left\{\mathsf{L}_0^{\mathrm{d}} = \ell_0^{\mathrm{d}}\right\} P\left\{\mathsf{L}_0^{\mathrm{s}} = \ell_0^{\mathrm{s}}\right\}$$

$$\times P\left\{\mathsf{L}_1^{\mathrm{d}} = \ell_1^{\mathrm{d}}\right\} P\left\{\mathsf{L}_1^{\mathrm{s}} = \ell_1^{\mathrm{s}}\right\}.$$

---

[13]The first probability expression in the bracket is the last joint-probability term in the *denominator* of $\Lambda_{\mathrm{pnal}}(j_1, \ell_0^{\mathrm{d}}, \ell_0^{\mathrm{s}})$ in (4.92). The second probability expression in the bracket is the last joint-probability term in the *numerator* of (4.92).

The conditional probability can be obtained using similar steps leading to (4.92), resulting in

$$P\{\mathsf{V}_{1:j_2} \in \mathcal{R}^c : \mathsf{J}_1 = j_1, \mathsf{L}_0^{\mathrm{d}} = \ell_0^{\mathrm{d}}, \mathsf{L}_0^{\mathrm{s}} = \ell_0^{\mathrm{s}}, \mathsf{L}_1^{\mathrm{d}} = \ell_1^{\mathrm{d}}, \mathsf{L}_1^{\mathrm{s}} = \ell_1^{\mathrm{s}}\}$$

$$= \underbrace{\left[\prod_{k=1}^{j_2-\ell_{\max}^{\mathrm{m}}} \frac{P\left\{\mathsf{V}_{k:k+\ell_{\max}^{\mathrm{m}}-1} \in \mathcal{R}^c \mid \mathsf{J}_1 = j_1, \mathsf{L}_0^{\mathrm{d}} = \ell_0^{\mathrm{d}}, \mathsf{L}_0^{\mathrm{s}} = \ell_0^{\mathrm{s}}, \mathsf{L}_1^{\mathrm{d}} = \ell_1^{\mathrm{d}}, \mathsf{L}_1^{\mathrm{s}} = \ell_1^{\mathrm{s}}\right\}}{P\left\{\mathsf{V}_{k+1:k+\ell_{\max}^{\mathrm{m}}-1} \in \mathcal{R}^c \mid \mathsf{J}_1 = j_1, \mathsf{L}_0^{\mathrm{d}} = \ell_0^{\mathrm{d}}, \mathsf{L}_0^{\mathrm{s}} = \ell_0^{\mathrm{s}}, \mathsf{L}_1^{\mathrm{d}} = \ell_1^{\mathrm{d}}, \mathsf{L}_1^{\mathrm{s}} = \ell_1^{\mathrm{s}}\right\}} \right]}_{\triangleq \Lambda_{\mathrm{pnal\text{-}nal}}(j_1, \ell_0^{\mathrm{d}}, \ell_0^{\mathrm{s}}, \ell_1^{\mathrm{s}}, \ell_1^{\mathrm{d}})}$$

$$\times P\left\{\mathsf{V}_{j_2-\ell_{\max}^{\mathrm{m}}+1:j_2} \in \mathcal{R}^c \mid \mathsf{J}_1 = j_1, \mathsf{L}_0^{\mathrm{d}} = \ell_0^{\mathrm{d}}, \mathsf{L}_0^{\mathrm{s}} = \ell_0^{\mathrm{s}}, \mathsf{L}_1^{\mathrm{d}} = \ell_1^{\mathrm{d}}, \mathsf{L}_1^{\mathrm{s}} = \ell_1^{\mathrm{s}}\right\}, \quad (4.95)$$

where $j_2 \triangleq j_1 + \ell_1^{\mathrm{d}} + \ell_1^{\mathrm{s}} + \ell_{\max}^{\mathrm{m}}$.[14]

Equation (4.95) can be interpreted with the help of Fig. 4-16 as follows. The condition $\{\mathsf{J}_1 = j_1, \mathsf{L}_0^{\mathrm{d}} = \ell_0^{\mathrm{d}}, \mathsf{L}_0^{\mathrm{s}} = \ell_0^{\mathrm{s}}, \mathsf{L}_1^{\mathrm{d}} = \ell_1^{\mathrm{d}}, \mathsf{L}_1^{\mathrm{s}} = \ell_1^{\mathrm{s}}\}$ indicates that the segment of the observed symbols consists of (a) the last j_1 symbols of an MSS with length $\ell_0^{\mathrm{d}} + \ell_0^{\mathrm{s}} + \ell_{\max}^{\mathrm{m}}$, (b) all symbols of the next MSS with length $\ell_1^{\mathrm{d}} + \ell_1^{\mathrm{s}} + \ell_{\max}^{\mathrm{m}}$, and (c) $\ell_{\max}^{\mathrm{m}} - 1$ marker symbols (see Fig. 4-16a). These observed symbols generate a total of j_2 decision variables. Each of the $j_2 - \ell_{\max}^{\mathrm{m}} + 1$ terms in the numerator is a $\ell_{\max}^{\mathrm{m}}$-joint probability, and each of the $j_2 - \ell_{\max}^{\mathrm{m}}$ terms in the denominator is a $(\ell_{\max}^{\mathrm{m}} - 1)$-joint probability. Different terms in the numerator correspond to different segments of length $\ell_{\max}^{\mathrm{m}}$, which are time-shifted versions of one another (see Fig. 4-16b). Similarly, different terms in the denominator correspond to different segments of length $\ell_{\max}^{\mathrm{m}} - 1$, which are also time-shifted versions of one another (see Fig. 4-16c). In general, these joint-probability terms need to be obtained numerically.

By comparing Fig. 4-16 and Fig. 4-15, it will be apparent that most of the $\ell_{\max}^{\mathrm{m}}$-joint probabilities and $(\ell_{\max}^{\mathrm{m}} - 1)$-joint probabilities in (4.95) have already appeared in (4.92) for the evaluation of p_{nal}. The remaining joint probability terms need to be evaluated, and these terms correspond to the segments near the boundary of the MSSs. Hence, the effort to obtain $p_{\mathrm{nal\text{-}nal}}$ after we have obtained p_{nal} is minimal from a numerical point of view.

---

[14]Recall that $\mathsf{J}_2 = j_1 + \ell_1^{\mathrm{d}} + \ell_1^{\mathrm{s}} + \ell_{\max}^{\mathrm{m}}$ when conditioned on $\mathsf{J}_1 = j_1$, $\mathsf{L}_1^{\mathrm{d}} = \ell_1^{\mathrm{d}}$, and $\mathsf{L}_1^{\mathrm{s}} = \ell_1^{\mathrm{s}}$.

$\ell_{\max}^{m} - 1$ marker symbols ℓ_0^{d} data symbols ℓ_0^{s} silence symbols

| c_2 | c_3 | $\cdots$ | $c_{\ell_{\max}^{m}}$ | D_1 | D_2 | $\cdots$ | $D_{\ell_0^{d}}$ | I_1 | I_2 | $\cdots$ | $I_{\ell_0^{s}}$ | c_1 |

observation begins here j_1 observed symbols

lm_11_marker_symbols ℓ_1^{d} data symbols ℓ_1^{s} silence symbols

| c_2 | $\cdots$ | $c_{\ell_{\max}^{m}}$ | $\tilde{D}_1$ | $\tilde{D}_2$ | $\cdots$ | $\tilde{D}_{\ell_1^{d}}$ | $\tilde{I}_1$ | $\tilde{I}_2$ | $\cdots$ | $\tilde{I}_{\ell_1^{s}}$ | c_1 | c_2 | $\cdots$ | $c_{\ell_{\max}^{m}}$ |

$\ell_1^{d} + \ell_1^{s} + \ell_{\max}^{m}$ observed symbols $\ell_{\max}^{m} - 1$ marker symbols

(a) Sequence of symbols satisfying the condition $\{L_1^{d} = \ell_1^{d}, L_1^{s} = \ell_1^{s}, J_1 = j_1, L_0^{d} = \ell_0^{d}, L_0^{s} = \ell_0^{s}\}$

| $\cdots$ | $D_{\ell_0^{d}}$ | I_1 | I_2 | $\cdots$ | $I_{\ell_0^{s}}$ | c_1 |

| V_1 | V_2 | V_3 | | $\cdots$ | | V_{j_1} |

$\ell_{\max}^{m}$ decision variables

$\ell_{\max}^{m}$ decision variables

| c_2 | $\cdots$ | $c_{\ell_{\max}^{m}}$ | $\tilde{D}_1$ | $\tilde{D}_2$ | $\cdots$ | $\tilde{D}_{\ell_1^{d}}$ | $\tilde{I}_1$ | $\tilde{I}_2$ | $\cdots$ | $\tilde{I}_{\ell_1^{s}}$ | c_1 | c_2 | $\cdots$ | $c_{\ell_{\max}^{m}}$ |

| $\cdots$ | V_{j_2} |

$\cdots$ $\ell_{\max}^{m}$ decision variables

(b) Blocks of length $\ell_{\max}^{m}$, each of which corresponds to a different $\ell_{\max}^{m}$-joint probability term in the numerator

| $\cdots$ | $D_{\ell_0^{d}}$ | I_1 | I_2 | $\cdots$ | $I_{\ell_0^{s}}$ | c_1 |

| V_1 | V_2 | V_3 | | $\cdots$ | | V_{j_1} |

$\ell_{\max}^{m} - 1$ decision variables

$\ell_{\max}^{m} - 1$ decision variables

| c_2 | $\cdots$ | $c_{\ell_{\max}^{m}}$ | $\tilde{D}_1$ | $\tilde{D}_2$ | $\cdots$ | $\tilde{D}_{\ell_1^{d}}$ | $\tilde{I}_1$ | $\tilde{I}_2$ | $\cdots$ | $\tilde{I}_{\ell_1^{s}}$ | c_1 | c_2 | $\cdots$ | $c_{\ell_{\max}^{m}}$ |

| $\cdots$ | V_{j_2} |

$\cdots$ $\ell_{\max}^{m} - 1$ decision variables

(c) Blocks of length $\ell_{\max}^{m} - 1$, each of which corresponds to a different $(\ell_{\max}^{m} - 1)$-joint probability term in the denominator
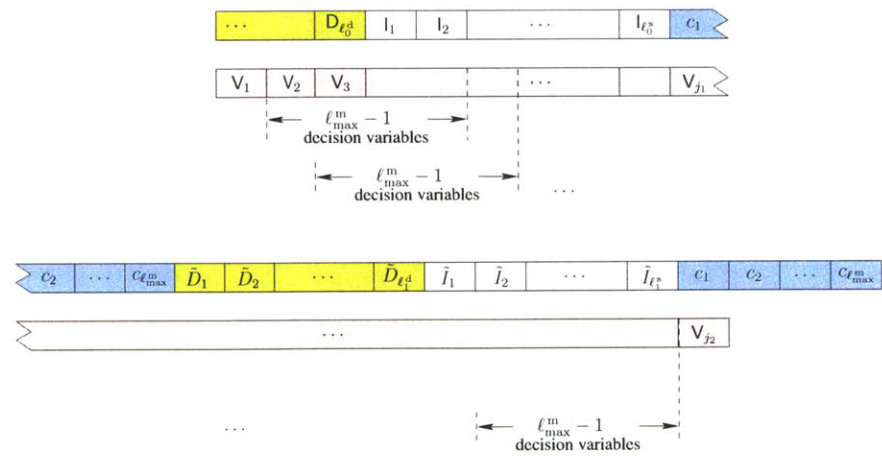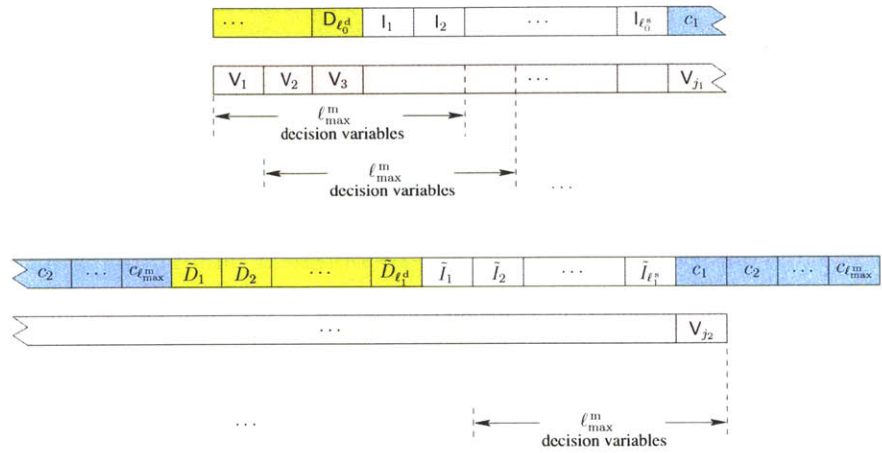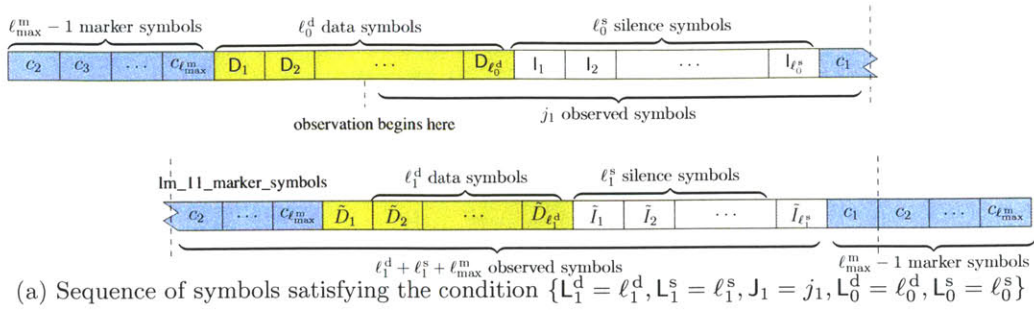
Figure 4-16: Pictorial representation of the MSSs helps to aid the interpretation of equation (4.95).

137

Derivation for $p_{\text{nal-det}}$

A similar approach to the previous case gives

$$p_{\text{nal-det}} = P\left\{\mathsf{V}_{1\,:\,\mathsf{J}_2-1} \in \mathcal{R}^c, \mathsf{V}_{\mathsf{J}_2} \in \mathcal{R}\right\}$$

$$= \sum_{\ell_0^{\text{d}}=1}^{\ell_{\text{max}}^{\text{d}}} \sum_{\ell_0^{\text{s}}=0}^{\ell_{\text{max}}^{\text{s}}} \sum_{j_1=1}^{\ell_0^{\text{d}}+\ell_0^{\text{s}}+\ell_{\text{max}}^{\text{m}}} \sum_{\ell_1^{\text{d}}=1}^{\ell_{\text{max}}^{\text{d}}} \sum_{\ell_1^{\text{s}}=0}^{\ell_{\text{max}}^{\text{s}}} P\{\mathsf{V}_{1\,:\,\mathsf{J}_2-1} \in \mathcal{R}^c, \mathsf{V}_{\mathsf{J}_2} \in \mathcal{R} :$$

$$\mathsf{J}_1 = j_1, \mathsf{L}_0^{\text{d}} = \ell_0^{\text{d}}, \mathsf{L}_0^{\text{s}} = \ell_0^{\text{s}}, \mathsf{L}_1^{\text{d}} = \ell_1^{\text{d}}, \mathsf{L}_1^{\text{s}} = \ell_1^{\text{s}}\}$$

$$\times \left(\frac{1}{\ell_0^{\text{d}} + \ell_0^{\text{s}} + \ell_{\text{max}}^{\text{m}}}\right) P\left\{\mathsf{L}_0^{\text{d}} = \ell_0^{\text{d}}\right\} P\left\{\mathsf{L}_0^{\text{s}} = \ell_0^{\text{s}}\right\}$$

$$\times P\left\{\mathsf{L}_1^{\text{d}} = \ell_1^{\text{d}}\right\} P\left\{\mathsf{L}_1^{\text{s}} = \ell_1^{\text{s}}\right\},$$

where the conditional probability can be obtained numerically from the expansion below:

$$P\{\mathsf{V}_{1\,:\,j_2-1} \in \mathcal{R}^c, \mathsf{V}_{j_2} \in \mathcal{R} : \mathsf{J}_1 = j_1, \mathsf{L}_0^{\text{d}} = \ell_0^{\text{d}}, \mathsf{L}_0^{\text{s}} = \ell_0^{\text{s}}, \mathsf{L}_1^{\text{d}} = \ell_1^{\text{d}}, \mathsf{L}_1^{\text{s}} = \ell_1^{\text{s}}\}$$

$$= \Lambda_{\text{pnal-nal}}(j_1, \ell_0^{\text{d}}, \ell_0^{\text{s}}, \ell_1^{\text{s}}, \ell_1^{\text{d}})$$

$$\times P\left\{\mathsf{V}_{j_2-\ell_{\text{max}}^{\text{m}}+1\,:\,j_2-1} \in \mathcal{R}^c, \mathsf{V}_{j_2} \in \mathcal{R} \,\middle|\, \mathsf{J}_1 = j_1, \mathsf{L}_0^{\text{d}} = \ell_0^{\text{d}}, \mathsf{L}_0^{\text{s}} = \ell_0^{\text{s}}, \mathsf{L}_1^{\text{d}} = \ell_1^{\text{d}}, \mathsf{L}_1^{\text{s}} = \ell_1^{\text{s}}\right\}$$

$$= \Lambda_{\text{pnal-nal}}(j_1, \ell_0^{\text{d}}, \ell_0^{\text{s}}, \ell_1^{\text{s}}, \ell_1^{\text{d}})$$

$$\times \left[P\left\{\mathsf{V}_{j_2-\ell_{\text{max}}^{\text{m}}+1\,:\,j_2-1} \in \mathcal{R}^c \,\middle|\, \mathsf{J}_1 = j_1, \mathsf{L}_0^{\text{d}} = \ell_0^{\text{d}}, \mathsf{L}_0^{\text{s}} = \ell_0^{\text{s}}, \mathsf{L}_1^{\text{d}} = \ell_1^{\text{d}}, \mathsf{L}_1^{\text{s}} = \ell_1^{\text{s}}\right\}\right.$$

$$\left.- P\left\{\mathsf{V}_{j_2-\ell_{\text{max}}^{\text{m}}+1\,:\,j_2} \in \mathcal{R}^c \,\middle|\, \mathsf{J}_1 = j_1, \mathsf{L}_0^{\text{d}} = \ell_0^{\text{d}}, \mathsf{L}_0^{\text{s}} = \ell_0^{\text{s}}, \mathsf{L}_1^{\text{d}} = \ell_1^{\text{d}}, \mathsf{L}_1^{\text{s}} = \ell_1^{\text{s}}\right\}\right],$$

$$(4.96)$$

for $j_2 \triangleq j_1 + \ell_1^{\text{d}} + \ell_1^{\text{s}} + \ell_{\text{max}}^{\text{m}}$. All terms in (4.96) have appeared in (4.95) for the evaluation of $p_{\text{nal-nal}}$.[15] Hence, the effort to obtain $p_{\text{nal-det}}$ after we have obtained $p_{\text{nal-nal}}$ is minimal from a numerical point of view.

---

[15]The first probability expression in the bracket is the last joint-probability term in the *denominator* of (4.95). The second probability expression in the bracket is the last joint-probability term in the *numerator* of (4.95).

Derivation for c_{nal}

We write c_{nal} as

$$c_{\text{nal}} = P\left\{\mathsf{V}_{\mathsf{J}_2+1\,:\,\mathsf{J}_3} \in \mathcal{R}^c \,\middle|\, \mathsf{V}_{\mathsf{J}_2-\ell_{\max}^{\mathrm{m}}+2\,:\,\mathsf{J}_2} \in \mathcal{R}^c\right\}$$

$$= \sum_{\ell_1^{\mathrm{d}}=1}^{\ell_{\max}^{\mathrm{d}}} \sum_{\ell_1^{\mathrm{s}}=0}^{\ell_{\max}^{\mathrm{s}}} \sum_{\ell_2^{\mathrm{d}}=1}^{\ell_{\max}^{\mathrm{d}}} \sum_{\ell_2^{\mathrm{s}}=0}^{\ell_{\max}^{\mathrm{s}}} \frac{P\left\{\mathsf{V}_{\mathsf{J}_2-\ell_{\max}^{\mathrm{m}}+2\,:\,\mathsf{J}_3} \in \mathcal{R}^c \,\middle|\, \mathsf{L}_1^{\mathrm{d}} = \ell_1^{\mathrm{d}}, \mathsf{L}_1^{\mathrm{s}} = \ell_1^{\mathrm{s}}, \mathsf{L}_2^{\mathrm{d}} = \ell_2^{\mathrm{d}}, \mathsf{L}_2^{\mathrm{s}} = \ell_2^{\mathrm{s}}\right\}}{P\left\{\mathsf{V}_{\mathsf{J}_2-\ell_{\max}^{\mathrm{m}}+2\,:\,\mathsf{J}_2} \in \mathcal{R}^c \,\middle|\, \mathsf{L}_1^{\mathrm{d}} = \ell_1^{\mathrm{d}}, \mathsf{L}_1^{\mathrm{s}} = \ell_1^{\mathrm{s}}, \mathsf{L}_2^{\mathrm{d}} = \ell_2^{\mathrm{d}}, \mathsf{L}_2^{\mathrm{s}} = \ell_2^{\mathrm{s}}\right\}}$$

$$\times\, P\left\{\mathsf{L}_1^{\mathrm{d}} = \ell_1^{\mathrm{d}}\right\} P\left\{\mathsf{L}_1^{\mathrm{s}} = \ell_1^{\mathrm{s}}\right\} P\left\{\mathsf{L}_2^{\mathrm{d}} = \ell_2^{\mathrm{d}}\right\} P\left\{\mathsf{L}_2^{\mathrm{s}} = \ell_2^{\mathrm{s}}\right\}.$$

$$(4.97)$$

To simplify the index, we let $\mathsf{W}_j \triangleq \mathsf{V}_{j+\mathsf{J}_2-\ell_{\max}^{\mathrm{m}}+1}$, for $j \geq 1$. Then, c_{nal} is given by

$$c_{\text{nal}} = \sum_{\ell_1^{\mathrm{d}}=1}^{\ell_{\max}^{\mathrm{d}}} \sum_{\ell_1^{\mathrm{s}}=0}^{\ell_{\max}^{\mathrm{s}}} \sum_{\ell_2^{\mathrm{d}}=1}^{\ell_{\max}^{\mathrm{d}}} \sum_{\ell_2^{\mathrm{s}}=0}^{\ell_{\max}^{\mathrm{s}}} \frac{P\left\{\mathsf{W}_{1\,:\,\mathsf{J}_3-\mathsf{J}_2+\ell_{\max}^{\mathrm{m}}-1} \in \mathcal{R}^c \,\middle|\, \mathsf{L}_1^{\mathrm{d}} = \ell_1^{\mathrm{d}}, \mathsf{L}_1^{\mathrm{s}} = \ell_1^{\mathrm{s}}, \mathsf{L}_2^{\mathrm{d}} = \ell_2^{\mathrm{d}}, \mathsf{L}_2^{\mathrm{s}} = \ell_2^{\mathrm{s}}\right\}}{P\left\{\mathsf{W}_{1\,:\,\ell_{\max}^{\mathrm{m}}-1} \in \mathcal{R}^c \,\middle|\, \mathsf{L}_1^{\mathrm{d}} = \ell_1^{\mathrm{d}}, \mathsf{L}_1^{\mathrm{s}} = \ell_1^{\mathrm{s}}, \mathsf{L}_2^{\mathrm{d}} = \ell_2^{\mathrm{d}}, \mathsf{L}_2^{\mathrm{s}} = \ell_2^{\mathrm{s}}\right\}}$$

$$\times\, P\left\{\mathsf{L}_1^{\mathrm{d}} = \ell_1^{\mathrm{d}}\right\} P\left\{\mathsf{L}_1^{\mathrm{s}} = \ell_1^{\mathrm{s}}\right\} P\left\{\mathsf{L}_2^{\mathrm{d}} = \ell_2^{\mathrm{d}}\right\} P\left\{\mathsf{L}_2^{\mathrm{s}} = \ell_2^{\mathrm{s}}\right\}.$$

$$(4.98)$$

The ratio of conditional probabilities in the summation can be obtained by expanding the numerator using similar steps leading to (4.92): for the length $n \triangleq \ell_2^{\mathrm{d}} + \ell_2^{\mathrm{s}} + 2\ell_{\max}^{\mathrm{m}} - 1$,[16]

$$\frac{P\left\{\mathsf{W}_{1\,:\,n} \in \mathcal{R}^c \,\middle|\, \mathsf{L}_1^{\mathrm{d}} = \ell_1^{\mathrm{d}}, \mathsf{L}_1^{\mathrm{s}} = \ell_1^{\mathrm{s}}, \mathsf{L}_2^{\mathrm{d}} = \ell_2^{\mathrm{d}}, \mathsf{L}_2^{\mathrm{s}} = \ell_2^{\mathrm{s}}\right\}}{P\left\{\mathsf{W}_{1\,:\,\ell_{\max}^{\mathrm{m}}-1} \in \mathcal{R}^c \,\middle|\, \mathsf{L}_1^{\mathrm{d}} = \ell_1^{\mathrm{d}}, \mathsf{L}_1^{\mathrm{s}} = \ell_1^{\mathrm{s}}, \mathsf{L}_2^{\mathrm{d}} = \ell_2^{\mathrm{d}}, \mathsf{L}_2^{\mathrm{s}} = \ell_2^{\mathrm{s}}\right\}}$$

$$= \Lambda_{\text{cnal}}(\ell_1^{\mathrm{d}}, \ell_1^{\mathrm{s}}, \ell_2^{\mathrm{d}}, \ell_2^{\mathrm{s}})\, P\{\mathsf{W}_{n-\ell_{\max}^{\mathrm{m}}+1\,:\,n} \in \mathcal{R}^c :$$

$$\mathsf{L}_1^{\mathrm{d}} = \ell_1^{\mathrm{d}}, \mathsf{L}_1^{\mathrm{s}} = \ell_1^{\mathrm{s}}, \mathsf{L}_2^{\mathrm{d}} = \ell_2^{\mathrm{d}}, \mathsf{L}_2^{\mathrm{s}} = \ell_2^{\mathrm{s}}\}, \quad (4.99)$$

---

[16]Recall that $\mathsf{J}_3 - \mathsf{J}_2 = \mathsf{T}_2 = \ell_2^{\mathrm{d}} + \ell_2^{\mathrm{s}} + \ell_{\max}^{\mathrm{m}}$ when conditioned on $\mathsf{L}_2^{\mathrm{d}} = \ell_2^{\mathrm{d}}$ and $\mathsf{L}_2^{\mathrm{s}} = \ell_2^{\mathrm{s}}$.

where $\Lambda_{\text{cnal}}(\ell_1^{\text{d}}, \ell_1^{\text{s}}, \ell_2^{\text{d}}, \ell_2^{\text{s}})$ is given by

$$\Lambda_{\text{cnal}}(\ell_1^{\text{d}}, \ell_1^{\text{s}}, \ell_2^{\text{d}}, \ell_2^{\text{s}}) \triangleq \frac{1}{P\left\{\mathsf{W}_{1\,:\,\ell_{\max}^{\text{m}}-1} \in \mathcal{R}^c \;\middle|\; \mathsf{L}_1^{\text{d}} = \ell_1^{\text{d}}, \mathsf{L}_1^{\text{s}} = \ell_1^{\text{s}}, \mathsf{L}_2^{\text{d}} = \ell_2^{\text{d}}, \mathsf{L}_2^{\text{s}} = \ell_2^{\text{s}}\right\}}$$

$$\times \left[\prod_{k=1}^{n-\ell_{\max}^{\text{m}}} \frac{P\left\{\mathsf{W}_{k\,:\,k+\ell_{\max}^{\text{m}}-1} \in \mathcal{R}^c \;\middle|\; \mathsf{L}_1^{\text{d}} = \ell_1^{\text{d}}, \mathsf{L}_1^{\text{s}} = \ell_1^{\text{s}}, \mathsf{L}_2^{\text{d}} = \ell_2^{\text{d}}, \mathsf{L}_2^{\text{s}} = \ell_2^{\text{s}}\right\}}{P\left\{\mathsf{W}_{k+1\,:\,k+\ell_{\max}^{\text{m}}-1} \in \mathcal{R}^c \;\middle|\; \mathsf{L}_1^{\text{d}} = \ell_1^{\text{d}}, \mathsf{L}_1^{\text{s}} = \ell_1^{\text{s}}, \mathsf{L}_2^{\text{d}} = \ell_2^{\text{d}}, \mathsf{L}_2^{\text{s}} = \ell_2^{\text{s}}\right\}}\right]. \quad (4.100)$$

Equation (4.99) can be interpreted with the help of Fig. 4-17 as follows. The condition $\{\mathsf{L}_1^{\text{d}} = \ell_1^{\text{d}}, \mathsf{L}_1^{\text{s}} = \ell_1^{\text{s}}, \mathsf{L}_2^{\text{d}} = \ell_2^{\text{d}}, \mathsf{L}_2^{\text{s}} = \ell_2^{\text{s}}\}$ indicates that the segment of observed symbols consists of (a) the last $\ell_{\max}^{\text{m}} - 1$ symbols from an MSS, (b) entire $\ell_2^{\text{d}} + \ell_2^{\text{s}} + \ell_{\max}^{\text{m}}$ symbols from the next MSS, and (c) $\ell_{\max}^{\text{m}} - 1$ marker symbols (see Fig. 4-17a). These observed symbols generate a total of n decision variables. Each of the $n - \ell_{\max}^{\text{m}} + 1$ terms in the numerator is a $\ell_{\max}^{\text{m}}$-joint probability, and each of the $n - \ell_{\max}^{\text{m}} + 1$ terms in the denominator is a $(\ell_{\max}^{\text{m}} - 1)$-joint probability. Different terms in the numerator correspond to different segments of length $\ell_{\max}^{\text{m}}$, which are time-shifted versions of one another (see Fig. 4-17b). Similarly, different terms in the denominator correspond to different segments of length $\ell_{\max}^{\text{m}} - 1$, which are also time-shifted versions of one another (see Fig. 4-17c). In general, these joint-probability terms need to be obtained numerically.

A comparison of Fig. 4-17 and Fig. 4-16 shows that all $\ell_{\max}^{\text{m}}$-joint probabilities and $(\ell_{\max}^{\text{m}} - 1)$-joint probabilities in (4.99) and (4.100) have already appeared in (4.95) for the evaluation of $p_{\text{nal-nal}}$. Hence, the effort to obtain c_{nal} after we have obtained $p_{\text{nal-nal}}$ is minimal from a numerical point of view.

140

Derivation for c_{det}

A similar approach to the previous section gives

$$c_{\text{det}} = P\left\{\mathsf{V}_{\mathsf{J}_2+1:\mathsf{J}_3-1} \in \mathcal{R}^c, \mathsf{V}_{\mathsf{J}_3} \in \mathcal{R} \mid \mathsf{V}_{\mathsf{J}_2-\ell^{\mathrm{m}}_{\max}+2:\mathsf{J}_2} \in \mathcal{R}^c\right\}$$

$$= \sum_{\ell^{\mathrm{d}}_1=1}^{\ell^{\mathrm{d}}_{\max}} \sum_{\ell^{\mathrm{s}}_1=0}^{\ell^{\mathrm{s}}_{\max}} \sum_{\ell^{\mathrm{d}}_2=1}^{\ell^{\mathrm{d}}_{\max}} \sum_{\ell^{\mathrm{s}}_2=0}^{\ell^{\mathrm{s}}_{\max}} \frac{P\left\{\mathsf{W}_{1:n-1} \in \mathcal{R}^c, \mathsf{W}_n \in \mathcal{R} \mid \mathsf{L}^{\mathrm{d}}_1 = \ell^{\mathrm{d}}_1, \mathsf{L}^{\mathrm{s}}_1 = \ell^{\mathrm{s}}_1, \mathsf{L}^{\mathrm{d}}_2 = \ell^{\mathrm{d}}_2, \mathsf{L}^{\mathrm{s}}_2 = \ell^{\mathrm{s}}_2\right\}}{P\left\{\mathsf{W}_{1:\ell^{\mathrm{m}}_{\max}-1} \in \mathcal{R}^c \mid \mathsf{L}^{\mathrm{d}}_1 = \ell^{\mathrm{d}}_1, \mathsf{L}^{\mathrm{s}}_1 = \ell^{\mathrm{s}}_1, \mathsf{L}^{\mathrm{d}}_2 = \ell^{\mathrm{d}}_2, \mathsf{L}^{\mathrm{s}}_2 = \ell^{\mathrm{s}}_2\right\}}$$

$$\times\, P\left\{\mathsf{L}^{\mathrm{d}}_1 = \ell^{\mathrm{d}}_1\right\} P\left\{\mathsf{L}^{\mathrm{s}}_1 = \ell^{\mathrm{s}}_1\right\} P\left\{\mathsf{L}^{\mathrm{d}}_2 = \ell^{\mathrm{d}}_2\right\} P\left\{\mathsf{L}^{\mathrm{s}}_2 = \ell^{\mathrm{s}}_2\right\},$$

$$(4.101)$$

where $n \triangleq n(\ell^{\mathrm{d}}_2, \ell^{\mathrm{s}}_2) = \ell^{\mathrm{d}}_2 + \ell^{\mathrm{s}}_2 + 2\ell^{\mathrm{m}}_{\max} - 1$ and $\mathsf{W}_j \triangleq \mathsf{V}_{j+\mathsf{J}_2-\ell^{\mathrm{m}}_{\max}+1}$. The ratio of conditional probabilities in the summation can be written as

$$\frac{P\left\{\mathsf{W}_{1:n-1} \in \mathcal{R}^c, \mathsf{W}_n \in \mathcal{R}^c \mid \mathsf{L}^{\mathrm{d}}_1 = \ell^{\mathrm{d}}_1, \mathsf{L}^{\mathrm{s}}_1 = \ell^{\mathrm{s}}_1, \mathsf{L}^{\mathrm{d}}_2 = \ell^{\mathrm{d}}_2, \mathsf{L}^{\mathrm{s}}_2 = \ell^{\mathrm{s}}_2\right\}}{P\left\{\mathsf{W}_{1:\ell^{\mathrm{m}}_{\max}-1} \in \mathcal{R}^c \mid \mathsf{L}^{\mathrm{d}}_1 = \ell^{\mathrm{d}}_1, \mathsf{L}^{\mathrm{s}}_1 = \ell^{\mathrm{s}}_1, \mathsf{L}^{\mathrm{d}}_2 = \ell^{\mathrm{d}}_2, \mathsf{L}^{\mathrm{s}}_2 = \ell^{\mathrm{s}}_2\right\}}$$

$$= \Lambda_{\text{cnal}}(\ell^{\mathrm{d}}_1, \ell^{\mathrm{s}}_1, \ell^{\mathrm{d}}_2, \ell^{\mathrm{s}}_2)\left[P\left\{\mathsf{W}_{n-\ell^{\mathrm{m}}_{\max}+1:n-1} \in \mathcal{R}^c \mid \mathsf{L}^{\mathrm{d}}_1 = \ell^{\mathrm{d}}_1, \mathsf{L}^{\mathrm{s}}_1 = \ell^{\mathrm{s}}_1, \mathsf{L}^{\mathrm{d}}_2 = \ell^{\mathrm{d}}_2, \mathsf{L}^{\mathrm{s}}_2 = \ell^{\mathrm{s}}_2\right\}\right.$$

$$\left. -\, P\left\{\mathsf{W}_{n-\ell^{\mathrm{m}}_{\max}+1:n} \in \mathcal{R}^c \mid \mathsf{L}^{\mathrm{d}}_1 = \ell^{\mathrm{d}}_1, \mathsf{L}^{\mathrm{s}}_1 = \ell^{\mathrm{s}}_1, \mathsf{L}^{\mathrm{d}}_2 = \ell^{\mathrm{d}}_2, \mathsf{L}^{\mathrm{s}}_2 = \ell^{\mathrm{s}}_2\right\}\right], \quad (4.102)$$

where all terms in the right-hand side of (4.102) have already appeared in (4.99) for the evaluation of c_{nal}.[17] Hence, the effort to obtain c_{det} after we have obtained c_{nal} is minimal from a numerical point of view.

---

[17] The first probability expression in the bracket is the last joint-probability term in the denominator of (4.100). The second probability expression in the bracket is the last joint-probability term in (4.99).
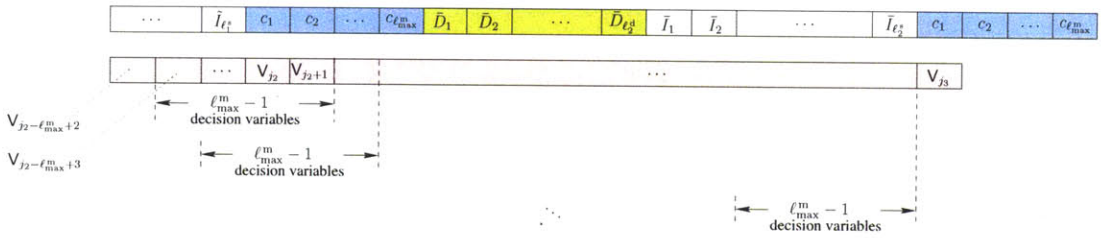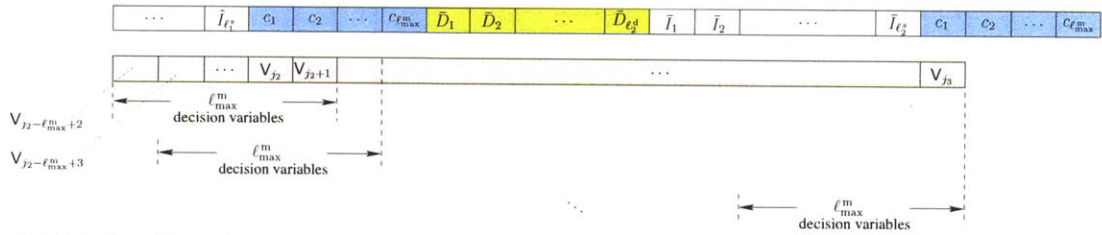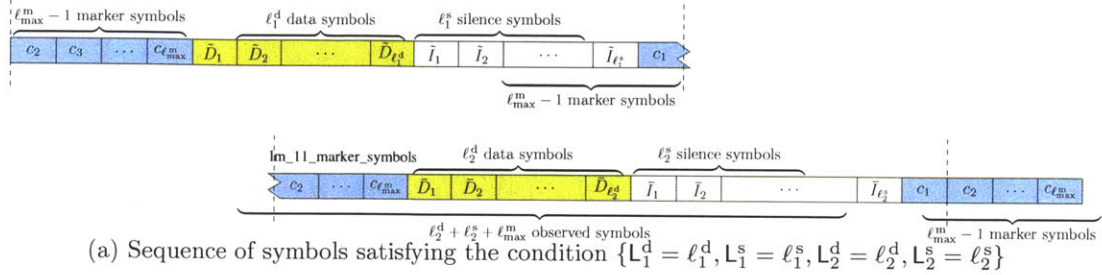
(a) Sequence of symbols satisfying the condition $\{\mathsf{L}_1^{\mathrm{d}} = \ell_1^{\mathrm{d}}, \mathsf{L}_1^{\mathrm{s}} = \ell_1^{\mathrm{s}}, \mathsf{L}_2^{\mathrm{d}} = \ell_2^{\mathrm{d}}, \mathsf{L}_2^{\mathrm{s}} = \ell_2^{\mathrm{s}}\}$

(b) Blocks of length $\ell_{\max}^{\mathrm{m}}$, each of which corresponds to a different $\ell_{\max}^{\mathrm{m}}$-joint probability term in the numerator

(c) Blocks of length $\ell_{\max}^{\mathrm{m}} - 1$, each of which corresponds to a different $(\ell_{\max}^{\mathrm{m}} - 1)$-joint probability term in the denominator

Figure 4-17: Pictorial representation of the MSSs helps to aid the interpretation of equation (4.99).

4.5   Applications to Time-Aware Networks

In this section, we illustrate applications of the first-passage-time distributions developed in Section 4.1–Section 4.4. We will consider three aspects of synchronization in time-aware networks: synchronization of two clocks, synchronization of a network of clocks, and synchronization of frames. Our main contributions in this this section are

- a characterization of time to synchronize a pair of clocks and a network of clocks in terms of the average and the outage;

- applications of first-passage-time distributions to clock synchronization;

- applications of first-passage-time distributions to network synchronization; and

- applications of first-passage-time distributions to frame synchronization.

These applications demonstrate utility of our first-passage-time distributions.

This section is organized as follows In Section 4.5.1, we illustrate application of our solution to clock synchronization. In Section 4.5.2, we illustrate application of our solution to network synchronization. In Section 4.5.3, we illustrate application of our solution to frame synchronization.

4.5.1   Calibration Time Between Two Clocks

To illustrate an application of first-passage-time problems that involve Brownian motion with polynomial drift, we consider a problem in synchronization of two clocks. We will describe a problem statement, a system model, and a solution.

Problem Statement

Consider a pair of clocks in a synchronous network. These two clocks need to maintain their times close to each other for coordination, communication, or other purposes. One clock serves as a reference clock. The other serves as a slave clock, a clock that will be calibrated to match the time of the reference clock. Suppose that, at time 0, the two clocks are calibrated to have the same time, a requirement that is ideal but

143

serves to give a best case analysis. We want to characterize the amount of time, measured by the reference clock, until the two clocks are out of sync.

The problem in synchronization translates into the following mathematical formulation. Let a random process Y_t denote the time difference between two clocks, where $Y_0 = 0$ (a perfect calibration) and t is time of the reference clock. Let an interval (a_Y, b_Y) denote a range of acceptable time differences, where $a_Y < 0 < b_Y$. Let a random variable $\breve{\tau}_{a_Y, b_Y}$ denote the amount of time until the two clocks are out of sync: $\breve{\tau}_{a_Y, b_Y} = \inf\{t \geq 0 : Y_t \notin (a_Y, b_Y)\}$, a first passage time. We will call $\breve{\tau}_{a_Y, b_Y}$ a calibration time because a clock needs to be calibrated at time $\breve{\tau}_{a_Y, b_Y}$. We want to summarize the probability distribution of $\breve{\tau}_{a_Y, b_Y}$ by a single number that captures an essence of the calibration time.

Two questions remain for discussion: what is a proper model for Y_t? and how to characterize $\breve{\tau}_{a_Y, b_Y}$ by a single number? For the first question, we will model Y_t as a scaled Brownian motion with quadratic drift. For the second question, we will characterize the calibration time in two ways: an average (one single number) and an outage (another single number). We now discuss these questions in detail.

System Model

We model Y_t as

$$Y_t = \sigma B_t + \breve{c} + \breve{q}t + \breve{\mu}t^2, \qquad\qquad t \geq 0,$$

where σ, $\breve{c}$, $\breve{q}$, and $\breve{\mu}$ are constants that depend on the clocks. Brownian motion B_t represents a white frequency modulation noise. Constant σ represents severity of white frequency modulation noise. Constants $\breve{c}$ and $\breve{q}$ represent phase and frequency errors from the calibration at time 0. Constant $\breve{\mu}$ represents aging effect. Our model is a simplification of a general model, which accounts for other types of noise and allows $\breve{c}$, $\breve{q}$, and $\breve{\mu}$ to be random variables [70] [16, Sec. 5.2; p. 250]. Our model is reasonable when the frequency white noise is a dominant type of noise [46].
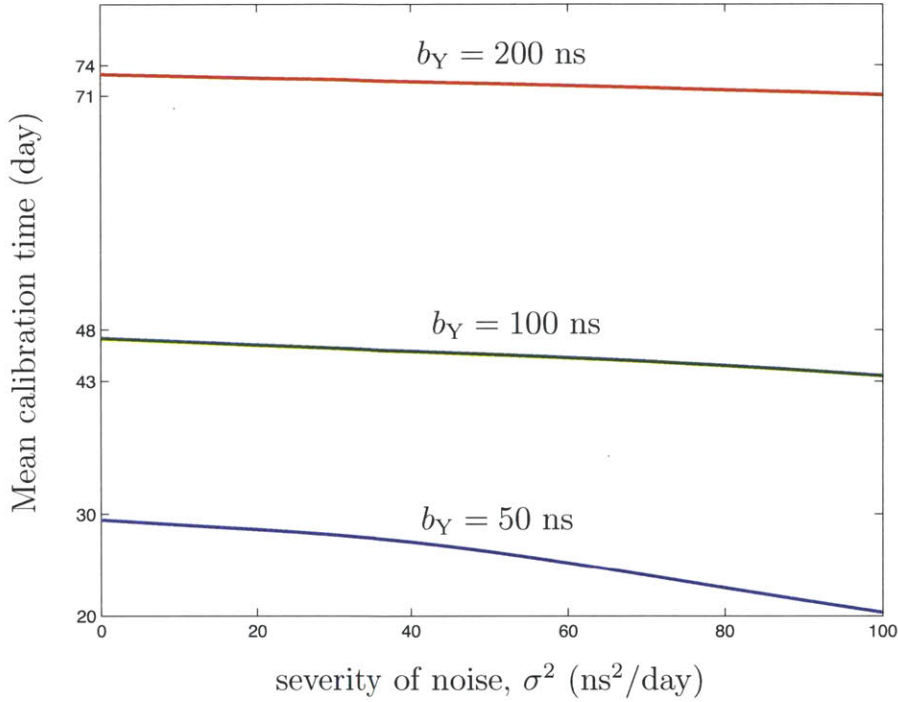
144

Figure 4-18: A clock needs to be calibrated often if noise is large or if the maximum allowable time difference is small.

Performance Measure

We characterize the calibration time from two perspectives: average and outage. The average is defined to be the expectation $\mathbb{E}\left\{\breve{\tau}_{a_\mathrm{Y},b_\mathrm{Y}}\right\}$, which gives us the mean calibration time or the average duration until the slave clock needs to be calibrated. The outage depends on a parameter $0 < p < 1$, where p is a target for the probability that the time differences remain in an interval $(a_\mathrm{Y}, b_\mathrm{Y})$. The outage at level p is defined to be time t_0 such that $\mathbb{P}\left\{\breve{\tau}_{a_\mathrm{Y},b_\mathrm{Y}} > t_0\right\} = p$. The outage tells us to calibrate the clock at time t_0 if we want to be $100p$-percent confident that the two clocks are in sync. The average and the outage are obtained numerically from the PDF of $\breve{\tau}_{a_\mathrm{Y},b_\mathrm{Y}}$.

Numerical Examples

We set $\breve{c} = 0$ because of a perfect calibration at time 0 and set $\breve{q}$, $\breve{\mu}$, σ, a_Y, and b_Y to typical values for certain atomic clocks: $\breve{q} = 1$ ns/day, and $\breve{\mu} = 2.37 \times 10^{-2}$ ns/day^2 (or 10^{-13} / year) (for MASER standard; see Table 2.1), and $a_\mathrm{Y} = -b_\mathrm{Y}$ (a symmetric
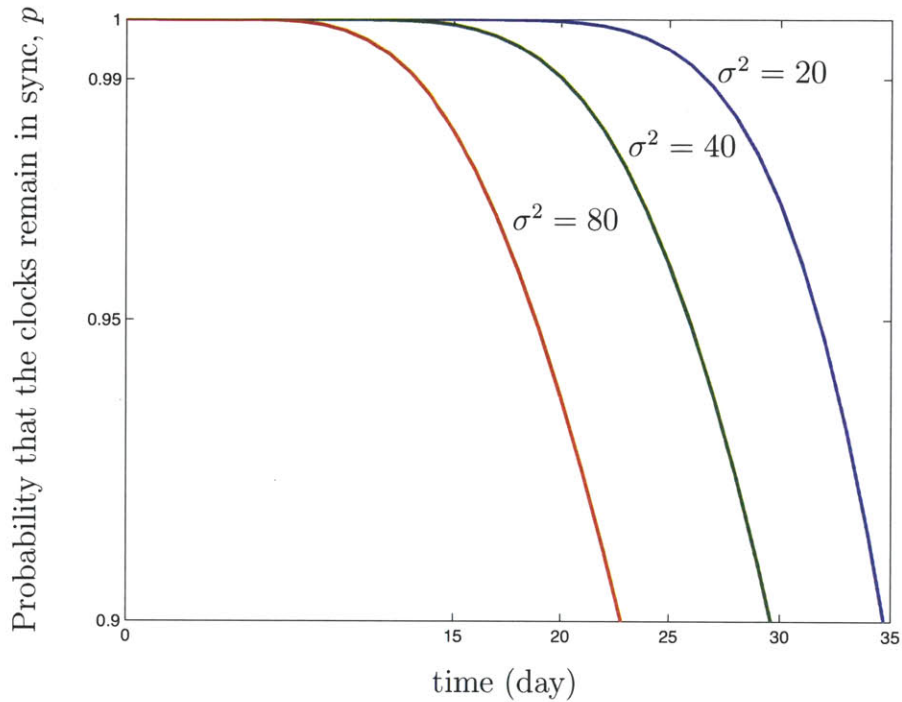
Figure 4-19: A clock with large noise (σ^2, in ns^2/day) is likely to lose synchronization with the reference clock.

boundary) [84] [16, p. 292]. Typical values of σ and b are 40 ns^2/day and 100 ns [84]. But we will vary σ^2 and b in the numerical examples to show the effects of noise and boundary. Using these typical values of the parameters, we characterize averages and outages of the calibration time.

Averages of the calibration time appear in Fig. 4-18 as a function of severity σ^2 of noise and the maximum allowable time difference b_Y. For each curve with fixed b_Y, the mean calibration time decreases as σ^2 increases. This trend is consistent with intuition: the slave clock needs to be calibrated more often if the clocks are more noisy. On the other hand, for a fixed σ^2, the mean calibration time increases as b_Y increases. This trend is also intuitive: the slave clock needs to be calibrated less often if it is allowed to deviate more from the reference clock. For typical values of $\sigma^2 = 40$ ns^2/day and $b_Y = 100$ ns, the average curve suggests that the slave clock be calibrated at day 46. This example summarizes the calibration time in terms of the average.

146

Another way to summarize the calibration time comes from outage curves or complementary CDFs in Fig. 4-18. In the figure, the outage curves share a common value of $b_Y = 100$ ns but they use different values of σ^2. Notice that each curve is a decreasing function of time. This trend is consistent with intuition: as time progresses, the clocks are less likely to remain in sync. When σ^2 decreases, the curve moves away from the y-axis. This trend is also intuitive: the slave clock needs to be calibrated less often if the clocks are less noisy. For a typical value of $\sigma^2 = 40$ ns^2/day and for a level $p = 0.9$, the outage curve suggests that the slave clock be calibrated at day 30. Outages and averages are applications of our first passage time problems to synchronization.

4.5.2 Calibration Time in a Network

To illustrate an application of first-passage-time problems that involve multi-dimensional Brownian motions with polynomial drifts, we consider a problem in network synchronization. We will describe a problem statement, a system model, and a solution.

Problem Statement

Consider a network that consists of n clocks. These clocks need to maintain the absolute time close to a reference clock, for coordination, communication, or other purposes. Suppose that, at time 0, the n clocks are calibrated to have the same time as the time at the reference clock, a requirement that is ideal but serves to give a best case analysis. We want to characterize the amount of time, measured by the reference clock, until k out of n clocks are simultaneously out of sync with the reference clock. Here, k depends on a specific application and ranges from $k = 1$ (the most restricted requirement on time synchronism) to $k = n$ (the least restricted requirement on time synchronism). Parameter k controls how stringent the synchronization requirement is.

The problem in synchronization translates into the following mathematical formulation. For each $i = 1, 2, \ldots, n$, let a random process $Y_t^{(i)}$ denote the time difference

147

between clock i and the reference clock, where $\mathsf{Y}_0^{(i)} = 0$ (a perfect calibration) and t is time of the reference clock. Let an interval $(a_\mathsf{Y}, b_\mathsf{Y})$ denote a range of acceptable time differences, where $a_\mathsf{Y} < 0 < b_\mathsf{Y}$. For each $k = 1, 2, \ldots, n$, let a random variable $\tau_{a_\mathsf{Y}, b_\mathsf{Y}}(k)$ denote the amount of time until any k clocks are simultaneously out of sync:

$$
\begin{aligned}
&\tau_{a_\mathsf{Y}, b_\mathsf{Y}}(k) \\
&= \inf\left\{ t \geq 0 : \exists \mathcal{J} \subset \{1, 2, \ldots, n\} \text{ such that } |\mathcal{J}| = k \text{ and } \forall j \in \mathcal{J} \ \mathsf{Y}_t^{(j)} \notin (a_\mathsf{Y}, b_\mathsf{Y}) \right\},
\end{aligned}
$$

which is a first passage time. We will call $\tau_{a_\mathsf{Y}, b_\mathsf{Y}}(k)$ a calibration time because the network needs to be calibrated at time $\tau_{a_\mathsf{Y}, b_\mathsf{Y}}(k)$. Similar to the case of two clocks in Section 4.5.1, we want to summarize the probability distribution of $\tau_{a_\mathsf{Y}, b_\mathsf{Y}}(k)$ by the average and the outage, which capture the essence of the calibration time.

System Model

We model $\mathsf{Y}_t^{(i)}$ as

$$
\mathsf{Y}_t^{(i)} = \sigma \mathsf{B}_t^{(i)} + \check{c} + \check{q}t + \breve{\mu}t^2, \qquad t \geq 0, i = 1, 2, \ldots, n,
$$

where σ, $\check{c}$, $\check{q}$, and $\breve{\mu}$ are parameters of clocks, defined in Section 4.5.1, and where $\mathsf{B}_t^{(1)}, \mathsf{B}_t^{(2)}, \ldots, \mathsf{B}_t^{(n)}$ are independent Brownian motions representing white frequency modulation noise. Our model is reasonable when the white frequency modulation noise is a dominant type of noise [46] and when n clocks are the same type, so the coefficients in the quadratic drifts are identical.

Performance Measure

Similar to Section 4.5.1, we characterize the calibration time from two perspectives: average and outage. The average is defined to be the expectation $\boldsymbol{E}\left\{\tau_{a_\mathsf{Y}, b_\mathsf{Y}}(k)\right\}$, which gives us the mean calibration time or the average duration until k out of n clocks are simultaneously out of sync. The outage depends on a parameter $0 < p < 1$, where p is a target for the probability that the time differences remain in an interval $(a_\mathsf{Y}, b_\mathsf{Y})$.

148

The outage at level p is defined to be time t_0 such that $\boldsymbol{P}\left\{\tau_{a_Y,b_Y}(k) > t_0\right\} = p$. The outage tells us to calibrate the network at time t_0 if we want to be $100p$-percent confident that $n - k + 1$ clocks or more stay in sync with the reference clock. The average and the outage are obtained from the CDF of $\tau_{a_Y,b_Y}(k)$ for $k = 1$ (see (4.67) or (4.69)). For the other cases of k, we bound the average and the outage using the bounds on the CDF (see (4.68) or (4.70)).

Numerical Examples

We set $\check{c} = 0$ (a perfect calibration at time 0) and set $\check{q} = 1$ ns/day, $\check{\mu} = 2.37 \times 10^{-20}$ ns/day^2, and $b_Y = -a_Y = 100$ ns (see a justification of these parameters in Section 4.5.1). We will vary σ^2 around its typical value that appears in [84], to show the effects of noise. Using these parameters, we characterize averages and outages of the calibration time.

In the figures that we will plot, the parameters n and k vary to reflect different characteristic of networks. The number of clocks in the network is set to $n = 4, 20, 100$ to represent a small, medium, and large networks, resepctively. The number of clocks that are allowed to go out of sync in a network of size n is also varied. We will set $k = 1, k = 2, k = \lceil n/2 \rceil, k = n$ to represent various degrees of requirement on synchronism, where $\lceil x \rceil$ denote the smallest integer that is greater than or equal to x. For $k = 1$, the synchronization occurs immediately when $k = 1$ out of n clocks is out of sync with respect to the reference clock. The value of $k = 1$ gives us the most conservative way to synchronize the network. For $k = 2$, the synchronization occurs when $k = 2$ out of n clocks are simultaneously out of sync. For $k = \lceil n/2 \rceil$, the synchronization occurs when at least half of the clocks are simultaneously out of sync. For $k = n$, the synchronization occurs when all of the clocks are simultaneously out of sync. For the case that $k = 1$, we will have the curves for the expectation and the outage since we have exact expression for the CDF of the calibration time. For the case that $k \geq 2$, we have an upper bound and a lower for the average calibration and an upper bound and a lower bound for the outage. Figures 4-20–fig:mean:kn shows the plots for $k = 1, 2, \lceil n/2 \rceil, n$, respectively.
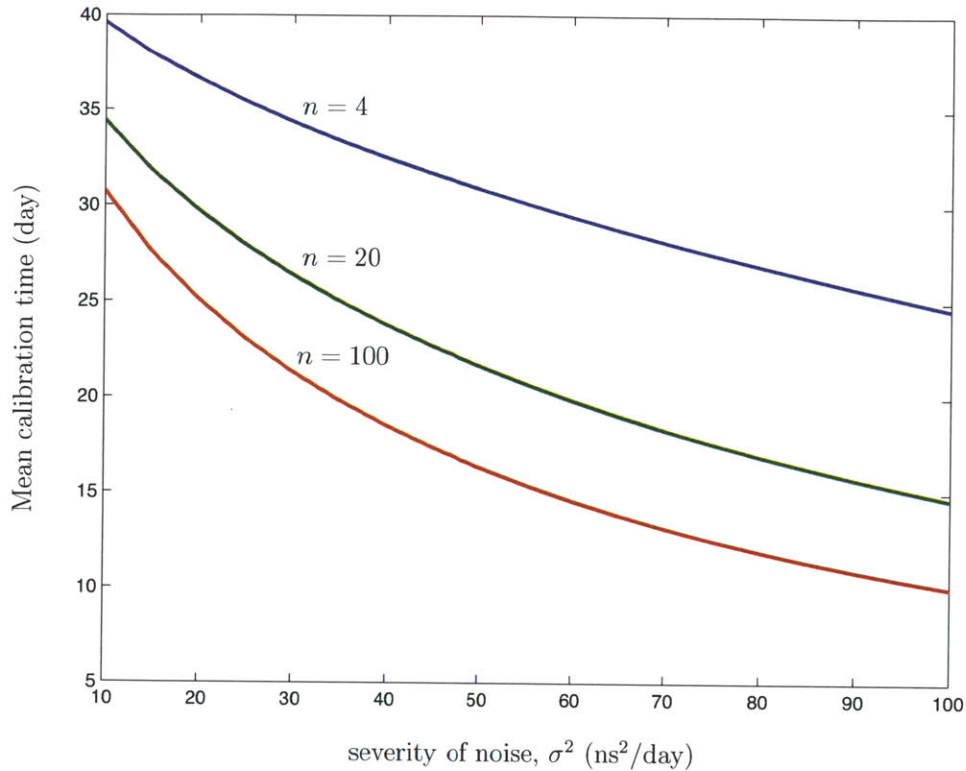
149

Figure 4-20: For $k = 1$, mean time to calibrate the network decreases as the network size n increases and as the clock noise σ^2 increases over a typical range.

For $k = 1$, the mean calibration time appears in Fig. 4-20 as a function of severity σ^2 of noise and the number n of clocks. For a fixed σ^2, we observe from the figure that as n increases, the mean calibration time decreases. This finding is intuitive: as the number of clocks in the network increases, it is more likely for any $(k = 1)$ of the clocks to become out of sync, resulting in short calibration time. For a fixed n, we observe from the figure that as σ^2 increases, the mean calibration time decreases. This finding is also intuitive: when the clocks become more noisy, it is more likely for any $(k = 1)$ of the clocks to become out of sync, resulting in short calibration time. The figure gives insight into the calibration of the network for $k = 1$, the most conservative requirement for synchronization.

For $k = 2$, the upper bound and lower bound for the mean calibration time appear in Fig. 4-21 as a function of severity σ^2 of noise and the number n of clocks. The bounds provide insight into the mean calibration time and are reasonably close to
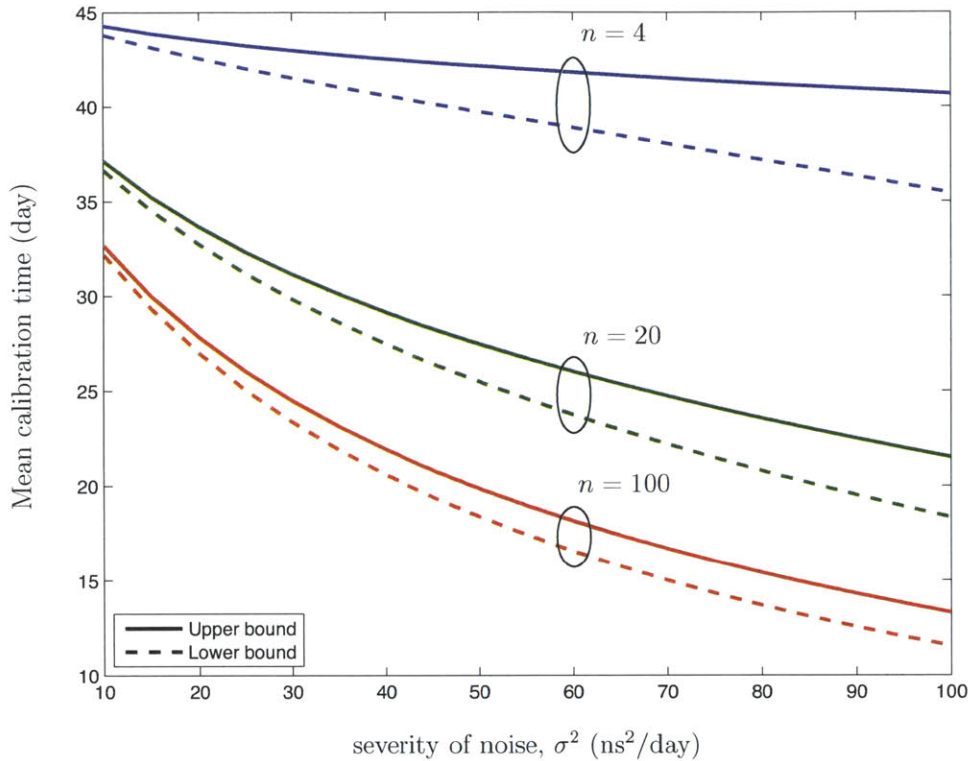
150

Figure 4-21: For $k = 2$, the upper bound and the lower bound on the mean time to calibrate the network give insight into how often a network of n clocks needs to be calibrated. The mean time decreases as the network size n increases and as the clock noise σ^2 increases over a typical range.

each other. For example, the maximum difference between the upper bound and the lower bound over the range of typical σ^2 in the figure is less than six days, giving us a relatively precise range of the mean calibration time. Using these bounds, we can draw conclusions about the general trends of the mean calibration time.

From Fig. 4-21, at each σ^2, we observe that as n increases from 4 to 20 and to 100, the bounds decrease. The bounds for different n's are not overlapped, implying that the mean calibration time must also decrease when n increases from 4 to 20 and to 100. This finding about the mean calibration time is intuitive: as the number of clocks in the network increases, it takes short time for two clocks to become simultaneously out of sync. For a fixed n, we observe from the bounds that in general as σ^2 increases, the mean calibration time decreases. This finding is also intuitive: when the clocks
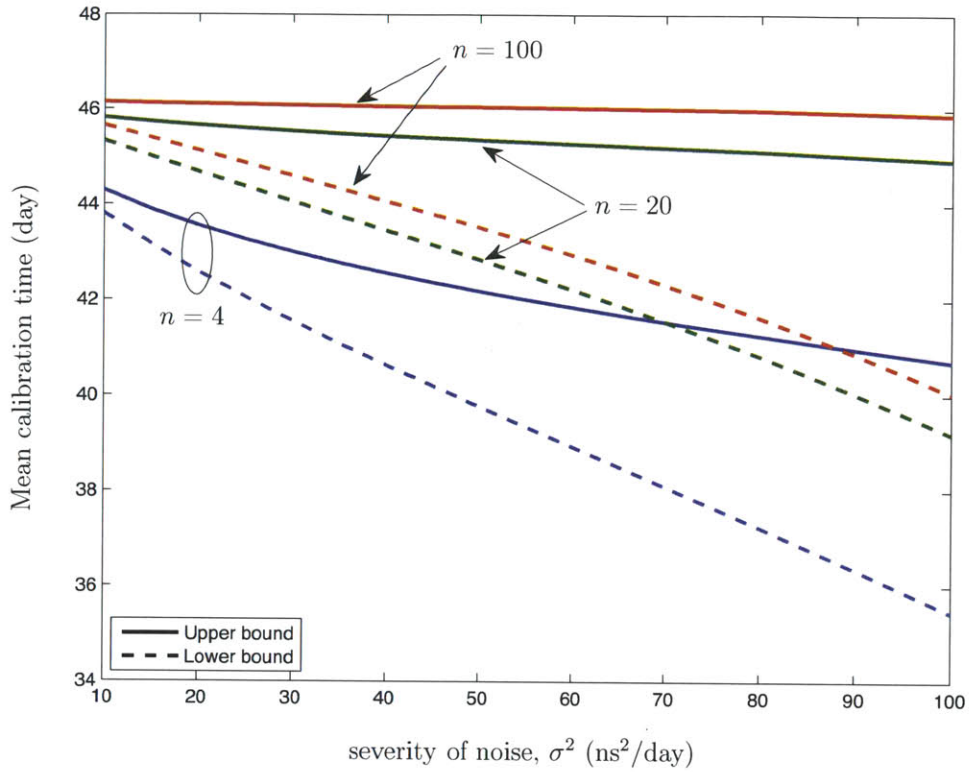
151

Figure 4-22: For $k = \lceil n/2 \rceil$, the larger the network size, the more difficult for half of the clocks to simultaneously become out of sync.

become more noisy, it is more likely that any two clocks become simultaneously out of sync, resulting in short calibration time. The bounds for the mean calibration time provide insight into the calibration time of the network.

For $k = \lceil n/2 \rceil$, the upper bound and lower bound for the mean calibration time appear in Fig. 4-22 as a function of severity σ^2 of noise and the number n of clocks. The bounds provide insight into the mean calibration time and are reasonably close to each other. For example, the maximum difference between the upper bound and the lower bound over the range of typical σ^2 in the figure is less than six days, giving us a relatively precise range of the mean calibration time. Using these bounds, we can draw conclusions about the general trends of the mean calibration time.

From Fig. 4-22, at each σ^2, we observe that as n increases from 4 to 20 and to 100, the upper bound and the lower bound increase. This finding about the bounds is intuitive: as the number of clocks in the network increases, it takes long time for half
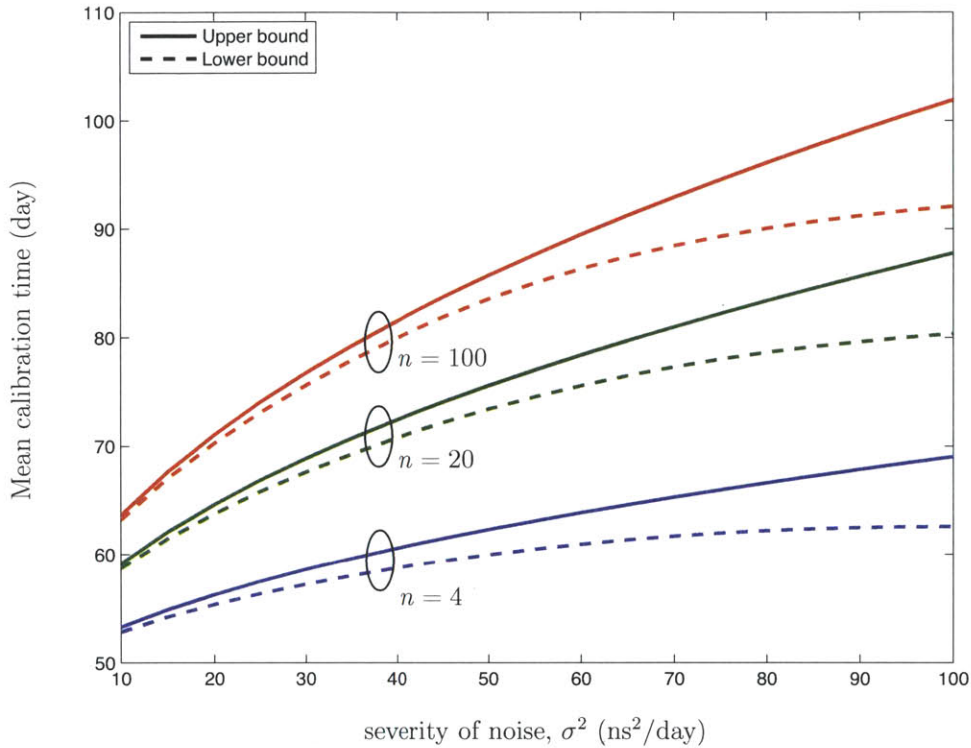
Figure 4-23: For $k = n$, the larger the network size, the more difficult for all of the clocks to simultaneously become out of sync.

of the clocks to become simultaneously out of sync. For a fixed n, we observe from the bounds that in general as σ^2 increases, the mean calibration time decreases. This observation implies that, for the range of σ^2 in the figure, the noisy the clock, the more likely that half of the clocks become simultaneously out of sync. The bounds for the mean calibration time provide insight into the calibration time of the network.

For $k = n$, the upper bound and lower bound for the mean calibration time appear in Fig. 4-23 as a function of severity σ^2 of noise and the number n of clocks. The bounds provide insight into the mean calibration time and are reasonably close to each other. For example, the maximum difference between the upper bound and the lower bound over the range of typical σ^2 in the figure is less than ten days, giving us a relatively precise range of the mean calibration time. Using these bounds, we can draw conclusions about the general trends of the mean calibration time.

From Fig. 4-23, at each σ^2, we observe that as n increases from 4 to 20 and to

100, the bounds increase. The bounds for different n's are not overlapped, implying that the mean calibration time must also increase when n increases from 4 to 20 and to 100. This finding about the bounds is intuitive: as the number of clocks in the network increases, it is more difficult for all of the clocks to become simultaneously out of sync, resulting in long calibration time for a large network. For a fixed n, we observe from the bounds that in general as σ^2 increases, the mean calibration time increases. This finding is at first surprising but arises from the range of σ^2 that appears in the figure. For this range of σ^2, clocks that have been out of sync have returned to become in sync, due to increasing volatility of the time error (as σ^2 increases). As a result, we observe that the mean calibration time increases as σ^2 increases from $\sigma^2 = 10$ to $\sigma^2 = 100$. When σ^2 approaches infinity, the mean calibration time approaches zero.[18] Hence, at some σ^2 larger than 100, we expect the mean calibration time to decrease. Again, the bounds for the mean calibration time provide insight into the calibration time of the network.

Another way to summarize the calibration time comes from outage curves or complementary CDFs in Figs. 4-24–4-27. In the figure, the outage curves and the bounds share common values of $b_Y = 100$ ns and $\sigma^2 = 40$ ns^2/day but they use different values of n, the number of clocks in the network. Notice that for $n = 1$, we provide the outage curve (see Fig. 4-24). For other values of n, we provide upper bounds and lower bounds for the outage curves (see Figs. 4-25–4-27). We now discuss each figure in detail.

For $k = 1$, the outage curve appears in Fig. 4-24 for different values of n, the number of clocks in the network. For a fixed n, the curve is decreasing as time increases. This finding is intuitive: as the time progresses, the probability that the network remains in sync decreases. As n increases from 4 to 20 and to 100, the outage curves move toward the y-axis. This finding is consistent with intuition: as the number of clocks increases, the probability that the network remains in sync decreases. The outage curves give us insight into how often clocks in the network need to be calibrated.

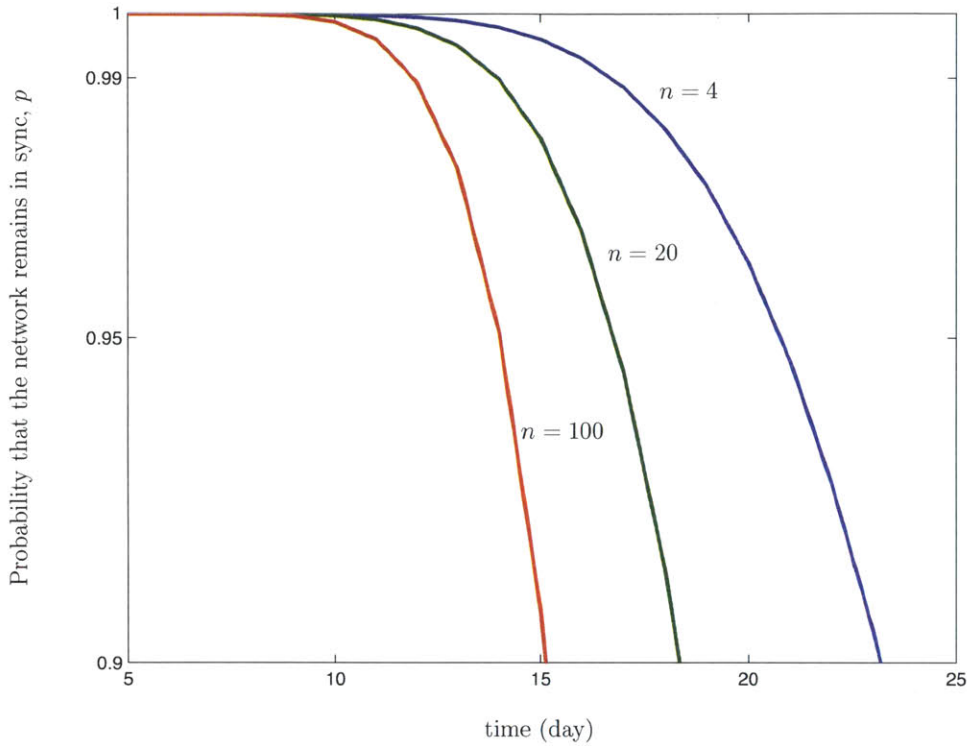[18]This statement is a consequence of continuity of measure [99, Thm. 1.19(d)].

Figure 4-24: For $k = 1$, time to calibration from the standpoint of outage is consistent with time to calibration from the standpoint of average in Fig. 4-20: the larger the network, the shorter the time to calibration.

For $k = 2$, the upper bounds and lower bounds for the outage curves appear in Fig. 4-25 for different values of n. The bounds are reasonably close to each other. For example, the maximum difference between the upper bound and the lower bound over the range of typical σ^2 in the figure is less than two days, giving us a relatively precise range of calibration time (from the perspective of outage probability). As n increases from 4 to 20 and to 100, the bounds move toward the y-axis. This finding is intuitive and arises from the similar reason as for the case of $k = 1$ in Fig. 4-24: the more clocks, the more likely that two of them become out of sync at a given time. The bounds for the outage curve provide insight into the calibration time of the network.

For $k = \lceil n/2 \rceil$, the upper bounds and lower bounds for the outage curves appear in Fig. 4-26 for different values of n. The bounds are reasonably close to each other. For
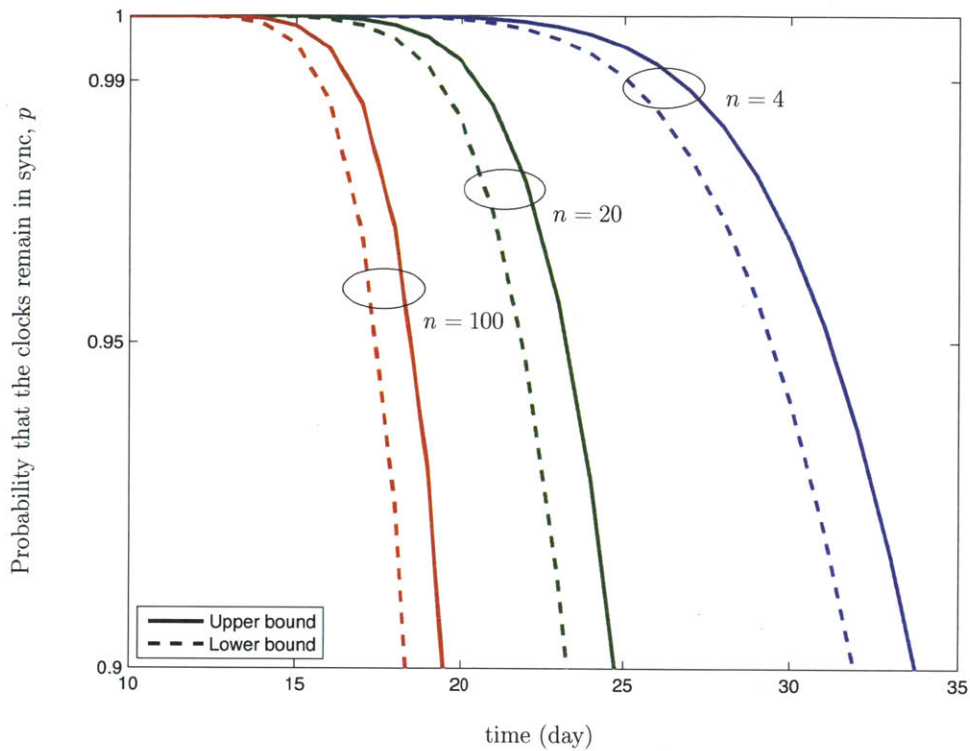
155

Figure 4-25: For $k = 2$, time to calibration from the standpoint of outage is consistent with time to calibration from the standpoint of average in Fig. 4-21: the larger the network, the shorter the time to calibration.

example, the maximum difference between the upper bound and the lower bound over the range of typical σ^2 in the figure is less than two days, giving us a relatively precise range of calibration time (from the perspective of outage probability). As n increases from 4 to 20 and to 100, the bounds move away from the y-axis. This finding is intuitive since the network is calibrated when half of the clocks are simultaneously out of sync: the more clocks, the more difficult for half of them to become simultaneously out of sync at a given time. The bounds for the outage curve provide insight into the calibration time of the network.

For $k = n$, the upper bounds and lower bounds for the outage curves appear in Fig. 4-27 for different values of n. The bounds are reasonably close to each other. For example, the maximum difference between the upper bound and the lower bound in the figure is less than two days, giving us a relatively precise range of calibration
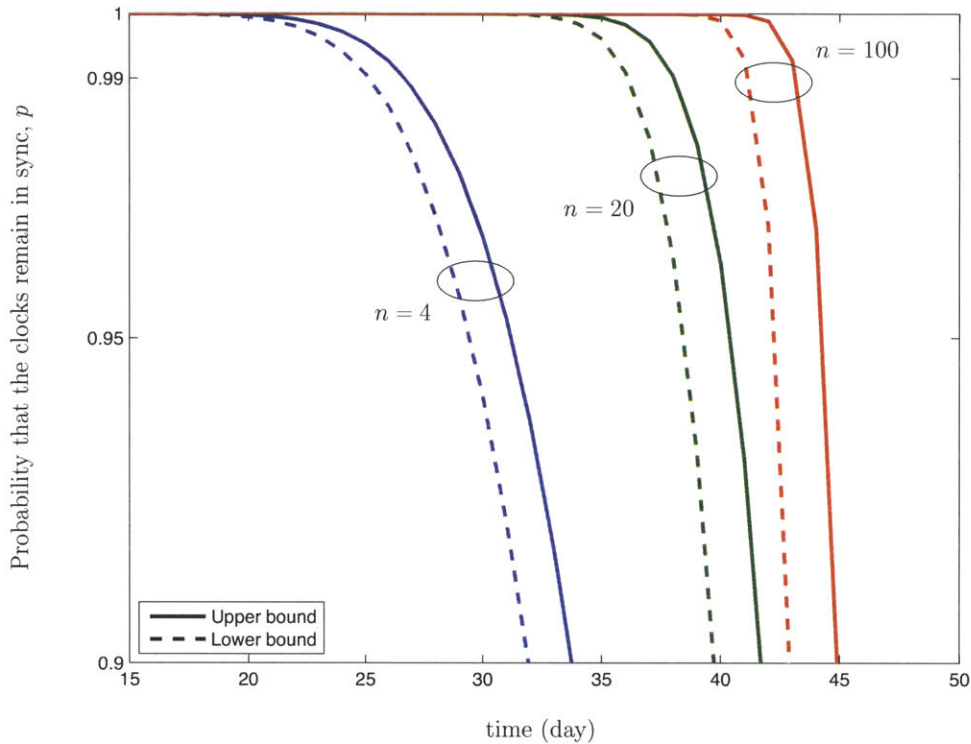
Figure 4-26: For $k = \lceil n/2 \rceil$, time to calibration from the standpoint of outage is consistent with time to calibration from the standpoint of average in Fig. 4-22: the larger the network, the longer the time to calibration.

time (from the perspective of outage probability). As n increases from 4 to 20 and to 100, the bounds move away from the y-axis. This finding is intuitive since the network is calibrated when all of the clocks are simultaneously out of sync: the more clocks, the more difficult for all of them to become simultaneously out of sync at a given time. The bounds for the outage curve provide insight into the calibration time of the network.

4.5.3 A Processing Delay During the Synchronization Phase

To illustrate our analytical framework developed in Section 4.4, we consider the simplest scenario, involving continuous transmission of binary symbols over the AWGN channel. These symbols constitute packets that nodes exchange during the synchronization phase.
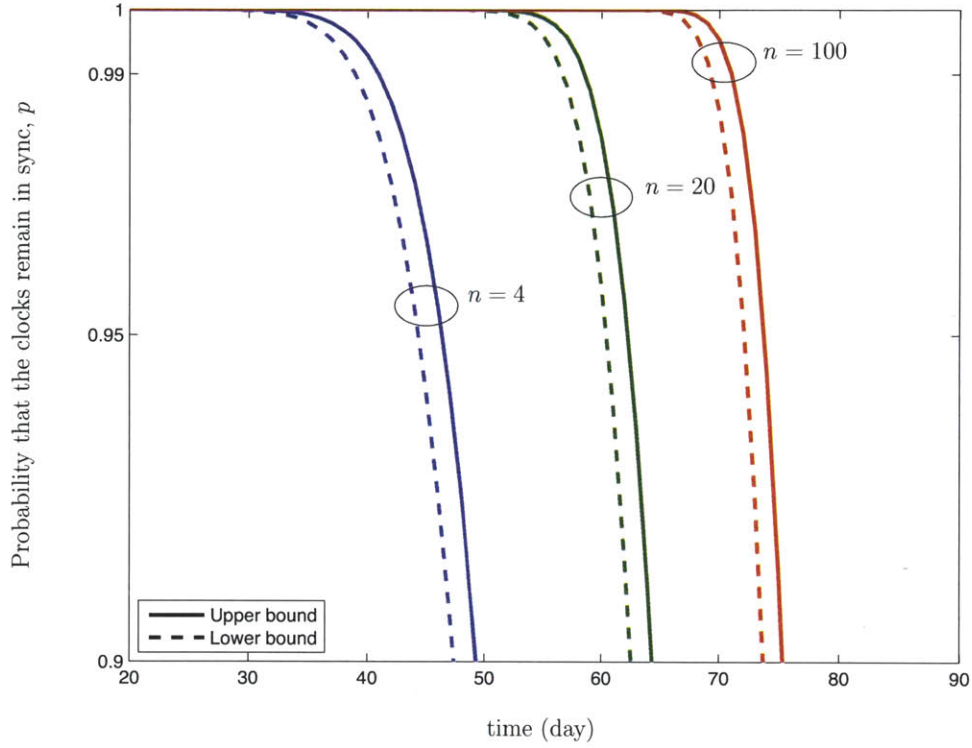
Figure 4-27: For $k = n$, time to calibration from the standpoint of outage is consistent with time to calibration from the standpoint of average in Fig. 4-23: the larger the network, the longer the time to calibration.

Case Study

Transmitted data symbols, $\{D_j\}$, are assumed to be IID and equally likely to take a value of -1 or $+1$. The length L_i^d of frame number i is uniform over the set, $\{\ell_{min}^d, \ell_{min}^d + 1, \ldots, \ell_{max}^d\}$, and $L_i^s = 0$. The transmitter injects a marker with good correlation properties into the beginning of each frame. The data and marker symbols are converted into waveforms for transmission, which are impaired by AWGN.

The frame synchronizer decides whether a marker begins at index j by considering two hypotheses. Let H_1 denote the hypothesis that a marker begins at index j, whereas H_0 denotes the hypothesis that a marker does not begin at index j:

$$H_1 : X_i = c_{i-j+1} + N_i, \qquad (i = j, j+1, \ldots, j+\ell_{max}^m - 1)$$

$$H_0 : X_i = D_i + N_i, \qquad (i = j, j+1, \ldots, j+\ell_{max}^m - 1).$$

158

Here, $\{N_i\}$ are IID Gaussian random variables with zero mean and variance σ^2. We eliminate the cases where there is a mixture of data and marker symbols from our hypothesis, since segments of well-designed markers should mimic a sequence of random data [24, 25].

We will employ a decision rule based on soft correlation with the decision function g_1 in (4.80). The threshold for decision rule, denoted by η, is chosen according to the Neyman-Pearson criteria [10, p. 216]. Hence, our decision rule becomes

$$V_j \triangleq \sum_{k=1}^{\ell_{\max}^{\mathrm{m}}} c_k X_{j+k-1} \underset{H_0}{\overset{H_1}{\gtrless}} \eta.$$

Selection of Threshold

Let the random variable $H \in \{H_1, H_0\}$ denote the true hypothesis. Using Neyman-Pearson criteria, we select a threshold η such that the probability of false alarm equals a desired level, α:

$$P\{V_j > \eta \mid H = H_0\} = \alpha. \tag{4.103}$$

We now evaluate the false alarm probability as follows.

Without loss of generality, we will set the time index $j = 1$. Under hypothesis $H = H_0$, decision variable V_1 involves a sum of IID Bernoulli random variables, $\sum_{k=1}^{\ell_{\max}^{\mathrm{m}}} c_k D_k$, and a sum of normal random variables, $\sum_{k=1}^{\ell_{\max}^{\mathrm{m}}} c_k N_k$. The probability of false alarm at a given threshold η equals [25, eq. (51)]

$$P\{V_j > \eta \mid H = H_0\} = \frac{1}{2^{\ell_{\max}^{\mathrm{m}}}} \sum_{k=0}^{\ell_{\max}^{\mathrm{m}}} \binom{\ell_{\max}^{\mathrm{m}}}{k} Q\left(\frac{\eta - \ell_{\max}^{\mathrm{m}} + 2k}{\sqrt{\sigma^2 \ell_{\max}^{\mathrm{m}}}}\right),$$

where $Q(x)$ is Gaussian Q-function [91, eq. 2.1-97]. We then obtain η by numerically solving the nonlinear equation (4.103) using a technique such as the bisection method. The probability of false alarm for various σ^2 is depicted in Fig. 4-28.

Remark 1. *The bisection method requires an initial point η_0 to begin the iteration. One approach to select a good initial point is to approximate V_j by a Gaussian random*
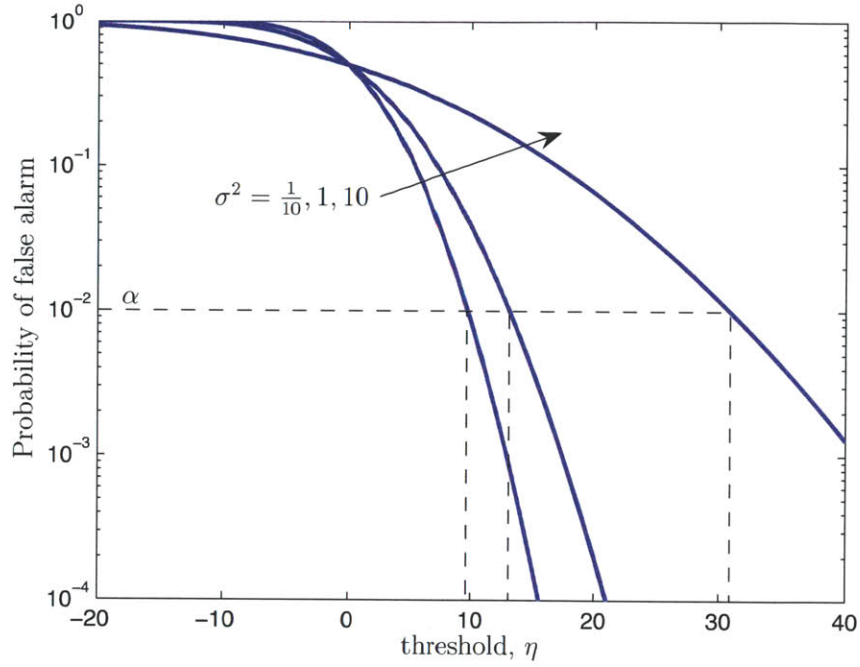
Figure 4-28: The threshold is selected to achieve the probability of false alarm at a desired level, α. The figure shows $\alpha = 10^{-2}$ and the marker length $\ell_{\max}^m = 16$.

variable. This approximation is motivated by the central limit theorem. Mathematically, for large $\ell_{\max}^m$ the false alarm probability, $P\{V_j > \eta \mid H = H_0\}$, is approximated by

$$Q\left(\frac{\eta}{\sqrt{\ell_{\max}^m(1+\sigma^2)}}\right).$$

Under this approximation, the initial point is given by

$$\eta_0 = Q^{-1}(\alpha)\sqrt{\ell_{\max}^m(1+\sigma^2)},$$

which is easy to obtain using standard mathematical packages. The Gaussian approximation turns out to be very good (Fig. 4-29), implying that the bisection method will terminate in a few steps.

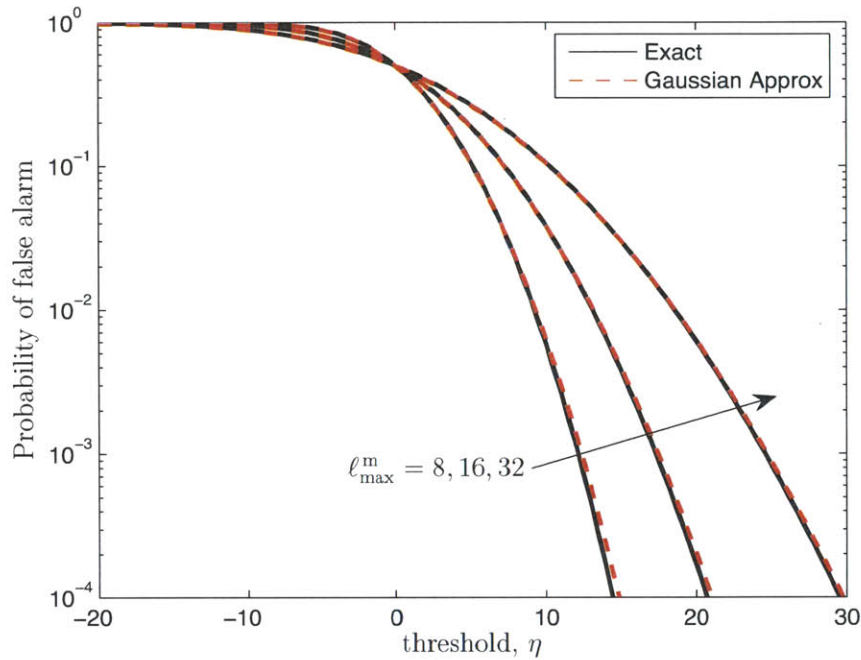**Remark 2.** *To obtain the transition probabilities, we follow the approach described in*

Figure 4-29: The Gaussian approximation can be used to approximate the probability of false alarm ($\sigma^2 = 1$).

Section 4.4.5. Each joint probability term in that section is obtained by conditioning on data symbols, if applicable, and then integrating the joint pdf of the Gaussian random variables over the appropriate region, defined by the threshold.[19] As an example, a joint probability term that needs to be evaluated is

$$P\left\{\mathsf{W}_1 \leq \eta, \mathsf{W}_2 \leq \eta, \ldots, \mathsf{W}_{\ell_{\max}^m} \leq \eta\right\}$$

where

$$\mathsf{W}_j = \sum_{k=1}^{\ell_{\max}^m} c_k(\mathsf{D}_{k+j-1} + \mathsf{N}_{k+j-1}) \qquad (j = 1, 2, 3, \ldots, \ell_{\max}^m).$$

---

[19]If the joint probability term is generated by the marker symbols only, then the conditioning is unnecessary.
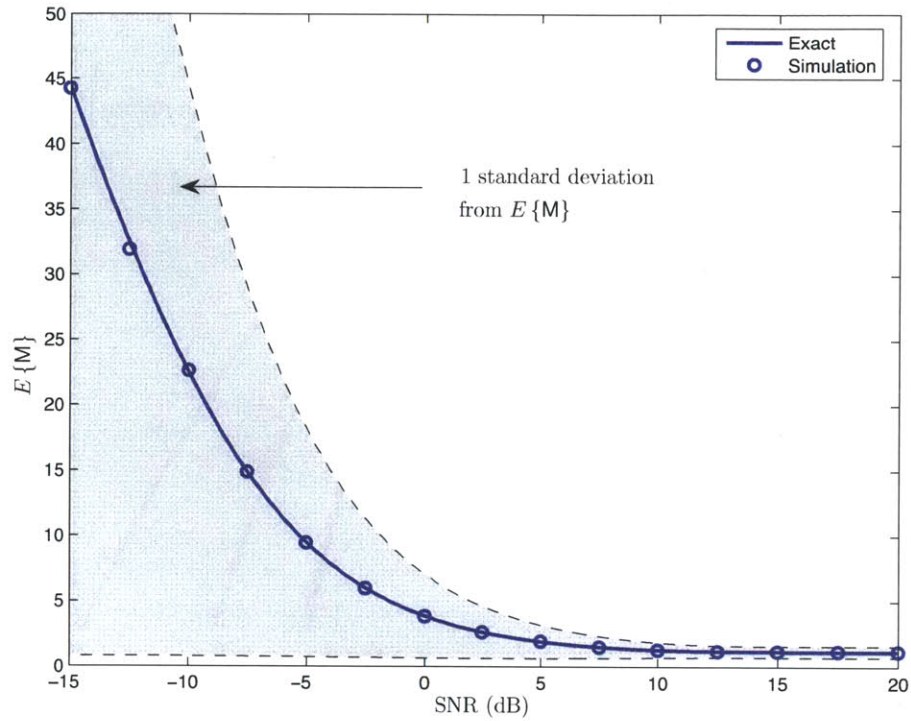
161

Figure 4-30: The expected number of MSSs required for a correct acquisition measures the amount of time to complete frame synchronization.

To evaluate this probability, we write

$$P\left\{\mathsf{W}_1 \le \eta, \mathsf{W}_2 \le \eta, \ldots, \mathsf{W}_{\ell_{\max}^m} \le \eta\right\}$$

$$= E\{\, P\{\mathsf{W}_1 \le \eta, \mathsf{W}_2 \le \eta, \ldots, \mathsf{W}_{\ell_{\max}^m} \le \eta \,:\, \mathsf{D}_1, \mathsf{D}_2, \ldots, \mathsf{D}_{2\ell_{\max}^m - 1}\} \,\},$$

where the expectation is over the data symbols $\{\mathsf{D}_j\}$. Conditioned on $\{\mathsf{D}_j = d_j\}$ for $d_j \in \{-1, +1\}$, the random vector $(\mathsf{W}_1, \mathsf{W}_2, \ldots, \mathsf{W}_{\ell_{\max}^m})$ has a multivariate normal distribution, whose CDF can be obtained efficiently using, for example, the method in [47].[20]
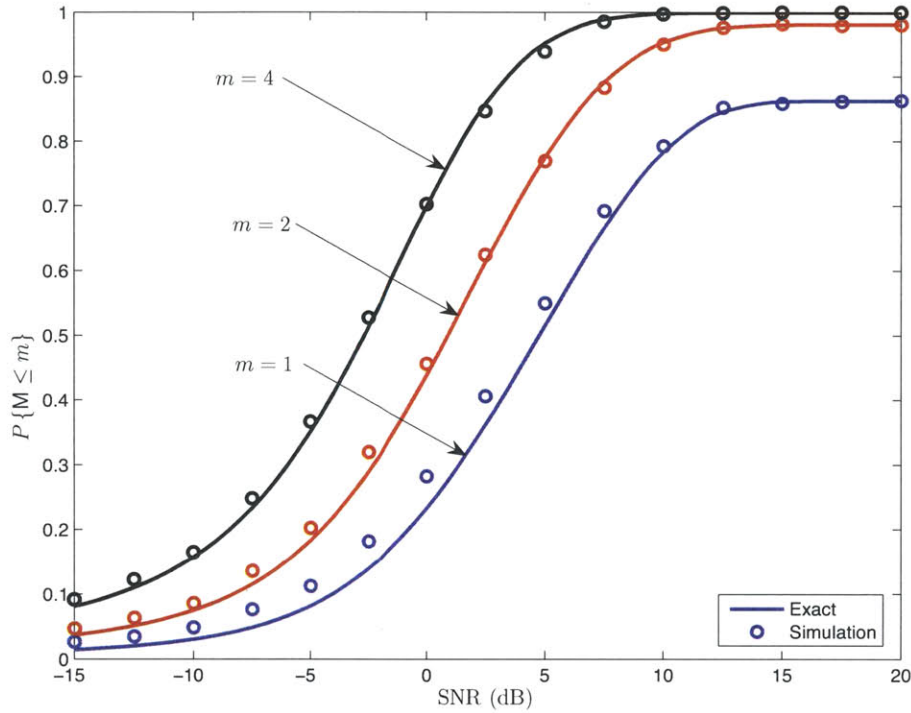
Figure 4-31: As the duration m to acquire the marker increases, the probability of correct acquisition within the given duration increases.

Discussion

For the purpose of illustration, we consider a false alarm level of $\alpha = 1\%$, a marker of length $\ell_{\max}^{\mathrm{m}} = 8$, and a frame length $\mathsf{L}_i^{\mathrm{d}}$ that is uniform on $\{30, 31, \ldots, 40\}$. Marker symbols are selected to be $(c_1, \ldots, c_8) = (+1, -1, +1, +1, +1, -1, -1, -1)$ to ensure good correlation properties [102]. Using these parameters, we evaluate the performance metrics in Section 4.4.2.

Figure 4-30 shows the expected time to complete the marker acquisition as a function of the SNR, $1/\sigma^2$. The expected time decreases with an increase in SNR as one would expect and reaches an asymptotic value, which is slightly greater than 1 in a high SNR regime.[21] This behavior can be attributed to the fact that the errors can still occur due to the data symbols replicating the marker. To eliminate this type of

---

[20]When $\ell_{\max}^{\mathrm{m}}$ is large, the conditioning on $\{\mathsf{D}_j\}$ may be too time-consuming. In that case, one may consider appropriate approximations.

[21]Note that changing the value of α will affect the asymptotic value.
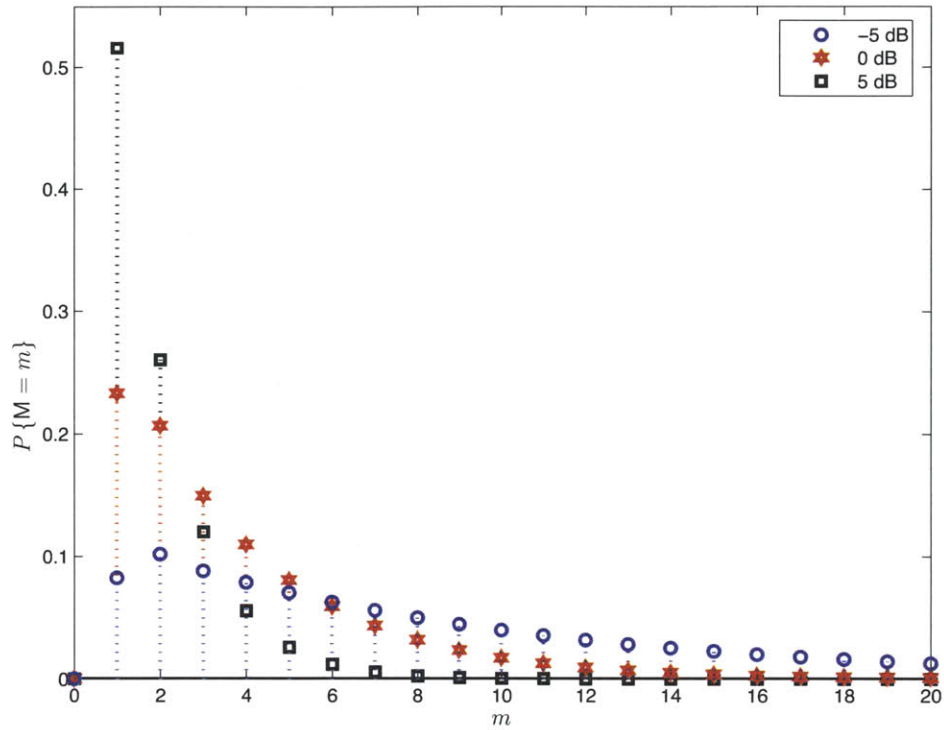
Figure 4-32: The PMF of M is obtained from the performance metric $P\{\mathsf{M} \leq m\}$.

decision error, the transmitter must modify the sequence of transmitted symbols, for example, using an approach similar to [7, p. 88].[22]

Figure 4-31 shows the probability of correct acquisition within a given duration, measured in terms of the number m of MSSs. For the purpose of illustration, we consider $m = 1, 2, 4$. The probability of correct acquisition increases with m as one would expect, indicating that the longer the duration spent to detect a marker, the more likely that the marker acquisition will be correct. The probabilities $P\{\mathsf{M} \leq m\}$ in the high SNR regime are related to the events of data symbols replicating the marker. In Figs. 4-30–4-31, we also report the simulation results, which confirm the validity of our analysis.

The performance metric $P\{\mathsf{M} \leq m\}$ can be used to obtain the PMF of M as well as the moments of M. For illustration purposes, we plot the PMF of M in Fig. 4-32 and the standard deviation of M as a shaded area around $E\{\mathsf{M}\}$ in Fig. 4-30.[23]

---

[22]This approach, however, can cause problems in some cases [43].

[23]It is more convenient to obtain $E\{\mathsf{M}\}$ through the closed-form expression in (4.84) although

164

Notice in Fig. 4-32 that the PMF of M for low SNR is spread, thus resulting in a large standard deviation as can be observed in Fig. 4-30.

$E\{M\}$ can also be obtained from the pmf.

Chapter 5

Conclusion

In this research, we solve first-passage-time problems and demonstrate the applications to network synchronization. The main results of this research are divided into five components, which address the five objectives of this thesis. In the first component, we derive the probability distribution of the first time that Brownian motion with quadratic drift exits from a boundary consisting of two constants. In the second component, we derive the probability distribution of the first time that Brownian motion with polynomial drift exits from a boundary consisting of two constants. In the third component, we derive and bound the probability distribution of the first time that a multi-dimensional Brownian motion with polynomial drift exits from a boundary described by an open set in the Euclidean space. In the forth component, we derive the probability distribution of the amount of time to achieve frame synchronization using the framework of first passage time. In the fifth component, we illustrate applications of our first-passage-time distributions to time-aware networks. The five components of this thesis are summarized below.

Brownian Motion with Quadratic Drift

We solve first-passage-time problems in which random process is Brownian motion with quadratic drift and the boundary consisting of two constants. Our goal is to obtain the probability distribution of the first time that Brownian motion with quadratic

drift crosses a two-sided boundary.

Our approach is to use transformation methodology. Brownian motion with quadratic drift is not a time-homogenous Markov process, necessitating a new technique to solve the first-passage-time problem. We apply five types of transformations: transformations of the probability measure, the time, the stochastic integral, the conditional expectation, and the unconditional expectation. In the derivation, the most challenging step is an evaluation of a conditional expectation that is a functional of a Brownian motion. To address this challenge, we transform the conditional expectation into an expectation, using an integral transform. Our approach yields an explicit expression of the first-passage-time distribution.

Our solution to the first-passage-time problem is special because few of first-passage-time problems are solved explicitly. The solution covers the case of Brownian motion without drift and Brownian motion with linear drift as special cases. As a simple extension, we provide the probability distribution for the case of a scaled Brownian motion with an arbitrary initial position. This variation is solved by a reduction to the problem of Brownian motion with quadratic drift. We expect our work to have practical utility because first-passage-time problems appear in many disciplines.

Brownian Motion with Polynomial Drift

We solve first-passage-time problems in which random process is Brownian motion with polynomial drift and the boundary consists of two constant barriers. The goal is to obtain the probability distribution of the first time that Brownian motion with polynomial drift crosses a two-sided boundary.

Our approach is to use transformation methodology. Like the case of quadratic drift, Brownian motion with polynomial drift is not a time-homogenous Markov process, making this first-passage-time problem difficult. Given that a quadratic drift is a special case of polynomial drift, the five type transformations still apply. In particular, we use transformations of the probability measure, the time, the stochastic integral, the conditional expectation, and the unconditional expectation. The dis-

168

tinction from the quadratic drift is at the last two transformations, which need to be adjusted for the polynomial drift. Our approach yields an expression of the PDF.

The main results on polynomial drift have several consequences. A class of polynomials is a dense subset of a class of continuous functions. As a consequence, we are able to solve first-passage-time problems for a class of drifts that contain not only polynomials but also elementary functions such as the sinusoidal, exponential, logarithmic, and square-root functions. In addition, we extend the results to the cases of one constant barrier, a moving barrier, and a scaled Brownian motion starting from an arbitrary location. We verify our methods by comparing our PDFs to the known PDFs for the square-root boundary. Given a large class of drifts that can be solved, we expect our work to have practical utility.

Multi-Dimensional Brownian Motion with Polynomial Drift

We solve first-passage-time problems, in which random process is a multi-dimensional Brownian motion with polynomial drift and a boundary that belongs to a family of open sets in the Euclidean space. The goal is to derive and bound the probability distribution of the first time that multi-dimensional Brownian motion with polynomial drift crosses a boundary.

Our approach to obtain and bound the probability distribution is to use reduction and ordered statistics. In particular, we reduce a mute-dimensional problem to several one-dimensional problems that involve Brownian motion with polynomial drift. Then, we relate the first passage time to the ordered statistic that depends on the shape of the boundary. These order statistics are not identically distributed but their distributions are straightforward to derive. Our approach yields a lower bound and an upper bound for the probability distribution of the first passage time.

The strength of our solution is that the bounds are simple to evaluate even for a random process with large dimension. In certain shape of the boundary, the lower bound equals the probability distribution of the first passage time. In general, the first-passage-time problems involving multi-dimensional Brownian motion is difficult to solve. Our solutions give insight into the probability distribution of the first passage

169

time.

A Discrete-Time Process With Certain Correlations

We solve first-passage-time problems in which random process is a discrete-time process with a certain correlation and the boundary is a constant. Our goal is to obtain the explicit expressions for the two most important performance measures for frame synchronization: the expected time to complete frame synchronization and the probability of correct acquisition within a given duration. The first metric is suitable for characterizing performance of transmission systems without delay constraints, while the second one is suitable for systems with delay constraints. The derivations of these explicit solutions turn out to involve probabilities and conditional probabilities of first passage times.

Our approach to obtain the performance metrics is to decompose the amount of time to correct acquisition as a random sum and apply rules of probability (such as Bayes' theorem, the law of total probability, and the law of large number), stopping time, and renewal theory. The strength of our approach is that these metrics can be expressed in terms of few parameters, which we refer to as the transition probabilities. The transition probabilities depend on the SNR, the decision rule, and the fading conditions. We discuss approaches to obtain the transition probabilities. Once the transition probabilities have been obtained for a given SNR, they can be used to evaluate the performance of a frame synchronization system.

Our framework yields the explicit expressions for performance metrics of frame synchronization. The results give insight into frame synchronization for both the continuous transmission of variable-length frames and bursty transmission of frames.

Applications to Time-Aware Networks

We demonstrate applications of first-passage-time distributions that we developed to network synchronization. We consider three examples: a synchronization of two clocks, a synchronization of a network of clocks, and frame synchronization.

Our approach to illustrate the applications of first-passage-time distribution is to express key quantities in a time-aware network as first passage times. For example, the time until the network loses synchronization is the first passage time of a multi-dimensional random process. The time until a node correctly acquires a packet is a function of the first-passage-time distributions for a discrete-time process. Since we know the probability distributions of the first-passage-time (from the previous four components of this research), we are able to derive the performance measures of these key quantities in time-aware networks.

The results give insight into synchronization time in a networks. We consider three aspects of synchronization in a time-aware network: synchronization of two clocks, synchronization of a network of clocks, and frame synchronization. In the case of two clocks, we plot the average and the outage of the calibration time as a function of key parameters such as severity of clock noise and the maximum allowable time error. In the case of the network of clocks, we plot the average and the outage of the network calibration time as a function of key parameters such as severity of clock noise and the size of the network. In the case of frame synchronization, we plot the average time to achieve frame synchronization and the probability to achieve frame synchronization within a given duration, as a function of key parameters such as the SNR. We provide interpretations of the results from these plots. The results from this component of the research provide valuable insights into the performance of time-aware networks and can serve as a guideline for the design of clocks and a deployment of networks.

In conclusion, this research solves various first-passage-time problems. The first-passage-time problems are difficult to solve since the problems often involve an infinite set of dependent random variables. Here, we are able to solve the first-passage-time problems for explicit solution for the Brownian motion with quadratic drift, for a special case of multi-dimensional Brownian motion with polynomial drift, and for the discrete time process with certain correlations. In the other first-passage-time problems that we solve here, we are able to bound the probability distribution (for the general case of multi-dimensional Brownian motion with polynomial drift) and able

to obtain the probability distribution with a combination of analytical and numerical methods (for the case of Brownian motion with polynomial drift). The class of first-passage-time problems that we solve in this research is large, covering various types of random processes and boundaries. We demonstrate applications of these first-passage-time problems to network synchronization, as an illustration. We expect our contributions to be useful and have practical utility since first-passage-time problems occur in many fields.

Appendix A

Other Important Proofs For the Discrete-Time Process

A.1 Justification of Equation (4.83)

To simplify the analysis, we assume, without loss of generality, that attempts to perform frame synchronization continue indefinitely even after a correct marker acquisition. This assumption implies that M_i is well-defined for any $i \geq 1$.

To prove the claim, we begin by defining auxiliary random variables:

$$\mathsf{Y}_i \triangleq \begin{cases} 1, & \text{if attempt } i \text{ yields a correct acquisition;} \\ 0, & \text{otherwise,} \end{cases}$$

for $i \geq 1$, and

$$1_{\mathcal{E}} \triangleq \begin{cases} 1, & \text{if event } \mathcal{E} \text{ occurs;} \\ 0, & \text{otherwise.} \end{cases} \tag{A.1}$$

Hence,

$$\mathsf{K} = \inf\{i \geq 1 : \mathsf{Y}_i = 1\}. \tag{A.2}$$

Let $S_K \triangleq M = M_1 + M_2 + \cdots + M_K$. Then, similar to the proof of Wald's identity,

$$E\{S_K\} \overset{(a)}{=} \sum_{k=1}^{\infty} E\{S_K 1_{\{K=k\}}\}$$

$$\overset{(b)}{=} \sum_{k=1}^{\infty} \sum_{i=1}^{k} E\{M_i 1_{\{K=k\}}\}$$

$$\overset{(c)}{=} \sum_{i=1}^{\infty} \sum_{k=i}^{\infty} E\{M_i 1_{\{K=k\}}\}$$

$$= \sum_{i=1}^{\infty} E\{M_i 1_{\{K \geq i\}}\}, \tag{A.3}$$

where (a) is a summation over disjoint regions, (b) is due to the definition of S_k and linearity of expectation, and (c) is due to [99, Corr. to Thm. 1.27]. To show that M_i and $1_{\{K \geq i\}}$ are independent for any i, we write

$$1_{\{K \geq i\}} = 1 - 1_{\{K \leq i-1\}}$$

$$= 1 - 1_{\{Y_1=1 \text{ or } Y_2=1 \text{ or } \ldots \text{ or } Y_{i-1}=1\}} \qquad \text{(from eq. (A.2))}$$

which shows that $1_{\{K \geq i\}}$ is a function of $Y \triangleq (Y_1, Y_2, \ldots, Y_{i-1})$. Random vector Y is independent of M_i because different acquisition attempts examine disjoint MSSs.[1] A continuation of (A.3) gives

$$E\{S_K\} = \sum_{i=1}^{\infty} E\{M_i\} E\{1_{\{K \geq i\}}\} \qquad \text{(independence)}$$

$$= \sum_{i=1}^{\infty} E\{M_1\} P\{K \geq i\} \qquad \text{(identically distributed)}$$

$$= E\{M_1\} E\{K\},$$

which proves the claim.[2]

---

[1]In other words, Y and M_i are independent because past decisions, which occurred at discrete times 1 to $i - 1$, do not affect the future outcome at time i.

[2]Note that the claim is not a direct application of Wald's identity [38, p. 369] because we do not require K to be a stopping time, do not require $E\{K\} < \infty$, and do not require $E\{M_i\} < \infty$.

A.2 Probability of Correct Acquisition

The probability of correct acquisition is given by

$$
p_{\text{cAcq}} = P\left\{\bigcup_{i=1}^{\infty} \{V_{1:J_i-1} \in \mathcal{R}^c, V_{J_i} \in \mathcal{R}\}\right\}
$$

$$
= \sum_{i=1}^{\infty} P\{V_{1:J_i-1} \in \mathcal{R}^c, V_{J_i} \in \mathcal{R}\} \quad \text{(disjoint union)}
$$

$$
= \underbrace{P\{V_{1:J_1-1} \in \mathcal{R}^c, V_{J_1} \in \mathcal{R}\}}_{=p_{\text{det}}}
$$

$$
+ \underbrace{P\{V_{1:J_2-1} \in \mathcal{R}^c, V_{J_2} \in \mathcal{R}\}}_{=p_{\text{nal-det}}}
$$

$$
+ \sum_{i=3}^{\infty} P\{V_{1:J_i-1} \in \mathcal{R}^c, V_{J_i} \in \mathcal{R}\}.
$$

Terms in the infinite sum can be simplified into

$$
P\{V_{1:J_i-1} \in \mathcal{R}^c, V_{J_i} \in \mathcal{R}\}
$$

$$
= \underbrace{P\{V_{1:J_2} \in \mathcal{R}^c\}}_{=p_{\text{nal-nal}}}
$$

$$
\times \left[\prod_{k=2}^{i-2} P\{V_{J_k+1:J_{k+1}} \in \mathcal{R}^c \mid V_{J_k-\ell_{\max}^{\text{m}}+2:J_k} \in \mathcal{R}^c\}\right]
$$

$$
\times P\{V_{J_{i-1}+1:J_i-1} \in \mathcal{R}^c, V_{J_i} \in \mathcal{R} : V_{J_{i-1}-\ell_{\max}^{\text{m}}+2:J_{i-1}} \in \mathcal{R}^c\}
$$

$$
= p_{\text{nal-nal}}(c_{\text{nal}})^{i-3}c_{\text{det}} \quad \text{(Time invariance)},
$$

where $\prod_{k=2}^{1}(\cdot) \triangleq 1$, $(c_{\text{nal}})^0 \triangleq 1$, and the parameters c_{nal} and c_{det} are defined in (4.85). Hence,

$$
p_{\text{cAcq}} = p_{\text{det}} + p_{\text{nal-det}} + \sum_{i=3}^{\infty} p_{\text{nal-nal}}(c_{\text{nal}})^{i-3}c_{\text{det}}.
$$

If $c_{\text{nal}} = 1$, then $c_{\text{det}} = 0$ and $p_{\text{cAcq}} = p_{\text{det}} + p_{\text{nal-det}}$. Otherwise, the infinite sum is a geometric series. Putting both cases of c_{nal} together yields (4.86).

A.3 Expected Time to Acquire a Marker

The expected time to acquire a marker equals

$$E\left\{\mathsf{M}_1\right\} = \sum_{i=1}^{\infty} P\left\{\mathsf{M}_1 \geq i\right\}$$

$$= 1 + \sum_{i=2}^{\infty} P\left\{\mathsf{M}_1 \geq i\right\},$$

since $\mathsf{M}_1 \geq 1$. The probability in the infinite sum can be obtained by observing that $\left\{\mathsf{M}_1 \geq i\right\} = \left\{\mathsf{V}_{1:\mathsf{J}_{i-1}} \in \mathcal{R}^c\right\}$. Hence,

$$P\left\{\mathsf{M}_1 \geq 2\right\} = P\left\{\mathsf{V}_{1:\mathsf{J}_1} \in \mathcal{R}^c\right\} = p_{\mathrm{nal}}$$

$$P\left\{\mathsf{M}_1 \geq 3\right\} = P\left\{\mathsf{V}_{1:\mathsf{J}_2} \in \mathcal{R}^c\right\} = p_{\mathrm{nal\text{-}nal}},$$

and for $i \geq 4$,

$$P\left\{\mathsf{M}_1 \geq i\right\}$$

$$= P\left\{\mathsf{V}_{1:\mathsf{J}_2} \in \mathcal{R}^c\right\} \times \prod_{k=2}^{i-2} P\left\{\mathsf{V}_{\mathsf{J}_k+1:\mathsf{J}_{k+1}} \in \mathcal{R}^c \mid \mathsf{V}_{\mathsf{J}_k-\ell_{\mathrm{max}}^{\mathrm{m}}+2:\mathsf{J}_k} \in \mathcal{R}^c\right\}$$

$$= p_{\mathrm{nal\text{-}nal}}\left(c_{\mathrm{nal}}\right)^{i-3} \qquad \text{(Time invariance)}.$$

Hence

$$E\left\{\mathsf{M}_1\right\} = 1 + p_{\mathrm{nal}} + p_{\mathrm{nal\text{-}nal}} + \sum_{i=4}^{\infty} p_{\mathrm{nal\text{-}nal}}\left(c_{\mathrm{nal}}\right)^{i-3}.$$

which simplifies into (4.87).

The expression for $E\left\{\mathsf{M}_1\right\}$, which involves three cases, can be understood intuitively as follows. The condition $0 < p_{\mathrm{nal\text{-}nal}} \leq 1$ means that with non-zero probability a marker detector examines more than two MSSs. The condition $c_{\mathrm{nal}} = 1$ implies that if the marker detector examines more than two MSSs, then the marker detector will never terminate. The condition $0 < p_{\mathrm{nal\text{-}nal}} \leq 1$ together with $c_{\mathrm{nal}} = 1$ in the third case

implies that M_1 is unbounded, resulting in $E\{M_1\} = \infty$. The condition $p_{\text{nal-nal}} = 0$ in the second case implies that with probability one the marker detector terminates within one MSS or two MSSs, resulting in the expected duration $E\{M_1\}$ between 1 and 2 inclusively. The remaining case occurs when the detector terminates after examining a finite number of MSSs, resulting in $1 \leq E\{M\} < \infty$.

A.4   Justification of (4.88)

The base case (4.88a) is obvious. The recursive case (4.88b) proceeds as follows:

$$
\begin{aligned}
&\gamma(k+1, m) \\
&= \sum_{n=1}^{\infty} P\{M_1 + M_2 + \cdots + M_k + M_{k+1} \leq m \; : \; M_{k+1} = n\} P\{M_{k+1} = n\} \\
&= \sum_{n=1}^{\infty} P\{M_1 + M_2 + \cdots + M_k \leq m - n\} P\{M_{k+1} = n\} \\
&= \sum_{n=1}^{m-k} \gamma(k, m-n) P\{M_1 = n\},
\end{aligned}
$$

where we have used the fact $M_1 + M_2 + \cdots + M_k \geq k$ in the last equation.

A.5   Justification of (4.91)

We will investigate properties of a generic arrival process, which include the marker arrival process $\{J_i\}$ as a special case. Then we will justify (4.91) through the properties of this generic arrival process.

Consider an arbitrary arrival process with the interarrival times $\{L_i + S_i\}$ for $i \geq 1$, where $L_i \geq 0$, $S_i \geq 1$, $\{L_i\}$ are IID, $\{S_i\}$ are IID, and $\{L_i\}$ and $\{S_i\}$ are independent. As an example, L_i is the length of a frame, and S_i is the length of a silent transmission plus the length of the marker. Suppose that we begin to observe the arrival process at random time. Let $L_{i^*} + S_{i^*}$ be the interarrival time containing the beginning of the observation. We wish to obtain the PMF of L_{i^*}.

We use an argument based on renewal theory to write, for $\ell \geq 0$,

$$P\{L_{i^*} = \ell\} = \lim_{n \to \infty} \frac{\sum_{\substack{1 \leq i \leq n \\ L_i = \ell}} (L_i + S_i)}{\sum_{i=1}^{n} (L_i + S_i)} \qquad \text{almost surely,}$$

where the argument of the limit is the portion of time that gives rise to the event $\{L_{i^*} = \ell\}$. Separating the summation in the numerator and introducing an auxiliary random set,

$$\mathcal{I}(\ell, n) \triangleq \{i : 1 \leq i \leq n \text{ and } L_i = \ell\},$$

into the expression give, almost surely,

$$P\{L_{i^*} = \ell\} = \lim_{n \to \infty} \left(\frac{\ell |\mathcal{I}(\ell, n)| + \sum_{i \in \mathcal{I}(\ell, n)} S_i}{\sum_{i=1}^{n} (L_i + S_i)} \right)$$

$$= \lim_{n \to \infty} \left(\frac{\frac{\ell |\mathcal{I}(\ell, n)|}{n} + \frac{|\mathcal{I}(\ell, n)|}{n} \frac{\sum_{i \in \mathcal{I}(\ell, n)} S_i}{|\mathcal{I}(\ell, n)|}}{\frac{1}{n} \sum_{i=1}^{n} (L_i + S_i)} \right),$$

which simplifies into

$$\frac{\ell \left(\lim_{n \to \infty} \frac{|\mathcal{I}(\ell, n)|}{n} \right) + \left(\lim_{n \to \infty} \frac{|\mathcal{I}(\ell, n)|}{n} \right) \left(\lim_{n \to \infty} \frac{\sum_{i \in \mathcal{I}(\ell, n)} S_i}{|\mathcal{I}(\ell, n)|} \right)}{\lim_{n \to \infty} \frac{1}{n} \sum_{i=1}^{n} (L_i + S_i)}$$

Writing

$$\frac{|\mathcal{I}(\ell, n)|}{n} = \frac{1}{n} \sum_{i=1}^{n} 1_{\{L_i = \ell\}},$$

where 1 is the indicator function, defined in (A.1), and applying the strong law of large number [38, Thm. 8.3.5] to the limits result in

$$P\{L_{i^*} = \ell\} = \frac{\ell P\{L_1 = \ell\} + P\{L_1 = \ell\} E\{S_1\}}{E\{L_1 + S_1\}},$$

or equivalently,

$$P\left\{L_{i^*} = \ell\right\} = \left(\frac{\ell + E\left\{S_1\right\}}{E\left\{L_1\right\} + E\left\{S_1\right\}}\right) P\left\{L_1 = \ell\right\}. \tag{A.4}$$

We make the following observations regarding (A.4). If L_i takes values in a set $\mathcal{L}$ of integers, then L_{i^*} also takes values in the same set of integers. This characteristic of L_{i^*} is expected, since L_{i^*} is one of $\{L_i : i \geq 1\}$. In addition, for all ℓ, the right-hand sides of (A.4) are non-negative and sum to 1. This characteristic implies that (A.4) is a valid PMF. Moreover, if $L_i = \ell_c$ and $S_i = s_c$ are constants, then (A.4) becomes

$$P\left\{L_{i^*} = \ell\right\} = \begin{cases} 1, & \text{if } \ell = \ell_c; \\ 0, & \text{otherwise,} \end{cases}$$

which agrees with intuition. Furthermore, the expectation of L_{i^*} satisfies[3]

$$E\left\{L_{i^*}\right\} = \frac{E\left\{L_1^2\right\} + E\left\{L_1\right\} E\left\{S_1\right\}}{E\left\{L_1\right\} + E\left\{S_1\right\}}$$

$$\geq E\left\{L_1\right\},$$

indicating that L_{i^*} tends to be larger than L_1. This characteristic is intuitive, since the random instant that our observation begins is likely to fall into a large interarrival time. These observations help to validate (A.4).

Using (A.4) with

$$L_i = \mathsf{L}_i^{\mathrm{d}}, S_i = \mathsf{L}_i^{\mathrm{s}} + \ell_{\max}^{\mathrm{m}}, \ell = \ell_0^{\mathrm{d}}, \text{ and } L_{i^*} = \mathsf{L}_0^{\mathrm{d}}$$

gives (4.91a). Similarly, using (A.4) with

$$L_i = \mathsf{L}_i^{\mathrm{s}}, S_i = \mathsf{L}_i^{\mathrm{d}} + \ell_{\max}^{\mathrm{m}}, \ell = \ell_0^{\mathrm{s}}, \text{ and } L_{i^*} = \mathsf{L}_0^{\mathrm{s}}$$

gives (4.91b).

---

[3]The inequality follows from the fact that variance $E\left\{L^2\right\} - (E\left\{L\right\})^2$ is non-negative for any random variable L, or more generally, from the Schwarz inequality [99, Thm. 3.5].

A.6 Value of $\tilde{N}(k)$

We decompose

$$\tilde{N}(k) = \tilde{N}_{\mathrm{nal}}(k) + \tilde{N}_{\mathrm{det}}(k),$$

where $\tilde{N}_{\mathrm{nal}}(k)$ denotes the number of k-joint probabilities required to evaluate the transition probabilities p_{nal}, $p_{\mathrm{nal\text{-}nal}}$, and c_{nal}, and $\tilde{N}_{\mathrm{det}}(k)$ denotes the number of k-joint probabilities required to evaluate the transition probabilities p_{det}, $p_{\mathrm{nal\text{-}det}}$, and c_{det}. To obtain $\tilde{N}_{\mathrm{nal}}(k)$, we consider six distinct cases.

Case 1a: $\mathsf{L}_i^{\mathrm{s}} = 0$ and $1 \leq k \leq \ell_{\max}^{\mathrm{m}} - 2$. Then, $\tilde{N}_{\mathrm{nal}}(k) = 1$, which corresponds to the k-joint probability term generated by the sequence of k data symbols and the marker.

Case 2a: $\mathsf{L}_i^{\mathrm{s}} \geq 2\ell_{\max}^{\mathrm{m}} - 2$ and $1 \leq k \leq \ell_{\max}^{\mathrm{m}} - 2$. Then, $\tilde{N}_{\mathrm{nal}}(k) = k$, which corresponds to the k-joint probability terms generated by the sequences of d data symbols, $k - d - 1$ silence symbols, and the marker, for $d = 0, 1, 2, \ldots, k - 1$.

Case 3a: $\mathsf{L}_i^{\mathrm{s}} = 0$ and $k = \ell_{\max}^{\mathrm{m}} - 1$. By inspection of Fig. 4-16, $\tilde{N}_{\mathrm{nal}}(\ell_{\max}^{\mathrm{m}} - 1)$ is the number of $(\ell_{\max}^{\mathrm{m}} - 1)$-joint probability terms generated by the sequence of $c_3, c_4, \ldots, c_{\ell_{\max}^{\mathrm{m}}}$, $(2\ell_{\max}^{\mathrm{m}} - 2)$ data symbols, the marker, and $(\ell_{\max}^{\mathrm{m}} - 1)$ data symbols. Hence, $\tilde{N}_{\mathrm{nal}}(\ell_{\max}^{\mathrm{m}} - 1) = 3\ell_{\max}^{\mathrm{m}} - 2$.

Case 4a: $\mathsf{L}_i^{\mathrm{s}} \geq 2\ell_{\max}^{\mathrm{m}} - 2$ and $k = \ell_{\max}^{\mathrm{m}} - 1$. By inspection of Fig. 4-16, $\tilde{N}_{\mathrm{nal}}(\ell_{\max}^{\mathrm{m}} - 1)$ is the number of $(\ell_{\max}^{\mathrm{m}} - 1)$-joint probability terms generated by the sequence of $c_3, c_4, \ldots, c_{\ell_{\max}^{\mathrm{m}}}$, $(2\ell_{\max}^{\mathrm{m}} - 2)$ data symbols, $(2\ell_{\max}^{\mathrm{m}} - 2)$ silence symbols, the marker, and $(\ell_{\max}^{\mathrm{m}} - 1)$ data symbols. Hence, $\tilde{N}_{\mathrm{nal}}(\ell_{\max}^{\mathrm{m}} - 1) = 5\ell_{\max}^{\mathrm{m}} - 4$.

Case 5a: $\mathsf{L}_i^{\mathrm{s}} = 0$ and $k = \ell_{\max}^{\mathrm{m}}$. By inspection of Fig. 4-16, $\tilde{N}_{\mathrm{nal}}(\ell_{\max}^{\mathrm{m}})$ is the number of $\ell_{\max}^{\mathrm{m}}$-joint probability terms generated by the sequence of $c_2, c_3, \ldots, c_{\ell_{\max}^{\mathrm{m}}}$, $(2\ell_{\max}^{\mathrm{m}} - 1)$ data symbols, the marker, and $(\ell_{\max}^{\mathrm{m}} - 1)$ data symbols. Hence, $\tilde{N}_{\mathrm{nal}}(\ell_{\max}^{\mathrm{m}}) = 3\ell_{\max}^{\mathrm{m}} - 1$.

Case 6a: $\mathsf{L}_i^{\mathrm{s}} \geq 2\ell_{\max}^{\mathrm{m}} - 2$ and $k = \ell_{\max}^{\mathrm{m}}$. By inspection of Fig. 4-16, $\tilde{N}_{\mathrm{nal}}(\ell_{\max}^{\mathrm{m}})$ is the number of $\ell_{\max}^{\mathrm{m}}$-joint probability terms generated by the sequence of $c_2, c_3, \ldots, c_{\ell_{\max}^{\mathrm{m}}}$, $(2\ell_{\max}^{\mathrm{m}} - 1)$ data symbols, $(2\ell_{\max}^{\mathrm{m}} - 1)$ silence symbols, the marker, and $(\ell_{\max}^{\mathrm{m}} - 1)$ data

symbols. Hence, $\tilde{N}_{nal}(\ell_{max}^m) = 5\ell_{max}^m - 2$.

After deriving p_{nal}, $p_{nal\text{-}nal}$, and c_{nal}, we already have most of the joint probability terms that are also required for the derivation of p_{det}, $p_{nal\text{-}det}$, and c_{det}. The remaining k-joint probability terms are the first terms of the right-hand side of (4.93) for $k = 1, 2, 3, \ldots, \ell_{max}^m - 2$. We now consider two distinct cases.

Case 1b: $\mathsf{L}_i^s = 0$ and $1 \leq k \leq \ell_{max}^m - 2$. Then, $\tilde{N}_{det}(k) = 1$, which corresponds to the k-joint probability term generated by the sequence of k data symbols and $c_1, c_2, \ldots, c_{\ell_{max}^m - 1}$.

Case 2b: $\mathsf{L}_i^s \geq 2\ell_{max}^m - 2$ and $1 \leq k \leq \ell_{max}^m - 2$. Then, $\tilde{N}_{det}(k) = k + 1$, which corresponds to the k-joint probability terms generated by the sequences of d data symbols, $k - d$ silence symbols, and $c_1, c_2, \ldots, c_{\ell_{max}^m - 1}$, for $d = 0, 1, 2, \ldots, k$.

Combining the results from cases 1a–6a and cases 1b–2b gives the bounds for $\tilde{N}(k)$ in (4.90).

Bibliography

[1] J. Abate and P. P. Valkó, "Multi-precision Laplace transform inversion," *Internat. J. Numer. Methods Engrg.*, vol. 60, 2004.

[2] M. Abramowitz and I. A. Stegun, Eds., *Handbook of Mathematical Functions with Formulas, Graphs, and Mathematical Tables*. United States Department of Commerce, 1972, tenth printing.

[3] D. W. Allan, "Statistics of atomic frequency standards," *Proc. IEEE*, vol. 54, no. 2, pp. 221–230, Feb. 1966.

[4] R. H. Barker, "Group synchronization of binary digital systems," in *Communication Theory*, W. Jackson, Ed. New York: Academic-Butterworth, 1953.

[5] R. J. Barton and H. V. Poor, "Signal detection in fractional gaussian noise," *IEEE Trans. Inf. Theory*, vol. 34, no. 5, pp. 943–959, Sep. 1988.

[6] C. W. Baum and V. V. Veeravalli, "A sequential procedure for multihypothesis testing," *IEEE Trans. Inf. Theory*, vol. 40, no. 6, pp. 1994–2007, Nov. 1994.

[7] D. P. Bertsekas and R. G. Gallager, *Data Networks*, 2nd ed. New Jersey, 07632: Prentice-Hall, 1992.

[8] D. P. Bertsekas and J. N. Tsitsiklis, *Introduction to Probability*. Athena Scientific, 2002.

[9] G.-G. Bi, "Performance of frame sync acquisition algorithms on the awgn channel," *IEEE Trans. Commun.*, vol. 32, no. 10, pp. 1196–1201, Oct. 1983.

[10] P. J. Bickel and K. Doksum, *Mathematical Statistics: Basic Ideas and Selected Topics*, 2nd ed. Upper Saddle River, NJ: Prentice Hall, 2001, vol. 1.

[11] F. Black and J. C. Cox, "Valuing corporate securities: Some effects of bond indenture provisions," *J. of Finance*, vol. 31, no. 2, pp. 351–367, 1976.

[12] I. F. Blake and W. C. Lindsey, "Level-crossing problems for random processes," *IEEE Trans. Inf. Theory*, vol. IT-19, no. 3, pp. 295–315, May 1973.

[13] A. N. Borodin and P. Salminen, *Handbook of Brownian Motion—Facts and Formulae*. Basel, Switzerland: Birkhäuser, 1996.

[14] ——, *Handbook of Brownian Motion—Facts and Formulae*, 2nd ed. Basel, Switzerland: Birkhäuser, 2002.

[15] W. R. Braun, "Performance analysis for the expanding search PN acquisition algorithm," *IEEE Trans. Commun.*, vol. 30, pp. 424–435, Mar. 1982.

[16] S. Bregni, *Synchronization of Digital Telecommunications Network*. West Sussex, England: John Wiley & Sons, Ltd., 2002.

[17] R. M. Capocelli and L. M. Ricciardi, "Diffusion approximation and first passage time problem for a model neuron," *Biol. Cybernet.*, vol. 8, no. 6, pp. 214–223, Jun. 1971.

[18] C. Carbonelli, A. A. D'Amico, U. Mengali, and M. Morelli, "Channel acquisition and tracking for DS-CDMA uplink transmissions," *IEEE Trans. Commun.*, vol. 53, pp. 1930–1939, Nov. 2005.

[19] C. Carbonelli and U. Mengali, "Synchronization algorithms for UWB signals," *IEEE Trans. Commun.*, vol. 54, pp. 329–338, Feb. 2006.

[20] D. Cassioli, M. Z. Win, and A. F. Molisch, "The ultra-wide bandwidth indoor channel: From statistical model to simulations," *IEEE J. Sel. Areas Commun.*, vol. 20, no. 6, pp. 1247–1257, Aug. 2002.

[21] S. Chandrasekhar, "Stochastic problems in physics and astronomy," *Rev. Modern Phys.*, vol. 15, no. 1, pp. 1–89, Jan. 1943.

[22] C.-C. Chen and M. Z. Win, "Frequency noise measurement of diode-pumped Nd:YAG ring lasers," *IEEE Photonics Technol. Lett.*, vol. 2, no. 11, pp. 772–774, Nov. 1990.

[23] M. Chiani and M. G. Martini, "Optimum synchronization of frames with unknown, variable lengths on gaussian channels," in *Proc. IEEE Global Telecomm. Conf.*, Dallas, TX, Dec. 2004, pp. 4087–4091.

[24] ——, "Practical frame synchronization for data with unknown distribution on AWGN channels," *IEEE Commun. Lett.*, vol. 9, no. 5, pp. 456–458, May 2005.

[25] ——, "On sequential frame synchronization in AWGN channels," *IEEE Trans. Commun.*, vol. 54, no. 2, pp. 339–348, Feb. 2006.

[26] C.-C. Chong, Y.-E. Kim, S. K. Yong, and S.-S. Lee, "Statistical characterization of the UWB propagation channel in indoor residential environment," *Wireless Communications and Mobile Computing, Wiley InterScience*, vol. 5, no. 5, pp. 503–512, Aug. 2005.

[27] C.-C. Chong and S. K. Yong, "A generic statistical-based UWB channel model for high-rise apartments," *IEEE Trans. Antennas Propag.*, vol. 53, pp. 2389–2399, 2005.

[28] E. A. Coddington, *An Introduction to Ordinary Differential Euqations.* New York: Dover Publications, 1989.

[29] G. E. Corazza, "On the MAX/TC criterion for code acquisition and its application to DS-SSMA systems," *IEEE Trans. Commun.*, vol. 44, pp. 1173–1182, Sep. 1996.

[30] G. E. Corazza, C. Caini, A. Vanelli-Coralli, and A. Polydoros, "DS-CDMA code acquisition in the presence of correlated fading–Part I: Theoretical aspects," *IEEE Trans. Commun.*, vol. 52, no. 7, pp. 1160–1168, Jul. 2004.

[31] ——, "DS-CDMA code acquisition in the presence of correlated fading–Part II: Application to cellular networks," *IEEE Trans. Commun.*, vol. 52, no. 8, pp. 1397–1407, Aug. 2004.

[32] G. E. Corazza and A. Polydoros, "Code acquisition in CDMA cellular mobile networks–Part I:theory," in *Proc. IEEE 5$\underline{th}$ Int. Symp. on Spread Spectrum Techniques & Applications*, Sun City, SOUTH AFRICA, Sep. 1998, pp. 454–458.

[33] D. A. Darling and A. J. F. Siegert, "The first passage problem for a continuous Markov process," *Ann. of Math. Stat.*, vol. 24, no. 4, pp. 624–639, Dec. 1953.

[34] A. J. de Lind van Wijngaarden and T. J. Willink, "Frame synchronization using distributed sequences," *IEEE Trans. Commun.*, vol. 48, pp. 2127 – 2138, Dec. 2000.

[35] J. L. Doob, *Stochastic Processes.* New York: John Wiley & Sons, 1953.

[36] V. P. Dragalin, A. G. Tartakovsky, and V. V. Veeravalli, "Multihypothesis sequential probability ratio tests - part I: Asymptotic optimality," *IEEE Trans. Inf. Theory*, vol. 45, no. 7, pp. 2448–2461, Nov. 1999.

[37] ——, "Multihypothesis sequential probability ratio tests - part II: Accurate asymptotic expansions for the expected sample size," *IEEE Trans. Inf. Theory*, vol. 46, no. 4, pp. 1366–1383, Jul. 2000.

[38] R. M. Dudley, *Real Analysis and Probability*, 2nd ed. New York, NY: Cambridge University Press, 2003.

[39] J. Durbin, "Boundary-crossing probabilities for the brownian motion and poisson processes and techniques for computing the power of the Kolmogorov-Smirnov test," *J. Appl. Probab.*, vol. 8, no. 3, pp. 431–453, Sep. 1971.

[40] P. Embrechts and H. Schmidli, "Modelling of extremal events in insurance and finance," *Math. Methods Oper. Res.*, vol. 39, no. 1, pp. 1–34, Feb. 1994.

[41] W. J. Ewens, *Mathematical Population Genetic.* New York: Springer, 1937.

[42] M. Feng, "Complete solution of the Schrödinger equation for the time-dependent linear potential," *Phys. Rev. A*, vol. 64, no. 3, pp. 034 101-1 – 034 101-3, Aug. 2001.

[43] D. Fiorini, M. Chiani, V. Tralli, and C. Salati, "Can we trust in HDLC?" *ACM SIGCOMM Computer Commun. Review*, vol. 24, no. 5, pp. 61–80, Oct. 1994.

[44] W. Fischer, E. Wallmeier, T. Worster, S. P. Davis, and A. Hayter, "Data communications using ATM: architectures, protocols, and resource management," *IEEE Commun. Mag.*, vol. 32, pp. 24–33, Aug. 1994.

[45] P. Flandrin, "On the spectrum of fractional brownian motions," *IEEE Trans. Inf. Theory*, vol. 35, no. 1, pp. 197–199, Jan. 1989.

[46] L. Galleani, L. Sacerdote, P. Tavella, and C. Zucca, "A mathematical model for the atomic clock error," *Metrologia*, vol. 40, no. 3, pp. S257–S264, Jun. 2003.

[47] A. Genz, "Numerical computation of multivariate normal probabilities," *J. Computational and Graphical Statistics*, vol. 1, no. 2, pp. 141–149, Jun. 1992.

[48] C. N. Georghiades, "Optimum delay and sequence estimation from incomplete data," *IEEE Trans. Inf. Theory*, vol. 36, no. 1, pp. 202–208, Jan. 1990.

[49] C. N. Georghiades and D. L. Snyder, "The expectation-maximization algorithm for symbol unsynchronized sequence detection," *IEEE Trans. Commun.*, vol. 39, no. 1, pp. 54–61, Jan. 1991.

[50] S. Gezici, E. Fishler, H. Kobayashi, H. V. Poor, and A. F. Molisch, "A rapid acquisition technique for impulse radio," in *Proc. IEEE Pacific Rim Conf. on Commun., Computers and Signal Processing*, vol. 2, Victoria, Canada, Aug. 2003, pp. 627 – 630.

[51] S. Glisic and M. D. Katz, "Modeling of code acquisition process for Rake receivers in CDMA wireless networks with multipath and transmitter diversity," *IEEE J. Sel. Areas Commun.*, vol. 19, pp. 21–32, Jan. 2001.

[52] S. W. Golomb and R. A. Scholtz, "Generalized Barker sequences," *IEEE Trans. Inf. Theory*, vol. 11, no. 4, pp. 533– 537, Oct. 1965.

[53] S. W. Golomb and M. Z. Win, "Recent results on polyphase sequences," *IEEE Trans. Inform. Theory*, vol. 44, no. 2, pp. 817–824, Mar. 1998.

[54] I. S. Gradshteyn and I. M. Ryzhik, *Table of Integrals, Series, and Products*, 6th ed. San Diego, CA: Academic Press, Inc., 2000.

[55] P. Groeneboom, "Brownian motion with a parabolic drift and airy functions," *Probab. Theory Related Fields*, vol. 81, pp. 79–109, 1989.

[56] M. Guenach, H. Wymeersch, H. Steendam, and M. Moeneclaey, "Code-aided ML joint frame synchronization and channel estimation for downlink MC-CDMA," *IEEE J. Sel. Areas Commun.*, vol. 24, no. 6, pp. 1105–1114, Jun. 2006.

[57] G. Hernándex-Del-Valle. (2009, May) On Schrödinger's equation, 3-dimensional Bessel bridges, and passage time problems. [Online]. Available: http://arxiv.org/abs/0905.1971v1

[58] J. K. Holmes, *Coherent Spread Spectrum Systems*, 1st ed. New York: Wiley-Interscience, 1982.

[59] E. A. Homier and R. A. Scholtz, "Hybrid fixed-dwell-time search techniques for rapid acquisition of ultra-wideband signals," in *International Workshop on Ultra Wideband System*, Oulu, Finland, Jun. 2003.

[60] M. K. Howlader, "Decoder-assisted noncoherent frame synchronization for burst OFDM-based packet transmission," in *Proc. IEEE Global Telecomm. Conf.*, St. Louis, MO, Nov. 2005, pp. 2927–2931.

[61] H. Huh and J. V. Krogmeier, "A unified approach to optimum frame synchronization," *IEEE Trans. Wireless Commun.*, vol. 5, no. 12, pp. 3700–3711, Dec. 2006.

[62] L. D. Kabulepa, A. G. Ortiz, and M. Glesner, "Design of an efficient OFDM burst synchronization scheme," in *IEEE Int. Symp. on Circuits and Systems*, vol. 3, Scottsdale, AZ, May 2002, pp. III–449 – III–452.

[63] I. Karatzas and S. E. Shreve, *Brownian Motion and Stochastic Calculus*, 2nd ed. New York: Springer, 1991.

[64] M. D. Katz and S. Glisic, "Modeling of code acquisition process in CDMA networks–quasi-synchronization systems," *IEEE Trans. Commun.*, vol. 46, pp. 1564–1568, Dec. 1998.

[65] ——, "Modeling of code acquisition process in CDMA networks–asynchronous systems," *IEEE J. Sel. Areas Commun.*, vol. 18, pp. 73–86, Jan. 2000.

[66] M. D. Katz, J. H. Iinatti, and S. Glisic, "Two-dimensional code acquisition in time and angular domains," *IEEE J. Sel. Areas Commun.*, vol. 19, pp. 2441–2451, Dec. 2001.

[67] ——, "Recent advances in multi-antenna based code acquisition," in *Proc. IEEE Int. Symp. on Spread Spectrum Techniques & Applications*, Sydney, Australia, Aug. 2004, pp. 199 – 206.

[68] ——, "Two-dimensional code acquisition in environments with a spatially nonuniform distribution of interference: Algorithm and performance," *IEEE Trans. Wireless Commun.*, vol. 3, pp. 1–7, Jan. 2004.

[69] M. S. Klamkin and D. J. Newman, "The philosophy and applications of transform theory," 1960, unpublished manuscript.

[70] W. C. Lindsey, F. Ghazvinian, W. C. Hagmann, and K. Dessouky, "Network synchronization," *Proc. IEEE*, vol. 73, no. 10, pp. 1445– 1467, Oct. 1985.

[71] W. C. Lindsey, *Synchronization Systems in Communication and Control*. Englewood Cliffs, NJ: Prentice-Hall, 1972.

[72] W. C. Lindsey and M. K. Simon, *Telecommunication Systems Engineering*. Englewood Cliffs, NJ: Prentice-Hall, 1973.

[73] B. B. Mandelbrot and J. W. V. Ness, "Fractional brownian motions, fractional noises and applications," *SIAM Review*, vol. 10, no. 4, pp. 422–437, Oct. 1968.

[74] X. Mao, *Stochastic Differential Equations and Applications*, 2nd ed. Chichester, UK: Horwood Publishing, 2007.

[75] A. Martin-Löf, "The final size of a nearly critical epidemic, and the first passage time of a Wiener process to a parabolic barrier," *J. Appl. Probab.*, vol. 35, no. 3, pp. 671–682, Sep. 1998.

[76] J. L. Massey, "Optimal frame synchronization," *IEEE Trans. Commun.*, vol. COM-20, no. 2, pp. 115–119, Apr. 1972.

[77] A. A. Novikov, "On stopping times for a Wiener process," *Theory Prob. and its Applications*, vol. 16, no. 3, pp. 449–456, 1971.

[78] B. Øksendal, *Stochastic Differential Equations*, 6th ed. New York: Springer, 2007.

[79] A. E. Payzin, "Analysis of a digital bit synchronizer," *IEEE Trans. Commun.*, vol. 31, no. 4, pp. 554– 560, Apr. 1983.

[80] D. B. Percival, "Stochastic models and statistical analysis for clock noise," *Metrologia*, vol. 40, no. 3, pp. S289–S304, Jun. 2003.

[81] G. Peskir and A. Shiryaev, *Optimal Stopping and Free-Boundary Problems*. Basel, Switzerland: Birkhäuser, 2006.

[82] R. L. Peterson, R. E. Ziemer, and D. E. Borth, *Introduction to Spread Spectrum Communications*, 1st ed. Englewood Cliffs, New Jersey 07632: Prentice Hall, 1995.

[83] R. L. Pickholtz, D. L. Schilling, and L. B. Milstein, "Theory of spread spectrum communications–A tutorial," *IEEE Trans. Commun.*, vol. COM-30, no. 5, pp. 855–884, May 1982.

[84] L. D. Piro, E. Perone, and P. Tavella, "Random walk and first crossing time: Applications in metrology," in *European Frequency and Time Forum International*, Warsaw, POLAND, Mar. 1998, pp. 388–391.

[85] A. Polydoros and S. Glisic, "Code synchronization: A review of principles and techniques," in *Proc. IEEE Int. Symp. on Spread Spectrum Techniques & Applications*, Oulu, Finland, Jul. 1994, pp. 115–137.

[86] A. Polydoros and M. K. Simon, "Generalized serial search code acquisition: The equivalent circular state diagram approach," *IEEE Trans. Commun.*, vol. COM-32, no. 12, pp. 1260–1268, Dec. 1984.

[87] A. Polydoros and C. L. Weber, "A unified approach to serial search spread-spectrum code acquisition—Part I: General theory," *IEEE Trans. Commun.*, vol. COM-32, no. 5, pp. 542–549, May 1984.

[88] ——, "A unified approach to serial search spread-spectrum code acquisition— Part II: A matched-filter receiver," *IEEE Trans. Commun.*, vol. COM-32, no. 5, pp. 550–560, May 1984.

[89] H. V. Poor, *Quickest Detection*. New York: Cambridge University Press, 2009.

[90] W. H. Press, S. A. Teukolsky, W. T. Vetterling, and B. P. Flannery, *Numerical Recipes in C*, 2nd ed. New York, NY 10011-4211: Cambridge University Press, 1995.

[91] J. G. Proakis, *Digital Communications*, 4th ed. New York, NY, 10020: McGraw-Hill, Inc., 2000.

[92] I. Ramachandran and S. Roy, "On acquisition of wideband direct-sequence spread spectrum signals," *IEEE Trans. Wireless Commun.*, vol. 5, pp. 1537–1546, Jun. 2006.

[93] L. M. Ricciardi and S. Sato, "Diffusion processes and first-passage-time problems," in *Lectures in applied mathematics and informatics*, L. M. Ricciardi, Ed. Manchester, UK: Manchester University Press, 1990, pp. 206–285.

[94] R. R. Rick and L. B. Milstein, "Parallel acquisition in mobile DS-CDMA systems," *IEEE Trans. Commun.*, vol. 45, pp. 1466–1476, Nov. 1997.

[95] ——, "Optimal decision strategies for acquisition of spread-spectrum signals in frequency-selective fading channels," *IEEE Trans. Commun.*, vol. 46, pp. 686–694, May 1998.

[96] H. Robbins and D. Siegmund, "Probability distributions related to the law of the iterated logarithm," *Proc. Natl. Acad. Sci. USA*, vol. 62, no. 1, pp. 11–13, Jan. 1969.

[97] P. Robertson, "A generalized frame synchronizer," in *Proc. IEEE Global Telecomm. Conf.*, Orlando, FL, Dec. 1992, pp. 365–369.

[98] M. Rudagavi, W. R. Heiiizelman, J. Webb, and R. Talluri, "Wireless MPEG-4 video communication on DSP chips," *IEEE Signal Process. Mag.*, vol. 17, no. 1, pp. 36–53, Jan. 2000.

[99] W. Rudin, *Real and Complex Analysis*, 3rd ed. McGraw-Hill, 1987.

[100] P. Salminen, "On the first hitting time and the last exit time for a Brownian motion to/from a moving boundary," *Adv. Appl. Probab.*, vol. 20, pp. 411–426, 1988.

[101] L. S. Schmidt, "Atomic clock models using fractionally integrated noise processes," *Metrologia*, vol. 40, no. 3, pp. S305–S311, Jun. 2003.

[102] R. A. Scholtz, "Frame synchronization techniques," *IEEE Trans. Commun.*, vol. COM-28, no. 8, pp. 1204–1213, Aug. 1980.

[103] W.-H. Sheen and S. Chiou, "Performance of multiple-dwell pseudo-noise code acquisition with I-Q detector on frequency-non selective multipath fading channels," *Wireless Network*, vol. 5, pp. 11–21, Sep. 1999.

[104] W.-H. Sheen and C.-C. Tseng, "Code acquisition with diversity combining for FFH/MFSK spread-spectrum systems," *IEE Proc. Commun.*, vol. 48, pp. 437–444, Dec. 1998.

[105] W.-H. Sheen, C.-C. Tseng, and H.-C. Wang, "Multiple-dwell and sequential code acquisition with diversity for FFH/MFSK spread-spectrum systems under band multitone jamming," *IEEE Trans. Commun.*, vol. 48, pp. 841–851, May 2000.

[106] W.-H. Sheen, J.-K. Tzeng, and C.-K. Tzou, "Effects of cell correlations in a mathched-filter PN code acquisition for direct-sequence spread-spectrum system," *IEEE Trans. Veh. Technol.*, vol. 48, pp. 724–732, May 1999.

[107] W.-H. Sheen and H.-C. Wang, "A new analysis of direct-sequence psudonoise code acquisition on Rayleigh fading channels," *IEEE J. Sel. Areas Commun.*, vol. 19, pp. 2225–2232, Nov. 2001.

[108] L. A. Shepp, "Radon-Nikodym derivatives of Gaussian measures," *Ann. of Math. Stat.*, vol. 37, no. 2, pp. 321–354, 1966.

[109] ——, "A first passage problem for Wiener process," *Ann. of Math. Stat.*, vol. 38, no. 6, pp. 1912–1914, Dec. 1967.

[110] ——, "The joint density of the maximum and its location for a Wiener process with drift," *J. Appl. Probab.*, vol. 16, pp. 423–427, 1979.

[111] O.-S. Shin and K. B. E. Lee, "Utilization of multipaths for spread-spectrum code acquisition in frequency-selective Rayleigh fading channels," *IEEE Trans. Commun.*, vol. 49, pp. 734–743, Apr. 2001.

[112] A. J. F. Siegert, "On the first passage time probability problem," *Phys. Rev.*, vol. 81, no. 4, pp. 617–623, Feb. 1951.

[113] F. Simoens, H. Wymeersch, H. Steendam, and M. Moeneclaey, "Synchronization for MIMO systems," in *Smart Antennas—State-of-the-Art*. Hindawi Publishing, 2005.

[114] M. K. Simon, J. K. Omura, R. A. Scholtz, and B. K. Levitt, *Spread Spectrum Communications Handbook*. New York, NY: McGraw-Hill, 2001.

[115] D. Slepian, "First passage time for a particular gaussian process," *Ann. of Math. Stat.*, vol. 32, no. 2, pp. 610–612, Jun. 1961.

[116] E. Sourour and S. C. Gupa, "Direct-sequence spread spectrum parallel acquisition in nonselective and frequency-selective fading Rician fading channels," *IEEE J. Sel. Areas Commun.*, vol. 10, pp. 535–544, Apr. 1992.

[117] A. Steingass, A. van Wijngaarden, and W. Teich, "Frame synchronization using superimposed sequences," in *Proc. IEEE Int. Symp. on Inf. Theory*, Ulm, GERMANY, Jun. 1997, p. 489.

[118] J. J. Stiffler, *Theory of Synchronous Communications*, 1st ed. Englewood Cliffs, New Jersey 07632: Prentice-Hall, 1971.

[119] D. W. Stroock, *Probability Theory, An Analytic View*, revised ed. Cambridge, United Kingdom: Cambridge University Press, 1999.

[120] ——, *An Introduction to Markov Processes*. Springer-Verlag Berlin Heidelberg, 2005, vol. 230.

[121] W. Suwansantisuk, *"Multipath Aided Rapid Acquisition,"* Master's thesis, Department of Electrical Engineering and Computer Science, Massachusetts Institute of Technology, Cambridge, MA, May 2004, thesis advisor: Professor Moe Z. Win.

[122] W. Suwansantisuk and M. Z. Win, "On the asymptotic performance of multi-dwell signal acquisition in dense multipath channels," in *Proc. IEEE Int. Zurich Seminar on Communications*, Zürich, Switzerland, Feb. 2006, pp. 174–177.

[123] ——, "Rapid acquisition techniques for spread spectrum signals," in *Proc. IEEE Int. Symp. on Inf. Theory*, Seattle, WA, Jul. 2006, pp. 947–951.

[124] ——, "Multipath aided rapid acquisition: Optimal search strategies," *IEEE Trans. Inform. Theory*, vol. 53, no. 1, pp. 174–193, Jan. 2007.

[125] ——, "Randomized search strategies for wideband signal acquisition," in *Proc. IEEE Int. Conf. on Commun.*, Cape Town, South Africa, May 2010, pp. 1–5.

[126] W. Suwansantisuk, M. Z. Win, and L. A. Shepp, "On the performance of wide-bandwidth signal acquisition in dense multipath channels," *IEEE Trans. Veh. Technol.*, vol. 54, no. 5, pp. 1584–1594, Sep. 2005, special section on *Ultra-Wideband Wireless Communications–A New Horizon*.

[127] ——, "Properties of the mean acquisition time for wide-bandwidth signals in dense multipath channels," in *Proc. 3rd SPIE Int. Symp. on Fluctuation and Noise in Communication Systems*, vol. 5847, Austin, TX, May 2005, pp. 121–135.

[128] R. Talluri, "Error-resilient video coding in the iso mpeg-4 standard," *IEEE Commun. Mag.*, vol. 36, pp. 112 – 119, Jun. 1998.

[129] V. V. Veeravalli and C. W. Baum, "Asymptotic efficiency of a sequential multi-hypothesis test," *IEEE Trans. Inf. Theory*, vol. 41, no. 6, pp. 1994–1997, Nov. 1995.

[130] S. R. S. Veradhan, *Stochastic Processes*. Providence, RI: American Mathematical Society, 2007.

[131] S. Vijayakumaran and T. F. Wong, "Best permutation search strategy for ultra-wideband signal acquisition," in *Proc. IEEE Semiannual Veh. Technol. Conf.*, Los Angeles, CA, Sep. 2004, pp. 1184 – 1187.

[132] ——, "On equal-gain combining for acquisition of time-hopping ultra-wideband signals," *IEEE Trans. Commun.*, vol. 54, pp. 479–490, Mar. 2006.

[133] A. J. Viterbi, *CDMA: Principles of Spread Spectrum Communication*, 1st ed. Reading, MA: Addison-Wesley, 1995.

[134] H.-C. Wang and W.-H. Sheen, "Variable dwell-time code acquisition for direct-sequence spread-spectrum systems on time-variant Rayleigh fading channels," *IEEE Trans. Wireless Commun.*, vol. 48, pp. 1037–1046, Jun. 2000.

[135] Y. Wang, S. Wenger, J. Wen, and A. K. Katsaggelos, "Error-resilient video coding techniques," *IEEE Signal Process. Mag.*, vol. 17, p. 612, Apr. 2000.

[136] A. Weinberg, "Generalized analysis for the evaluation of search strategy effects on PN acquisition performance," *IEEE Trans. Commun.*, vol. 31, pp. 37–49, Jan. 1983.

[137] M. Z. Win, C.-C. Chen, and R. A. Scholtz, "Optical phase-locked loop (OPLL) for an amplitude modulated communications link using solid state lasers," *IEEE J. Sel. Areas Commun.*, vol. SAC-13, no. 3, pp. 569–576, Apr. 1995.

[138] M. Z. Win, G. Chrisikos, and N. R. Sollenberger, "Performance of Rake reception in dense multipath channels: Implications of spreading bandwidth and selection diversity order," *IEEE J. Sel. Areas Commun.*, vol. 18, no. 8, pp. 1516–1525, Aug. 2000.

[139] M. Z. Win and Z. A. Kostić, "Virtual path analysis of selective Rake receiver in dense multipath channels," *IEEE Commun. Lett.*, vol. 3, no. 11, pp. 308–310, Nov. 1999.

[140] M. Z. Win and R. A. Scholtz, "On the energy capture of ultra-wide bandwidth signals in dense multipath environments," *IEEE Commun. Lett.*, vol. 2, no. 9, pp. 245–247, Sep. 1998.

[141] ——, "On the robustness of ultra-wide bandwidth signals in dense multipath environments," *IEEE Commun. Lett.*, vol. 2, no. 2, pp. 51–53, Feb. 1998.

[142] ——, "Characterization of ultra-wide bandwidth wireless indoor communications channel: A communication theoretic view," *IEEE J. Sel. Areas Commun.*, vol. 20, no. 9, pp. 1613–1627, Dec. 2002.

[143] M. Z. Win and J. H. Winters, "Virtual branch analysis of symbol error probability for hybrid selection/maximal-ratio combining in Rayleigh fading," *IEEE Trans. Commun.*, vol. 49, no. 11, pp. 1926–1934, Nov. 2001.

[144] Y.-C. Wu, Q. Chaudhari, and E. Serpedin, "Clock synchronization of wireless sensor networks," *IEEE Signal Process. Mag.*, vol. 28, no. 1, pp. 124 – 138, Jan. 2011.

[145] H. Wymeersch and M. Moeneclaey, "Code-aided ML joint delay estimation and frame synchronization," in *Signal Processing for Telecommunications and Multimedia, Multimedia Systems and Applications*, B. H. T.A. Wysocki and B. Wysocky, Eds., vol. 27. Springer-Verlag, 2005.

[146] H. Wymeersch, H. Steendam, H. Bruneel, and M. Moeneclaey, "Code-aided frame synchronization and phase ambiguity resolution," *IEEE Trans. Signal Process.*, vol. 54, no. 7, pp. 2747–2757, Jul. 2006.

[147] C. W. Yak, Z. Lei, S. Chattong, and T. T. Tjhung, "Timing synchronization and frequency offset estimation for ultra-wideband (UWB) multi-band OFDM systems," in *Proc. IEEE Int. Symp. on Personal, Indoor and Mobile Radio Commun.*, Berlin, Germany, Sep. 2005, pp. 471– 475.

[148] B. Yang, K. B. Letaief, R. S. Cheng, and Z. Cao, "Burst frame synchronization for OFDM transmission in multipath fading links," in *Proc. IEEE Semiannual Veh. Technol. Conf.*, Amsterdam, NETHERLAND, Sep. 1999, pp. 300–304.

[149] L.-L. Yang and L. Hanzo, "Serial acquisition of DS-CDMA signals in multipath fading mobile channels," *IEEE Trans. Veh. Technol.*, vol. 50, pp. 617–628, Mar. 2001.

[150] ——, "Serial acquisition performance of single-carrier and multicarrier DS-CDMA over Nakagami-m fading channels," *IEEE Trans. Wireless Commun.*, vol. 1, pp. 692–702, Oct. 2002.

[151] M. Zakai and J. Ziv, "On the threshold effect in radar range estimation," *IEEE Trans. Inf. Theory*, vol. 15, no. 1, pp. 167–170, Jan. 1969.

[152] W. Zhuang, "Noncoherent hybrid parallel PN code acquisition for CDMA mobile communications," *IEEE Trans. Veh. Technol.*, vol. 45, pp. 643–656, Nov. 1996.

[153] C. Zucca and P. Tavella, "The clock model and its relationship with the Allen and related variances," *IEEE Trans. Ultrason., Ferroelectr., Freq. Control*, vol. 52, no. 2, pp. 289–296, Feb. 2005.